1-1-2013

Subsurface discontinuity analysis & modeling for the federal waste disposal facility and compact waste disposal facility landfills

Shuang Cao
University of Mississippi

SUBSURFACE DISCONTINUITY ANALYSIS & MODELING FOR THE FEDERAL WASTE DISPOSAL FACILITY AND COMPACT WASTE DISPOSAL FACILITY LANDFILLS

A Thesis
presented in partial fulfillment of requirements
for the degree of Master of Science
in the Department of Geology and Geological Engineering
The University of Mississippi

By

SHUANG (CINDY) CAO

September 2013

ABSTRACT

This research considers discontinuities mapped by Waste Control Specialists LLC to support the site conditions and performance analysis of the Compact Waste Disposal Facility and the Federal Waste Disposal Facility excavations constructed near Andrews, Texas. Discontinuities observed in excavation walls contain a limited number of discontinuities showed evidence of previous fluid movement. While no networks of such discontinuities were observed in the field, the potential for such networks may exist. This research is significant in understanding the performance of these waste facilities by modeling multiple realizations of possible fracture configurations in three-dimensional spatial models of the type of discontinuities observed in the field. The results show the low-angle discontinuities vastly outnumber the near-vertical discontinuities and most hydraulically significant discontinuities are shown with near-vertical orientation. Relatively few hydraulically significant discontinuities were observed across all mapped faces within the set of low-angle discontinuities. Furthermore, the proportion of vertical to horizontal discontinuities decreases with decreasing grain size, and most Genetic units had discontinuities in the upper half of a Genetic unit that were roughly horizontal and very few showed evidence of hydraulic significance. Three-dimensional models were created of the discontinuities in each of the geologic lagers surrounding both facilities using DFNModeler. These models were created using a statistical representation of the hydraulically significant discontinuities observed in each of the geologic units observed in the mapped areas of both facilities. In general, the variation in discontinuity properties do not show significant trends beyond the consistency with the geologic characteristics of each bed or layer, supporting a

bedded but otherwise statistically consistent spatial model of the units. The model results showed a mean of maximum fracture network volume or compartment hull volume of 95.72 m^3 and 188.59 m^3 for the CWF and FWF, respectively. The maximum effective diameter or one-dimensional span of such hulls is small (3.57 m to 6.82 m) relative to the height of width of the excavation walls. The largest proportion of compartment hulls had a volume smaller than 8 m^3 and a few hulls were larger than 18 m^3. There is no evidence found in models of either the CWF or FWF that there is any credible potential for fluid flow within possible networks of discontinuities within these units in either the vertical direction or horizontal direction.

DEDICATION

This thesis is dedicated to everyone who helped me and guided me through my own times of stress and anxiety. In particular, I thank my parents, without tireless encouragement I would have given up long ago.

LIST OF ABBREVIATIONS AND SYBOLS

CEUS	Central and Eastern U.S
CGU	Compact Waste Disposal Facility Genetic Unit
CWF	Compact Waste Disposal Facility
CWFGU	Compact and Federal Waste Disposal Facilities Combined Genetic Unit
DFNModeler	Discrete Fracture Network Modeler
FWF	Federal Waste Disposal Facility
FGU	Federal Waste Disposal Facility Genetic Unit
HSD	Hydraulically Significant Discontinuities
NHSD	Non-Hydraulically Significant Discontinuities
USGS	U.S. Geological Survey
WCS	Waste Control Specialists LLC

ACKNOWLEDGMENTS

I express my deepest appreciate to my advisor, Dr. Joel S. Kuszmaul and my committee member, Dr. Robert M. Holt, and Dr. Adnan Aydin. I could not have financed my studies without the assistantship provided by the Department of Geology and Geological Engineering.

In addition, I thank Dr. Joel S. Kuszmaul help me dealing with my future plan. Also, I thank Dr. Jin Guohai and Dr. Chunmiao Zheng Hands of University of Alabama for providing access to important software.

Lastly, I acknowledge the emotional support from my boyfriend and fellow students. You made this part of my life enjoyable and enriching.

TABLE OF CONTENTS

LSIT OF FIGURES

LSIT OF TABLES

CHAPTER I

INTRODUCTION

1.0 An Overview of the Thesis

Discontinuity properties have a large influence on the engineering behavior of soil and rock masses, affecting the design of excavations, slopes, landfills and mines. In engineering practice, a discontinuity is a plane or surface that marks a change in physical or chemical characteristics in a soil or rock mass. The presence of discontinuities will make a soil or rock mass anisotropic, may provide the principle conduits for fluid flow, and may have an influence on rock mass deformability which may not be good for engineering design and construction. Understanding the effect of such discontinuities requires a detailed understanding of the number and nature of discontinuities present in a rock mass. This research involves the mapping and analysis of a set of discontinuities present in the rock in which waste disposal facilities have recently been created.

The research data comes from the discontinuity mapping activities which are conducted in the Compact Waste Disposal Facility (CWF) and the Federal Waste Disposal Facility (FWF) landfill excavations during the period between March 9, 2011 and July 26, 2011. "All mapping activities occurred concurrently with the excavation of the landfills and were completed within 24 hours of the excavation of the mapping face" (Holt. et al., 2011). For the CWF landfill, there are six mapped levels. For FWF landfill, nine levels are mapped. For both CWF and FWF

sites, two near-vertical faces are excavated in the southeast corner of each landfill. At both CWF and FWF sites, all levels are included within the upper part of the Cooper Canyon Formation of the Dockum Group (Holt. et al., 2011).

Discontinuities observed in the CWF and FWF contain some special discontinuities that show evidence of previous fluid movement. This research is significant in understanding the performance of these waste facilities. Examining and creating a three-dimensional model of the discontinuity data gives a better view and understanding for fracture network analysis. The results are able to show how the discontinuities are distributed in each genetic unit within the mapped corners of the CWF and FWF landfills. The discontinuity properties are examined and analyzed by statistics methods. Furthermore, the results consider the discontinuities in each genetic unit and geologic unit in CWF and FWF landfills using stereo plots or hemispherical projections. Since some discontinuities are unusual and show evidence of previous fluid movement, the results assess the biggest influence which shows in both the hydraulically significant discontinuities (HSD) and non-hydraulically significant discontinuities (NHSD). Integrated all the results, it presents an in-depth explanation of those discontinuities. And the results display a comprehensive view for examining the issue of discontinuity networks.

From this research, landfill site characterizations are examined, and the potential for discontinuities networks are examined. This research also provides a unique opportunity for understanding the geologic frame work of the upper part of the Cooper Canyon Formation of the Dockum Group. Furthermore, spatial analysis of the discontinuity data is conducted that gives a more detailed and comprehensive condition for the landfills. Finally, a three-dimensional model for HSD is created to display a comprehensive view of those discontinuities; any networks of

discontinuities are considered to examine the potential for fluid flow within such possible networks.

1.1 Working Basis

The research data is provided by Waste Control Specialists LLC (WCS). This research is mainly based on a subsurface discontinuity mapping project named "Subsurface Discontinuity Mapping for the Federal Waste Disposal Facility and Compact Waste Disposal Facility Landfills" which was conducted in 2011. There is an abundance of prior work that guides this research.

As a result, some field data and information comes from previous field work which is needed for this research, such as field water potential measurements and information for each discontinuity. At this time, the WCS waste disposal facilities are in service, so no field work was conducted during this research. While partial field measurements and lab tests results are reviewed and used. More details of data information are introduced in Chapter II. Furthermore, the site characterizations that affect disposal landfill performance are described. So this research provides the opportunity to understand landfill site characterization in this research. Since there is no field observation conducted, previous literature were used to summarize and understand all site characterizations. More details of site characterizations are introduced in Chapter I. Based on the previous project, some existing theories are also used. For example, a series of genetically-related units are identified during the mapping of the CWF and FWF, and the unit boundaries are selected in the mapping project. This identification and classification is highly significant, so it is used and referred to in this research. More details of this theory are discussed in Chapter II and III.

1.2 Site Characteristics

1.2.1 Location

The research area is located at a land disposal facility which is built for low level radioactive material from a variety of sources, all to be managed by Waste Control Specialist LLC (WCS). WCS is a hazardous and radioactive waste processing and disposal company. And the WCS land disposal facility is located about 31 miles (50 km) west of the City of Andrews, Texas and 6 miles (10 km) east of the City of Eunice, New Mexico. The land disposal facilities are located about 1.5 mile (2.4 km) east of the Texas-New Mexico State boundary and 1 mile (1.6 km) north of Texas Highway 176. Figure 1.1 shows the facility location with identifiable landmarks (Waste Control Specialists LLC, 2007).

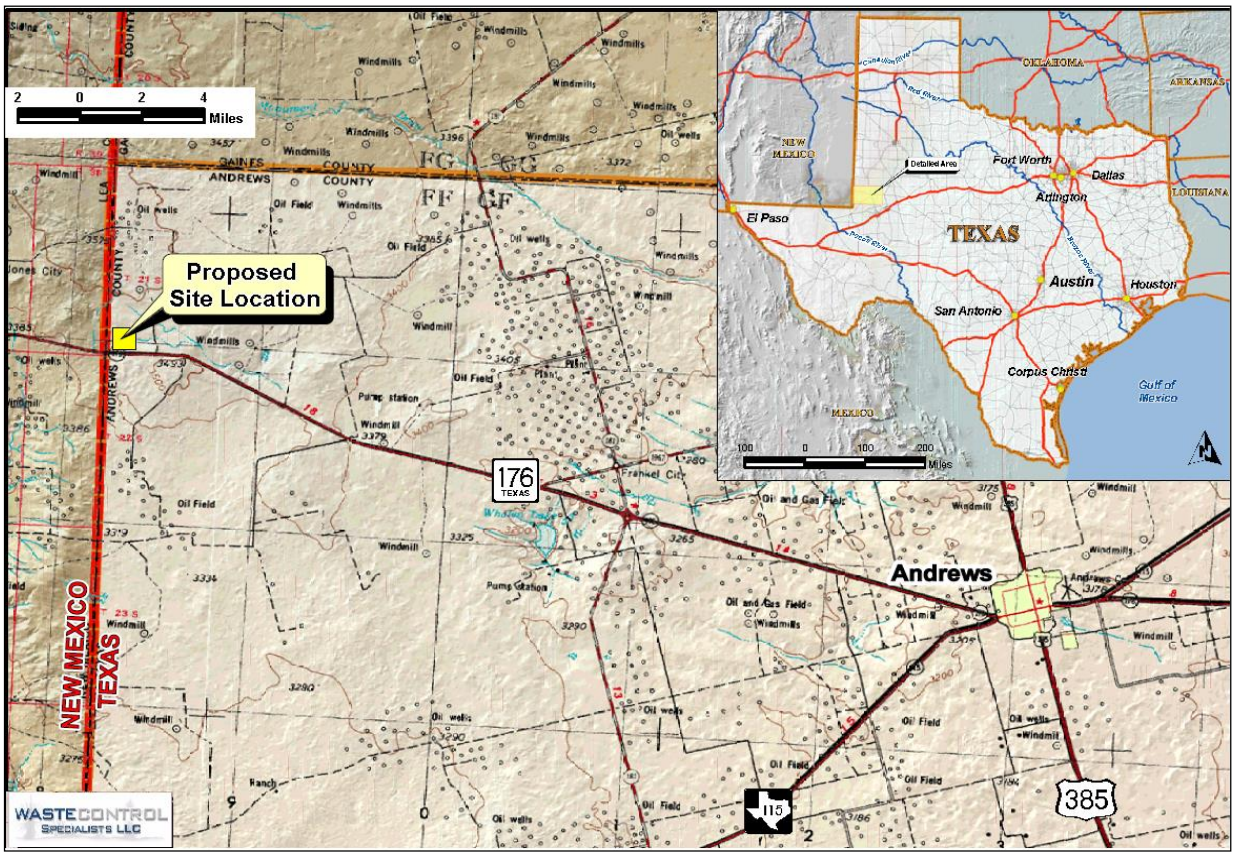

Figure 1.1 Research Site Location Map (Waste Control Specialists LLC, 2007)

All discontinuity data are collected and mapped concurrently with the excavation of those disposal facilities. The data come from two main disposal facilities, one disposal facility is called the Compact Waste Disposal Facility (CWF) and another facility is called the Federal Waste Disposal Facility (FWF) landfill. The CWF discontinuity data comes from six mapped excavation levels, and the FWF discontinuity data comes from nine mapped excavation levels. For each level, two near-vertical faces are mapped in the southeast corner of each landfill. Figure 1.2 and 1.3 shows the discontinuity data observation windows.

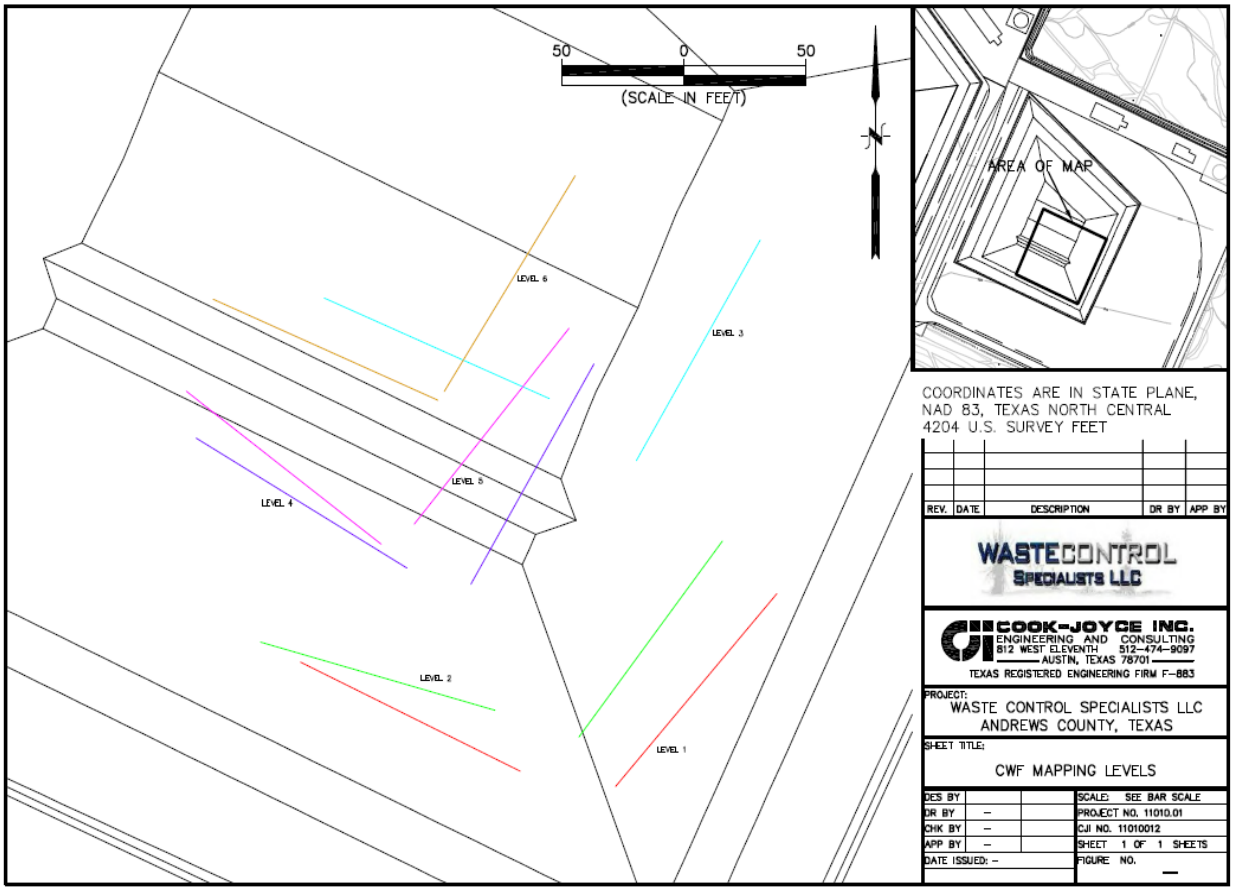

Figure 1.2 Location of Mapping Levels and Faces in CWF (Holt et al., 2010)

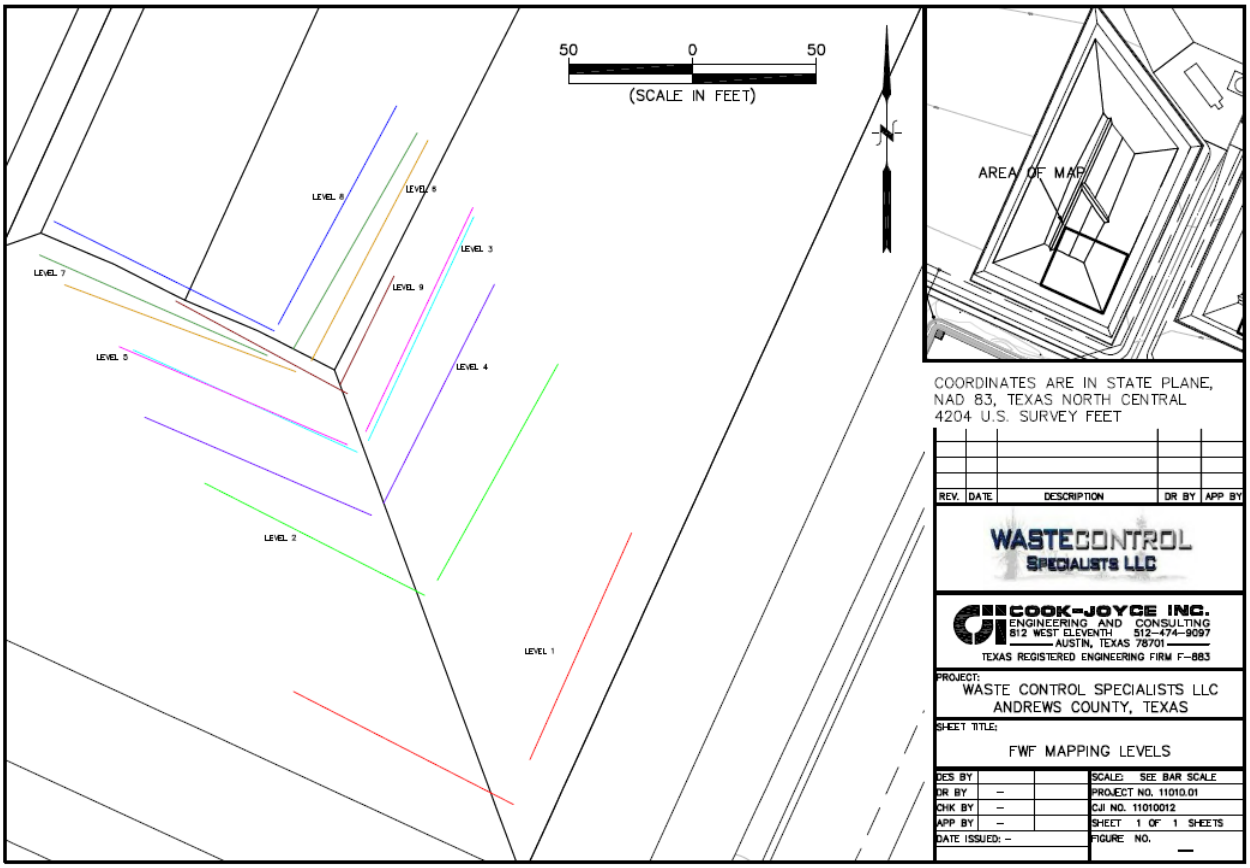

Figure 1.3 Location of Mapping Levels and Faces in FWF (Holt et al., 2010)

1.2.2 Climate and Vegetation

The WCS land disposal facility site is located between Andrews County, Texas and Lea County, New Mexico. The climatic regions are identified separately in these two states, which makes the area surrounding the site located in two climatic regions: Southern High Plains in Texas and Southeastern Plains in New Mexico. Southern High Plains is referred to the area surrounding the site because the majority of the set is located within Texas. The climate in the area surrounding the site is classified as a semiarid environment which is characterized by low annual humidity, low annual precipitation and high average annual temperature or simply as having a warm, dry summer and mild, dry winter (Waste Control Specialists LLC, 2007).

The highest mid-day mean relative humidity in January is around 50 percent. During the summer and fall, the relative humidity values are generally higher than those for winter and spring (Waste Control Specialists LLC, 2007).

As presented in Figure 1.4, the average annual precipitation in this area ranges from 14 to 18 inches. The majority of the precipitation increases from May through October when the region receives most rainfall while some precipitation occurs during early spring.

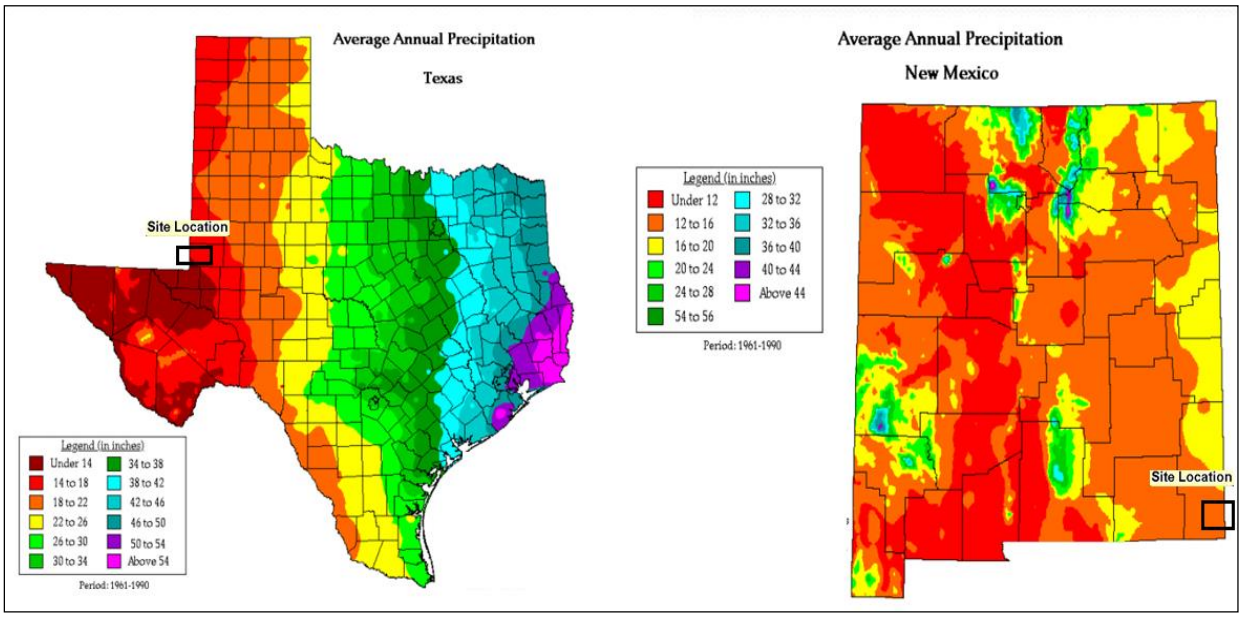

Figure 1.4 Texas and New Mexico Average Annual Precipitation Map (SCAS, 2000)

The difference between the average daily maximum and average daily minimum temperatures is approximately 30 ℉ throughout the year. According to the records from the National Weather Service (NWS) Cooperative Station, the average maximum daytime temperature ranged from low 60s ℉ in the winter to the low 90s ℉ in the summer and the average minimum nighttime temperature ranged from 30s ℉ in the winter to the about 60s ℉ in the summer (Waste Control Specialists LLC, 2007).

For vegetation information, the WCS land disposal facility site is located in the High Plains region, which is part of the central Great Plains. As Figure 1.5 shows, the natural

vegetation in this site is low desert grassland with scattered shrubs, cacti and forbs. The cover type is majorly Harvard Shin Oak-Mesquite Brush.

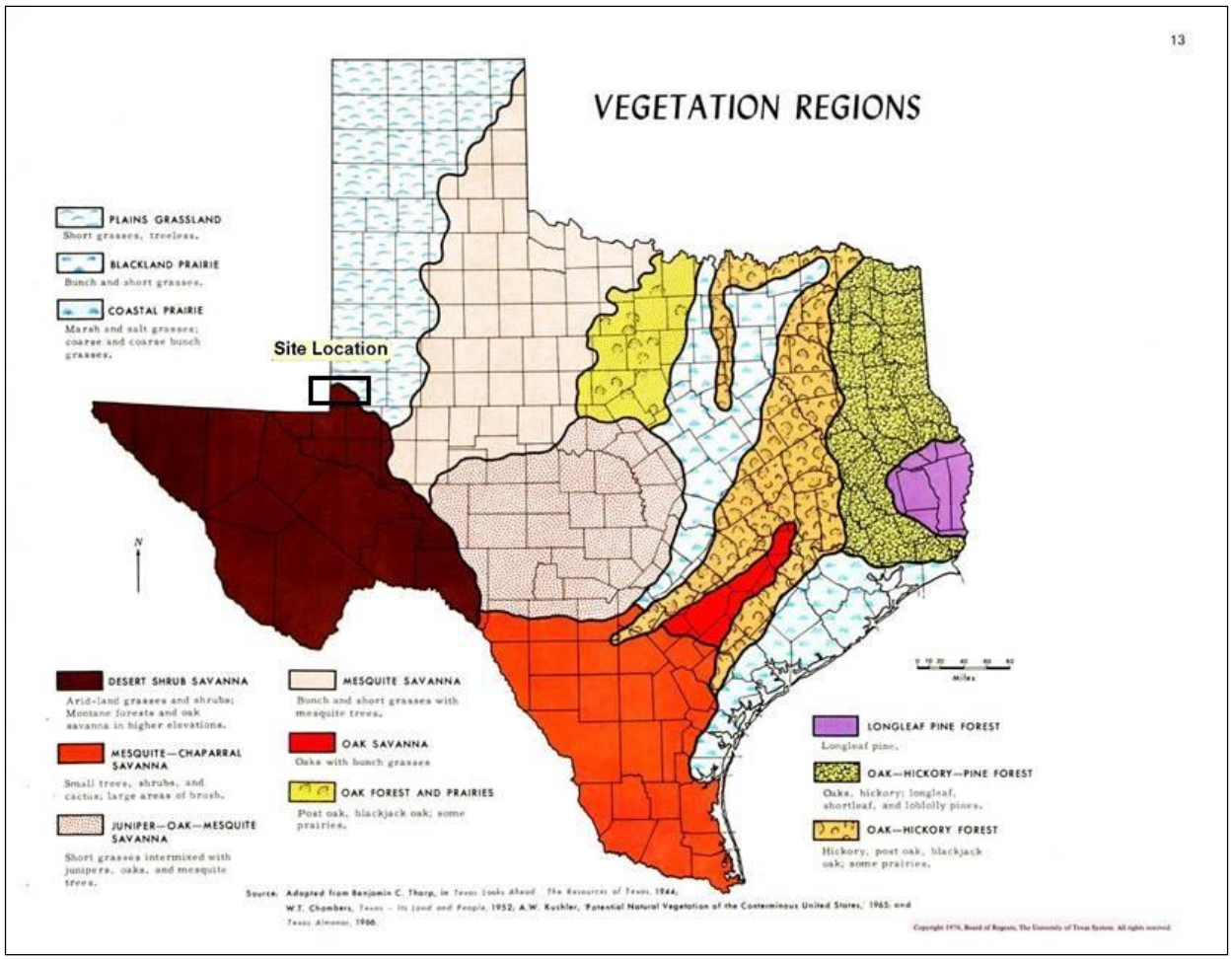

Figure 1.5 Site Location Vegetation Regions (Board of Regents, 1976)

1.2.3 Topography and Drainage

The WCS land disposal facility site is located in west Texas and the southern portion of the High Plains. Figure 1.6 shows the physiographic regions of the Texas Panhandle and adjacent areas of Texas and New Mexico. The Southern High Plains is an elevated area of undulating plains with low relief encompassing a large area of western Texas and eastern New Mexico (Waste Control Specialists LLC, 2007).

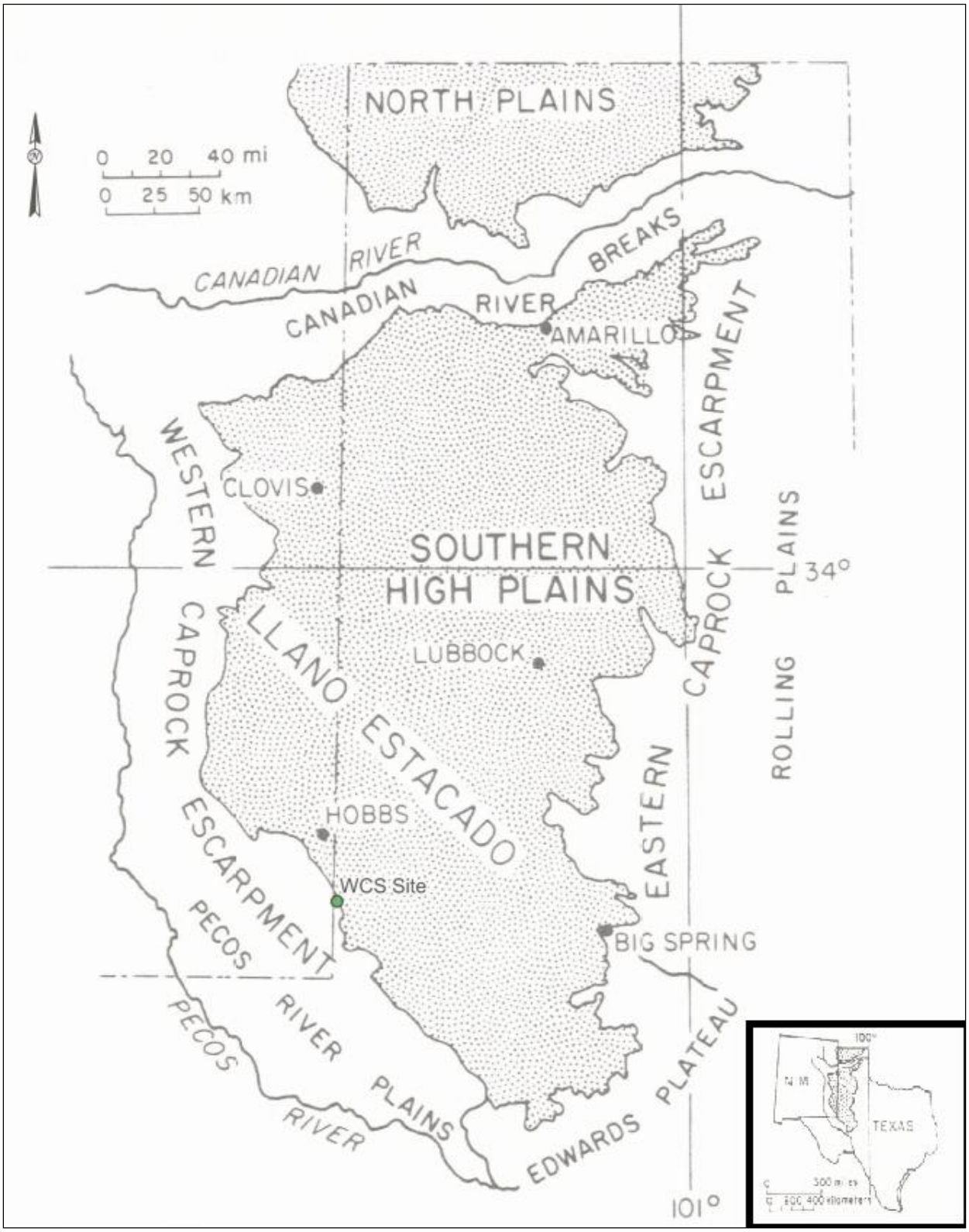

Figure 1.6 Physiographic Regions of the Texas Panhandle and Adjacent Areas of Texas and New Mexico (Waste Control Specialists LLC, 2007)

The WCS site is on the southwestern slope of the surface water drainage divide between the Pecos River and the Colorado River (Cook-Joyce,Inc, 2007). This slope is southwest toward Monument Draw, New Mexico, and topographic relief in this area is a gentle southwestward slope of about 50 ft (15m) per mile (Cook-Joyce,Inc, 2007). For the WCS land disposal facility, the maximum elevation is around 3500 ft (1067 m); the minimum elevation is about 3415 ft (1040 m). Regional topographic map shows the area is only of contrast between depositional plains and large erosional surfaces locally altered by subterranean solution and near-surface collapse. Figure 1.7 illustrates the altitude range is from about 5000ft (1.5 km) in North West to about 2,700ft (0.8 km) near Big Spring in South East. In the WCS facility, some small surface depressions and a few established playa basins are presented. Outside the WCS facility, local topographic features include Baker Spring to the west and small playas or solution pans (localized dissolution of the caprock caliche at or near ground surface) between Baker Spring and the facility (Cook-Joyce, Inc., 2007).

Although the fluvial scars of Pleistocene drainage channels occur throughout southeastern New Mexico and west Texas, there are presently no though-flowing streams. The nearest surface water drainage around the WCS land disposal facility is Monument Draw in Lea County, New Mexico. It is a southward-draining ephemeral draw about 3 miles (4.8 km) west of the WCS facility boundary (Cook-Joyce, Inc., 2007). 'The draw does not have through-going surface water drainage, and due to encroachment of Cenozoic alluvial and eolian deposits, loses surface expression after it enters Winkler County, Texas." (Cook-Joyce, Inc., 2007).

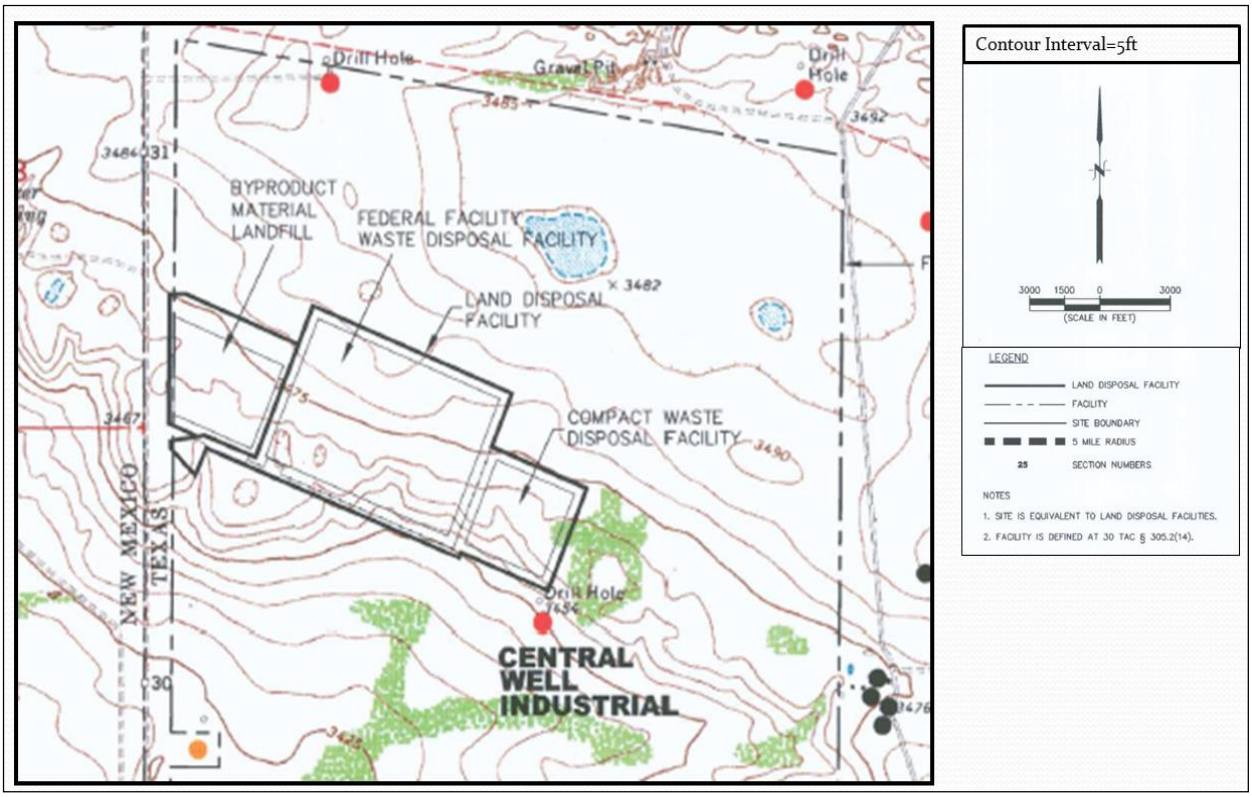

Figure 1.7 Topographic Map for WCS Site (Waste Control Specialists LLC, 2007)

1.2.4 Regional and Site Geology

The research site lies within the Central Basin Platform of the Permian Basin. "The Permian rocks comprise marine shales, limestones, sandstone, marls and anhydrite and the salt deposits of the Salaso and Rustler Formations in the late Permian time" (Waste Control Specialists LLC, 2007). The landfills are built for low level radioactive material from a variety of sources all to be managed by WCS. The nature of the geologic units at the site is critical to the successful isolation of these waste materials. The geologic formations encountered in the vicinity of the WCS facility contains, from oldest to youngest, the Triassic Dockum Group, the Cretaceous Trinity Group Antlers Formation, the late Tertiary Ogallala Formation, late Tertiary/Quaternary Gatuna Formation or Cenozoic Alluvium, the Pleistocene windblown sands of the Blackwater Draw Formation, and Holocene windblown sands and playa deposits.(Cook-Joyce, Inc., 2007). The regional geologic observations show that the data collection area lies

within the upper part of the Cooper Canyon Formation of the Dockum Group. The Cooper Canyon Formation has about 500 ft (152 m) thickness in the WCS vicinity. "In the WCS facilities area, the claystones of the Dockum Group Cooper Canyon Formation are overlain primarily by the early Cretaceous Antlers sandstone and gravels, except for the southwest corner of the facility where the late-Tertiary-early Quaternary Gatuna Formation is present over the Dockum Group" (Cook-Joyce, Inc., 2007). Figure 1.8 shows a site-specific stratigraphic column for those geologic formations.

For WCS site, it is situated over the north central of a prominent Paleozoic structural feature named the Central Basin Platform. "The Central Basin Platform is a deep-seated horst-like structure that extends northwest to southeast from southeastern New Mexico to eastern Pecos County, Texas" (Cook-Joyce, Inc., 2007). "Patterns of sedimentation at and around the WCS site since the Cooper Canyon was deposited indicate broad uplift and limited periods of subsidence across the region" (Holt et al., 2010). Holt et al. (2010) reported that the tectonic stresses did not induce fracturing within the Dockum, and they also indicated that the Dockum was unsaturated during its depositional phase and it remained above sea-level.

There are specific geologic features occurring in Duckum that should be related to their depositional environment. Arcuate slickensided surfaces are common throughout the mudrock sequences (Holt et al., 2010). The outcrop revealed that master slickensides that defined the lower boundary of gilgai. "The slickensided surfaces and gilgai are consistent with repeated subaerial exposure and soil development in a vertic regime and indicate and arid to semi-arid environment with repeated wetting and drying" (Holt et al., 2010).

In general, this feature is caused by paleosols formed in a relatively dry depositional environment that had wet and dry periods as a distinctive features. Modern analogs would be

known as vertisols, which commonly have extensive shrinkage cracking and can have a mound feature known as gilgai. Chertkov, (2005) suggests a number of possible mechanisms for the origin of these features, all involving loading and soil movement along shear planes (slickensides) after the failure of soil material near vertical cracks formed during shrinking and swelling of soils with significant expansive clay content.

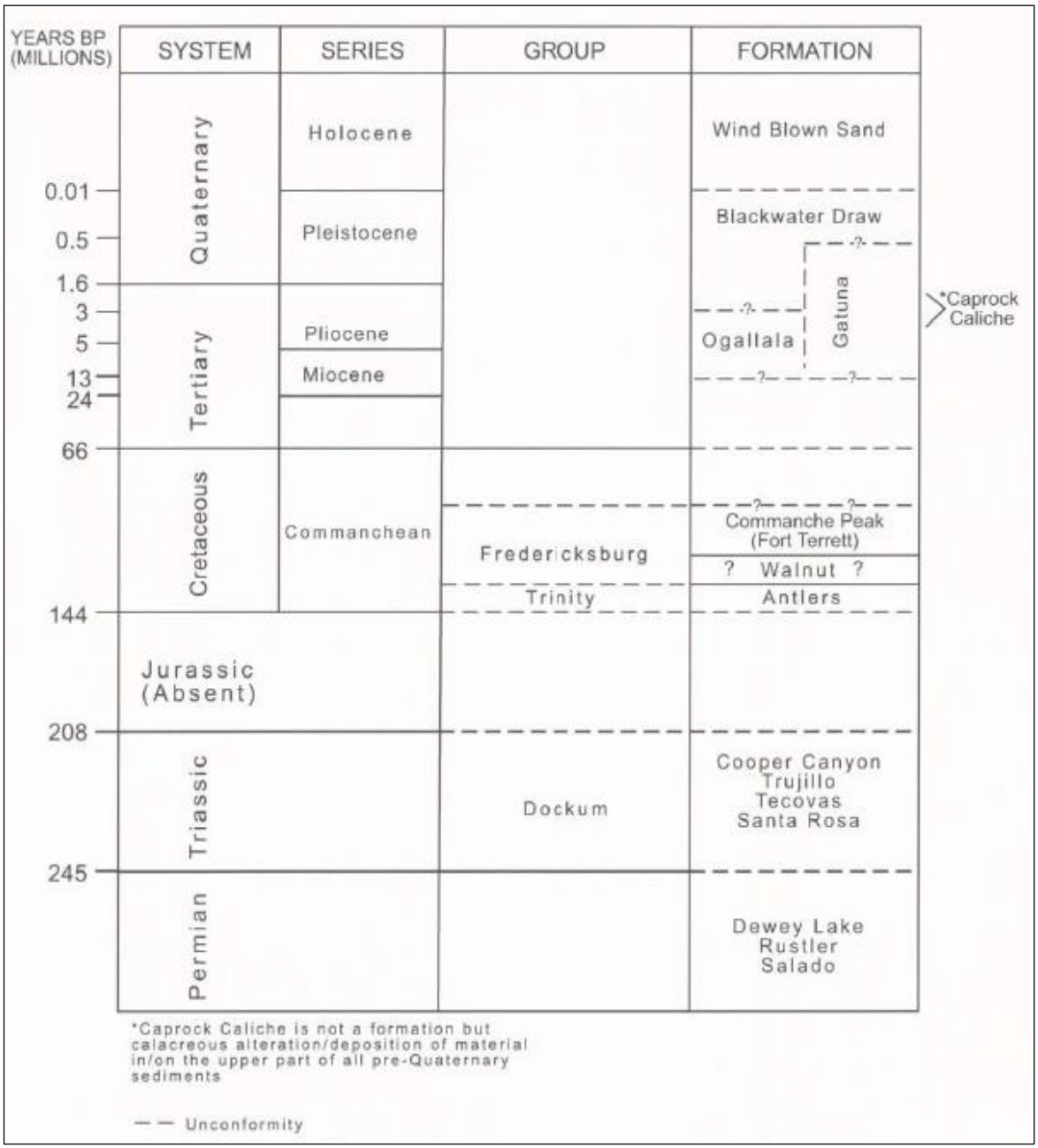

Figure 1.8 WCS Site-Specific Stratigraphic Chart (Cook-Joyce, Inc., 2007)

The model of horizontal shrinkage cracks determines the key parameter to be the maximum vertical size of gilgai. Chertkov (2005) reports, before gilgai formation, a dry soil contains both subvertical and subhorizontal cracks. During the wet season, water infiltrates through the upper soil surface and along vertical crack walls. As a result of soil swelling, the vertical cracks close. Due to the softness of the upper wetted soil, a volume of air-filled horizontal cracks is retained which is subject to extension upward (mounding) in response to the increased horizontal confinement caused by swelling or expanding soil pressures.

For example, in units of southeast of New Mexico, Eren (2005) reports that most fractures formed by progressive loading during burial are essentially parallel or subparallel to bedding orientation (Eren, 2005). But the slickensides observed (Holt et al. 2011) on those features suggest that they are likely to have experienced displacement along the features that are likely due in part to swelling or shrinkage effects. Many features formed in response to swelling or shrinkage during cycles of wet and dry seasons would have a different orientation. Typically the shrinkage cracks would be vertical (Chertkov, 2005) or close to vertical in orientation.

The discontinuity data were collected from Southeast part of WCS which located in CWF and FWF at the northwestern corner of Andrews County, Texas. "At the site, the Cooper Canyon consists of thicker (~45 ft) mudrock sequences showing varying degrees of pedogenic alteration intercalated with thinner (~10-20 ft) gray siltstone-sandstone zones, known locally as the 80-foot, 125-foot, 180-foot, and 225-foot zones" (e.g., Holt et al., 2011). For the siltstone-sandstone zones, it shows little pedogenic alteration. The existing geologic and discontinuity maps were created during the excavation of the CWF and FWF. All the discontinuity data comes from the maps which are prepared in the field at a scale of 1 in (0.025 m) equals 5 ft (4.572m), and they describe freshly exposed, near-vertical walls, each approximately 100 ft (30.48m) long, on both

the east face and south face in the Southeast corner of each excavation. The existing data not only contain the maps of the discontinuities but also characteristic features of all discontinuities. These features include geologic unit, length, strike, dip, roughness, curvature, termination type, aperture, and notes regarding fill and other observations. Ground water flow through here such as the Dockum is slow and limited by very low hydraulic conductivity (Holt et al., 2010).While most discontinuities show no evidence of past fluid movement (such features are considered NHSD), there are some features with evidence of staining or past fluid movement (such features are considered HSD) it is believed that the latter features may influence the landfill performance. Beyond this discontinuity data, there are other WCS related reports addressing the geology and hydrogeology of the local units which are also useful in assessing the site geology. Holt and Hughes (2008) report, for example, that Cooper Canyon claystones and mudstones are within the vadose zone, commonly defined as the region above the permanent water table. Furthermore, some wells were drilled, cored and sampled for hydraulic properties and matric potential measurements which supplement the mapping information to provide useful information regarding hydrologic properties of these units.

1.2.5 Seismicity

The historical earthquake in WCS land disposal facility site area can be divided into two periods: prior to 1962 and after 1962. Before 1962 is the pre-instrumental period when the epicentral locations and magnitudes are largely based upon felt reports. In this period, there is little evidence for seismicity in the CBP which is probably because of the lack of significant population. After 1962 is the instrumental period when seismographic coverage of the site region was initiated (URS Corporation, 2004).

As the Figure 1.9 shown, from the historical record, three significant earthquakes happened in this area: 1931 Valentine Earthquake, 1992 Rattlesnake Canyon Earthquake and 1995 Alpine Earthquake. Among which the 1992 Rattlesnake Canyon Earthquake is the most significant earthquake in the vicinity of the WCS site, this earthquake has an estimated magnitude range from M_b 4.6 to M 5.0 (URS Corporation, 2004). The earthquake was felt in southeastern New Mexico and west Texas; it is reasonable to assume this earthquake would have been felt at the WCS set according to the felt reports distribution (URS Corporation, 2004). With the first motion data, this earthquake was interpreted as a reverse fault, with movement consistent with east-west maximum horizontal compressive stress orientation. But with the scant data available, focal depth estimates could not able to be closely constrained, which could not rule out high water pressure water injection as a mechanism for this earthquake (URS Corporation, 2004).

As Figure 1.9 shown, the epicenter of the earthquake in 1992 is 19 miles (30km) to the southwest of WCS facilities site. For considering other earthquakes, only a few events above M3.0 have occurred with 30km range of the WCS site. Also, no faults offsets are known to exist in the units within 100km of the WCS site. The result of the probabilistic seismic hazard analyses of the WCS site shows low seismic hazard even associated with petroleum recovery activities (URS Corporation, 2004).

As some research show the southeastern New Mexico-west Texas corner is displayed as a high-hazard "bulls-eye" because of the cluster of earthquake contained in the USGS catalog in this location. For example, the USGS released a set of "landmark" National Hazard Maps for earthquake ground shaking in 1996. WCS has argued (URS Corporation, 2004) that the USGS National Hazard Map values for the WCS site are too high because they used inappropriate

approaches. In particular, the WCS site and the Southern Great Plains are included as part of the CEUS craton, and a maximum magnitude of M 7.0 is used for Gaussian smoothing for CEUS craton. The maximum magnitude of M 7.0 is, in the WCS argument, definitely too high for the WCS site and the Southern Great Plains. Secondly, the CEUS attenuation relationships used by the USGS are not appropriate for most of the site region (Waste Control Specialists LLC, APP 2.5.2, 2007). As a result, the comprehensive seismic analysis indicates that the WCS site is in a seismically stable zone.

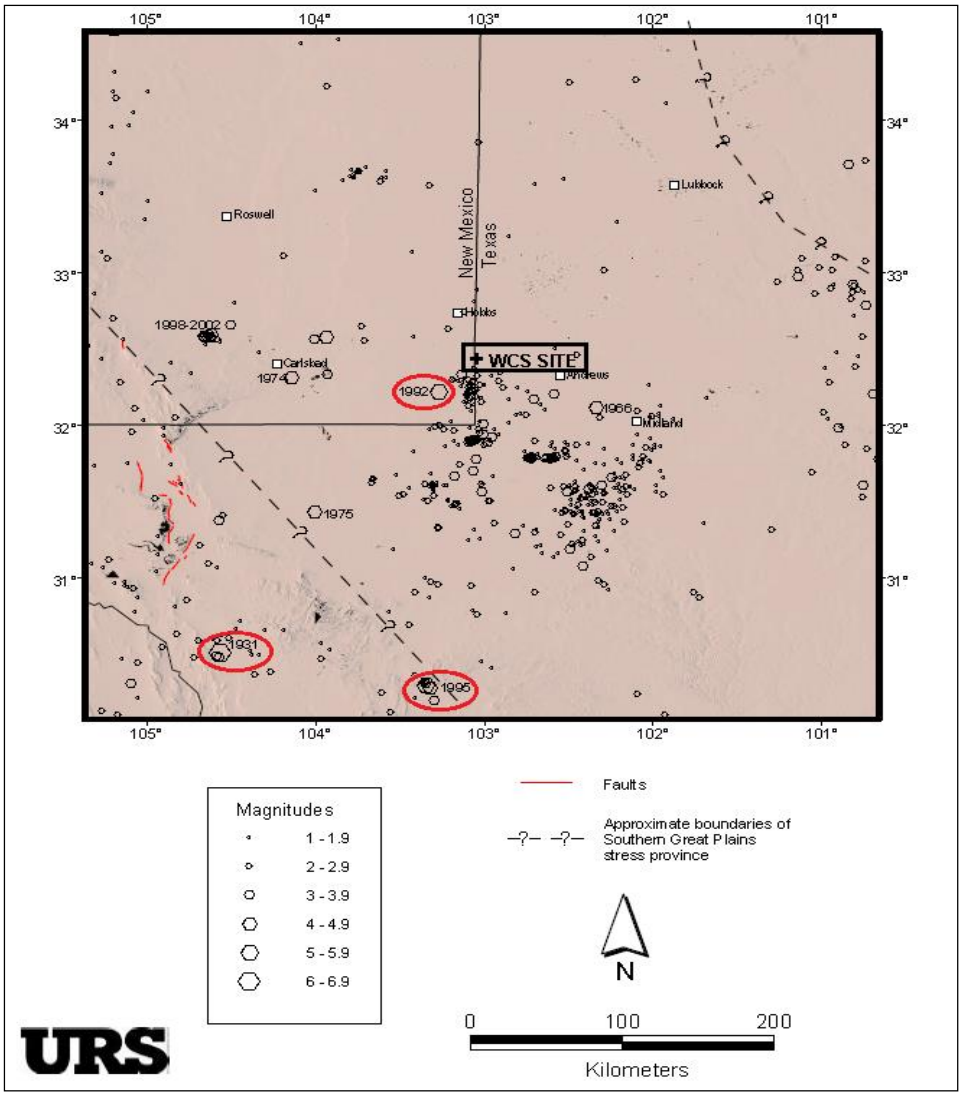

Figure 1.9 Historical Seismicity and Significant Earthquakes in the WCS Site Region 1849 to 2004 (URS Corporation, 2004)

1.3 Objectives

The research is intended as a master graduate thesis. It includes the following objectives. Firstly, describing the site characterizations that affect disposal landfill performance. Understanding and learning landfill site characterization. All information come from previous literature which includes climate information, topography information, drainage information, vegetation information, and regional geology information, site geology information, hydrogeology information and regional seismicity information are summarized in this research.

Second, describe and characterize the discontinuities for each genetic and geology unit in CWF and FWF landfills. Discover the anisotropy for the discontinuity properties in CWF and FWF landfills by using statistics analysis. Make an estimation map for each property of discontinuities. Find out what factors have the biggest influence on both HSD and NHSD. Discover which properties of discontinuities have the significant influence on the class of hydraulic significant discontinuities. Third, create three-dimensional spatial or geometric models for HSD in the map sections of the CWF and FWF landfills. Use the resulting model to example the potential for interpreting hydraulic significant discontinuity network that will be considered to examine the potential for fluid flow within such possible networks.

CHAPTER II

SPATIAL ANALYSIS

2.0 Introduction to Spatial Analyses

There were many different types of discontinuities observed within the upper Cooper Canyon formation. These included bedding, bioturbation, desiccation cracks, as well as paleopedogenic features. “A large proportion of the discontinuities mapped and described are longer, variably undulatory surfaces that are associated with paleopedogenesis.”(Holt et al., 2011) Identifying the anisotropy for the discontinuity properties in CWF and FWF landfills is significant for a more complete characterization of the discontinuities, their origin and expected hydrologic impact. As a consequence, spatial analysis is conducted for all the discontinuity data. Describe and characterize the discontinuities for each genetic and geology unit in CWF and FWF landfills is necessary. Find out what factors have the biggest influence on both HSD and NHSD is meaningful. Through the spatial analysis, it is important to discover which properties of discontinuities have the significant influence for the specialty of hydraulic significant discontinuities.

In the analyses that follow, the observed discontinuities are considered as a whole and also in distinct subgroups to examine who discontinuities vary within and between such groups. These subgroup classifications include sets grouped by common geologic unit, by common

genetic unit, by vertical location within a genetic unit, and by orientation (near-vertical discontinuities vs other discontinuities).

In order to do the spatial analysis, some methodologies are import. First, stereo plots or hemispherical projections are prepared to consider the orientation of mapped discontinuities for each geologic unit and genetic unit in both CWF and FWF. The HSD and NHSD features are plotted using different symbols in some stereoplots to permit the consistency of orientation between these two classes of discontinuities. To facilities the spatial analysis, a vertical coordinates is needed for each discontinuity. This method reveals a significant sense for those different discontinuities. Second, the quantitative analysis is acted on the discontinuity properties. Those discontinuity characters are classified and analyzed by using statistic method. Third, the methods of geostatistics for analyses of discontinuity are used. It discovers the anisotropy for discontinuity properties by using variogram analysis and Kriging method. Kriging will be applied to some properties of discontinuity data. Furthermore, by using Kriging method, some discontinuity properties prediction maps for both CWF and FWF are conducted.

2.1 Data from Field Mapping

2.1.1 Resources

As Chapter I introduced, at this time, the WCS waste disposal facilities are in service, so no field work were conducted. So, the previously collected data obtained at the time of the excavation of the CWF and FWF are used. That work was fully described by Holt et al. (2011), but is summarized here to introduce the procedures used and the data obtained.

The results from discontinuity maps of 30 different vertical faces from the main basis of the data used in this investigation. The maps were prepared in the field at a scale of 1 in (0.025m)

equals 5 ft (4.5m), and they describe freshly exposed, near-vertical walls, each approximately 100 ft (30.48m) long, on both the east face and south face in the Southeast corner of each excavation. All discontinuities present in the field were mapped if they were longer than about 1 ft (Holt et al., 2011). With roughly excavation steps or stages of about equal depth, a vertical face was left intact and cleaned to permit discontinuity mapping. The vertical faces did not create a full coverage (there were some gaps between sampled depths) nor did the staggered faces constitute a single plan of mapping. In particular, consider the eastern walls of the CWF, where Figure 1.2 shows the exact location of each of the mapped faces. The composite view of the six levels mapped are shown in Figure 2.1, which is included here as an example. The composite view of all four faces is shown in Appendix A. On those maps, some discontinuities have characteristics indicated some hydraulic significance which have been highlighted in red on map layers. Furthermore, the geologic unit, genetic unit, as well as their descriptions is included in maps. Figure A-1 and A-2 in Appendix A are discontinuity maps for both east side and south side of CWF. Figure A-3 and A-4 in Appendix A are discontinuity maps for both east side and south side of FWF.

To supplement the mapping of the discontinuities, some descriptive information of each mapped discontinuity is included in Table A-1 through Table A-4 in Appendix A. The useful raw data contains fracture number, geologic unit, genetic unit, strike, dip, roughness, curvature, termination type, aperture and HSD sign. To facilitate this research, new variables are added to represent the horizontal and vertical coordinates of each end of every mapped discontinuity (digitized directly from the maps). From these end points, the coordinates of the midpoint of the line connecting the two points are used to represent the spatial location of each discontinuity. So this point used to locate the discontinuity might not directly fall on the discontinuity,

particularly in the case of a discontinuity with significant curvature. Finally, the two end points of each discontinuity are used to identify the separation distance, which is used in this research to represent the discontinuity length.

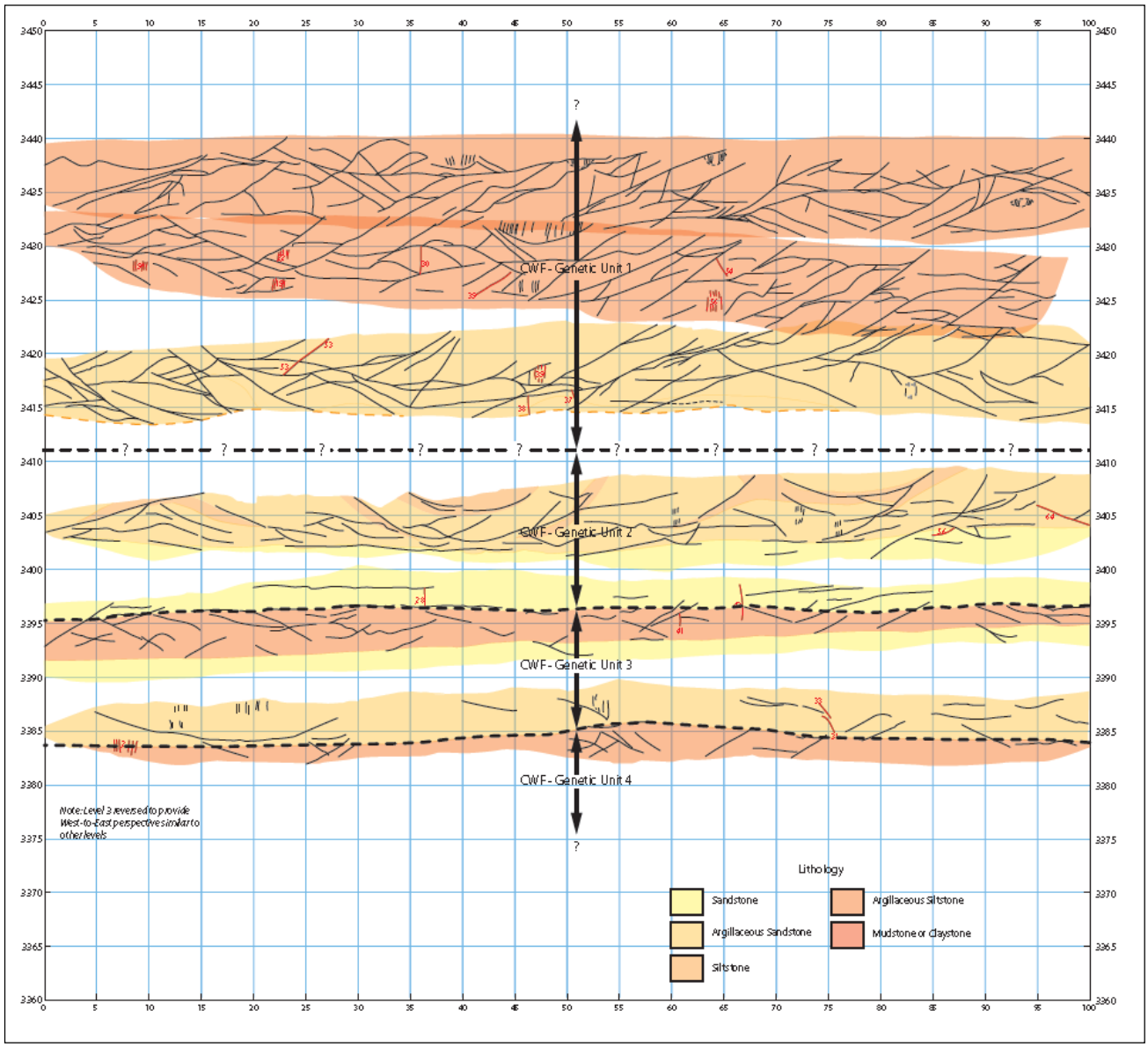

Figure 2.1 Vertical Composite of the Mapped Faces on the East Side of the CWF (Holt. et al., 2010)

Strike and dip were measured in the field using Brunton compasses set. The current magnetic declination was set to about 7.2 degrees east of true north. Roughness was estimated using scale of the size of the hand. The Range was set up from 1 to 5. 1 represented as smooth

like a plate of glass and 5 represented as rough and shard enough to be painful. Curvature was also estimated using s scale of 1 to 5. "The intersection of the discontinuity with the mapping surface would be nearly a straight line to be described by 1. An estimate of 5 indicates that the discontinuity curves through about 90 degrees" (Holt. et al., 2011). There are three termination types: AT, IN, OBS. AT means a termination "at" another discontinuity. In signified an upper termination with the rock. OBS indicates situations where the uppermost termination type is obscured and could not be determined. Aperture were measured based on evidence of pre-construction filling and aperture. The HSD are marked as number 1 and those HSD are recognized based on real HSD and potential HSD. The real HSD were recorded based on the stain which was taken as an indicator of possible vertical fluid movement, therefore designated the discontinuity as hydraulically significant during field work. The potential HSD were defined based on discontinuity dip angle, curvature and pedogenic alteration. The total number of real HSD in CWF is 75, and the total number of real HSD in FWF is 86. After classification and estimation, the total number of potential HSD in CWF is 120, and the total number of potential HSD is 132. With both real HSD and potential HSD data, HSD models become more conservative when the number of data is large than reality.

As Figure A-1 through Figure A-4 shown, the geologic unit and genetic unit are illustrated. For geologic unit, mudstone sequence shows varying degree of pedogenic alteration intercalated with thinner gray siltstone-sandstone zones. For siltstone-sandstone zones, it shows little pedogenic alteration and well-developed stratification consistent with bed form development and filled desiccation cracks (Holt. et al., 2011). As a consequence, five different geologic units are described and presented in both CWF and FWF. There are sandstone (Geologic Unit 1), argillaceous sandstone (Geologic Unit 2), siltstone (Geologic Unit 3),

argillaceous siltstone (Geologic Unit 4) and mudstone (Geologic Unit 5). All the different geologic units are presented in different color in Figure A-1 through Figure A-4.

Since there are related paleosol profiles, a series of genetically-related units were selected in both CWF and FWF. The genetically-related units in both CWF and FWF were also correlated and the origin units were also interpreted and discussed (Holt. et al., 2011). For the CWF, discontinuities are located in four Genetic Units on both the east face and south face which are 90 ft (27.432m) deep and 100 ft (30.48m) long. The FWF discontinuities are distributed across six Genetic Units on both the east face and south face. The horizontal span of the FWF mapped area is 100 ft (30.48m) that is essentially the same as the CWF mapped area, but the FWF excavations and maps extend approximately 20 ft (6.096m) deeper.

In CWF, it includes four different Genetic Units on both east side and south side. CWF Genetic Unit 1 (CGU-1) is greater than 25 ft (7.62 m) thick which contain poorly-sorted to well-sorted, argillaceous sandstone at base and upward to argillaceous siltstone and silt mudstone and finally to slightly-sandy mudstone. CWF Genetic Unit 2 (CGU-2) is least 15 ft (4.57m) which consists of very fine to medium, poorly-sorted sandstone at the base grading upward to argillaceous fine sandstone at the top. CWF Genetic Unit 3(CGU-3) is about 12 ft (3.66m) and it consists of argillaceous sandstone at the base and sandy mudstone at the top. CWF Genetic Unit 4 (CGU-4) is within unknown thickness. It contains sandy mudstone and argillaceous siltstone with a moderately well-developed pedogenic fabric and abundant slickensided surface (Holt. et al., 2011).

In FWF, it includes six different Genetic Units on both east side and south side. FWF Genetic Unit 1(FGU-1) has unknown original thickness due to upper contact of the Cooper Canyon erosion. It consists of sandy siltstone, intercalated with silty sandstone and the lower

contact is diffuse. FWF Genetic Unit 2(FGU-2) displays abundant slickensided surfaces. It consists of silty and sandy mudstone with well-developed pedogenic fabrics. The thickness is unknown due to unobserved lower contact. FWF Genetic Unit 3(FGU-3) is about 20 ft (6m) which contains argillaceous, silty sandstone at base and upward to sandy and silty mudstone. FWF Genetic Unit 4(FGU-4) is about 15 ft (4.57m) thick with argillaceous sandstone which displays abundant stratification. The sequence is mudstone overlying the sandstone and upward from siltstone to mudstone. FWF Genetic Unit 5(FGU-5) is about 13 ft (3.96m) and it consists of sandy siltstone and argillaceous sandstone and upward to mudstone. FWF Genetic Unit 6(FGU-6) is not discussed in this research and it consists of very fine silty sandstone that is moderately calcareous on west side of south face and north side of east face and weakly calcareous elsewhere (Holt. et al., 2011).

For CWF and FWF, there is a correction between them. Table 2.1 illustrates the general correction and notes for CWF and FWF. Except the uppermost genetic unit in the FWF, FGU-1, other remaining units in FWF shows good correlation with genetic unit in CWF. Based on this correction, the CWF genetic units and FWF genetic units are combined which shown in Table 2.1. The combined genetic units are named as CFGU-A, B, C, D, E, and F.

Table 2.1 Correlation between CWF and FWF Genetic Units (Holt. et al., 2011)

Combined Genetic Units	CWF Genetic Units	FWF Genetic Units	Notes
CFGU-A		FGU-1	Absent at the CWF
CFGU-B	CGU-1	FGU-2	Lower part has less clay in the CWF
CFGU-C	CGU-2	FGU-3	Lower part is laterally equivalent to the 80-Foot Zone; has less clay in the CWF
CFGU-D	CGU-3	FGU-4	Eastern part of the CWF is sandier
CFGU-E	CGU-4	FGU-5	Lower part unexcavated in CWF
CFGU-F	CGU-5	FGU-6	125-foot zone; not mapped in CWF

2.1.2 Data Processing

With all the raw discontinuity data and geologic and genetic units' information, the useful data id selected and processed. First, all maps with data are digitized using ArcGIS. Every discontinuity was digitized to have three coordinates including left point, middle point, and right point identified. ArcGIS and Excel are used. The first coordinate is the left most or starting point of the discontinuity and the second coordinate is the right most or end point of discontinuity. The third coordinate is calculated by averaging first coordinate and second coordinate. The calculated third coordinate indicates the center of main position of each discontinuity. Furthermore, the discontinuity linear length is estimated. Since there are both the left most point coordinate and the right most point of coordinate for each discontinuity, the linear length are estimated by

$$L = \sqrt{(X_2 - X_1)^2 + (Y_2 - Y_1)^2} \tag{2.1}$$

Where L is defined as estimated linear length for each discontinuity, X_2 and Y_2 are the left most or end point coordinates, X_1 and Y_1 are the right most or end point coordinates.

For both the CWF and FWF, the south face of discontinuities and east face of discontinuities in each genetic unit are combined in some of analyses completed to date. Depending on the correction between CWF and FWF genetic units, the data from CWF and FWF is also combined across the six genetic units. The results are illustrated in the Table 2.1.

2.2 Methodology of Spatial Analysis

2.2.1 Stereo plot-Hemispherical Projection

All discontinuities were identified, numbered, and mapped. Spatial analysis is not only conducted on CWF and FWF, but also conducted on combined Geologic Unit and Genetic Units across the CWF and FWF. In order to find out the regular patterns of discontinuity orientation,

the method used here is stereographic projection. “The stereographic projection simplifies graphical solutions to problems involving the relative orientations of planes in space” (Goodman, 1989). The discontinuity characteristics are analyzed by using this method. Software StereoStat are used to reveal the general patterns of discontinuities in geologic unit, genetic unit for both CWF and FWF. Stereoplots of poles not only measure the approximate plane of mapped discontinuities for each geologic unit and each new genetic unit in both CWF and FWF, but also the HSD and NHSD features are plotted using different symbols in some stereoplots. This method permits the consideration of more detailed analysis for HSD and NHSD and it facilitates the examination of the general patterns and differences that may exist between HSD and NHSD in different genetic and geologic units. Finally, the percentage of HSD and NHSD in each general pattern is also calculated to support the analysis.

Furthermore, the vertical coordinates also are added in stereoplots which show as “Y scale” to indicate whether each discontinuity belongs to upper part of a genetic unit or lower part of a genetic unit. This method only is applied on combined Genetic Unit. The Y scale is estimated by

$$Y_{SCALE} = Y_{mid} / Y_{\max} \tag{2.2}$$

where Y_{scale} is identified whether each discontinuity belongs to upper part of a genetic unit or lower part of a genetic unit, Y_{mid} is the vertical coordinates of each discontinuity. Y_{max} is the thickness of each genetic unit. With the coordinate data created in the early stages of this research for each discontinuity, the resulting vertical position within a genetic unit (known by the variable name “Y scale”) is established, so it is easy to identify whether a discontinuity is located in upper part or lower part of its respective genetic unit. If Y scale is smaller than 0.5,

it means this discontinuity is located in the lower part of a genetic unit. If Y scale is equal or larger than 0.5, it reveals this discontinuity falls in the upper part of its genetic unit. Stereoplots with the Y scale variable includes used a different color to look for different trends within the upper and lower parts of each genetic unit.

2.2.2 Geostatistics Analysis and Kriging

To examine spatial variations within the discontinuity data, it is useful to examine for trends and for Kriging a number of properties of the discontinuities. Kriging is an advanced geostatistical procedure which can generates an estimated surface from a scattered set of points with the variable of interest (there are several variables to be considered). For this research, geostatistics analysis (Ordinary Kriging) is conducted on five properties of each discontinuity data which are strike, dip, roughness, curvature, as well as length. Ordinary Kriging is the most general and widely used of Kriging method which assumes the constant mean is unknown. This is commonly taken as reasonable assumption unless there is a scientific reason to reject it (ESRI, 2013). Histograms of each properties of discontinuity are made to check whether the data is roughly consistent with a normal distribution. If the data does not accord with a normal distribution, it becomes necessary to make data transformations to find a variable space in which the transformed variable follows the normal distribution. Furthermore, the variable (or transformed variable) is assumed to be stationary when the distribution is invariant under translation. Meanwhile, the random function needs to be homogeneous so that the inference will be feasible (Boykova, 1998).

The first step for geostatistical analysis is making a structural analysis for original data to create a variagrom and an appropriate model that fits the observed data. In other words, it creates the variograms and covariance functions to estimate the statistical dependence (called spatial

autocorrelation) values that depend on the model of autocorrelation (fitting a model). (ESRI, 2013) Then, the prediction is applied by Kriging method (making a prediction). For first step, the function of varigram will be used to make analysis. The equation is defined as (Cressie 1993):

$$2\gamma(x, y) = \mathrm{var}\big(Z(x) - Z(y)\big) = E\Big(\big(Z(x) - \mu(x)\big) - \big(Z(y) - \mu(y)\big)^2\Big) \qquad (2.3)$$

where γ(x, y) is called the semivariogram, Z(x, y) is the spatial random field. The calculation of variograms and Kriging are very difficult so that the suitable software were used in process of data analyzing. For this research, the data are two-dimensional and the applied a software is GS+.

In this case, the directional variograms will be calculated for five properties of discontinuity which made by software GS+. Meanwhile, the semivariogram models will be applied to these variograms to find the best fitted variogram model. For variogram modeling, this research uses several different candidate model to find the best fit that includes linear variogram model, exponential variogram model, spherical variogram model, and Gaussian variogram model. As previously discussed, the semivariogram describes the spatial autocorrelation of the measured sample points. "Because of a basic principle of geography (things that are closer are more alike), measured points that are close will generally have a smaller difference squared than those farther apart. Once each pair of locations is plotted after being binned, a model is fit through them. Range, sill, and nugget are commonly used to describe these models" (ESRI, 2013). The common semivariogram models functions are defined as following equations.

The exponential variogram model:

$$r(h) = (s - n)(1 - \exp(-h/(ra))) + n1_{(0,\infty)}(h) \qquad (2.4)$$

The spherical variogram model:

$$r(h) = (s-n)((\frac{3h}{2r} - \frac{h^3}{2r^3})1_{(0,r)}(h) + 1_{[r,\infty)}(h)) + n1_{(0,\infty)}(h) \quad (2.5)$$

The Gaussian variogram model:

$$r(h) = (s-n)(1-\exp(-\frac{h^2}{r^2 a})) + n1_{(0,\infty)}(h) \quad (2.6)$$

where the parameter a had different values in different references, E.g. a= 1/3 is the value used in (Chiles and Delfiner 1999). The 1_A(h) function is 1 if $h \in A$ and 0 otherwise.

The variogram is made and calculated in GS+. For this research, directional variograms are calculated in different directions and use the ranges of multiple variograms to draw an ellipse of anisotropy. This step is well suited for these layered units for estimation. In this case, discontinuity properties show different autocorrelation structures in the vertical direction, however, the horizontal direction shows similar correlation. Anisotropic semivariogram models are developed to reflect vertical differences. The directional bands are specified by azimuthal direction and angular tolerance. After making the anisotropic variograms for the data, using GS+, the Kriging method is applied to make a precise interpolation between the points. Kriging is a good way to find the best linear unbiased estimator so that the estimated properties maps for discontinuity are obtained.

2.3 Results of Spatial Analysis

2.3.1 Stereoplots Analysis

Stereoplots of poles to the measured plane of mapped discontinuities are created. The preliminary finding reveals general patterns of abundant discontinuities that have shallow dip

(poles clustered around the center of the stereoplot) and near-vertical discontinuities (poles around the rim of the stereoplot). Composite stereoplots illustrates these two basic sets of discontinuities for both geologic unit and genetic unit in the CWF and FWF. For both geologic unit and genetic unit complete dataset, a dip of 70° has been proposed (Holt et al., 2011) and used here as the boundary for these two discontinuity sets. The observations on the east facing and south facing are combined. And poles to the plane are projected onto the lower hemisphere. The observations of the dip angles which are small and equal than 70° are shown as unfilled circle. The observations of the dip angles which are bigger than 70° are shown as filled circle. The red cross with filled circle and unfilled circle are shown as HSD. Frequency and proportions of HSD and all discontinuities are represented in two different dip angle (<= 70°, >70°) set. Figure 2.2shows the poles to discontinuities observed on the mapped faces of the whole CWF. Figure 2.3 shows the poles to discontinuities observed on the mapped faces of the FWF. Figure 2.4 shows all discontinuities mapped in both CWF and FWF for which a planer representation is valid. Appendix B includes a set of stereonet representation of poles to the planar feature observed in all separate geologic unit and combined genetic unit of the CWF and FWF. For both CWF and FWF, HSD are far outnumbered by NHSD. The stereonet plot of HSD in CWF and FWF are similar. "Although various combinations of lithology and sedimentary features are recorded and designated in the field, the units have basic common characteristics" (Holt. et al., 2011). To compare the HSD and NHSD to different geologic unit and genetic unit, the relationship of discontinuities to geologic and genetic unit have been compared in HSD frequency and distinguished on HSD and NHSD within stereoplots through Figure B-1 to Figure B-20 in Appendix B.

Table 2.2 contains frequency and proportions of HSD and all discontinuities by geologic unit and genetic unit. The percentage of HSD and NHSD is calculated for each data subset. The majority of HSD are part of the steeply dipping discontinuity set.

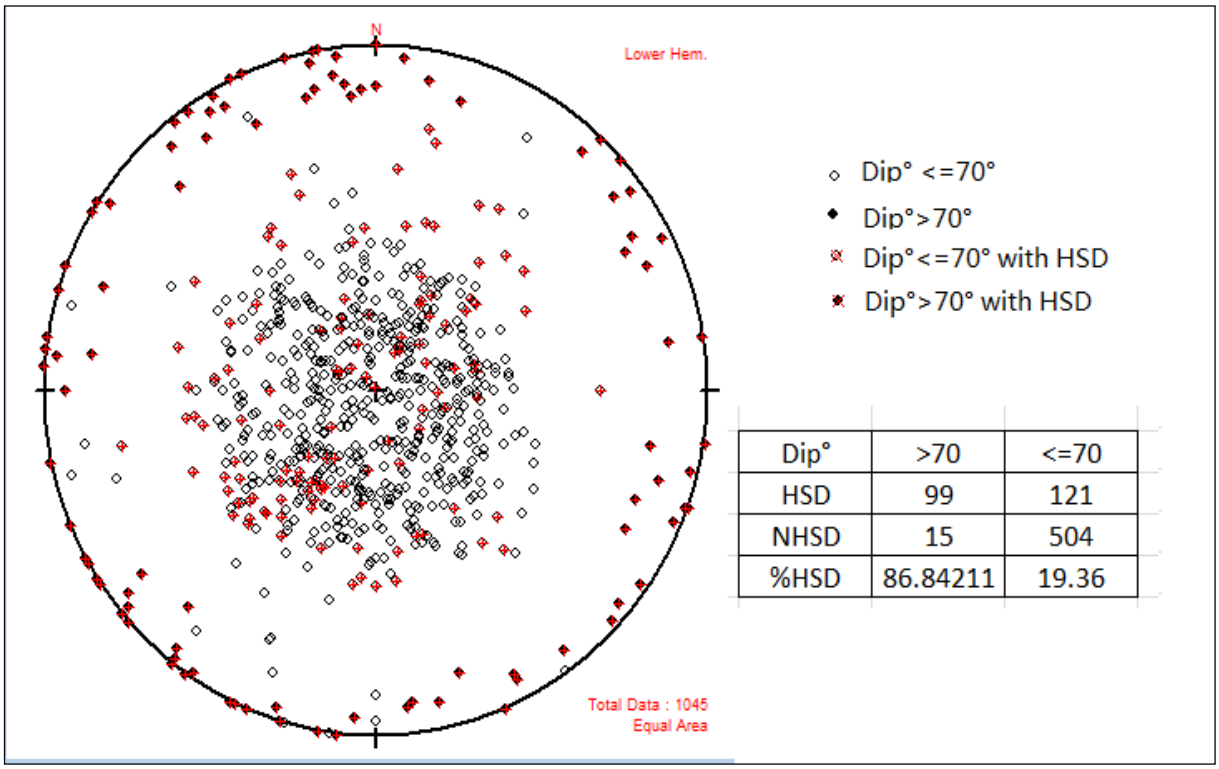

Dip°	>70	<=70
HSD	99	121
NHSD	15	504
%HSD	86.84211	19.36

Figure 2.2 Stereoplot of All Discontinuities Mapped in the CWF

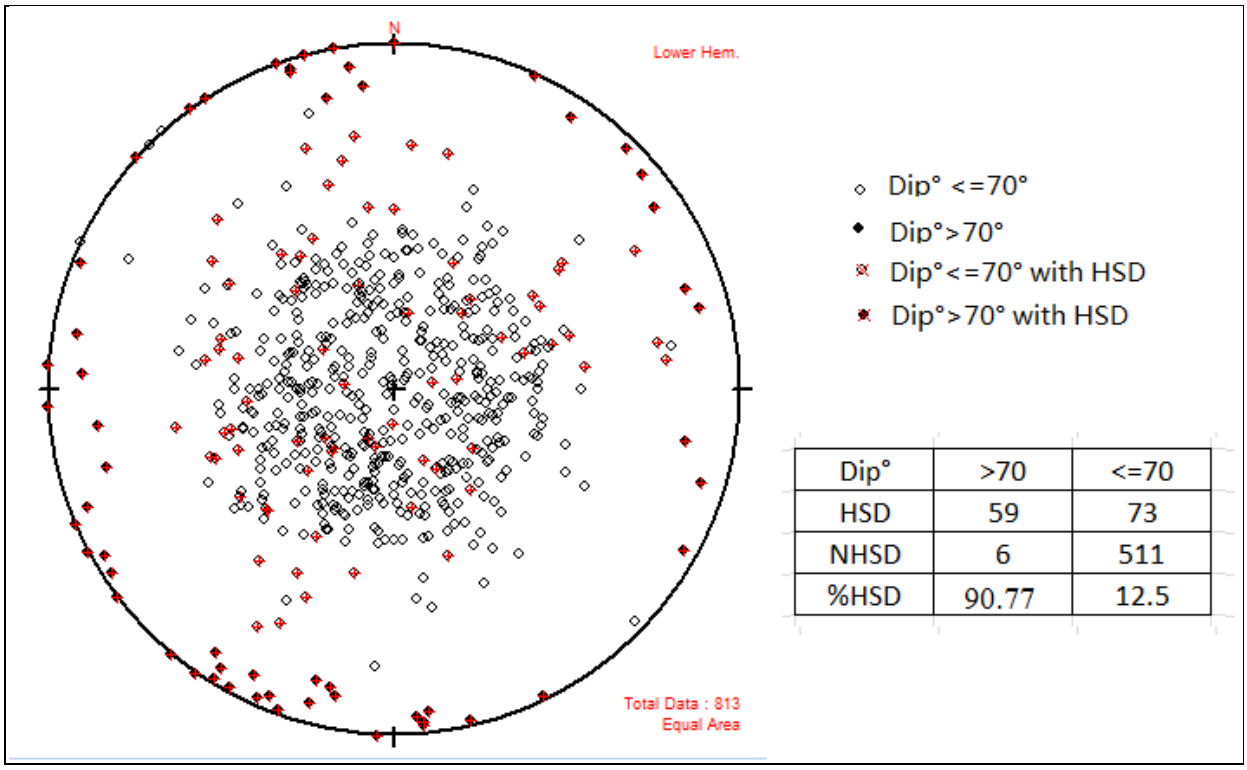

Dip°	>70	<=70
HSD	59	73
NHSD	6	511
%HSD	90.77	12.5

Figure 2.3 Stereoplot of All Discontinuities Mapped in the FWF

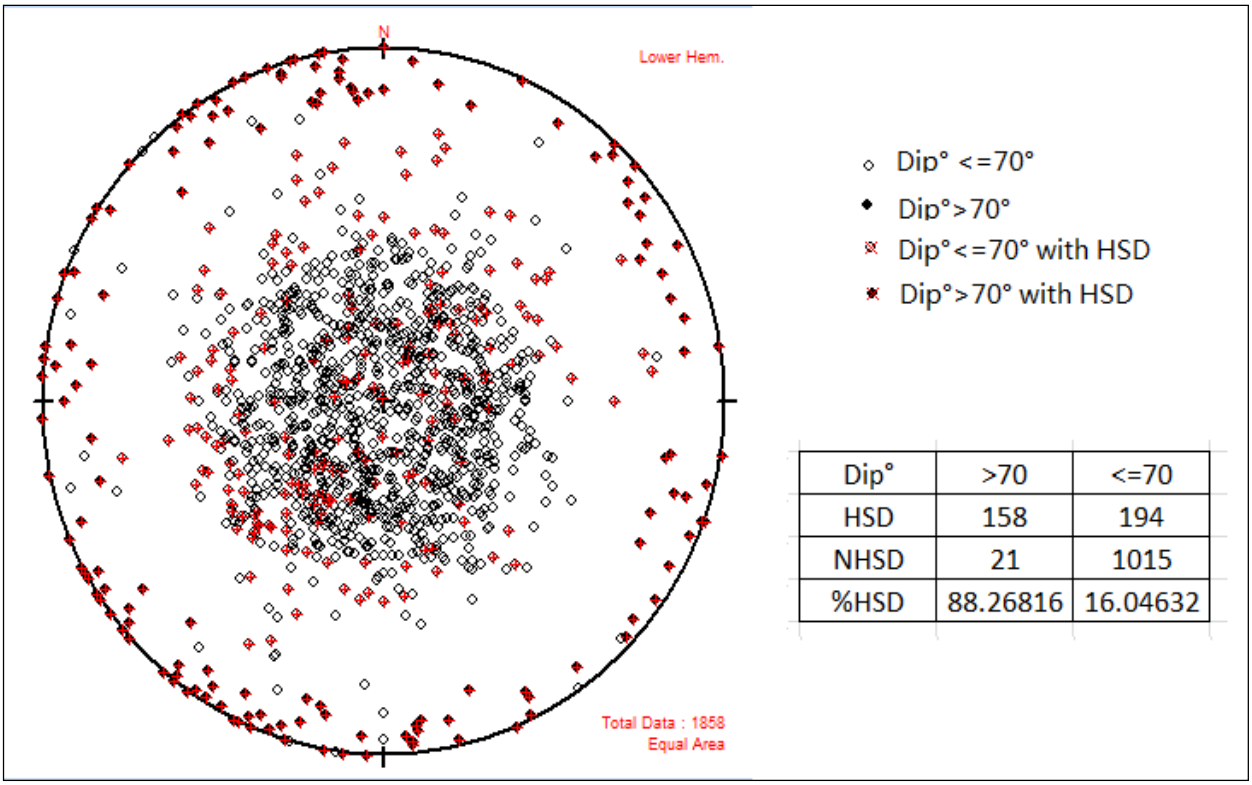

Dip°	>70	<=70
HSD	158	194
NHSD	21	1015
%HSD	88.26816	16.04632

Figure 2.4 Stereoplot of All Discontinuities Mapped in both CWF and FWF

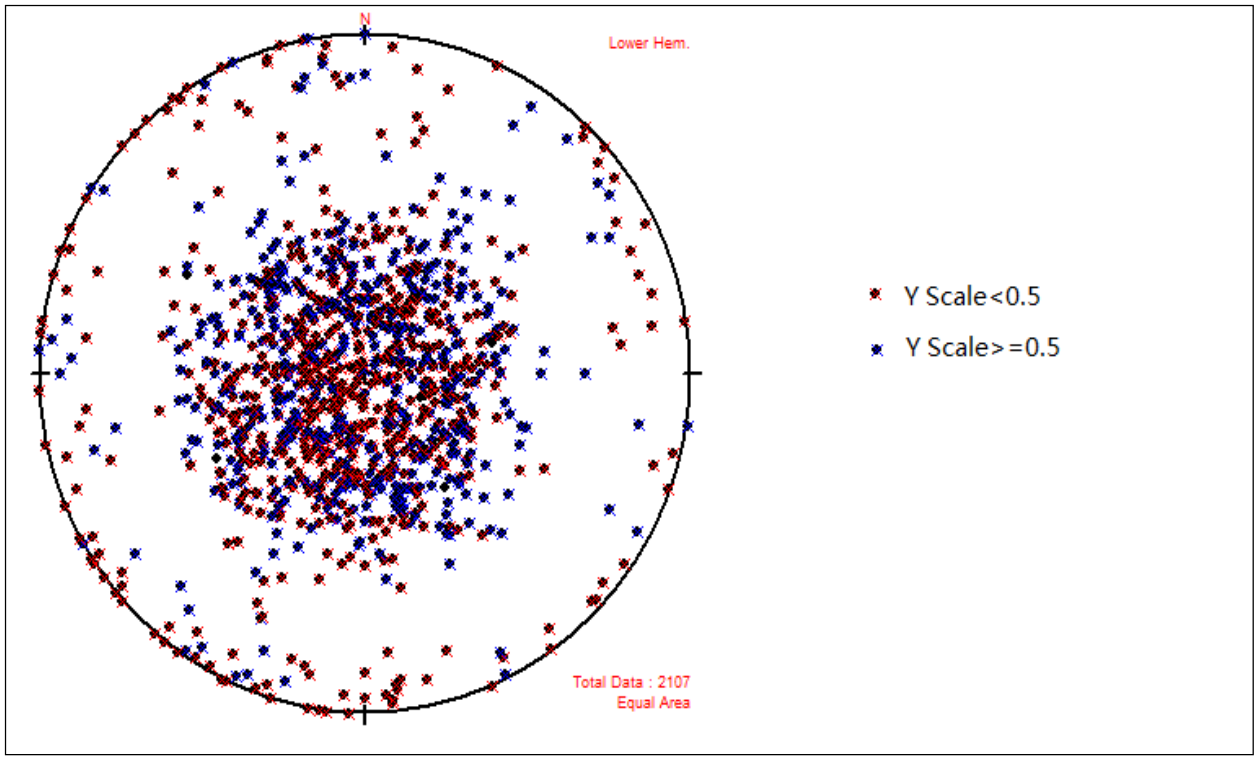

Figure 2.5 Stereoplot of All Discontinuities with Y_{scale} Mapped in both CWF and FWF

Table 2.2 Frequency and Proportions of HSD and All Discontinuities by Geologic Unit and Genetic Unit

Geologic Unit		Sandstone		Argillaceous Sandstone		Siltstone		Argillaceous Siltstone		Mudstone		ALL	
		Geologic Unit 1		Geologic Unit 2		Geologic Unit 3		Geologic Unit 4		Geologic Unit 5		ALL Geologic Unit	
	Dip	>70	<=70	>70	<=70	>70	<=70	>70	<=70	>70	<=70	>70	<=70
CWF	HSD	3.00	3.00	54.00	25.00	0.00	0.00	42.00	41.00	0.00	52.00	99.00	121.00
	NHSD	1.00	14.00	6.00	204.00	0.00	0.00	7.00	257.00	1.00	29.00	15.00	504.00
	%HSD	75.00	17.65	90.00	10.92	0.00	0.00	85.71	13.76	0.00	64.20	86.84	19.36
FWF	HSD	0.00	1.00	16.00	4.00	28.00	33.00	15.00	29.00	0.00	6.00	59.00	73.00
	NHSD	0.00	10.00	0.00	71.00	4.00	105.00	2.00	297.00	0.00	28.00	6.00	511.00
	%HSD	0.00	9.09	100.00	5.33	87.50	23.91	88.24	8.90	0.00	17.65	90.77	12.50
ALL	HSD	3.00	4.00	70.00	29.00	28.00	33.00	57.00	70.00	0.00	58.00	158.00	194.00
	NHSD	1.00	24.00	6.00	275.00	4.00	105.00	9.00	554.00	1.00	57.00	21.00	1015.00
	%HSD	75.00	14.29	92.11	9.54	87.50	23.91	86.36	11.22	0.00	50.43	88.27	16.05
Genetic Unit		FGU-1		CGU-1&FGU-2		CGU-2&FGU-3		CGU-3&FGU-4		CGU-4&FGU-5		CGU-5&FGU-6	
		Genetic Unit A		Genetic Unit B		Genetic Unit C		Genetic Unit D		Genetic Unit E		Genetic Unit F	
	Dip	>70	<=70	>70	<=70	>70	<=70	>70	<=70	>70	<=70	>70	<=70
ALL	HSD	18.00	20.00	82.00	59.00	44.00	25.00	14.00	32.00	1.00	22.00	12.00	0.00
	NHSD	2.00	38.00	16.00	444.00	2.00	220.00	0.00	219.00	0.00	138.00	0.00	0.00
	%HSD	90.00	34.48	83.67	11.73	95.65	10.20	100.00	12.75	100.00	13.75	100.00	0.00

For both CWF and FWF, the initial findings reveal almost the same number of discontinuities falls in the lower part and upper part of genetic units, however, during field observations, the discontinuities in the upper portion of a genetic unit appear more likely to be from the horizontal set than discontinuities in the lower portion of a genetic unit. Figure 2.5 shows almost the same number of discontinuities fall in the lower part and upper part of genetic units for the CWF and FWF. A filled circle with the red cross represents a Y_{scale} value smaller than 0.5 which means located in the lower part of genetic units. A filled circle with blue cross represents a Y_{scale} value larger or equal to 0.5, which means located in the upper part of genetic units. To test the Figure 2.5 results, each genetic unit is separated and analyzed. The results followed the field observation, which reveals there are more horizontal discontinuities in the upper portion of each genetic unit and more near-vertical discontinuities in the lower portion of each genetic unit. Table 2.3 represents the percentages of discontinuities in the lower part and the upper part of a genetic units dip angle smaller than 70° and larger or equal to 70°.

Table 2.3 Proportion of Discontinuity Distribution in Each Genetic Unit

	Dip <=70°		Dip >70°		ALL	
	Yscale< 0.5	Yscale>= 0.5	Yscale< 0.5	Yscale>= 0.5	Yscale< 0.5	Yscale>= 0.5
	Lower	Upper	Lower	Upper	Lower	Upper
CFGU-A	48	8	15	1	63	9
%	85.71	14.29	93.75	6.25	87.50	12.50
CFGU-B	257	215	68	28	325	243
%	54.45	45.55	70.83	29.17	57.22	42.78
CFGU-C	124	117	33	14	157	131
%	51.45	48.55	70.21	29.79	54.51	45.49
CFGU-D	73	175	13	4	86	179
%	29.44	70.56	76.47	23.53	32.45	67.55
CFGU-E	73	87	0	1	73	88
%	45.63	54.38	0.00	100.00	45.34	54.66
CFGU-F	0	0	11	1	11	1
%	0	0	91.67	8.33	91.67	8.33
Total	575	602	129	60	704	662
%	48.85	51.15	68.25	31.75	51.54	48.46

2.3.2 Geostatistics Analysis and Kriging Maps

For initial input data, first, the histograms are made to exam how these discontinuity properties are distributed. The histogram of Length is shown in Figure 2.6, which is included here as an example. In Appendix C, Figure C-1 to Figure C-5 illustrates all histograms of discontinuity properties. The CWF and FWF reveal consistency, supporting a view that discontinuity conditions are stationary across that range. To find out what factors have the biggest influence on both HSD and NHSD, the mean and standard deviation of each property for HSD and NHSD are calculated. Table 2.4 represents the calculation results. To realize the Kriging analysis, some histogram of properties which do not fit a normal distribution are transformed and also listed in appendix C Figure C-1 to Figure C-5. Figure 2.6 also shows an example of the transformation for Length.

Table 2.4 Statistical Calculation of Each Property for CWF and FWF

		Strike		Dip		Curvature		Roughness		Length	
		Mean	Std Dev	Mean	Std Dev	Mean	Std Dev	Mean	Std Dev	Mean	Std Dev
CWF	HSD	191.09	134	63.49	24.97	2.09	0.68	2.61	0.67	3.34	2.89
	NHSD	179.97	135.15	26.33	14.01	2.43	0.69	2.61	0.65	5.7	4.33
FWF	HSD	206.71	130.74	59.69	25.58	2.24	0.64	2.43	0.63	3.96	3.76
	NHSD	174.05	137.53	27.59	12.4	2.57	0.71	2.52	0.51	6	3.87
CWF &FWF	HSD	197.61	132.66	61.89	25.26	2.16	0.67	2.53	0.66	3.6	3.29
	NHSD	177.19	136.24	27.38	13.7	2.5	0.7	2.56	0.59	5.85	4.12

To realize the Kriging prediction map, some data that does not fit a normal distribution must be transformed. GS+ is the software used here for Kriging analysis. The first step is to input all discontinuity data with their coordinates. Then, using transformation methods, the user must make the variances more constant throughout the sampled area and the transformed data to become more consistent with the normal distribution. In this research, the Log transformation method is used for strike, dip and length, while roughness and curvature are not transformed. Next, the directional variogram analyses are made.

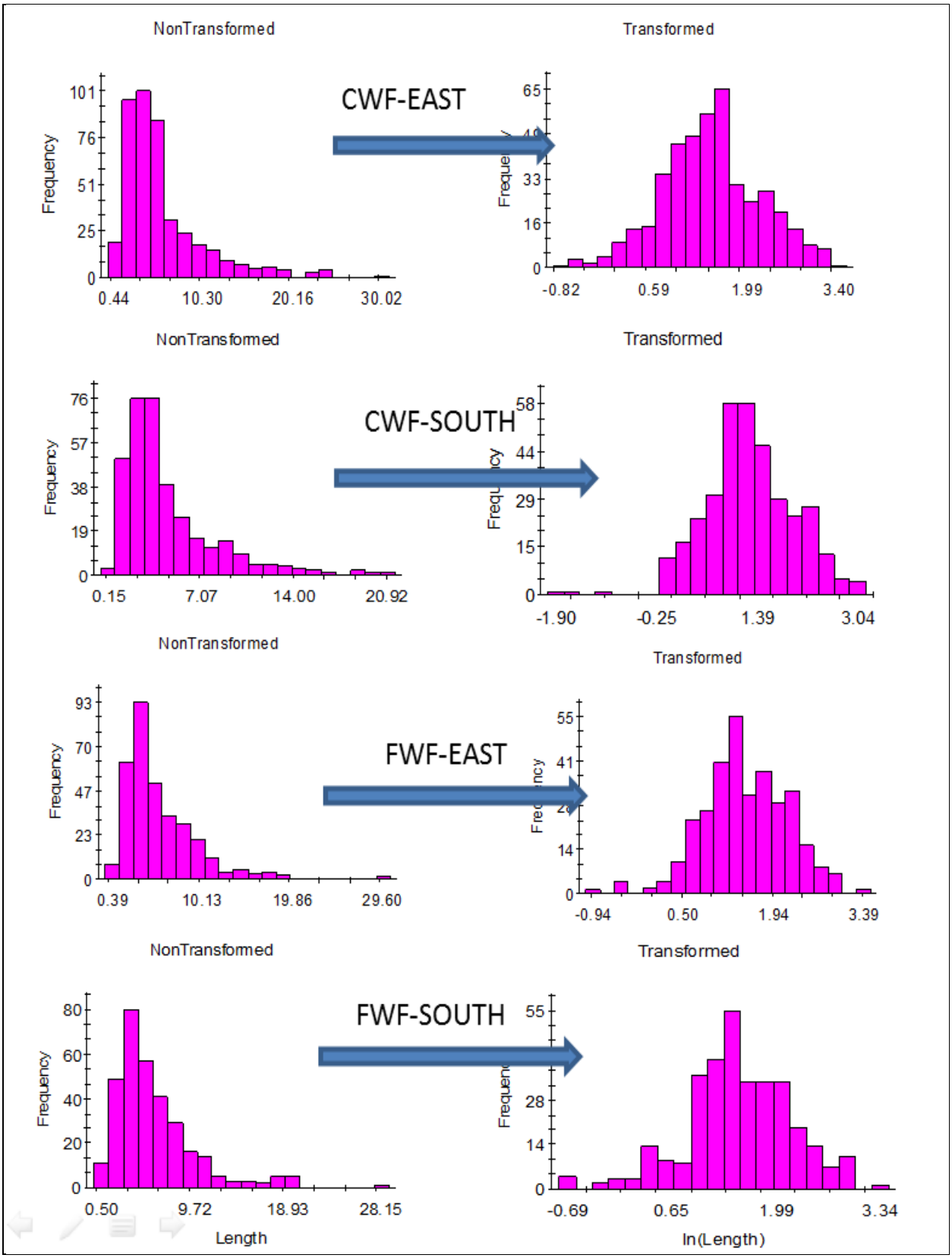

Figure 2.6 Histogram of Discontinuity Length for CWF and FWF

The different variograms are fitted by different models, with the user selecting the model that best fits each dataset. After making the variogram model for those data, it is possible to estimate every point from the initial data by using the points around it. The Kriging type used here is ordinary and all prediction maps are made as anisotropy maps. All fitted models are illustrated through Figure C-6 to Figure-10 in Appendix C. Figure 2.7 is shown as an example here which illustrates the semivariograms and best fitted model for Roughness. Table 2.5 includes all model parameters for the CWF and FWF, and it indicates the nugget effect accounts for most of the variability for strike data in the east face and the south face of the CWF and FWF. On the contrary, the reduced significance of the nugget effect is evident in other properties for both the east face and the south face of the CWF and FWF. For dip angle, length, curvature and roughness, the nugget effects are smaller than it is for strike which means the data are well structured. The possible reason for the large nugget effect for strike is the data does not seem to fit a normal distribution, even after transformation. In general, the nugget effects for all other data are small and acceptable.

To get the final prediction map of discontinuity properties, Kriging is applied for the CWF and FWF for both east faces and south faces. For CWF, the size of Kriging area is about 100 ft (30.48m) ×65 ft (19.812m). For FWF, the size of Kriging area is about 100 ft (30.48m) ×80 ft (24.284m). The maps were made by using GS+. Finally, the estimation maps for east side and south side are obtained which shown through Figure C- 6 to Figure C-10 in Appendix C. Figure 2.8 is shown as an example of estimation maps for roughness.

Table 2.5 Parameters for Variogram Models of Each Property in CWF and FWF

Location	Property	Varigram Nugget Effect	Transformation Type	Model Type	Range Minor	Range Major	Anisotropy	Sill
CWF-EAST	Strike	1.135	Log	Linear	218.200	218.300	Ture	2.692
	Dip	0.269	Log	Exponential	260.945	443.870	Ture	0.798
	Curvature	0.406	No	Spherical	3.820	3.821	Ture	0.546
	Roughness	0.331	No	Gaussian	6.175	6.175	Ture	0.454
	Length	0.542	Log	Linear	948.000	1656.000	Ture	1.210
CWF-South	Strike	1.610	Log	Linear	430.700	641.600	Ture	3.698
	Dip	0.395	Log	Gaussian	11.414	28.081	Ture	0.642
	Curvature	0.352	No	Linear	78.261	85.271	Ture	0.640
	Roughness	0.318	No	Gaussian	66.820	130.816	Ture	0.642
	Length	0.519	Log	Linear	721.400	931.900	Ture	1.193
FWF-EAST	Strike	1.441	Log	Linear	4524.000	6209.000	Ture	3.072
	Dip	0.256	Log	Linear	240.000	240.100	Ture	0.635
	Curvature	0.377	No	Linear	436.200	436.200	Ture	0.892
	Roughness	0.185	No	Spherical	11.152	11.152	Ture	0.273
	Length	0.410	Log	Linear	452.300	452.300	Ture	0.950
FWF-South	Strike	1.202	Log	Spherical	12.476	15.507	Ture	1.624
	Dip	0.404	Log	Linear	667.600	878.500	Ture	0.981
	Curvature	0.514	No	Linear	443.800	443.800	Ture	1.193
	Roughness	0.197	No	Gaussian	6.210	13.800	Ture	0.274
	Length	0.326	Log	Spherical	11.651	13.873	Ture	0.460

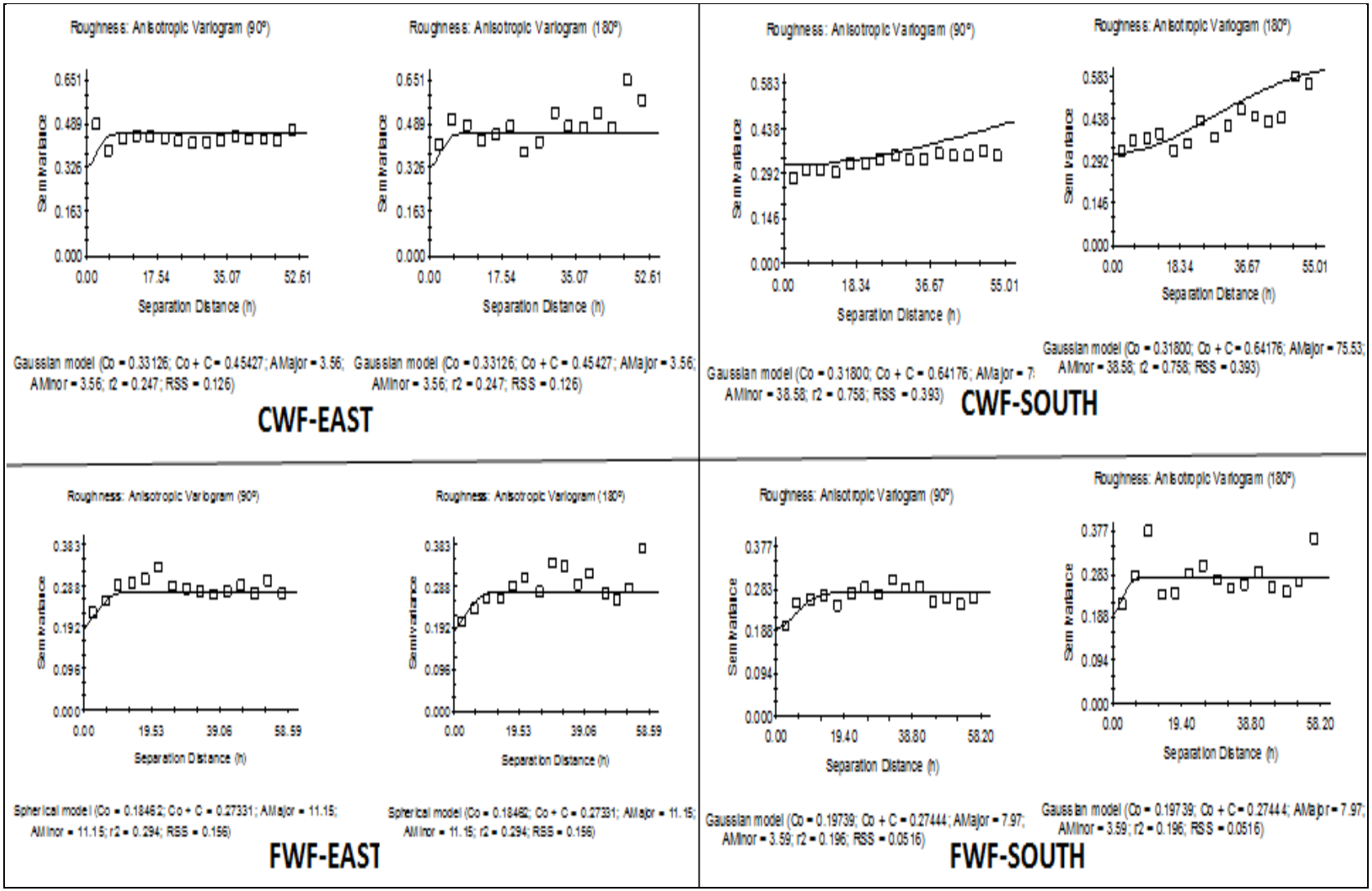

Figure 2.7 Fitted Variogram Models of Roughness for CWF and FWF

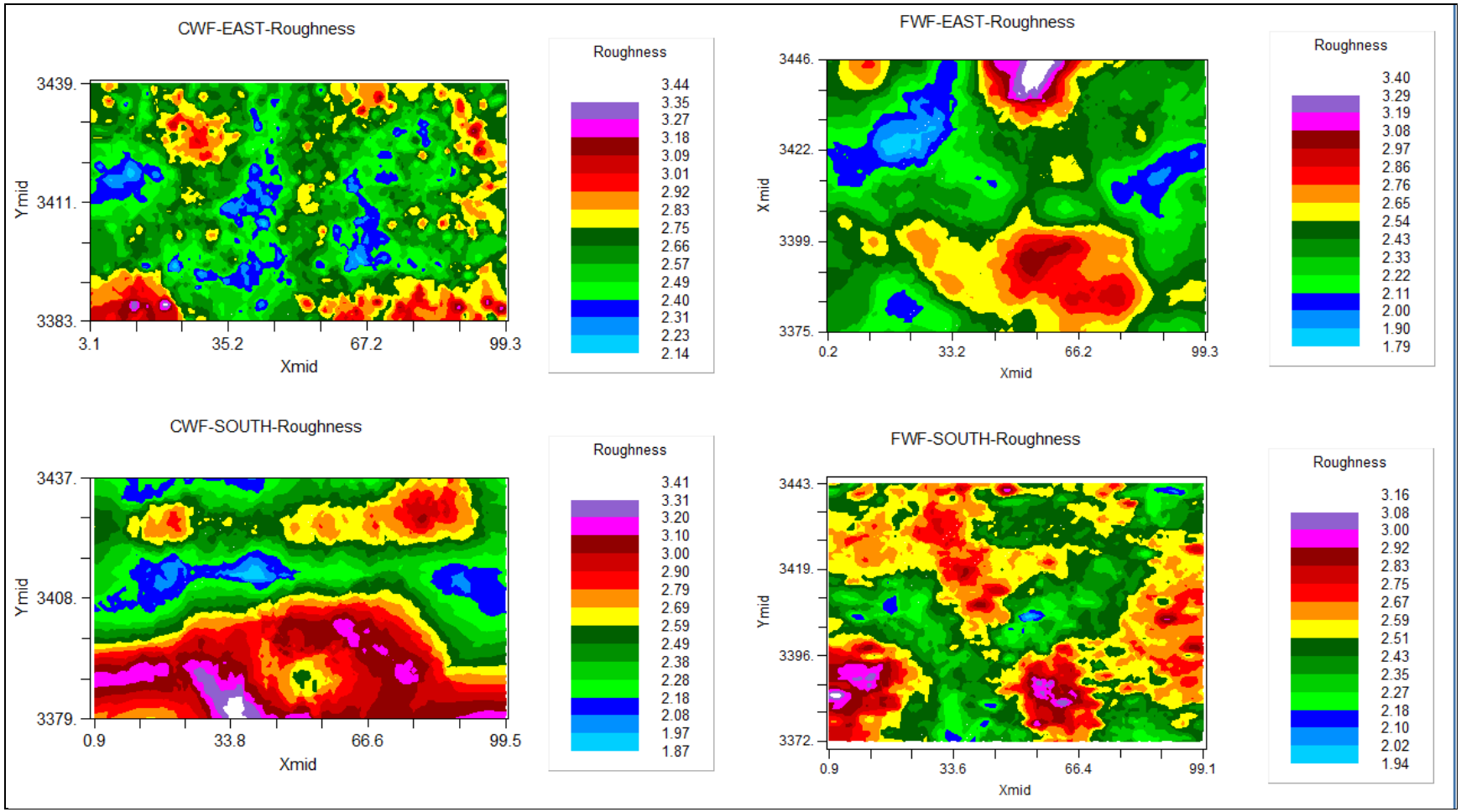

Figure 2.8 Kriging Prediction Maps of Roughness for CWF and FWF

CHAPTER III

THREE-DIMENSIONAL MODEL

3.0 Introduction of Three-Dimensional Model

Three-dimensional model is made here that can perform a good and comprehensive view for HSD. It provides a good understand and view for the CWF and FWF landfills. Furthermore, it helps to estimate if HSDs will affect the functionality of landfills. The three-dimensional models are created after statistical analysis of each discontinuity property. DFNModeler is applied to realize the three-dimensional model and compartmentalization analysis. Maximum volume for potential interconnectivity fracture network is calculated.

3.1 Background and Methodology

The consideration of potential for networks of HSD is the most significant aspect of this research, so building a three-dimensional model for those HSDs helps to discover the potential for any networks of HSDs that must be considered to examine the potential for fluid flow within such possible networks. The HSDs were defined in Chapter II, but it is worth reiterating that they included observed HSDs and potential HSDs for a conservative view of these potential pathways. “The field evidence is the basis for considering any particular discontinuity as hydraulically significant” (Holt. et al., 2011). The stain observed is taken as an indicator of possible vertical fluid movement and therefore designates the discontinuity as hydraulically significant. The HSD

data have the similar distribution to the distribution of all discontinuities. The total data set is also divided between those discontinuities with dips less than 70 ºand those with a dip greater than 70 º(Holt. et al., 2011). This result is the basis for dividing the discontinuities data into different fracture sets, with these two sets having distinctly different properties in the subsequent simulations.

To realize the three-dimensional model for those HSDs, an appropriate simulation software is selected DFNModeler (Pashin et al., 2008). "DFNModeler is a Windows application is designed for modeling discrete fracture network. The software has integrated fracture data input, generation of discrete fracture network, compartment and fluid migration pathway analysis, and visualization" (Jin and Pashin, 2007). Discrete fracture networks (DFN) are stochastic models of fracture architecture. This software are based on the statistical scaling properties of natural and induced fracture systems, and flow modeling in fractured media (Pashin et al. 2008). It includes statistical scaling rules derived from analysis of fracture length, height, spacing, orientation, and aperture. This software was developed to assess the potential risks associated with carbon sequestration in coal. The discrete fracture network (DFN) Modeling is created for risk assessment and it is used to assess risks in the Black Warrior Basin of Alabama, where coal bearing strata have high potential for carbon sequestration and enhanced coalbed methane recovery. One particularly valuable feature of DFNModelers is that it has the ability to generate and simulate discontinuities by conducting transmissivity analysis and compartmentalization analysis. The three-dimensional modeling is created that resemble the mapped discontinuities as closely as possible (Pashin et al. 2008). DFNModelers is the main software used for this modeling.

"DFNModeler software was written using Visual C++ programming language and includes an OpenGL visualization engine" (Pashin et al., 2008). It has five major functions. First, it enables input and editing of model data. Second it can generate the discrete fracture networks. Third it conducts the analysis to identify networks of connected fractures which are considered compartment hulls (this analysis being called compartmentalization) Such compartment hulls are potential fluid migration pathways, which are dominant in the case of geologic units of naturally low hydraulic conductivity. Fourth, the results can be visualized for interactive on a PC. Finally, DFN can be used to export model data and results. A brief technical overview and logic behind the DFNModeler is introduced as follow. Figure 3.1 illustrates the software modular architecture.

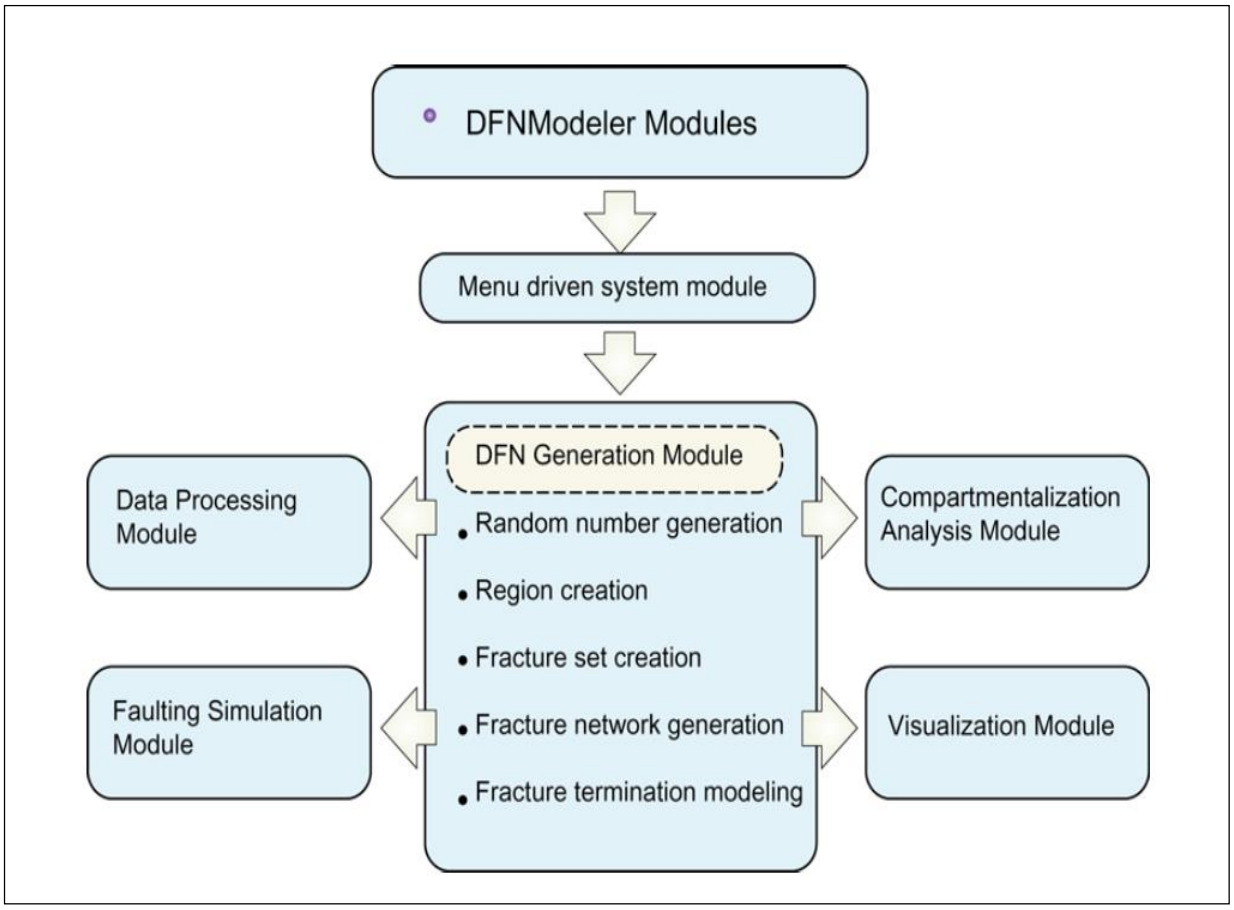

Figure 3.1 Diagram Showing Modular Architecture of DFNModeler Software (Pashin et al., 2008)

To realize the three-dimensional model of fracture network, the first step is defining regions for the whole simulation area. This action also is referred to as a fracture region. The fracture regions conceptually represent physical rock units with homogeneous discontinuity properties and consistent fracture abundance or clusters and they improve the realistic of the fracture generation in terms of computational geometry (Pashin et al., 2008). In general, each fracture region represents one physical geologic unit or lithologic unit. There are two different fracture regions types introduced in this software. One is a rectangular box which commonly represents a lithologic unit. The other one is a slab region that is used to represent a dipping rock formation or an inclined fracture zone. With the condition of this research, all fracture regions are defined using rectangular box fracture type. In each DFNModeler, each fracture region can includes multiple fracture sets.

After defining each fracture region, fracture sets can be established. A fracture set represents a group of fractures that have similar spatial properties. Fracture sets need to be different from one another by the fracture region in which they occur, orientation and geologic origin. "If any one of the above three factors is different, they should be included in different fracture sets" (Pashin et al., 2008). During this process, some geometric properties of a fracture set are defined which includes fracture set orientation, length, height, aperture, spacing and the frequency with which fractures terminate at pre-existing structures (i.e., cross-cutting relationships). Once the fracture regions and fracture sets are built, each fracture set can be assigned to fracture region and each fracture set can be mapped into a specific region to generate fractures based on that set's statistical properties. It is worth noting that a fracture set can only be assigned to one fracture region, whereas a fracture region can contain multiple fracture sets. In DFNModeler, the fractures are generated based on statistical distributions derived from fields.

For example, each fracture property is generated by statistical distribution which contains uniform, normal, log-normal, exponential, and Fisher distributions (Pashin et al., 2008). “The Fisher distribution was implemented specifically for directional data used for fracture orientations in DFNModeler (Ulrich, 1984; Wood, 1994). All other distributions were used for scalar data, such as the dimensions of fractures” (Pashin et al., 2008).

Once the fracture regions and fracture sets are defined, the DFN models are generated. The hierarchical algorithm is used to generate fracture to ensure the efficiency and speed. In DFNModeler, each fracture is represented as a polygon, which in turn is represented by an array of directed vertices (Pashin et al., 2008). Since there are no faults observed in research area, there is no faults present in the rock mass simulations.

The next step is the key function in DFNModeler which is called compartmentalization analysis. It is used to characterize the interconnectivity of fracture networks. This analysis process can determine if fractures intersect and how many fractures are interconnected to form a compartment. “A fracture compartment is defined as a convex polyhedron, or hull, that connects all vertices of intersecting fractures” (Pashin et al., 2008).

The compartment size is defined by the fracture networks network geometry. According to compartmentalization analysis documentation, DFNModel can first identify individual fracture networks and compute the bounding surface for each identified network. Then, the volume with the bounding surface and the horizontal extent of the network are calculated (Pointe at al., 1997). The generally action would be possible to compute the “bounding box” and the box volume and horizontal cross-section are used to surrogate compartment or rock mass volume and horizontal extent. However, this would lead to an overestimation in most cases of both volume and cross-section of the rock mass affected by the fracture network in question. In order to

reduce the potential for overestimates, DFNModeler calculates a bounding surface use convex hull. This convex is essentially a bounding surface with certain advantageous mathematical properties (Pointe at al., 1997). “For points with three-dimensional spatial coordinates, the convex hull is a convex polyhedron, which has the minimum volume of all possible convex polyhedra that bound the point set” (Pointe at al., 1997). Figure 3.2 shows a three-dimensional convex hull calculated using the QuickHull algorithm.

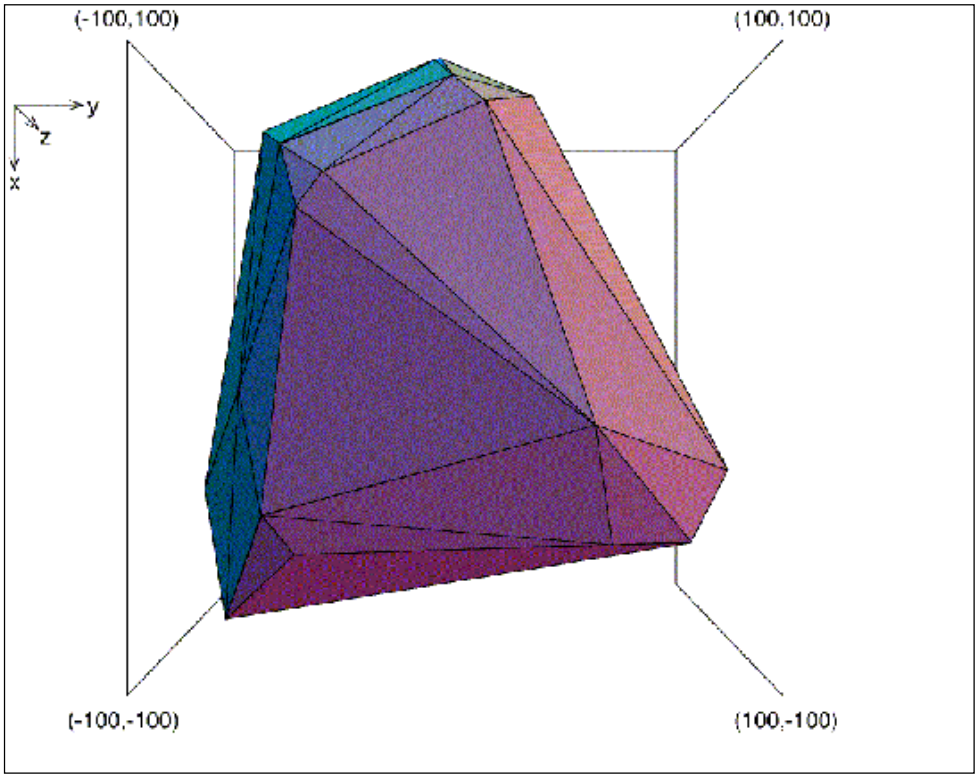

Figure 3.2 Convex Hull of Fracture Network (Pointe at al., 1997)

This compartment hull can represent how much rock mass may be potentially affected by this network of discontinuities are connected to have fluid flow ability. In other words, these compartment hulls boundaries define effective no-flow boundaries and all fractures with vertices forming the hull are in hydraulic communication (Pashin et al., 2008). Figure 3.3 shows an example of compartmentalization model. The colored polyhedral surrounding facture polygons are compartment hulls. It is worth noting, that compartment hulls can cross boundaries between

model regions or between simulated layers. This software also can define a well path and identify the flow pathway. However, in this research no well is built and the potential of fluid flow ability have already illustrated the objective of this research. As a result, the pathway analysis will not be performed. Instead, the size, number, and abundance of compartment hulls are used to describe the potential for the scale over which fluids might be readily transmitted in the modeled rock masses.

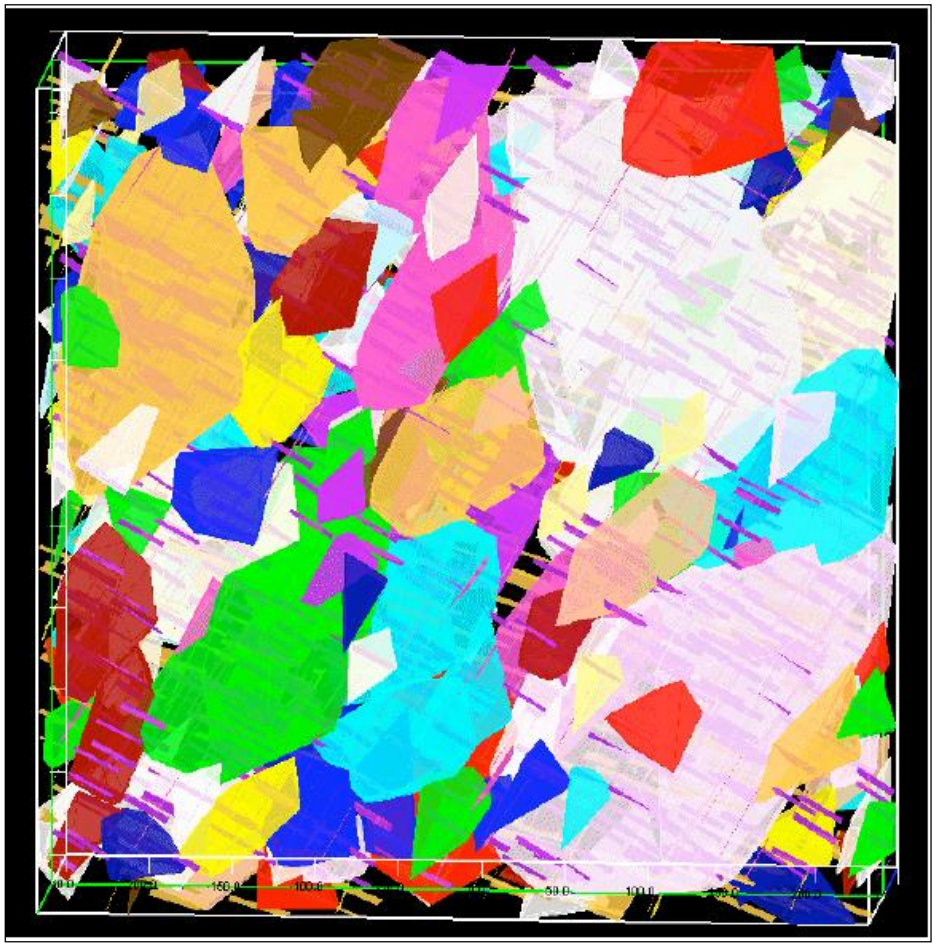

Figure 3.3 Compartmentalization Model Example Based on the DFN model (Pashin et al., 2008)

In this research, the first step begins with an analysis of the geology and statistical properties of the fracture networks that refer in particular to HSDs that form the basis of the DFN models. Then, the compartmentalization analysis is conducted to examine the potential for fluid

flow within such possible networks (HSD). The rock mass modeled in these three-dimensional simulations is not only built on the scale of the mapped or sampled window, but all simulations presented also are extended to the approximate size of the longest boundary of the CWF or FWF.

3.2 Application of DFNModeler

3.2.1 Fracture Networks-Hydraulically Significant Discontinuities (HSD)

The three-dimensional model is focus on Hydraulically Significant Discontinuities that were observed in the field, as these are considered to be the most likely possible pathway for fluid flow. As Chapter II indicated, the HSDs consist of confirmed HSDs and potential HSDs. The HSDs were mapped and identified for both CWF and FWF in the observation sample window. Those HSDs, or a statistical description of those HSD, are the main input data for the simulation. In those observation windows, there were no folds and faults exposed. The only geologic structures which may has significant impact on the possible vertical fluid movement are those Hydraulically Significant Discontinuities. Those discontinuities are distributed in different geologic units and they are separately characterized with a different statistical description within each geologic unit. Based on orientation, there are the two different fracture sets within each unit, as previously described.

The properties of each fracture set are characterized separately, considering orientation, termination, number of factures, fracture width, and fracture height (length). Furthermore, the hydraulic properties of the fractures themselves (not the rock material) are supplied to DFNModeler, which including aperture, transmissivity and storativity. Since a hydraulic analysis was not completed in this work, the values entered did not affect the results. Since the facture spacing function is not activated in this version, number of fracture is the only way to generate

the fractures. Furthermore, there are no faults and folds observed in the research area, so shear factures were not included in the model.

3.2.2 DFN Models

3.2.2.1 CWF and FWF Discontinuity Observation Windows

To build models in DFNModeler, the first step is assigning Fracture Regions. Fracture Regions are defined based on physical geologic units. For the CWF sampled window, there are six regions. The classification method is based on sequence and geologic unit of stratigraphic distribution.

The geologic units are defined within the CWF-Region as A, B, C, D, E, and F from top to bottom. Region A is 20 ft (6.096m) thick, 100 ft (30.48m) long and 100 (30.48m) ft wide. The elevation for Region A is assigned from 0 ft (0m) to -20 ft (6.096m). And the geologic unit for Region A is argillaceous siltstone. Region B is defined follow Region A. It is 18ft (5.4864m) thick, 100 ft (30.48m) long and 100 (30.48m) ft wide. The elevation is from -20 ft (-6.096m) to -38 ft (-11.58m).

The geologic unit is argillaceous sandstone. Region C is composited as sandstone which has 17ft (5.1816m) thickness, 100 ft (30.48m) long and 100 ft (30.48m) wide. The elevation is from -38 ft (-11.58m) to -55 ft (-16.764m). Region D is intercalated with region C and it is composited as mudstone. The thickness is 9 ft (2.7432) and it is also 100 ft (30.48m) long and 100 ft (30.48m) wide. Elevation is from -45ft (-3.716m) to -54ft (-16.4592m). Region E and F are both 5 ft (1.524m) thick and they are made by argillaceous sandstone and argillaceous siltstone, respectively. They are 100 ft (30.48m) long and 100 ft (30.48m) wide. The elevations are -55 ft (-16.764m) to -60 ft (20.1168m) and -60 ft (18.288m) to -65 ft (19.812m). The size of

the CWF observation window is 100 ft (30.48m) by 100 ft (30.48m) with a thickness of 65 ft (19.812m).

For the FWF sampled window, ten regions are defined based on different geologic unit. They are named as FWF-Regions A, B, C, D, E, F, G, H, I, and J. Ten different regions are arranged in turn from the top to bottom. The sequence is 10 ft (3.084 m) siltstone, 5 ft (1.524 m) argillaceous siltstone, 10 ft (3.084 m) siltstone, 10 ft (3.084 m) argillaceous siltstone, 10 ft (3.084 m) argillaceous sandstone, 15 ft (4.572 m) argillaceous siltstone, 2 ft (0.6096 m) sandstone, 3 ft (0.9144 m) mudstone, 5 ft (1.524 m) argillaceous siltstone and 5 ft (1.524 m) argillaceous sandstone. Each region is 100 ft (30.48m) long and 100 ft (30.48m) wide, excluding Region H and Region J. According to the discontinuity maps, region H (mudstone) is about 100 ft (30.48m) long but only 60 ft (18.288 m) wide. And Region J (argillaceous sand stone) is about 100 ft (30.48m) long and 45 ft (13.716m) wide. The mid elevations for each region are 5 ft (1.524 m), 12.5 ft (3.81m), 25 ft (7.62m), 35 ft (10.668m), 45 ft (13.716m), 57.5 ft (17.526m), 66 ft (20.1168m), 68.5 ft (20.8788m), 72.5 ft (22.098m), and 75.5 ft (23.0124m). The size of the FWF observation window is 100 ft (30.48m) by 100 ft (30.48m) with a thickness of 80 ft (24.384 m).

After defining the fracture regions for CWF and FWF, the fracture sets are assigned in each region. For each fracture region, there are two different fracture sets named as SET 1 and SET 2 based on the orientation. As Chapter II revealed, the HSD can be divided into two fracture sets, those with a dip angle is small than 70 °and those with a dip angle greater or equal to 70 °. For fracture set orientation, DFNModeler allows the user to assign fracture distribution as either uniform distribution or Fisher (normal) distribution. Fracture set properties' histograms were created and the best fit distribution of histograms is identified. Each fracture set orientation is

described using the Fisher distribution model; using parameters obtained from the mapped HSDs. Figures D-1 through Figure D-17 in Appendix D illustrate all the input fracture set properties' histograms. Table 3.1 contains a summary of each fracture set for the CWF. Table 3.2 contains a summary of each fracture set for the FWF. As the sets were modeled with the Fisher distribution, the concentration parameter (K_1) needs to be calculated and entered. For the research area, every fracture set is assigned as Fisher distribution. Table 3.1 and Table 3.2 contain the K_1 value for each fracture set in CWF and FWF. The Fisher dispersion parameter K_1 is generally found from the equation

$$K_1 = \frac{N_F}{N_F - |R|} \tag{3.1}$$

where $|R|$ is the magnitude of the vector sum of the unit vectors for orientation, and N_F is the number of fractures. *K* becomes very large as the dispersion of joint orientations becomes small (Goodman, 1989).

Table 3.1 Summarization of Each Fracture Set in Each Fracture Region for CWF

	CWF-Region A		CWF-Region B		CWF-Region C		CWF-Region D		CWF-Region E		CWF-Region F	
Fracture Set	Set 1	Set 2	Set 1	Set 2	Set 1	Set 2	Set 1	Set 2	Set 1	Set 2	Set 1	Set 2
NO.Fracture	28	41	23	43	5	3	11	1	6	11	9	1
NO. at	15	16	10	14	1	3	3	1	1	0	2	0
T%	53.57	39.02	43.48	32.56	20.00	100.00	27.27	100.00	16.67	0.00	22.22	0.00
Trend	218.18	155.34	243.61	187.77	242.40	214.00	180.91	286.00	227.17	86.00	222.00	87.00
Dip	45.14	84.34	34.48	85.24	26.80	84.00	26.64	90.00	35.00	83.00	50.00	76.00
Distribution	Normal	Normal	Normal	Normal	Normal	Normal	Normal	Uniform	Normal	Normal	Normal	Uniform
k	3.56	1.41	4.92	1.20	6.58	0.98	8.51	\	12.99	1.05	4.12	\
Height	LogNormal	LogNormal	LogNormal	LogNormal	Exponential	Exponential	LogNormal	Uniform	Exponential	Normal	Normal	Unifrom
Mean(ft)	4.43	2.47	5.81	2.31	6.86	1.69	3.91	1.11	2.36	1.44	3.10	4.53
Mean(m)	1.35	0.75	1.77	0.70	2.09	0.52	1.19	0.34	0.72	0.44	0.94	1.38
Std Dev(ft)	0.55	2.17	4.51	1.51	4.32	0.67	2.41	\	1.83	0.63	1.35	\
Std Dev(m)	0.17	0.66	1.37	0.46	1.32	0.20	0.73	\	0.56	0.19	0.41	\
Width1	Uniform	Uniform	Uniform	Uniform	Uniform	Uniform	Uniform	Uniform	Uniform	Uniform	Uniform	Uniform
Mean 1(m)	1.35	0.75	1.77	0.70	2.09	0.52	1.19	0.34	0.72	0.44	0.94	1.38
Width2	Uniform	Uniform	Uniform	Uniform	Uniform	Uniform	Uniform	Uniform	Uniform	Uniform	Uniform	Uniform
Mean 2(m)	2.70	1.51	3.54	1.41	4.18	1.03	2.38	0.68	1.44	0.88	1.89	2.76
Apperture	Exponential	Exponential	Uniform	Uniform	Uniform	Uniform	Uniform	Uniform	Uniform	Uniform	Uniform	Uniform
Mean(mm)	0.07	0.27	0.00	0.00	0.00	0.00	0.00	0.00	0.00	0.00	0.00	0.00
Std Dev(mm)	0.38	0.73	0.00	0.00	0.00	0.00	0.00	0.00	0.00	0.00	0.00	0.00
Mean(m)	7.00E-05	2.70E-04	0.00	0.00	0.00	0.00	0.00	0.00	0.00	0.00	0.00	0.00
Std Dev(m)	3.80E-04	7.30E-04	0.00	0.00	0.00	0.00	0.00	0.00	0.00	0.00	0.00	0.00

Then, fractures can be generated by selecting the Number of Fractures or Fracture Spacing. In this time, a specific number of fractures are assigned to a given fracture set within a fracture region. Fracture Spacing is not used to this research, because this method is not implemented in the current version of DFNModeler. Table 3.1 and Table 3.2 include the number of fractures in each fracture set of the CWF and FWF observation windows.

Table 3.2 Summarization of Each Fracture Set in Each Fracture Region for FWF

	CWF-Region A		CWF-Region B		CWF-Region C		CWF-Region D		CWF-Region E	
Fracture Set	Set 1	Set 2	Set 1	Set 2	Set 1	Set 2	Set 1	Set 2	Set 1	Set 2
NO.Fracture	20	18	7	3	13	11	4	11	4	16
NO. at	6	9	1	1	3	0	2	0	0	0
T%	30.00	50.00	14.29	33.33	23.08	0.00	50.00	0.00	0.00	0.00
Trend	211.20	178.17	171.86	160.67	215.00	228.82	201.75	132.91	318.25	235.44
Dip	43.85	84.72	47.71	90.00	29.15	85.82	33.50	81.55	31.50	84.69
Distribution	Normal	Normal	Normal	Normal	Normal	Normal	Normal	Normal	Normal	Normal
k	3.15	1.22	2.75	2.04	6.08	1.25	4.42	1.09	8.64	2.23
Height	LogNormal	Normal	LogNormal	Exponential	LogNormal	LogNormal	Exponential	LogNormal	Exponential	Normal
Mean(ft)	5.61	1.99	3.32	2.12	8.36	2.71	5.96	2.06	3.05	1.84
Mean(m)	1.71	0.61	1.01	0.65	2.55	0.83	1.82	0.63	0.93	0.56
Std Dev(ft)	6.28	0.63	1.86	0.52	5.30	1.19	2.84	0.91	1.54	0.67
Std Dev(m)	1.91	0.19	0.57	0.16	1.62	0.36	0.87	0.28	0.47	0.20
Width1	Uniform	Uniform	Uniform	Uniform	Unifrom	Unifrom	Uniform	Uniform	Uniform	Uniform
Mean 1(m)	1.71	0.61	1.01	0.65	2.55	0.83	1.82	0.63	0.93	0.56
Width2	Uniform	Uniform	Uniform	Uniform	Unifrom	Unifrom	Uniform	Uniform	Uniform	Uniform
Mean 2(m)	3.42	1.21	2.02	1.29	5.10	1.65	3.63	1.26	1.86	1.12
Apperture	Uniform	Uniform	Uniform	Uniform	Unifrom	Unifrom	Uniform	Uniform	Uniform	Uniform
Mean(mm)	0	0	0	0	0	0	0	0	0	0
Std Dev(mm)	0	0	0	0	0	0	0	0	0	0
Mean(m)	0	0	0	0	0	0	0	0	0	0
Std Dev(m)	0	0	0	0	0	0	0	0	0	0
	CWF-Region F		CWF-Region G		CWF-RegionH		CWF-Region I		CWF-Region J	
Fracture Set	Set 1	Set 2	Set 1	Set 2	Set 1	Set 2	Set 1	Set 2	Set 1	Set 2
NO.Fracture	10	1	1	0	0	0	8	0	0	0
NO. at	3	0	0	\	\	\	2	\	\	\
T%	30	0	0	\	\	\	25	\	\	\
Trend	252.50	77.00	82.00	\	\	\	238..875	\	\	\
Dip	37.40	88.00	44.00	\	\	\	43.38	\	\	\
Distribution	Normal	Uniform	Unifrom	\	\	\	Normal	\	\	\
k	4.45	\	\	\	\	\	4.58	\	\	\
Height	Normal	Uniform	Unifrom	\	\	\	LogNormal	\	\	\
Mean(ft)	3.56	1.87	4.16	\	\	\	5.70	\	\	\
Mean(m)	1.09	0.57	1.27	\	\	\	1.74	\	\	\
Std Dev(ft)	1.37	\	\	\	\	\	2.89	\	\	\
Std Dev(m)	0.42	\	\	\	\	\	0.88	\	\	\
Width1	Unifrom	Unifrom	Unifrom	\	\	\	Unifrom	\	\	\
Mean 1(m)	1.09	0.57	1.27	\	\	\	1.74	\	\	\
Width2	Unifrom	Unifrom	Unifrom	\	\	\	Unifrom	\	\	\
Mean 2(m)	2.17	1.14	2.54	\	\	\	3.47	\	\	\
Apperture	Uniform	Uniform	Uniform	\	\	\	Uniform	\	\	\
Mean(mm)	0	0	0	\	\	\	0	\	\	\
Std Dev(mm)	0	0	0	\	\	\	0	\	\	\
Mean(m)	0	0	0	\	\	\	0	\	\	\
Std Dev(m)	0	0	0	\	\	\	0	\	\	\

The fracture Width and Fracture Height (Length) describe the basic dimensions of fractures with a fracture set. In this circumstance, Fracture Height (Length) is a known parameter which is the linear length of each discontinuity within the mapped face. It can be used to specify the one dimension of fracture within the vertical mapped faces. This parameter also is described with an appropriate statistical distribution using parameters obtained from the mapping. Different models were chosen for different units, and the best model varied but included uniform, log normal, exponential, and power-law, depending upon the unit. For fracture width describes the horizontal dimension of fractures parallel to strike of each discontinuity. This parameter is unknown. Two hypotheses are built. First, the fracture width is assumed to be the same length as the fracture height which is named Assumption-A. Second, the fracture width is assumed to be twice as long as the fracture height which is named Assumption-B. The distribution type for this variable is selected as uniform distribution, an appropriate assumption for this variable with significant uncertainty. Table 3.1 and Table 3.2 contain all the information for the fracture width and fracture height (Length) of each geologic unit.

The fracture termination type is classified into three types in this research. It is assigned based on the uppermost end only of the discontinuity for consistency. The first type is AT, also known as "T" which means a termination "at" another discontinuity. The second type is assigned as IN, also known as "X". It indicates an upper termination within the rock. The third type is OBS that refers to situations where the uppermost termination type is obscured and could not be determined. In this simulation software, the termination percentage needs to be calculated. Table 3.1 and Table 3.2 include all the termination percentage for each fracture set of CWF and FWF. It is defined as comparing number of terminated tips to non-terminated tips. The equation is defined as

$$T\% = N_T /(N_T + N_R) \quad (3.2)$$

where N_T is defined as the total number of "T" type discontinuity, and N_R is the total number of other termination type's discontinuity.

Hydraulic properties information for fracture aperture, transmissivity and storativity are also assigned. For this research, fracture aperture is recorded based on evidence of pre-construction filling and aperture. There are only a few discontinuities for which pre-excavation where a nonzero aperture is evident. Almost 99% HSD have 0 mm aperture. Only small number of discontinuities (CWF-Region-A) have any aperture and these range from about 0 mm to 5mm. Transmissivity and storativity are defined as 0, as they are not used in this research; the transmissivity and storativity data do not affect the results and they are not important for the interconnection analysis.

With all fracture set information, the HSD networks in the CWF and FWF observation window area are readily quantified and are therefore suited for the development of DFN models. The compartmentalization analysis is applied and the compartments can then be used to assess the potential for through flow in rock on the periphery of the CWF and FWF observation window area. Multiple model realizations (using a different seed in each realization) were created for each excavation to permit consideration of multiple possible outcomes.

3.2.2.2 The Full CWF and FWF Models

Since all the HSD data for CWF and FWF observation window are qualified for DFN Modeling, it is reliable to extend from the observation windows close to the full size of the CWF and FWF excavation walls. Based on the CWF and FWF observation windows, the properties of the fracture regions and fracture set parameters are extended to actual CWF or FWF longest

(southern) excavation boundary. The statistical assumption here is that fracture properties obtained for the observation window are valid across the much longer full length each excavation. For the CWF, the full model size extends to 900 ft (274.32m) by 100 ft (30.48m) with a vertical thickness of 65 ft (19.812m), which close to the actual CWF dimension along the south face. By area or volume, the full model is 9 times as large as the models of the observation window. Each fracture region is expanded to its full size by retaining the same statistical properties, and retaining the same fracture density by increasing the number of fractures in proportion to the volume increase.

For the FWF, the full model size is extended to 2100 ft (640.08m) by 100 ft (30.48m) with a thickness of 80 ft (24.384m). In the case of the full-size FWF model, the fracture region size increase is 21 times larger than the model used for the observation window model. Thus, the number of fractures is 21 times those mapped in the FWF observation window. Figure 3.4 and Figure 3.5 shows the prepared models size for the full CWF and FWF. For both full CWF and FWF models, only the number of fractures is increased and the other properties of all fracture sets are maintained. The models are prepared and the compartmentalization analyses were conducted in multiple realizations (with a different seed in each realization).

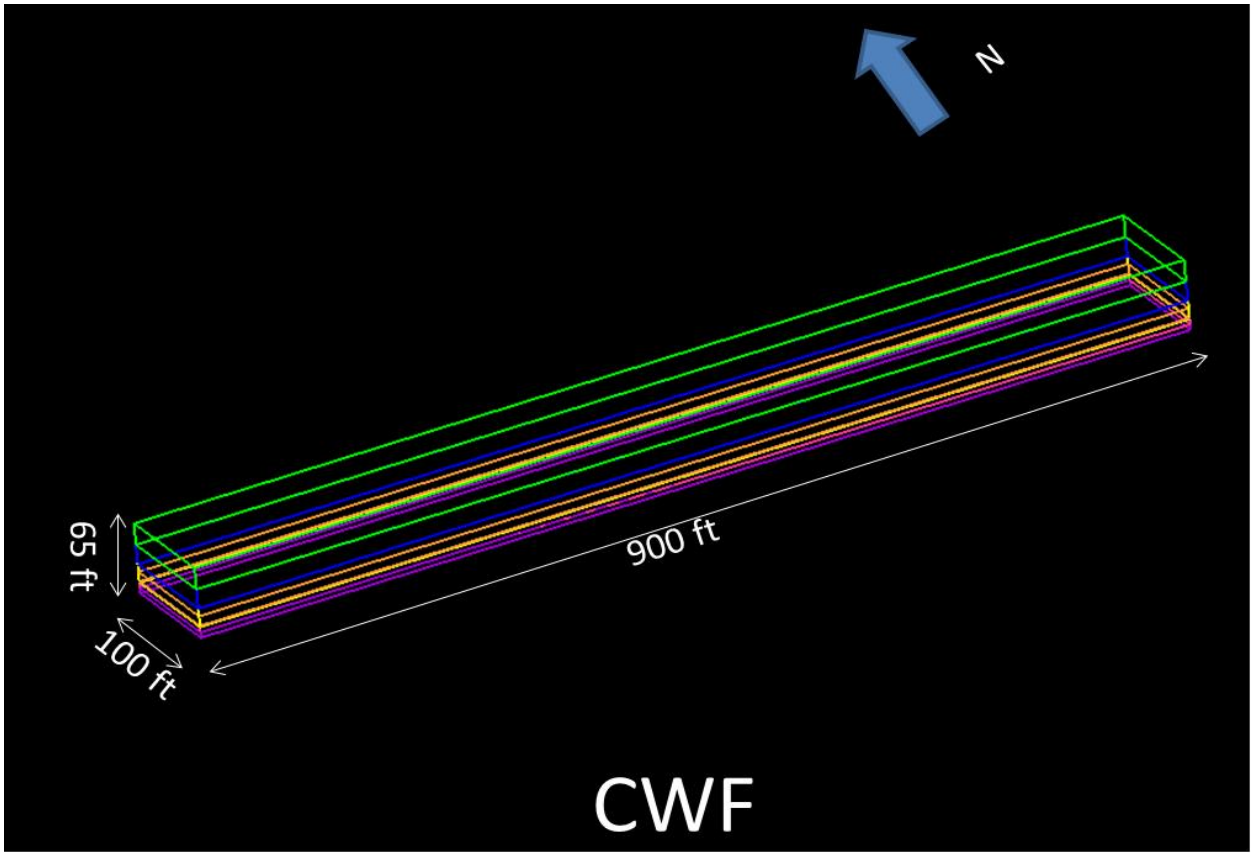

Figure 3.4 CWF Model Region Size

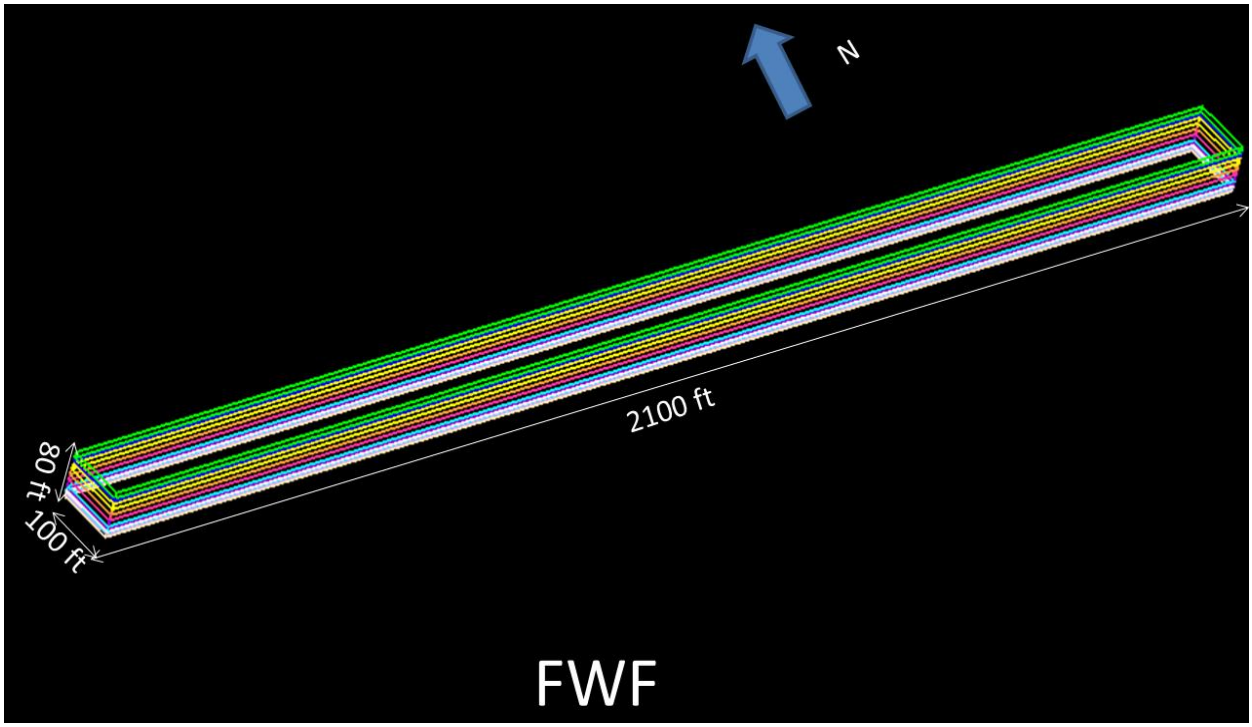

Figure 3.5 FWF Model Region Size

3.3 Results of DFNModeler Simulations

3.3.1 Compartmentalization Analysis

The compartmentalization analysis is conducted on the southern boundary of the CWF or FWF with two different hypotheses. In each excavation, the width of the rock mass (in the north-south direction) and the length and height of the simulated region matches the actual CWF or FWF longest (southern) excavation boundary. It becomes necessary to make an assumption about the extent of the mapped discontinuities into the mapped face. The nominal hypothesis adopted here is to assume that the fracture extent into the mapped face is on the order of the length along the mapped face. To examine the sensitivity to this assumption, we consider a second modeling assumption (Assumption-B) where the extent of the discontinuities into the mapped face is the very conservative assumption that the fractures extended into the mapped face at twice their mapped length.

The four simulated rock mass geometries are the CWF with a nominal assumption (Assumption-A) regarding fracture extent into the face, the CWF with the conservative assumption (Assumption-B) regarding fracture extent, the FWF with the nominal assumption (Assumption-A) regarding fracture extent, and the FWF with the conservative assumption (Assumption-B) regarding fracture extent.

A total of 33 simulations are completed for each of the four simulated rock mass cases. Four examples of the three-dimensional fracture and compartmentalization realizations for both of the different hypotheses for CWF and FWF are listed in Appendix E (Figure E-1 to Figure E-4). To get more reliable results for the full CWF and FWF models, 33 realizations are conducted to permit realistic variability of the possible results. That number was chosen to allow a mean

largest hull size that could be a realistic statistical representation of this property. Those realizations give a sufficient data of volume for each compartment hulls. The maximum compartments volumes, the total number of compartments hulls, and the frequency of compartments volume were created for each realization for the four different types of models. The results for these 132 realizations (33 realizations for each of two different sizes using two different assumed fracture dimensions) are recorded in Appendix E Table E-1.

The distributions of the maximum compartments volumes in 33 realizations are illustrated in Figure 3.6 for both the full CWF and FWF cases, with the results for both Assumption A and Assumption B are presented. Figure 3.7 reveals the mean frequency of compartments hulls falls in different volumes ranges, for these same cases. Within those compartments data, the volumes of interconnected fracture networks are identified. It may be true that the size of such networks might better be characterized by the vertical or areal extent, but hull volume is used here to be consistent with the customary interpretation of DFNModeler results.

If we were to treat each hull as roughly spherical, the representative diameters of the largest observed hull can be estimated for each realization to permit an approximate vertical dimension or maximum span of a potential fracture network. These are calculated and histograms of the maximum hull diameter are estimated for 33 realizations, as shown in Figure 3.8. Table 3.3 contains the maximum compartments volumes, the total number of compartments hulls, and the maximum representative diameter of hulls for 33 realizations of the four different types of simulations.

An example of one of these simulation results is shown for the full CWF case with the nominal assumption (Assumption-A) in Figure 3.9, where a total of 37 hulls are present. In this

illustrated case, the maximum hull volume is 15.7 m^3, with a representative diameter of 3.11 m. The full histogram of the volume of all hulls observed in this case is shown in Figure 3.10.

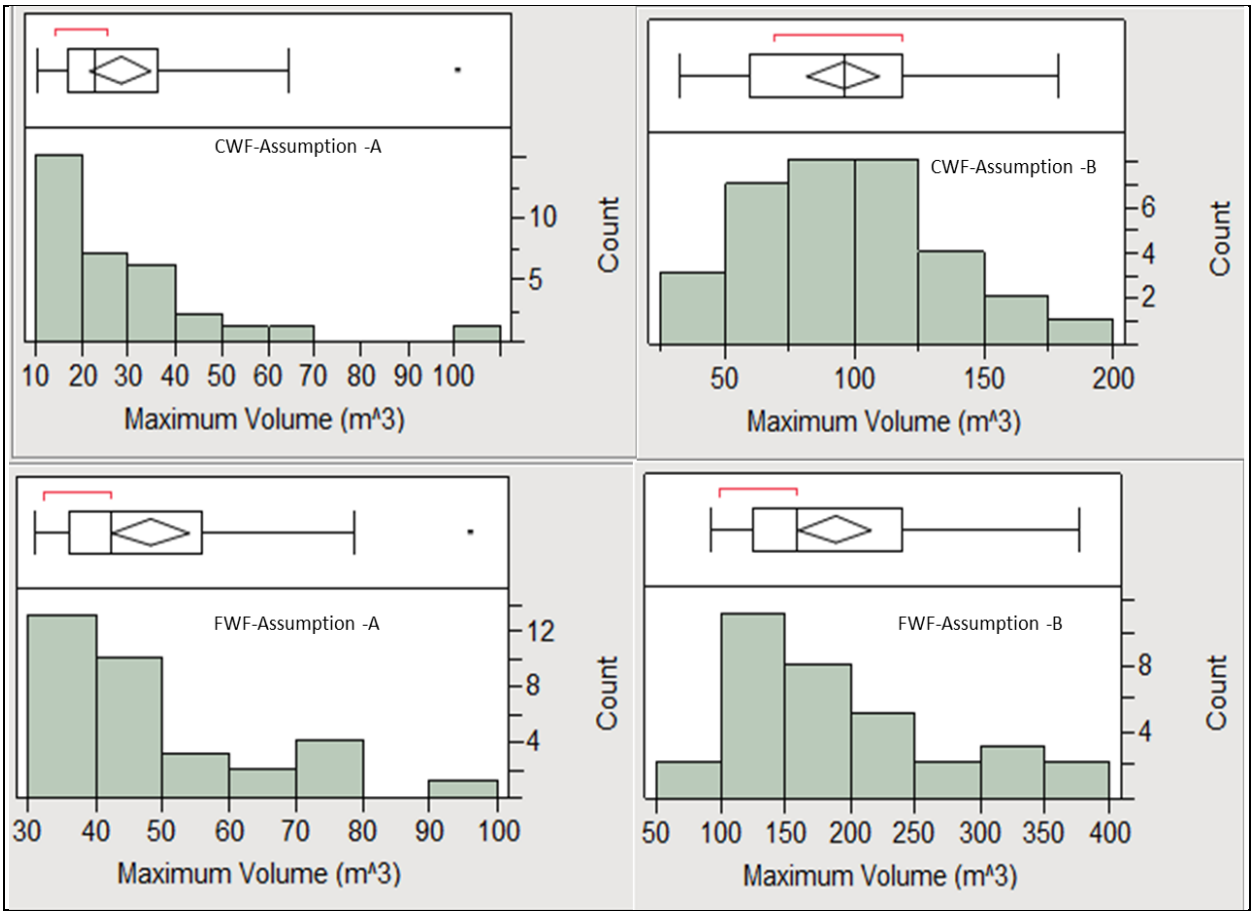

Figure 3.6 Histograms of Maximum Volume Compartments for CWF and FWF

Table 3.3 Compartments Statistics of 33 Realizations for CWF and FWF

Realization	CWF-A			CWF-B			FWF-A			FWF-B		
	Max. Vol (m^3)	Total No. Com	D (m)	Max Volume (m^3)	Total No. Com	D (m)	Max. Vol (m^3)	Total No. Com	D (m)	Max Volume (m^3)	Total No. Com	D (m)
1	25.2	45	3.64	59.9	69	4.85	36.0	43	4.10	115.0	119	6.03
2	10.3	34	2.70	170.0	72	6.87	42.4	36	4.33	107.0	125	5.89
3	18.0	38	3.25	103.0	74	5.82	41.7	52	4.30	213.0	144	7.41
4	18.2	29	3.26	51.1	70	4.60	45.1	55	4.42	148.0	127	6.56
5	51.0	35	4.60	84.8	75	5.45	73.7	58	5.20	106.0	132	5.87
6	15.7	37	3.11	50.5	71	4.59	69.4	55	5.10	360.0	143	8.83
7	25.2	45	3.64	141.0	64	6.46	36.0	43	4.10	125.0	130	6.20
8	10.3	34	2.70	118.0	80	6.09	42.4	36	4.33	220.0	138	7.49
9	18.0	38	3.25	149.0	64	6.58	41.7	52	4.30	274.0	144	8.06
10	13.3	45	2.94	75.0	78	5.23	45.1	57	4.42	182.0	132	7.03
11	28.0	36	3.77	179.0	72	6.99	73.7	58	5.20	151.0	129	6.61
12	37.8	34	4.16	103.0	74	5.82	33.3	49	3.99	219.0	137	7.48
13	19.1	43	3.32	51.1	70	4.60	37.4	37	4.15	153.0	139	6.64
14	17.6	33	3.23	84.8	75	5.45	53.2	69	4.67	141.0	128	6.46
15	38.8	39	4.20	50.5	71	4.59	38.4	49	4.19	304.0	143	8.34
16	23.4	41	3.55	141.0	64	6.46	36.5	56	4.12	180.0	120	7.01
17	30.4	41	3.87	96.0	54	5.68	56.3	54	4.76	246.0	130	7.77
18	64.8	27	4.98	110.0	68	5.94	39.6	64	4.23	159.0	112	6.72
19	47.2	44	4.48	32.4	65	3.96	49.2	56	4.55	148.0	121	6.56
20	15.9	49	3.12	103.0	75	5.82	56.1	46	4.75	135.0	125	6.36
21	17.3	39	3.21	118.0	84	6.09	48.5	47	4.52	233.0	119	7.63
22	32.6	38	3.96	145.0	87	6.52	78.7	55	5.32	102.0	118	5.80
23	13.3	32	2.94	59.6	76	4.85	41.2	42	4.29	319.0	127	8.48
24	101.0	33	5.78	102.0	66	5.80	70.7	42	5.13	255.0	145	7.87
25	25.5	36	3.65	99.8	76	5.75	45.9	56	4.44	123.0	130	6.17
26	48.7	33	4.53	160.0	70	6.74	35.5	52	4.08	98.6	124	5.73
27	14.2	40	3.00	82.0	73	5.39	95.8	51	5.68	377.0	133	8.96
28	15.7	39	3.11	86.0	66	5.48	32.7	50	3.97	195.0	122	7.19
29	38.1	27	4.17	68.6	70	5.08	31.1	58	3.90	159.0	124	6.72
30	21.9	37	3.47	85.1	62	5.46	66.5	53	5.03	301.0	141	8.31
31	34.7	41	4.05	119.0	74	6.10	34.3	66	4.03	92.8	117	5.62
32	22.5	45	3.50	37.9	75	4.17	32.3	44	3.95	157.0	134	6.69
33	19.6	40	3.35	42.7	66	4.34	36.2	51	4.10	125.0	127	6.20
Mean	28.3	37.8	3.7	95.7	71.2	5.6	48.4	51.3	4.5	188.6	129.7	7.0
Std	18.4	5.3	0.7	39.7	6.5	0.8	16.2	8.0	0.5	78.5	9.0	0.9

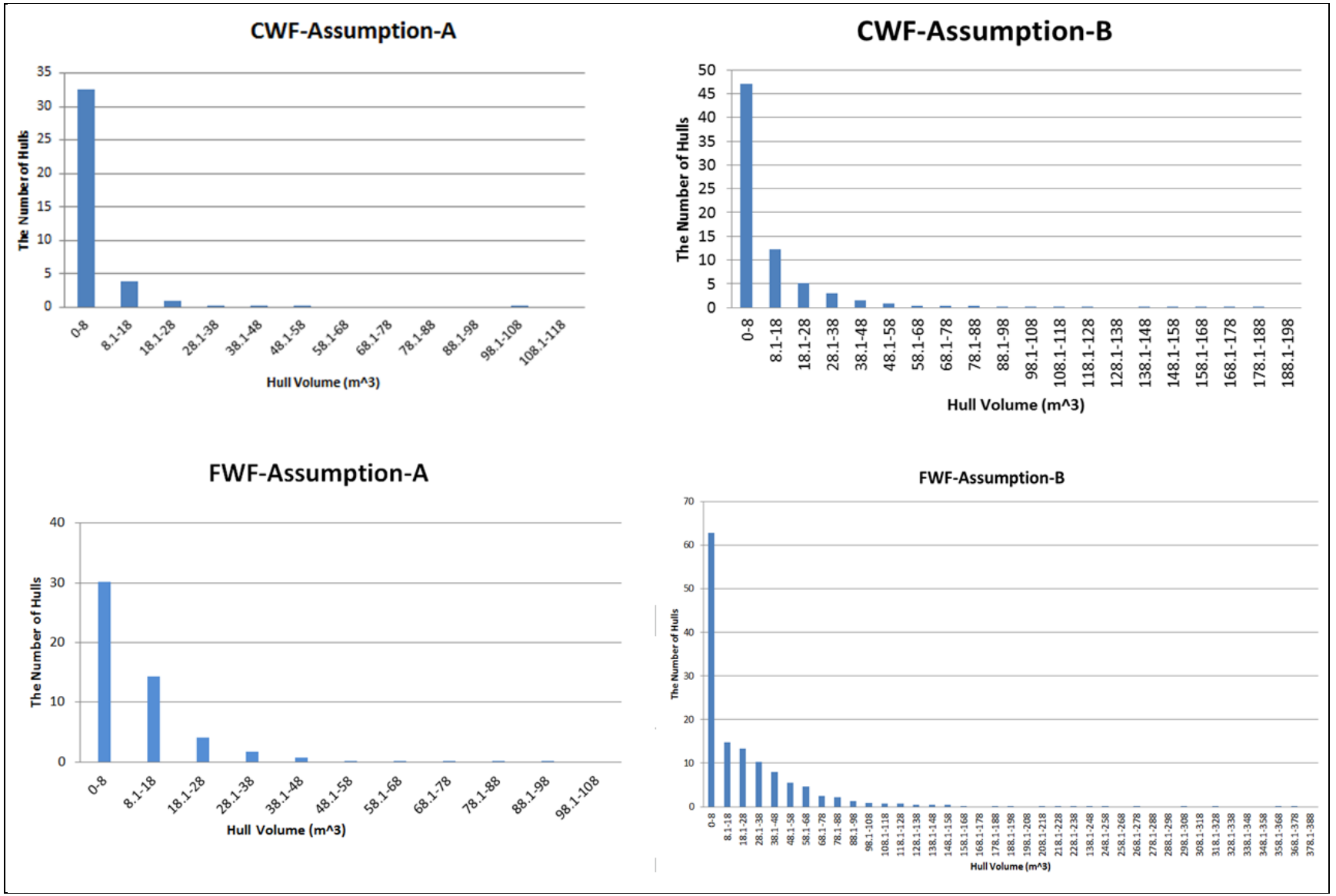

Figure 3.7 Mean Frequency of Compartments Volume for CWF and FWF

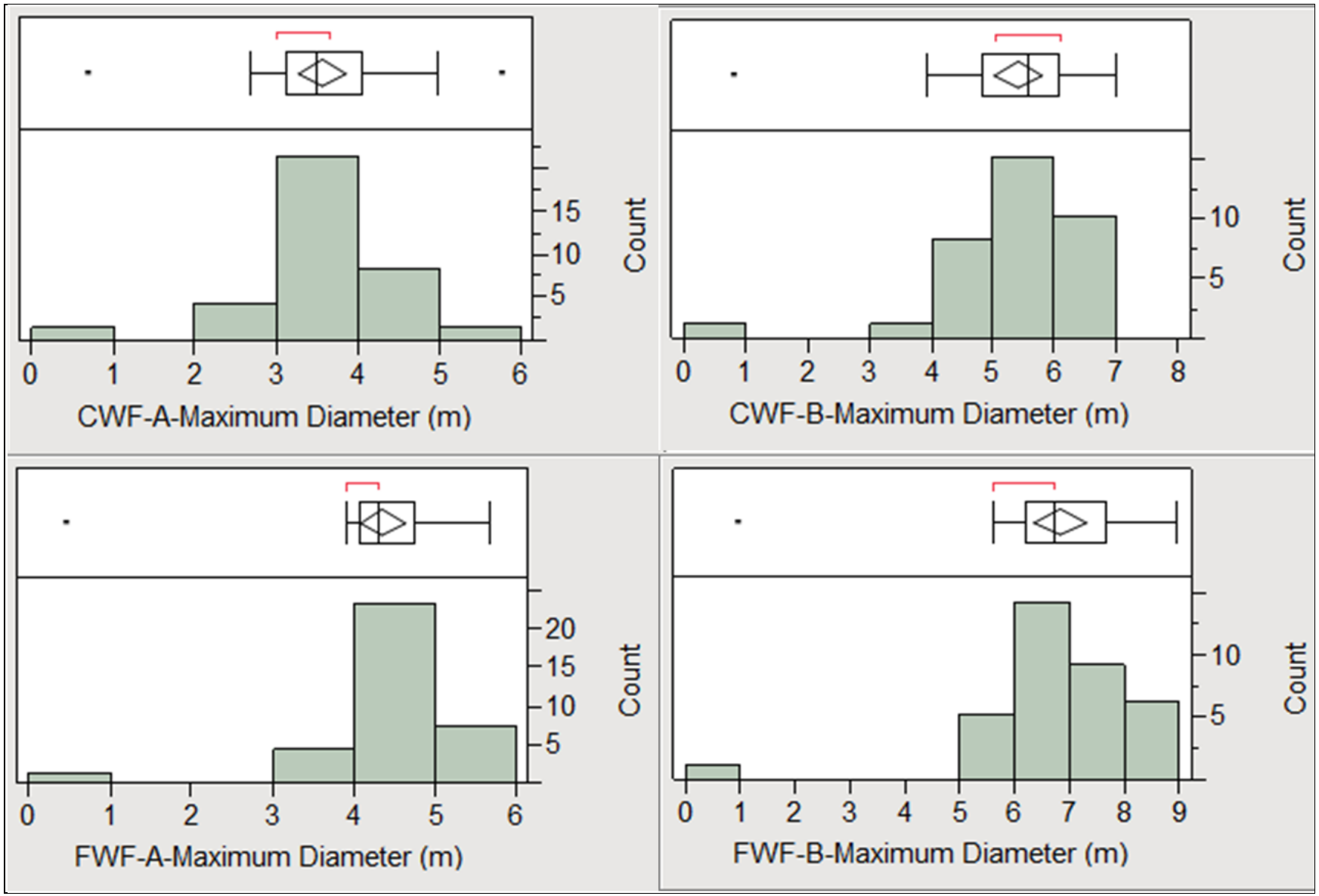

Figure 3.8 Histograms of Maximum Compartments Diameter for CWF and FWF

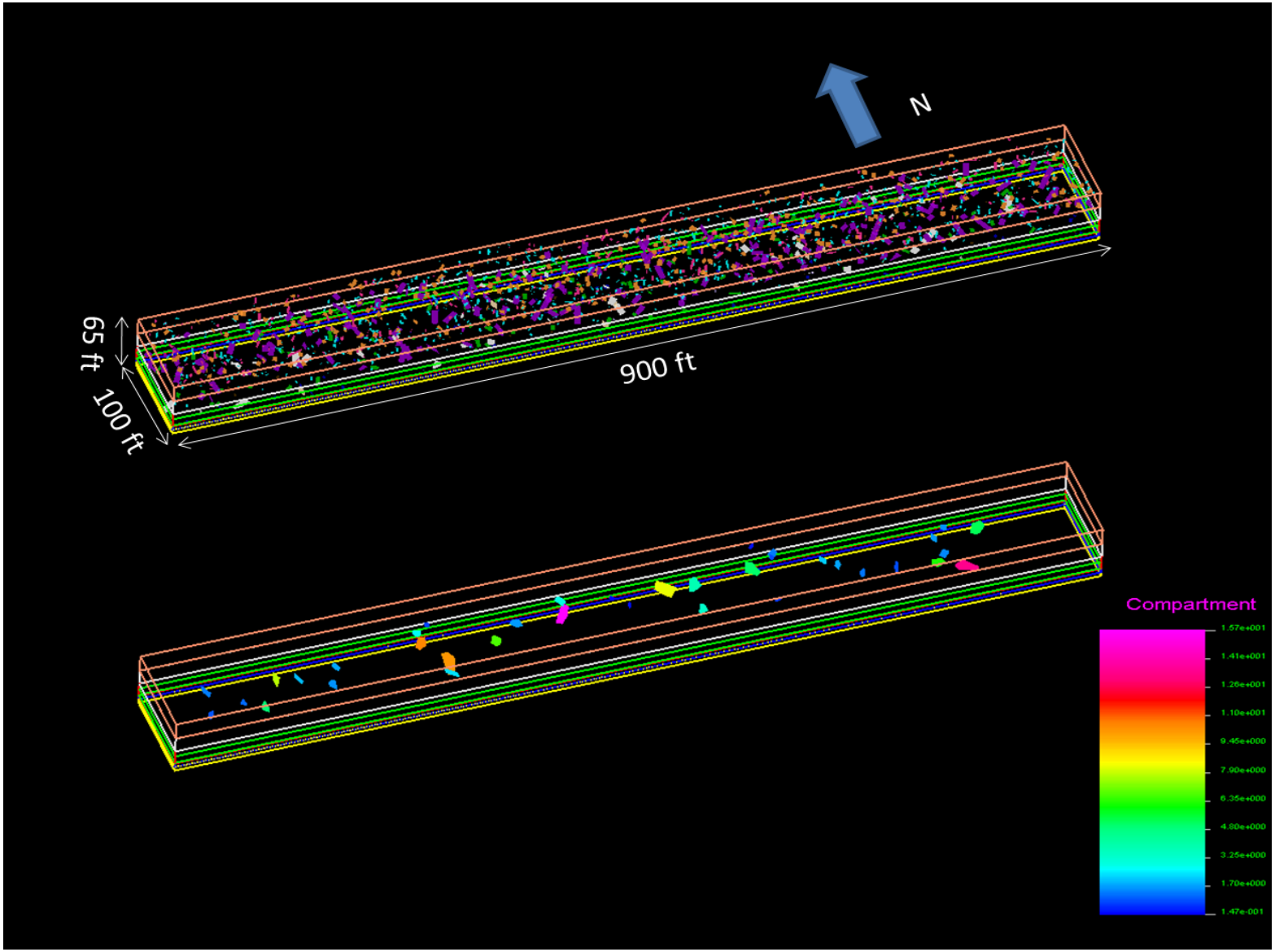

Figure 3.9 Example of Three-Dimensional Fracture Realization and Compartments Analysis for CWF Assumption-A Model

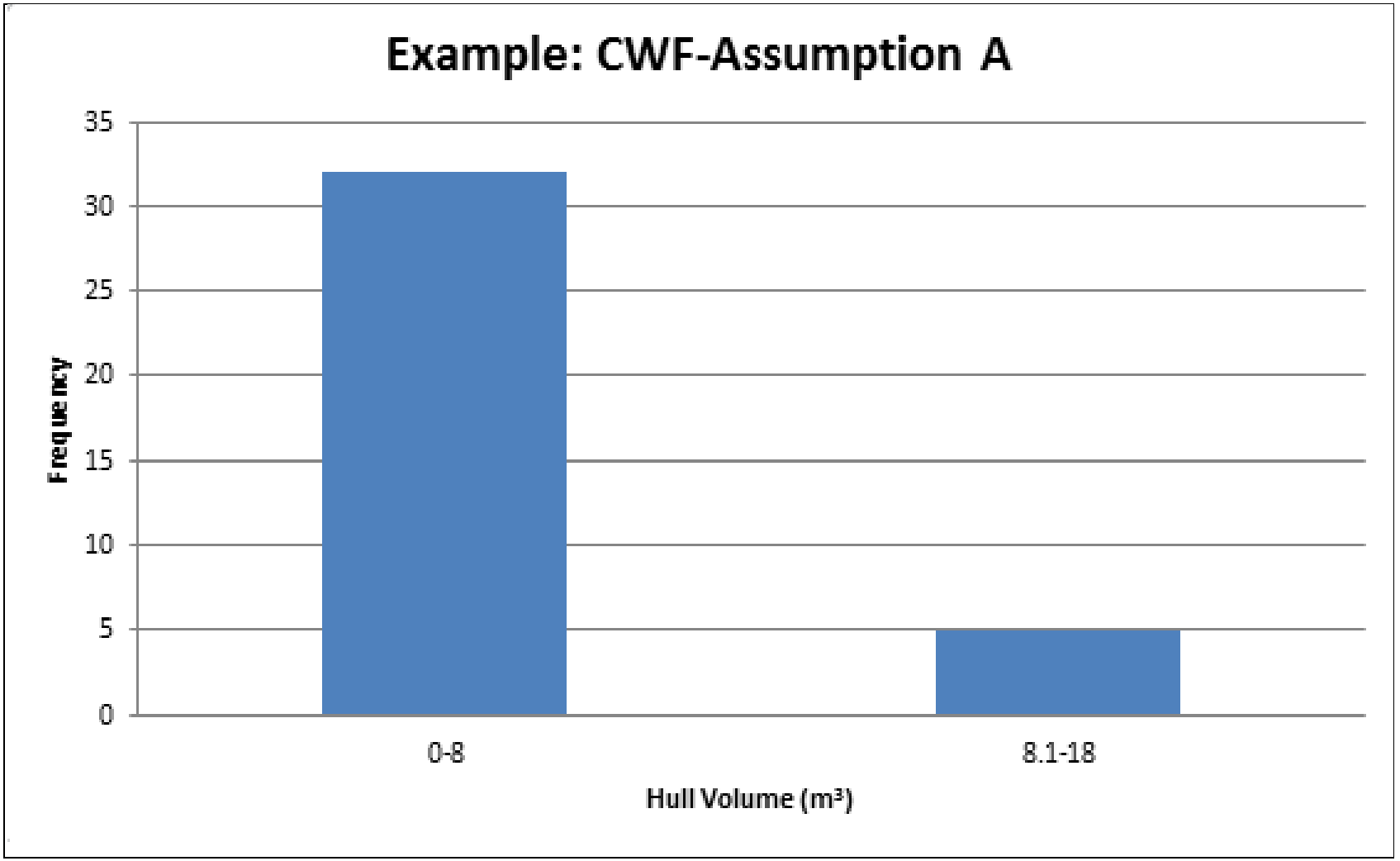

Figure 3.10 Histogram of Hull Volume Frequency for CWF Assumption-A Model

CHAPTER IV

CONCLUSIONS

4.0 **Stereoplots**

As Table 2.2 shown, for geologic unit 1 (sandstone) and geologic unit 2 (argillaceous sandstone), discontinuities that display a near vertical dip have a high proportion of discontinuities that class as HSD (75 to 92%), while discontinuities that display a subhorizontal orientation class as HSD much less frequently (only 5 to 17%). For geologic unit 3 (siltstone) and geologic unit 4 (Argillaceous siltstone), discontinuities again display a near vertical dip that have a high proportion of discontinuities that class as HSD (85 to 88%), while discontinuities that display a subhorizontal orientation class as HSD much less frequently (9 to 24%). For genetic unit 5 (Mudstone), except one discontinuity, all discontinuities are subhorizontal orientation. The HSD have 17% in FWF and 64% in CWF with subhorizontal orientation.

For Genetic Unit A, Genetic Unit B and Genetic Unit C, discontinuities show high proportion of NHSD with subhorizontal dip angle, while have only 10% to 35% of HSD show subhorizontal orientation. Most of HSD shows high percentage (84%-95%) with near-vertical orientation. For Genetic Unit D, Genetic Unit E, Genetic Unit F, discontinuities display a subhorizontal dip have much less proportion of discontinuities that class as HSD (10 to 14%). Furthermore, 100% HSD are shown with near-vertical orientation.

With combining both genetic unit and geologic unit observations for HSD in CWF and FWF, it is tempting to conclude that the low-angle discontinuities vastly outnumber the near-vertical discontinuities and most HSD are shown with near-vertical orientation. Only 16% HSD across all mapped faces are found within the set of low-angle discontinuities. Furthermore, it evidences that the proportion of vertical to horizontal discontinuities of all types decreases with decreasing grain size.

A complete set of the stereonets created to examine the vertical position within a genetic unit Figure B-21 through B-26 in Appendix B: Genetic unit A and F have a greater number of discontinuities with a Y_{scale} value which is small than 0.5. Genetic units B, C and E has almost the same number of discontinuities falling in the lower part and upper part of this genetic unit, genetic units D have more discontinuities with a Y_{scale} value which is bigger than 0.5, which clearly indicates that the various genetics units do not fall into the same pattern. Furthermore, table 2.3 shows the discontinuities in the upper portion of a genetic unit appear more to be from the horizontal set than discontinuities in the lower portion of a genetic unit.

Depending on previous finding, some discontinuities in genetic unit A are absent at the CWF and some discontinuities in genetic unit F are not mapped in CWF (simply because the CWF is shallower and did not extend to the depths where unit F would be located). It is reasonable to accept that for most Genetic units' discontinuities in the upper half of a genetic unit tend to be from the subhorizontal set

4.1 Geostatistics Analysis and Kriging Maps

Figures C-1 through Figure C-5 reveals that curvature and roughness are consistent with a normal distribution. The dip angle values are separated roughly into two different ranges, and this matched the results obtained in the analysis of the stereoplots. One set falls between 0° to

70° dip and another set falls from 70° to 90°, and the majority close to 90°. For curvature and roughness, which are both discretely distributed (recorded to the nearest 0.5 value, e.g. 2, 2.5, or 3), most of the values are either 2 or 2.5. For length, both CWF and FWF illustrate generally declining frequency with increased length, except the CWF south face where most of length values are close 4 ft (1.22m). For the CWF south face, the mode of the discontinuity length is approximately 3 ft (0.9m), which is reasonably similar to the remaining excavation faces. To prepare to Kriging prediction maps, the data which does not fit a normal distribution must be transformed, which is the case for strike, dip and length. The transformed data are shown in Appendix C Figure C-1through Figure C-5.

Furthermore, Table 2.1 illustrates that the dip angle is the most influence factor for HSD. The standard deviation is large and the results are distinctly different for the HSD and NHSD sets. Other properties have similar variability for the HSD and NHSD sets. The standard deviation for strike is large, which shows the great variability for both the HSD and NHD sets.

From Kriging prediction maps (Figure C- 11 to Figure C-14 in Appendix C), each property is estimated and a general sequence is discovered. By comparing each discontinuity property with different spatial position, the anisotropy for the discontinuity properties is revealed and is summarized below.

For the strike of discontinuities, the CWF east side is highly consistency with south side. Most CWF discontinuities are distributed between 100 ºto 150 º(Green color). Corresponding to Genetic Unit maps (Figure A-1, A-2), they are mostly found in the lower part of Genetic Unit 1 and Genetic Unit 2. Some low angle discontinuities between 0 ºto 30 ºare found in lower part of Genetic Unit 3 and Genetic unit 4 in East face of CWF. Furthermore, the strike is keeping the same pattern within the same Genetic Unit of CWF. However, the strikes of discontinuities in the

FWF are more variable. Most of the larger value strike orientations (>200 º) are found in Genetic Unit 3 and the most prominent part is discovered in argillaceous sandstone of Genetic Unit 3. As a consequence, there is no evident trend in discontinuity strike (or its variability) in either the CWF or FWF.

For discontinuity dip angle, both the CWF and FWF are fairly consistent. The majority of low dip angle discontinues, which fall between 5 ºto 20 ºare present in Genetic Unit 2 and the upper part of Genetic Unit 3 in the CWF and in Genetic Unit 3 in the FWF. Corresponding to geologic type, they are mostly found in argillaceous sandstone. Among high dip angle discontinuities, with dip from about 50 ºto 90 º, they are mostly revealed in the lower part Genetic Unit 1 (argillaceous sandstone) in the CWF and in Genetic Unit 2 in FWF. This finding is consistent with the correlation between CWF and FWF genetic units described by Holt et al. (2011).

The discontinuity length is estimated based on the left most point coordinate and the right most point of coordinate of discontinuity. In CWF, the south face and east face show consistent results, and that the longest linear length of discontinuities are exposed in lower part of Genetic Unit 1, which also is classified as an argillaceous sandstone. In the FWF, the longest linear length of discontinuities is revealed in Genetic Unit 2, for both the south face and east face, which also defined as sandy siltstone.

Discontinuity curvature maps show that the average of curvature for both the CWF and FWF are about 2.5 (mostly yellow to red color in Figure C-14). This result indicates that a higher curvature in a discontinuity is associated with shorter, the discontinuities. Furthermore, the east side of the CWF and FWF are smaller than the south side of the CWF and FWF and most of the observed curvature ratings fall between 1 and 2.5. The discontinuity roughness prediction maps

illustrates the CWF has slightly lower roughness values relative to the FWF. Repeating the same trend found for curvature, the east face of the CWF and FWF has lower roughness values relative to south face of CWF and FWF. In general, for both discontinuity curvature and roughness, any general trend or contrast is not obvious across the whole mapped data window.

4.2 DFN Models

The main results of DFN models are obtained in the full CWF and FWF models with two different hypotheses regarding discontinuity extent. An example of these results was presented in Figure 3.9, but the additional realizations are presented in Appendix E, Figure E-1 through Figure E-4, showing examples of realizations for the full CWF and FWF three-dimensional models. From those figures, a highly consistent of interconnection relationship is revealed and an estimate of the possible hull compartment size is possible. There are no extremely large fracture networks or hull compartments observed in the CWF and FWF models. In particular, there is no evidence found of any of the CWF and FWF models (even with very conservative assumptions) that there is any potential for fluid flow in either the vertical direction or horizontal direction. By characterizing the compartment volume in all realizations, the histograms and full results are illustrated in Figure 3.6 and Table 3.3. Figure 3.6 contains the histograms of maximum volume compartments in each realization for CWF and FWF. For hypothesis A, the mean of the maximum volume from all realizations from the full CWF model is 28.28 m^3 and the standard deviation is 18.43 m^3. The mean of the maximum volume from all realizations from the full of FWF model is 43.38 m^3 with 16.19 m^3 standard deviation. For hypothesis B, the mean maximum volume of the analogous CWF and FWF results are 95.72 $m^3$and 188.59 m^3, respectively. The standard deviations are 39.74 m^3 and 78.54 m^3.

Figure 3.7 illustrates the largest portion of compartments volumes are smaller than 8 m^3. With the Compartments volumes increased, the number of compartment hulls declines rapidly. Furthermore, the CWF and FWF are kept consistent. No matter for hypothesis A or hypothesis B, only small number of hulls is larger than 18 m^3 are in both CWF and FWF. Figure 3.8 was created to illustrate the span, effective diameter, or linear extent of the largest hull size observed in these realizations. Those results showed that the mean of the maximum effective diameter of hulls is around 3.57 m to 5.43 m, depending upon which hypothesis is applied in the CWF. Given the conservative nature of Assumption B, this provides a reasonable high end estimate of likely linear extent of the largest fracture network that might be reasonably expected. The FWF has larger effective diameter results, from 4.36 m to 6.82 m, depending on the assumption used regarding discontinuity extent into the mapped face. These results reveal that the one-dimensional distances or effective diameter of the largest hulls are small relative to the excavation height or width and cannot create have a significant influence on the landfill facility. In fact, the largest hull observed in any of the 132 realization considering all excavation models and all assumptions was 377 m^3, with an effective hull diameter of 8.96 m. Even this value, which might be unrealistic given the multiple conservative assumptions made in these realizations, is far less than the excavation height or width.

BIBLIOGRAPHY

Board of Regents, 1976, the University of Texas System, Retrieved from http://www.lib.utexas.edu/maps/atlas_texas/vegetation_regions.jpg

Boykova, Aatoaneta, 1999, "Moho discontinuity in Central Balkan Peninsula in the Light of the Geostatistical Structural Analysis," Physics of the Earth and Planetary Interiors, vol. 114, issues 1-2, pp. 49-58.

Chertkov, V. Y., 2005, "Some Possible Interconnections between Shrinkage Cracking and Gilgai," *Australian Journal of Soil Research*, vol. 43, pp. 67-71.

Chiles, J.-P., and Delfiner, P., 1999, *Geostatistics: Modeling Spatial Uncertainty*, New York: Wiley and Sons.

Cook-Joyce, Inc., 2007, Byproduct Material Landfill License Application No. R070516, Section2, Appendix 2.6.1.

Cressie, Noel A.C., 1993, *Statistics for Spatial Data*, Revised Edition, New York: John Wiley & Sons, Inc. 900 p.

Eren, M, 2005, "Origin of Stylolite Related Fractures in Atoka Bank Carbonates, Eddy County, New Mexico, U.S.A.," *Carbonates and Evaporites*, Vol. 20, Issue 1, pp. 42-49.

ESRI, 2013, *ArcGIS Desktop: Release 10*. Redlands, CA: Environmental Systems Research Institute.

Goodman, R.E., 1989, *Introduction to Rock Mechanics*, New York, John Wiley & Sons, pp. 141-178.

Holt, R.M., E. Hughes, 2008, "Report on hydrologic properties and conditions at the BPMP boreholes," Prepared for Waste Control Specialists LLC, P.O. Box 1129, Andrews, Texas.

Holt, R.M., G.E. Grisak, J.F. Pickens, D.W. Powers, J. Kuszmaul, E. E. Hughes, C. Griffith, S.L. Cook, 2010, "Conceptual Model Report," Submitted as an attachment to a letter from William P. Dornsife, WCS, to Susan Jablonski, Texas Commission on Environmental Quality, on June 24, 2010.

Holt, R.M., J. Kuszmaul, D.W. Powers, E. E. Hughes, 2011, "Subsurface Discontinuity mapping for The Feseral Waste Disposal Facility and Compact Waste Disposal Facility Landfills," attachment to letter from William P. Dornsife, WCS, to Susan Jablonski, Texas Commission on Environmental Quality, November 10, 2010.

Jin, Guohai, and Pashin, Jack C., 2007,"DFNModeler: An Efficient Discrete Fracture Network Modeler," in *Proceedings of the 2007 International Coalbed Methane Symposium*, Toronto: The Canadian Institute.

Pashin, J.C., G. Jin, Z. Cheng, C., S. Chen, and M. R. McIntyre, 2008, "Discrete Fracture Network Models for Risk Assessment of Carbon Sequestration in Coal," Final Technical Support to U.S. Department of Energy, prepared by Geological Survey of Alabama, 124 p.

Pointe, Paul R. La, Dershowitz, S.William, Foxford, Todd, 1997, "Reservoir Compartmentalization," Final Report to the U.S. Department of Energy, prepared by Golder Associates.

Spatial Climate Analysis service, 2000, Oregon State University, Retrieved from http://historymartinez.files.wordpress.com/2011/08/texas-climate-zones.png

URS Corporation, 2007, Byproduct Material Landfill License Application, No.R070516, Section2, Appendix 2.5.2.

Waste Control Specialists LLC (WCS), 2007, Byproduct Material Landfill License Application, No.R070516, Section2.

APPENDICES

APPENDIX LSIT OF FIGURES

APPENDIX LSIT OF TABLES

Appendix A

DISCONTINUITY DATA

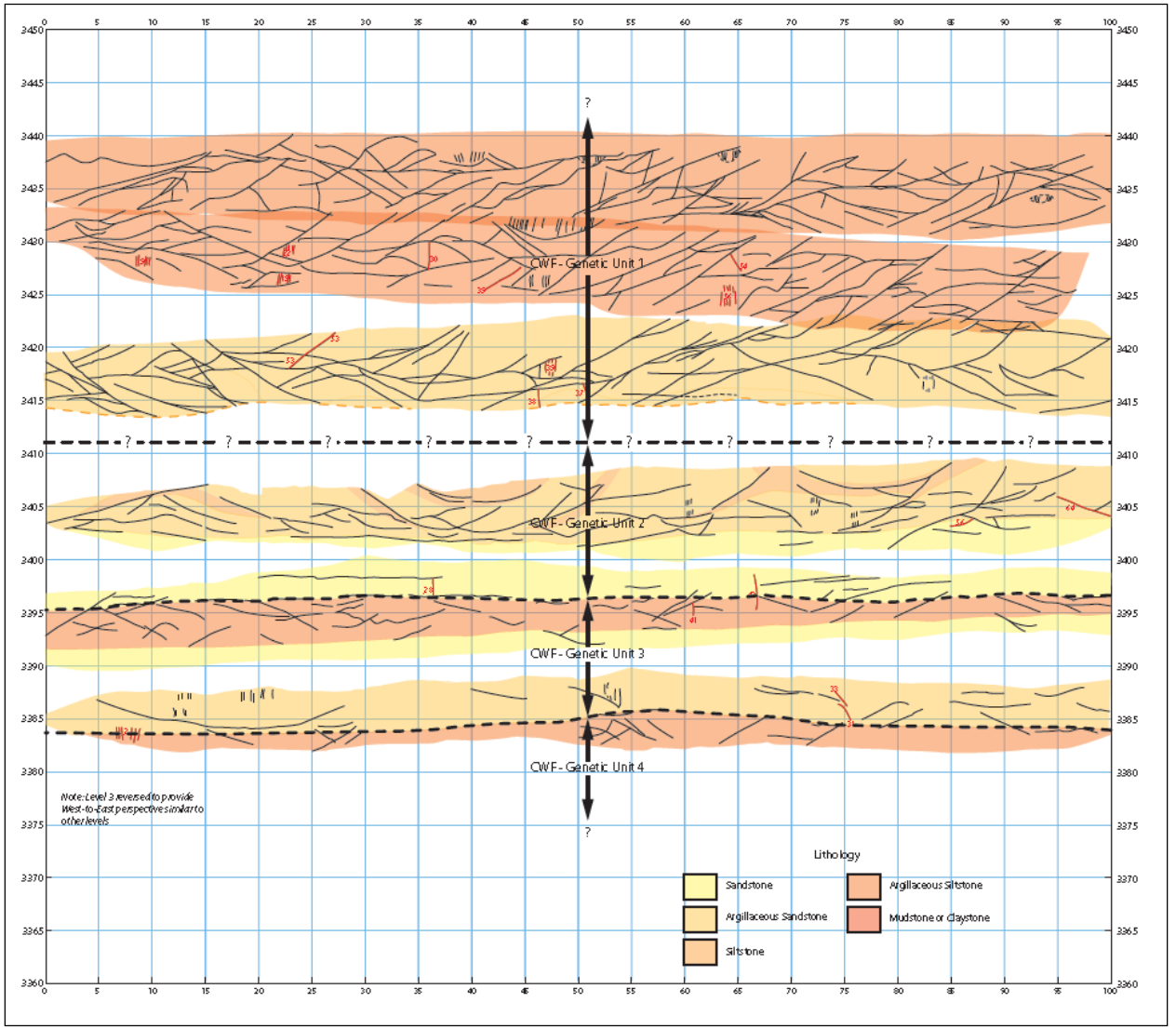

Figure A-1. Vertical Composite of the Mapped Faces on the East Side of the CWF (Holt. et al., 2010)

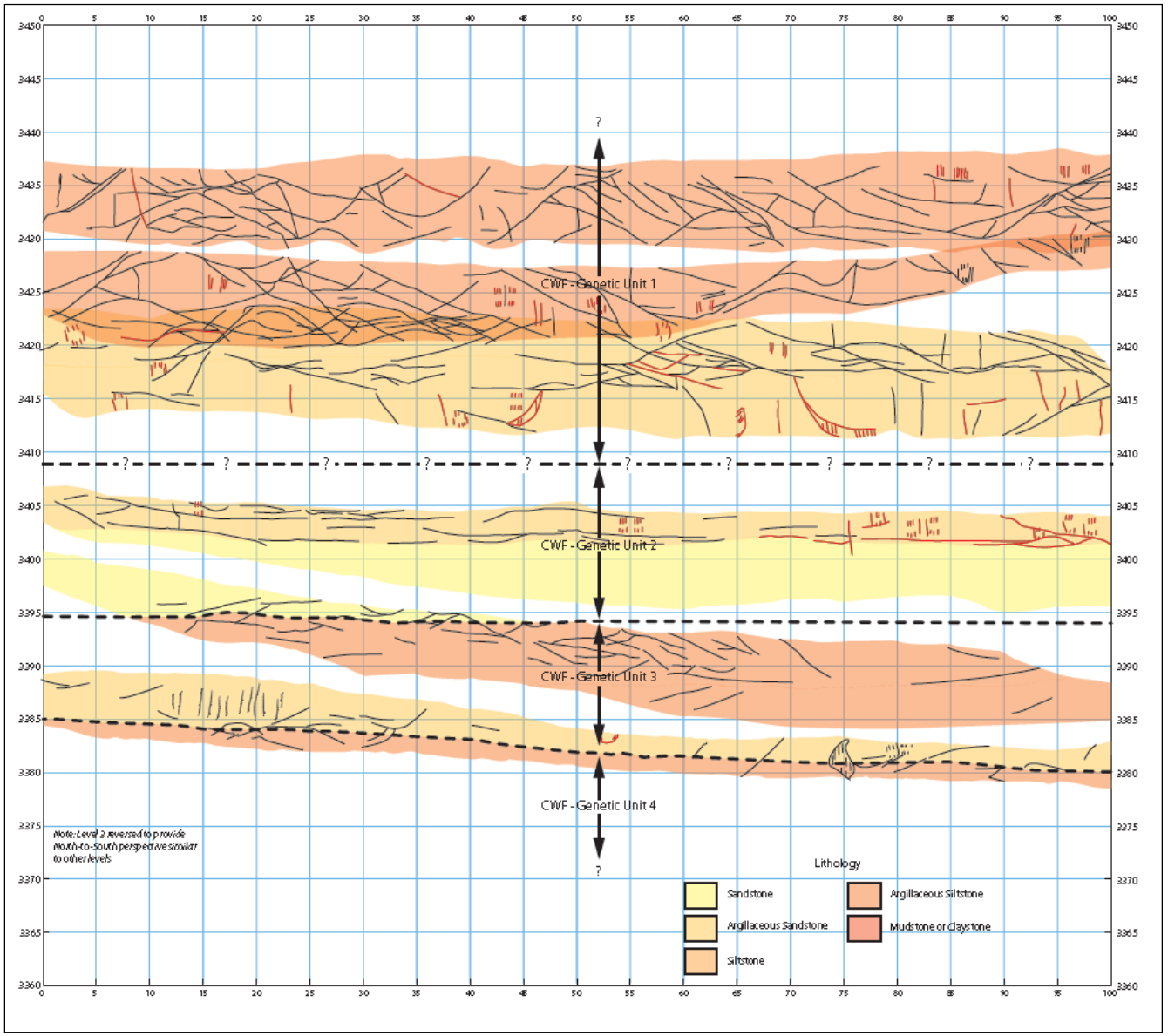

Figure A-2. Vertical Composite of the Mapped Faces on the South Side of the CWF (Holt. et al., 2010)

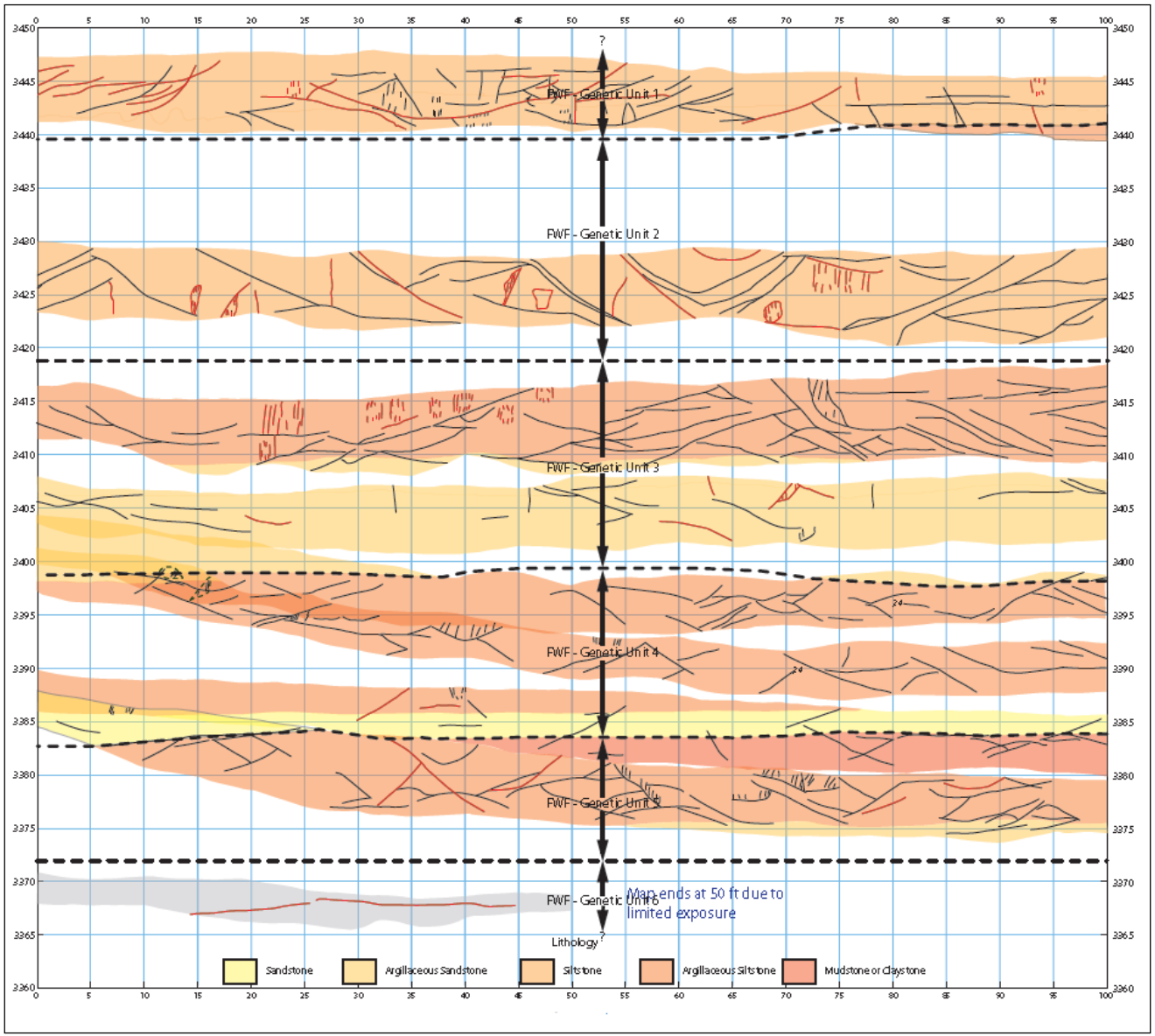

Figure A-3. Vertical Composite of the Mapped Faces on the East Side of the FWF (Holt. et al., 2010)

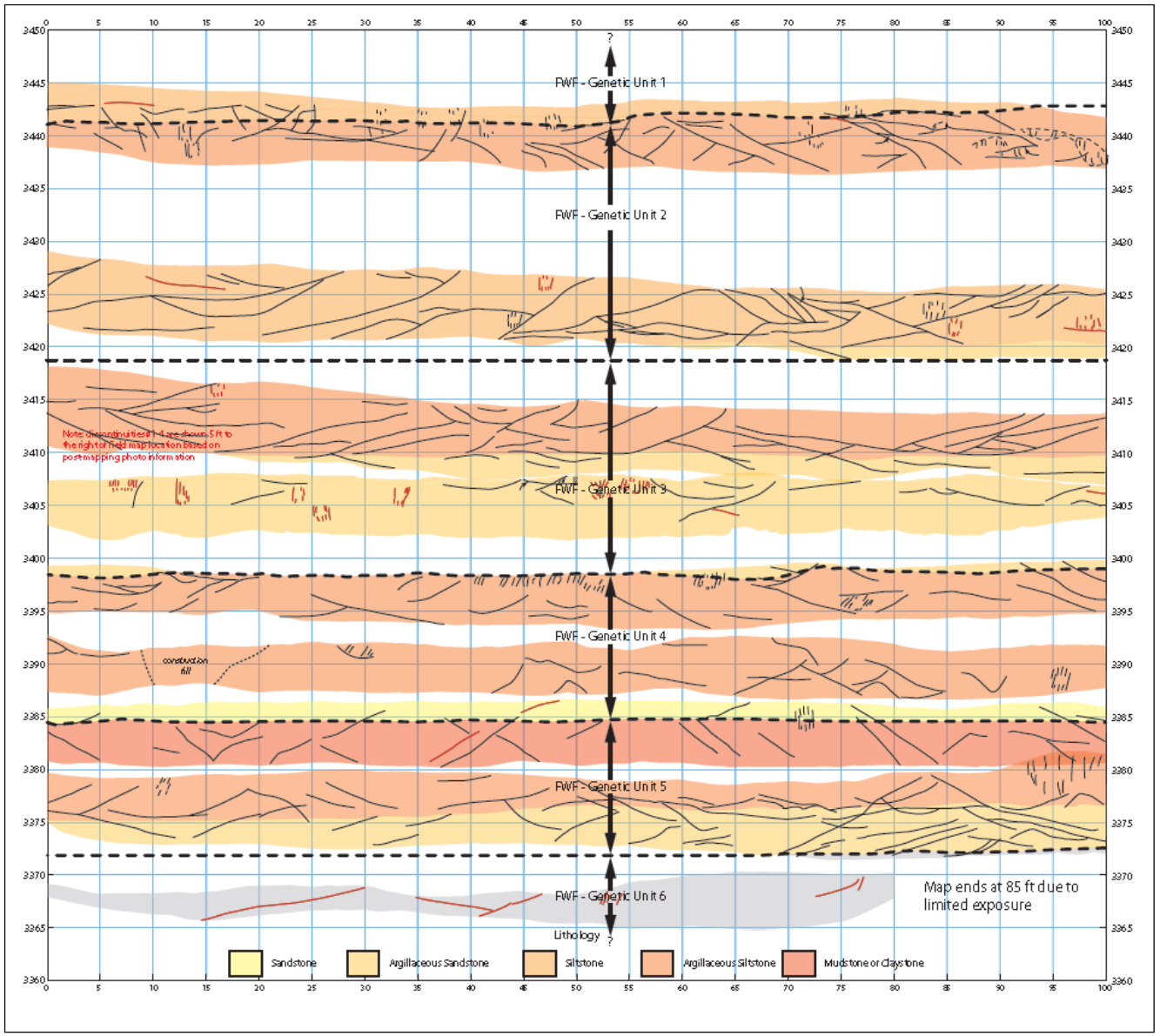

Figure A-4. Vertical Composite of the Mapped Faces on the South Side of the FWF (Holt. et al., 2010)

Table A-1 Discontinuity Data for East Face of CWF

Fracture No.	Geologic Unit	Strike (°)	Dip (°)	Curvature	Roughness	Termination	Aperture	Hydr. Sig?	Length	Genetic Unit	Xmid	Ymid
1	2	11	6S	2.5	3.5	At/in	0	0	6.44	2	91.49	3404.02
2	4	352	48E	2	2	at	0	1	9.91	1	7.70	3435.17
3	4	17	13E	1.5	2	at	0	0	5.27	1	9.59	3435.46
4	4	380	49N	2	3.5	at	0	1	4.52	1	10.37	3434.47
5	4	304	39N	1.5	3	at	0	0	3.15	1	11.98	3435.49
6	4	312	82S	1.5	4	at	0	1	1.16	1	11.86	3434.42
7	4	no single orientation		3	2	at	0	0	1.68	1	12.80	3435.32
8	4	no single orientation		2	2.5	at	0	0	3.17	1	14.04	3436.81
9	4	3	35E	2.5	2	at	0	0	8.94	1	16.54	3437.22
10	4	295	30N	1.5	2	at	0	0	10.45	1	18.18	3435.37
11	4	82	81S	1.5	3	at	0	1	2.91	1	20.05	3434.03
12	4	48	38S	2	2	at	0	0	16.67	1	30.16	3437.77
13	4	33	13S	2	3.5	at	0	0	4.42	1	24.23	3436.52
14	4	32	20E	2	2	at	0	0	4.75	1	25.99	3436.07
15	4	80	90	2	3	at	NA	1	2.56	1	25.48	3434.18
16	4	300	52S	1.5	2.5	at	0	1	8.13	1	29.00	3435.51
17	4	323	22N	2.5	3.5	at	0	0	3.56	1	28.78	3434.17
18	4	303	31S	2	2	at	0	0	5.15	1	31.37	3435.42
19	4	74	56S	3	2	at	0	0	5.37	1	31.97	3436.85
20	4	287	25N	1.5	2	at	0	0	10.07	1	37.30	3433.93
21	4	50	16N	2	2.5	at	0	0	2.93	1	36.16	3434.51
22	4	no single orientation		3	2	at	0	0	4.28	1	39.08	3437.68
23	4	39	37S	2.5	2	at	4 mm EI	0	1.38	1	38.45	3436.54
24	4	242	44N	3	2	at	0	0	12.79	1	42.86	3434.78
25	4	320	26N	1.5	2	at	0	0	2.27	1	40.89	3432.15
26	4	284	17N	2	2	at	0	0	4.58	1	45.39	3434.61
27	4	312	73N	2	2	at	0	1	2.95	1	52.28	3435.08
28	4	313	40N	2	2.5	at	0	1	3.55	1	55.38	3437.58

29	4	290	40N	2	2	at	0	1	2.42	1	56.58	3435.33
30	4	280	26N	2	3	at	0	0	7.27	1	60.77	3433.89
31	4	189	20N	3	3	at	0	0	4.76	1	59.30	3433.92
32	4	308	77N	2.5	4	at	0	0	3.21	1	59.24	3435.55
33	4	no single orientation		3	3	at	0	0	4.30	1	62.29	3433.33
34	4	56	47S	2	2.5	at	0	1	4.55	1	62.13	3434.33
35	4	320	41N	1.5	3	at	0	1	1.85	1	62.39	3435.08
36	4	46	19S	2	2	at	0	0	4.65	1	64.87	3434.13
37	4	17	33S	2.5	2 to 4	at	0	0	30.02	1	79.67	3434.96
38	4	323	32N	2.5	2	at	0	0	12.05	1	70.52	3435.34
39	4	dips to N up to 35°		3	2	at	0	0	1.90	1	65.12	3433.16
40	4	dips to N up to 35°		3	2	at	0	0	2.01	1	64.25	3433.12
41	4	dips up to ~43° to 47°		3	2	at	0	0	0.54	1	66.62	3432.64
42	4	52	25S	1.5	2.5	at	0	0	2.51	1	65.98	3432.48
43	4	323	77N	2	2.5	at	0	1	3.00	1	70.68	3437.01
44	4	320	21S	1.5	2.5	at	0	0	6.59	1	71.75	3432.37
45	4	64	27N	3	3	at	0	0	3.55	1	74.63	3437.29
46	4	too var, dips 34° to W		3	3	at	0	0	4.49	1	77.29	3436.99
47	4	294	68N	1.5	2	at	0	0	1.36	1	72.99	3433.82
48	4	268	17S	1.5	2.5	at	0	0	7.80	1	76.28	3433.47
49	4	30	29N	2.5	3.5	at	0	0	5.24	1	79.18	3432.97
50	4	71	16S	2	2	at	0	0	7.12	1	81.05	3434.51
51	4	308	19N	1.5	2.5	at	0	0	8.89	1	82.91	3433.41
52	4	280	~90	3	3.5	at	0	0	3.08	1	88.97	3434.67
53	4	300	~90	2.5	3	at	0	0	2.99	1	90.26	3435.05
54	4	variable	~40° to 120°	3	2	at	0	0	2.14	1	95.08	3436.52
55	4	345	16S	2.5	1.5	at	0	0	3.95	1	98.16	3435.43
56	4	46	29S	3	3	at	0	0	5.53	1	96.27	3434.63
57	4	296	27S	2.5	2.5	at	0	0	5.24	1	96.12	3434.51
58	4	54	46E	1.5	2	at	2mmEI	1	3.73	1	12.73	3431.15
59	4	52	38E	1.5	4	at	0	0	4.75	1	13.25	3429.83

60	4	38	30E	2	2.5	at	0	0	6.23	1	15.79	3428.93
61	4	25	22E	2	2	at	NA	0	4.08	1	18.63	3427.19
62	4	337	90	2	3	at	NA	1	1.00	1	21.90	3426.36
63	4	13	26W	1.5	2.5	at	0	0	3.15	1	22.57	3428.43
64	4	17	28W	3	3.5	at	0	0	4.67	1	26.09	3430.03
65	4	12	15N	2	3	at	0	0	10.16	1	29.02	3427.22
66	4	352	17W	2	2.5	at	0	0	8.97	1	31.34	3428.04
67	4	mound/tr	15 in dir	3.5	2.5	at	0	0	12.51	1	33.75	3428.75
68	4	87	24N	2	3.5	at	0	0	10.34	1	37.09	3427.01
69	4	330	90	1.5	2	at	0	1	2.66	1	35.98	3428.67
70	4	mound	14 in dir	3	2	at	0	0	2.85	1	37.66	3430.05
71	4	304	32S	3	2.5	at	0	0	8.26	1	42.11	3428.68
72	4	300	45N	2.5	2	at	0	0	2.25	1	41.88	3430.40
73	4	338	28N	1.5	2.5	at	0	0	4.08	1	41.83	3427.31
74	4	90	77N	2.5	2	at	0	0	1.05	1	46.75	3426.15
75	4	75	30S	2	2	at	0	0	3.45	1	44.53	3425.54
76	4	277	47N	1.5	2.5	at	0	1	2.43	1	53.40	3425.92
77	4	275	45N	1.5	2.5	at	0	1	2.10	1	53.48	3424.39
78	4	no single orientation		3	3	at	0	0	4.48	1	62.69	3429.35
79	4	no single orientation		3.5	3	at	0	0	12.03	1	67.21	3427.68
80	4	309	85N	2.5	2	at	0	1	1.89	1	64.22	3424.86
81	4	56	21S	1.5	3.5	at	0	0	2.87	1	66.90	3426.55
82	4	17	17N	2.5	3	at	0	0	2.69	1	69.31	3423.40
83	4	323	23N	3	2.5	at	0	0	12.03	1	74.30	3425.26
84	4	too variable	dips to E	3	2.5	at	0	0	8.64	1	72.59	3427.94
85	4	326	37E	2	2.5	at	1mEI	0	2.49	1	70.43	3425.60
86	4	52	28E	2	2	at	0	0	2.67	1	74.25	3427.76
87	4	73	20E	2.5	2	at	0	0	4.77	1	74.81	3424.53
88	4	90	47N	2	2.5	at	0	1	3.30	1	74.70	3423.50
89	4	320	24E	2	2.5	at	0	0	2.60	1	80.53	3427.77
90	4	no single orientation		5	3.5	at	0	0	2.07	1	80.21	3425.39

91	4	294	40N	3.5	3	at	0	0	3.19	1	81.05	3424.82
92	4	308	3N	2.5	3.5	at	0	0	3.26	1	79.87	3422.20
93	4	277	34N	2	2.5	at	0	0	1.42	1	78.89	3421.90
94	4	27	37E	2.5	3.5	at	0	0	6.02	1	84.41	3423.62
95	4	88	29N	1.5	4	at	0	0	1.67	1	85.75	3423.37
96	4	17	39E	2.5	3.5	at	0	0	3.18	1	92.39	3428.52
97	4	272	27S	1.5	3.5	at	0	0	1.42	1	92.53	3427.90
98	2	283	15S	4	3	at	0	0	3.06	1	4.04	3417.43
99	2	near level		2.5	3.5	at	0	0	8.95	1	4.62	3421.27
100	2	321	26S	4	3	at	0	0	10.15	1	9.86	3416.74
101	2	309	19S	3	2.5	at	0	0	6.03	1	7.74	3416.77
102	2	340	18S	1.5	1.5	at	0	0	2.44	1	12.40	3417.97
103	2	22	4S	2	2.5	at	0	0	3.21	1	11.08	3421.68
104	2	235	88S	2	3	at	0	1	1.34	1	17.01	3416.46
105	2	1	22W	2.5	3	at	0	0	17.99	1	17.56	3416.91
106	2	359	34S	2	2	at	0	0	1.65	1	18.49	3417.73
107	2	83	80N	2	2	at	0	1	1.91	1	22.43	3418.26
108	2	280	35S	2.5	2.5	at	0	0	14.26	1	28.96	3417.67
109	2	34	22N	3	3.5	at	0	0	2.52	1	32.77	3420.90
110	2	15	21N	2	2	at	0	0	9.43	1	38.70	3417.71
111	2	339	39N	1.5	3	at	0	0	2.33	1	39.62	3419.07
112	2	68	40N	2.5	2	at	0	0	5.35	1	40.89	3419.06
113	2	320	47N	2	1.5	at	0	1	2.25	1	46.00	3416.88
114	2	320	11S	1.5	2	at	0	0	3.72	1	48.66	3417.47
115	2	54	13S	3	1.5-2.5	at	0	0	3.20	1	50.16	3416.84
116	2	5	16S	5	3	at	0	0	23.79	1	58.62	3417.46
117	2	322	84N	2	1.5-3	at	0	1	1.61	1	53.65	3415.19
118	2	58	84S	2	2	at	0	1	1.49	1	52.41	3418.04
119	2	76	76S	1.5	1.5	at	0	1	1.19	1	53.63	3417.68
120	2	flat		2	2	at	0	0	2.59	1	53.12	3417.12
121	2	355	20S	3	2-3.0	at	0	0	3.65	1	55.66	3417.01

122	2	110	32S	5	2-3.0	at	0	0	24.54	1	67.11	3419.36
123	2	295	20W	3	3	at	0	0	6.78	1	63.21	3417.00
124	2	53	16N	3	2.5	at	0	0	19.15	1	73.78	3419.77
125	2	60	18N	2	2.5	at	0	0	3.93	1	67.48	3419.39
126	2	317	29S	2.5	2	at	0	0	8.77	1	70.52	3416.28
127	2	6	20N	3	1.5	at	0	0	6.84	1	73.45	3416.78
128	2	75	38N	2	1.5	at	0	0	4.11	1	76.42	3417.15
129	2	20	29N	2.5	2.5	at	0	0	2.52	1	78.95	3418.59
130	2	300	18N	2.5	2	at	0	0	5.10	1	85.83	3418.50
131	2	no single orientation		2.5	2	at	0	0	5.48	1	83.85	3417.54
132	2	322	23S	1.5	2	at	0	0	3.90	1	82.92	3415.42
133	2	28	30N	2	2.5	at	0	0	5.12	1	85.62	3414.49
134	2	343	25S	3	3	at	0	0	11.97	1	89.94	3416.58
135	2	297	24N	2	1.5	at	0	0	2.98	1	87.66	3418.40
136	2	280	24N	2	2.5	at	0	0	5.05	1	89.55	3418.52
137	2	103	12	4	3	at	0	0	5.12	1	93.69	3414.55
138	2	321	16N	3.5	2	at	0	0	5.60	1	97.23	3415.42
139	2	278	33S	2	2	at	0	0	2.51	1	96.79	3416.48
140	2	303	20N	1.5	3	at	0	0	1.46	1	99.27	3417.69
141	2	322	27N	1.5	2.5	at	0	0	2.77	2	3.14	3403.27
142	2	13	18N	2	3	at	0	0	4.60	2	4.89	3402.75
143	2	314	40N	2	2.5	at	0	1	2.91	2	8.83	3405.18
144	2	94	10S	2.5	3.5	at	0	0	5.64	2	24.17	3403.45
145	2	326	6S	3	3	at	0	0	2.23	2	21.82	3402.76
146	2	86	18S	3	3	at	0	0	2.82	2	23.39	3403.08
147	2	322	14N	3	3	at	0	1	2.91	2	26.21	3404.38
148	2	303	19S	2.5	2.5	at	0	0	2.53	2	27.39	3403.91
149	2	290	18	3	3.5	at	0	0	5.98	2	31.36	3403.57
150	2	320	10S	3	2.5	at	0	0	9.93	2	41.09	3403.94
151	4	299	17S	2.5	2	at	0	0	3.23	2	37.63	3405.83
152	2	354/78	33S/34N	4	3	at	0	0	8.95	2	50.38	3403.65

153	2	316	44N	2	2	at	0	1	2.26	2	62.04	3403.27
154	2	25	16S	4	2.5	at	0	0	12.18	2	63.88	3403.88
155	2	31	90	2	3	at	0	1	1.62	2	71.90	3404.99
156	2	308	38N	3	3.5	at	0	1	5.50	2	76.91	3403.78
157	4	83	26S	3	2.5	at	0	0	3.53	2	79.44	3406.26
158	2	76	7S	4	2	at	0	0	2.26	2	81.48	3405.01
159	2	305	29N	3.5	2.5	at	0	1	7.15	2	88.45	3405.66
160	1	74	36N	4	3	at	0	1	2.20	2	86.01	3403.45
161	1	82	22S	3	2.5	at	0	0	6.53	2	89.17	3403.62
162	2	46	20S	3.5	3.5	at	0	1	2.27	2	88.66	3404.75
163	1	287	76S	3	3	at	0	1	1.06	2	89.24	3403.48
164	2	82	39N	3	3	at	0	1	4.56	2	90.87	3406.10
165	1	277	90	2	2	at	0	1	1.61	2	36.37	3397.40
166	5	257	12N	3	2.5	at	0	0	4.19	3	4.65	3393.71
167	5	320	32S	4	2.5	at	0	0	5.52	3	6.68	3394.40
168	5	345	20S	2.5	2	at	0	0	2.40	3	24.48	3393.97
169	5	297	23S	3	1.5	at	0	0	2.79	3	28.56	3394.61
170	5	286	90	1.5	1.5	at	0	1	1.11	3	60.79	3395.32
171	5	346	25S	2.5	2	at	0	0	2.63	3	62.20	3395.39
172	1	78	86E	1.5	3	at	0	1	2.40	3	91.85	3393.98
173	1	314	30N	2	2	at	0	0	3.30	3	90.54	3394.08
174	5	35	36S	2	3	at	0	0	5.28	3	94.64	3395.80
175	5	too var		2.5	3	at	0	0	4.23	3	97.88	3395.69
176	2	11	21S	1.5	4.5	at	3 mm EI	0	4.79	3	69.74	3387.80
177	4	46	28E	3	2	at	0	0	3.80	4	52.08	3383.71
178	4	89	32N	1.5	2.5	at	0	0	1.14	4	52.97	3384.40
179	4	337	50N	1.5	2	at	0	1	3.06	4	53.53	3383.40
180	4	309	34S	1.5	3	at	0	0	2.90	4	57.77	3384.07
181	4	58	32N	2	3	in	0	0	4.28	1	10.69	3433.48
182	4	39	31S	3	3.5	in	0	0	9.98	1	21.90	3432.71
183	4	272	41N	2.5	2.5	in	0	0	3.59	1	34.96	3437.42

184	4	292	46N	2.5	2.5	in	0	0	1.46	1	38.70	3433.22
185	4	302	30S	2.5	3.5	in	0	0	2.11	1	42.29	3437.35
186	4	variable	~NW, 20-30°	3	3	in	0	0	2.90	1	42.87	3437.60
187	4	335	41N	2.5	3	in	0	0	2.02	1	52.73	3433.61
188	4	4	40E	1.5	3	in	0	1	6.37	1	55.78	3437.46
189	4	no single orientation		3	3	in	0	0	13.80	1	60.39	3431.93
190	4	73	28S	1.5	2	in	0	0	3.50	1	68.49	3431.95
191	4	300	12S	2	2	in	0	0	3.91	1	76.79	3432.18
192	4	too variable	dips to E	3	3	in	0	0	4.13	1	79.10	3436.54
193	4	84	26S	2	2	in	0	0	1.99	1	80.93	3436.11
194	4	310	18N	2	2	in	0	0	4.28	1	84.68	3436.67
195	4	337	25S	3	2	in	0	0	3.01	1	84.69	3436.18
196	4	75	34N	3.5	3	in	0	0	6.54	1	86.10	3433.15
197	4	111	76N	2.5	2.5	in	0	0	1.22	1	87.80	3436.42
198	4	51	34S	2	3	in	0	0	2.06	1	87.70	3431.32
199	4	304	27S	2	1.5	in	0	0	5.97	1	91.60	3436.41
200	4	307	24S	2.5	3	in	0	0	1.72	1	91.44	3437.17
201	4	342	28N	3	2	in	0	0	5.12	1	95.00	3437.50
202	4	50	24N	3	3.5	in	0	0	0.51	1	94.00	3434.04
203	4	82	13E	2	2	in	0	0	4.42	1	3.46	3430.48
204	4	variable	49N	4	2.5	in	0	0	14.40	1	11.06	3428.15
205	4	347	39N	4	3	in	0	0	7.97	1	7.59	3429.81
206	4	0	83E	1.5	2.5	in	NA	1	0.95	1	8.77	3428.17
207	4	285	30S	1.5	3.5	in	0	0	2.57	1	11.57	3427.74
208	4	42	34E	2.5	2	in	0	0	4.92	1	16.81	3430.92
209	4	280	32N	3	2.5	in	0	0	1.93	1	18.32	3426.13
210	4	302	29S	2	2	in	0	0	1.82	1	23.47	3431.15
211	4	0	11W	2	3	in	0	0	2.62	1	36.82	3425.85
212	4	72	18N	2.5	2.5	in	0	1	3.92	1	42.96	3426.52
213	4	321	34N	2	2.5	in	0	0	2.55	1	44.74	3426.61
214	4	320	10N	2	2	in	0	0	10.64	1	56.48	3426.30

215	4	279	20N	2.5	2	in	0	0	3.30	1	60.74	3423.86
216	4	189	90	1.5	2	in	0	1	1.99	1	64.81	3427.98
217	4	308	36E	3	2	in	0	0	2.57	1	66.78	3428.64
218	4	320	40N	2	3.5	in	0	1	6.00	1	67.59	3425.20
219	4	327	44N	2	2.5	in	0	1	1.90	1	70.43	3426.26
220	4	287	32E	3	2	in	0	0	3.58	1	80.71	3426.29
221	4	64	77E	3.5	2.5	in	0	0	1.87	1	80.86	3425.94
222	4	280	6N	2.5	3.5	in	0	0	11.67	1	89.36	3426.98
223	4	38	8E	2	3.5	in	0	0	3.63	1	84.73	3423.03
224	4	26	58E	3	3	in	0	0	2.35	1	91.58	3425.16
225	2	242	17N	2.5	3	in	0	0	10.64	1	40.50	3415.51
226	2	328	40N	2	3	in	0	1	8.81	1	41.08	3416.72
227	2	282	66S	2.5	2.5	in	0	1	1.40	1	49.27	3415.84
228	2	57	17N	2	2.5	in	0	0	3.94	1	53.41	3418.33
229	2	305	17S	1.5	1.5	in	0	0	9.07	1	89.22	3415.14
230	2	307	22S	2	1.5-2	in	0	1	5.98	1	86.93	3417.20
231	2	30	18N	3	2.5	in	0	0	5.34	1	95.32	3414.83
232	2	34	40S	3	3	in	0	0	12.04	2	8.64	3403.43
233	2	298	29S	2.5	3	in	0	0	2.51	2	10.96	3404.89
234	2	336	16S	2.5	3	in	0	0	7.26	2	14.48	3404.69
235	2	285	14S	2	3	in	0	0	5.08	2	12.46	3402.21
236	2	303	21S	2	2.5	in	0	0	3.02	2	16.54	3402.69
237	2	281	40S	2.5	2.5	in	0	1	21.74	2	33.88	3401.99
238	2	110	17	3	3.5	in	0	0	9.00	2	29.42	3404.35
239	2	34	23S	3.5	3.5	in	0	0	5.03	2	36.85	3404.36
240	2	15	37S	3	2	in	0	0	2.75	2	37.28	3402.41
241	2	111	35N	3	3	in	0	0	3.70	2	45.71	3402.40
242	2	274	24N	2	3.5	in	0	0	3.56	2	48.08	3405.04
243	2	276	26N	3	3	in	0	0	10.08	2	55.59	3406.18
244	2	21	26N	3	3	in	0	0	10.81	2	57.04	3404.36
245	2	23	9N	3	3.5	in	0	0	12.96	2	56.38	3401.78

246	2	274	84N	1.5	1.5	in	0	1	1.44	2	60.19	3404.80
247	2	288	21S	2.5	2.5	in	0	0	5.61	2	68.43	3404.32
248	2	15	10S	2	2	in	0	0	4.25	2	70.83	3402.58
249	1	23	21S	2	2.5	in	0	0	3.13	2	70.46	3401.50
250	4	70	23S	2.5	3.5	in	0	1	5.48	2	73.10	3406.02
251	2	247	15N	2.5	3	in	0	0	4.51	2	76.13	3402.62
252	2	316	20N	2.5	2.5	in	0	0	4.43	2	79.68	3403.51
253	2	51	25N	4	2.5	in	0	0	3.02	2	81.02	3405.13
254	1	77	16S	2	2	in	0	0	4.50	2	85.56	3402.65
255	2	47	13S	3.5	3	in	0	0	5.36	2	97.49	3405.00
256	1	279	19N	3.5	2	in	0	0	3.64	2	7.44	3395.51
257	1	22	10S	2.5	3	in	0	0	3.84	2	8.26	3396.53
258	1	294	30N	2	1.5	in	0	0	5.16	2	59.05	3395.67
259	1	278	90	2.5	2	in	0	0	3.30	2	66.60	3396.92
260	1	350	40N	1.5	1.5	in	0	0	1.58	2	73.30	3396.63
261	1	333	8N	2.5	2.5	in	0	0	13.39	2	78.43	3396.54
262	1	314	12N	2	1.5	in	0	0	2.25	2	76.03	3397.22
263	5	318	32N	2	2.5	in	0	0	3.67	3	4.70	3393.47
264	5	119	12	5	3	in	0	0	3.44	3	10.78	3393.02
265	5	318	23S	2.5	3	in	0	0	2.41	3	10.31	3393.14
266	5	292	29S	2.5	2.5	in	0	0	4.63	3	12.67	3395.06
267	5	299	26N	2.5	3	in	0	0	4.35	3	15.41	3392.76
268	5	297	10S	2.5	2	in	0	0	3.88	3	15.98	3396.20
269	5	56	42S	3.5	3	in	0	0	7.20	3	19.33	3395.24
270	5	297	24S	2.5	2	in	0	0	4.92	3	21.00	3395.40
271	5	84	18S	2	2	in	0	0	2.23	3	21.25	3392.52
272	5	14	17N	2.5	2.5	in	0	0	4.43	3	23.78	3394.60
273	5	62	1S	2	1.5	in	0	0	3.74	3	23.20	3396.32
274	5	60	17S	2	2	in	0	0	1.98	3	25.95	3395.70
275	5	300	30N	3.5	3.5	in	0	0	4.40	3	29.06	3394.29
276	5	317	23N	3.5	2	in	0	0	2.51	3	28.53	3395.42

277	5	27	11S	2.5	2	in	0	0	2.47	3	28.58	3396.03
278	5	21	12N	1.5	1.5	in	0	0	5.41	3	30.76	3396.64
279	5	276	19N	3	3	in	0	0	7.01	3	33.94	3394.89
280	5	300	27N	3	2	in	0	0	3.73	3	34.41	3393.10
281	5	68	12S	2	1.5	in	0	0	9.63	3	38.94	3396.58
282	5	301	11S	2	2	in	0	0	4.39	3	38.66	3395.59
283	5	81	36S	3	2.5	in	0	0	3.24	3	43.30	3394.37
284	5	52	4S	2	1.5	in	0	0	3.05	3	47.58	3395.93
285	1	8	32N	3	2	in	0	0	5.84	3	49.61	3392.67
286	5	313	29N	2	1.5	in	0	0	1.92	3	49.19	3393.34
287	5	296	14S	3.5	2	in	0	0	3.31	3	53.03	3395.68
288	5	40	14N	2	2	in	0	0	3.27	3	56.06	3397.49
289	5	341	25N	3	1.5	in	0	0	2.04	3	56.04	3396.22
290	5	86	39S	2.5	1.5	in	0	0	4.57	3	57.43	3394.50
291	5	24	40S	2.5	3.5	in	0	0	3.16	3	57.64	3393.49
292	5	305	26N	2	2	in	0	0	4.94	3	60.27	3395.83
293	5	314	15S	2.5	2	in	0	0	4.80	3	69.23	3395.83
294	5	320	29N	2	2.5	in	0	0	3.42	3	75.20	3394.88
295	5	303	19N	1.5	2.5	in	0	0	5.57	3	82.16	3395.77
296	5	1	15W	2	2	in	0	0	4.33	3	91.34	3395.80
297	2	22	73W	1.5	3.5	in	0	1	0.44	3	13.42	3387.15
298	2	11	73W	1.5	3.5	in	0	1	0.64	3	13.08	3385.66
299	2	23	87W	1.5	3.5	in	0	1	0.91	3	19.36	3387.24
300	2	17	78W	1.5	3.5	in	0	1	0.93	3	20.57	3387.40
301	2	26	44E	3	2.5	in	0	0	3.27	3	27.24	3384.54
302	2	83	48S	2.5	2	in	0	0	5.07	3	51.48	3387.09
303	2	no single orientation		4	4	in	3 mm EI	0	4.11	3	68.70	3387.71
304	2	49	83S	1.5	3.5	in	0	1	1.92	3	75.04	3385.66
305	2	352	21S	2	4.5	in	1 mm EI	0	1.98	3	73.60	3387.05
306	2	61	83S	1.5	4	in	0	1	1.75	3	74.72	3386.96
307	2	323	29N	2.5	4	in	0	0	4.59	3	78.87	3385.70

308	2	17	36W	2	4.5	in	2 mm EI	0	3.93	3	88.06	3387.47
309	2	29	4W	3.5	4	in	0	0	7.62	3	88.72	3386.53
310	2	310	13S	1.5	3.5	in	0	0	5.08	3	90.12	3384.60
311	2	55	27N	3.5	4.5	in	4 mm EI	0	4.66	3	95.26	3387.71
312	2	0	23W	1.5	4.5	in	0	0	3.19	3	98.46	3386.14
313	4	48	53W	3.5	2.5	in	0	0	1.28	4	8.43	3383.46
314	4	87	76S	2	1.5	in	0	1	4.53	4	17.40	3383.32
315	4	276	54S	2	1.5	in	0	1	2.28	4	26.29	3383.42
316	4	12	51E	2	2.5	in	0	1	4.71	4	27.14	3383.16
317	4	349	23E	1.5	3.5	in	0	0	1.71	4	28.90	3383.19
318	4	347	33W	2	3	in	0	0	2.90	4	53.53	3385.54
319	4	44	23W	1.5	2	in	0	0	2.48	4	51.29	3383.55
320	4	43	32S	2	2	in	0	0	4.44	4	55.35	3384.00
321	4	63	36S	2.5	2	in	0	0	2.35	4	55.35	3384.30
322	4	22	15W	1.5	4.5	in	0	0	2.66	4	57.18	3385.79
323	4	328	22E	1.5	3	in	0	0	5.27	4	65.57	3384.07
324	4	353	20S	2.5	2	in	0	0	4.18	4	69.94	3383.29
325	4	34	28E	1.5	2.5	in	0	0	2.35	4	73.19	3384.46
326	4	283	36N	1.5	3	in	0	0	4.01	4	73.19	3383.63
327	4	331	43N	1.5	2.5	in	0	1	4.42	4	80.33	3385.03
328	4	30	43E	4.5	1.5	in	0	0	5.77	4	95.90	3383.77
329	4	38	22W	4	2.5	obs	0	0	15.00	1	7.54	3437.96
330	4	350	13E	2	2.5	obs	0	0	15.45	1	8.14	3436.06
331	4	312	12W	2.5	3	obs	NA	0	5.09	1	17.57	3437.80
332	4	no single orientation		3	3	obs	0	0	7.64	1	20.62	3438.14
333	4	281	36N	2	2	obs	0	0	3.99	1	21.47	3439.08
334	4	73	30N	2.5	2	obs	0	0	6.85	1	31.66	3438.15
335	4	353	33S	2.5	2	obs	0	0	4.21	1	27.28	3438.44
336	4	284	30N	2	2.5	obs	0	0	5.20	1	34.14	3437.46
337	4	28	32E	1.5	3	obs	0	0	22.95	1	43.07	3435.76
338	4	48	35N	3	2.5	obs	NA	0	1.00	1	39.97	3437.97

339	4	72	38N	3.5	2.5	obs	0	0	18.39	1	48.85	3436.01
340	4	24	43N	3	3	obs	0	0	0.55	1	51.69	3437.74
341	4	283	22N	2	3	obs	0	0	17.16	1	57.30	3435.60
342	4	no single orientation		4	1.5	obs	0	0	17.26	1	58.77	3435.20
343	4	300	57N	2.5	3.5	obs	0	0	3.19	1	56.52	3436.95
344	4	dips ~30° to 300°		3	3	obs	0	0	0.91	1	64.53	3438.13
345	4	90	21S	2.5	2.5	obs	0	0	5.96	1	69.92	3431.86
346	4	287	16S	2.5	2	obs	0	0	4.18	1	72.65	3435.46
347	4	325	24N	1.5	3	obs	0	0	16.55	1	90.63	3433.89
348	4	32	22W	2	3	obs	NA	0	7.58	1	3.74	3431.94
349	4	variable	36E	2.5	4	obs	0	0	7.93	1	6.78	3432.30
350	4	no single orientation		4	3.5	obs	0	0	9.84	1	7.69	3431.70
351	4	no single orientation		5	2.5	obs	0	0	21.76	1	22.07	3432.71
352	4	85	31S	2.5	2.5	obs	0	0	5.78	1	7.38	3427.37
353	4	mound	13	3.5	2.5	obs	0	0	4.98	1	21.54	3426.33
354	4	333	34E	1.5	3.5	obs	0	0	5.35	1	21.05	3425.91
355	4	284	32N	1.5	3	obs	0	0	9.64	1	22.62	3430.21
356	4	60	88S	3	4	obs	NA	1	0.75	1	22.43	3429.02
357	4	300	30N	2	2	obs	0	0	6.54	1	34.65	3430.28
358	4	303	23S	2.5	2.5	obs	0	0	5.06	1	43.91	3430.16
359	4	328	25S	1.5	2.5	obs	0	0	4.80	1	45.09	3430.13
360	4	302	30 in dir	3	3.5	obs	NA	0	1.56	1	48.29	3431.25
361	4	43	31S	4	3	obs	0	0	16.69	1	51.77	3429.64
362	4	303	37N	2	3	obs	0	0	11.32	1	50.91	3428.11
363	4	54	25N	2	3.5	obs	0	0	16.95	1	55.25	3428.01
364	4	304	21N	2.5	2.5	obs	0	0	9.42	1	62.35	3428.61
365	4	304	42N	1.5	2	obs	0	1	11.51	1	61.86	3427.15
366	4	46	35N	3	2.5	obs	0	0	17.83	1	74.68	3425.77
367	4	324	40N	2.5	3	obs	0	0	5.12	1	69.81	3428.97
368	4	323	36N	1.5	4	obs	0	0	14.50	1	78.55	3425.68
369	4	268	35E	2.5	2.5	obs	0	0	19.74	1	87.03	3423.52

370	4	330	30N	1.5	2	obs	0	0	4.56	1	90.10	3421.73
371	4	313	20N	2	2.5	obs	0	0	11.64	1	90.60	3425.65
372	4	306	32N	2.5	3.5	obs	0	0	2.24	1	92.24	3427.17
373	4	no single orientation		4	3.5	obs	0	0	4.11	1	93.33	3424.64
374	4	33	18W	2.5	4	obs	0	0	3.02	1	93.52	3423.48
375	2	328	20N	1.5	2	obs	0	0	6.86	1	3.25	3414.39
376	2	87	24N	4.5	3	obs	0	0	10.68	1	5.25	3419.57
377	2	85	32S	3	2.5	obs	0	0	1.34	1	6.89	3421.97
378	2	290	14N	3	3	obs	0	0	10.10	1	12.82	3420.08
379	2	306	33N	2.5	3	obs	0	0	2.84	1	13.64	3421.79
380	2	292	30N	3.5	3	obs	0	0	7.61	1	18.66	3421.24
381	2	311	28N	3	3	obs	0	0	11.39	1	22.06	3420.56
382	2	305	25N	2	2.5	obs	0	0	24.53	1	31.13	3418.49
383	2	323	16N	3	3	obs	0	0	5.92	1	29.96	3422.00
384	2	358	33N	3.5	2.5	obs	0	0	9.48	1	34.84	3420.49
385	2	4	22S	2.5	1.5	obs	0	0	7.68	1	36.46	3420.88
386	2	377	16N	3.5	3	obs	0	0	14.15	1	43.51	3417.70
387	2	84	46N	1.5	2	obs	0	1	2.93	1	38.75	3420.66
388	2	357	34E	1.5	3	obs	0	0	5.22	1	42.11	3421.73
389	2	339	30N	1.5	1.5-3.5	obs	0	0	19.61	1	50.24	3418.35
390	2	310	55N	2.5	3	obs	0	0	7.83	1	62.64	3418.16
391	2	386	36N	3	2	obs	0	0	5.71	1	63.12	3420.02
392	2	288	38N	2	2-2.5	obs	0	0	9.16	1	65.19	3419.80
393	2	312	35N	1.5	2	obs	0	1	5.42	1	74.96	3419.67
394	2	78	35S	2	2	obs	0	0	12.27	1	79.62	3417.72
395	2	100	23E	3	2	obs	0	0	8.48	1	79.24	3420.41
396	2	315	46S	1.5	2	obs	0	1	6.07	1	84.17	3416.71
397	2	312	31S	2.5	1.5	obs	0	0	4.59	1	86.22	3419.12
398	2	307	19S	2.5	2	obs	0	0	11.53	1	94.79	3416.03
399	2	273	25N	2	2.5	obs	0	0	5.88	1	94.43	3419.10
400	2	305	24N	1.5	2.5	obs	0	0	3.86	1	95.83	3419.38

401	2	80	39S	3	3	obs	0	0	5.55	1	96.31	3417.63
402	2	104	23	3	2.5	obs	0	0	2.80	1	98.72	3416.39
403	4	294	16N	2	4	obs	0	0	15.47	2	7.71	3405.26
404	2	264	18S	2.5	3	obs	0	0	5.15	2	18.73	3404.87
405	4	317/318	32S/39N	5	3.5	obs	0	1	13.12	2	36.17	3405.81
406	4	52	26S	2	2.5	obs	0	0	5.24	2	37.44	3406.44
407	4	313	22N	2.5	3	obs	0	0	6.50	2	43.30	3406.20
408	4	277	38N	3	3.5	obs	0	1	7.91	2	48.88	3405.14
409	2	275	33N	5	4	obs	0	0	3.70	2	50.19	3407.10
410	4	286	34N	3	3.5	obs	0	0	6.67	2	65.28	3406.71
411	4	77	18S	2.5	3	obs	0	0	14.20	2	77.89	3408.71
412	2	287	90	2.5	2.5	obs	0	1	1.16	2	75.73	3403.72
413	4	334	39N	4	4	obs	0	1	7.31	2	79.76	3406.13
414	1	307	20N	2.5	3.5	obs	0	1	13.47	2	84.62	3404.84
415	2	125	18	4	4	obs	0	0	4.08	2	84.92	3406.13
416	2	305	23N	2.5	3	obs	0	0	2.07	2	93.81	3405.89
417	2	70	21N	3	4	obs	0	0	5.97	2	93.77	3407.85
418	2	84	36N	3	3	obs	0	0	1.70	2	99.21	3405.00
419	1	332	15N	2.5	2	obs	0	0	17.30	2	28.60	3398.35
420	1	297	6N	2	2	obs	0	0	8.36	2	71.26	3398.05
421	1	308	11N	2	2.5	obs	0	0	6.10	2	75.21	3398.12
422	5	300	26N	2	2.5	obs	0	0	4.01	3	97.48	3396.50
423	2	41	30N	4	4	obs	0	0	23.24	3	16.47	3386.55
424	2	21	20W	1.5	4	obs	2 mm EI	0	5.29	3	42.63	3387.39
425	2	4	90	1.5	3.5	obs	0	1	1.38	3	52.89	3387.74
426	2	308	88N	1.5	3.5	obs	0	1	1.73	3	53.91	3387.02
427	1	290	42S	2	3	obs	0	1	7.63	2&3	3.30	3394.89
428	5	290	42S	2	3	obs	0	1	7.63	2&3	3.30	3394.89
429	4	65	19S	3	2	obs/at	0	0	13.45	1	92.74	3432.65

Table A-2 Discontinuity Data for South Face of CWF

Fracture No.	Geologic Unit	Strike (°)	Dip (°)	Curvature	Roughness	Termination	Aperture	Hydr. Sig?	Length	Genetic Unit	Xmid	Ymid
1	4	344	11W	1.5	2.5	at	0	0	2.32	1	8.11	3434.28
2	4	75	35S	3	2	at	<1mm EI	0	6.61	1	12.72	3434.57
3	4	307	14W	2.5	3	at	0	0	2.94	1	11.32	3434.05
4	4	no single orientation		4	3	at	0	0	8.28	1	13.95	3431.17
5	4	349	12S	2	2	at	0	0	3.19	1	13.33	3431.65
6	4	365	14S	2	3	at	0	0	4.39	1	15.79	3431.83
7	4	315	35S	3	2.5	at	0	0	3.51	1	17.77	3434.47
8	4	7	20E	1.5	3	at	1mm EI	0	2.68	1	20.93	3434.93
9	4	302	75S	3	2.5	at	2mm EI	0	5.47	1	22.87	3432.72
10	4	340	8S	1.5	2	at	0	0	3.89	1	20.34	3432.86
11	4	335	34S	2	2	at	0	0	4.39	1	21.91	3431.42
12	4	78	78S	1.5	2	at	0	1	0.88	1	21.50	3431.33
13	4	82	26N	2	2	at	not avail.	0	5.63	1	36.50	3435.01
14	4	345	22N	2	2.5	at	0	0	5.79	1	44.03	3431.25
15	4	74	28N	2	2.5	at	0	0	10.42	1	51.78	3431.49
16	4	17	90	1	2.5	at	0	1	0.15	1	52.88	3426.90
17	4	6	86E	1.5	3	at	0	1	1.95	1	50.13	3431.83
18	4	69	30N	2	2	at	0	0	8.05	1	50.36	3432.28
19	4	32	36S	2	3	at	0	0	4.13	1	52.30	3434.27
20	4	276	14S	2.5	3	at	0	0	3.91	1	51.73	3434.82
21	4	61	45N	2.5	2.5	at	0	0	7.78	1	56.47	3433.50
22	4	3	27E	2	2	at	0	0	6.95	1	60.45	3431.06
23	4	56	38W	1.5	2.5	at	0	0	4.64	1	56.67	3433.89
24	4	310	40S	1.5	2.5	at	0	1	10.14	1	61.17	3433.83
25	4	42	29N	1.5	2.5	at	0	0	3.24	1	59.80	3433.00
26	4	319	32S	2	2.5	at	0	0	7.21	1	63.76	3431.16
27	4	280	28N	2.5	2.5	at	0	0	3.92	1	67.62	3430.17
28	4	25	15E	1.5	2.5	at	0	0	2.44	1	66.36	3429.33
29	4	67	13N	1.5	2	at	0	0	16.07	1	71.54	3431.88

30	4	no single orientation		2.5	2.5	at	0	0	11.73	1	76.38	3430.73
31	4	349	44N	2	3.5	at	0	1	2.86	1	72.78	3432.49
32	4	34	86E	2	3.5	at	0	1	1.88	1	83.45	3434.54
33	4	17	24E	3	3.5	at	0	0	9.84	1	89.53	3432.40
34	4	280	23S	2	3	at	0	0	2.60	1	88.69	3433.12
35	4	1	47E	2	3	at	0	1	1.57	1	94.25	3433.59
36	4	no single orientation		3	2.5	at	0	0	7.62	1	96.20	3432.70
37	4	311	57S	2.5	2	at	0	0	2.93	1	95.62	3432.31
38	4	28	26W	2	2.5	at	0	0	4.87	1	97.86	3431.76
39	4	78	28S	2	2.5	at	0	0	3.57	1	96.63	3433.48
40	4	349	31E	2	2	at	0	0	3.06	1	97.56	3434.43
41	4	322	47S	1.5	2	at	0	1	4.25	1	97.95	3434.20
42	4	57	17S	2	3	at	0	0	6.65	1	4.94	3423.25
43	4	40	30N	4	2	at	0	0	13.52	1	11.21	3422.91
44	4	351	16N	2.5	2.5	at	0	0	5.25	1	12.29	3420.97
45	4	83	18N	2.5	2.5	at	0	0	4.90	1	13.93	3421.23
46	4	303	40N	2.5	3.5	at	0	0	9.84	1	16.96	3424.51
47	4	278	24N	2	2.5	at	0	0	6.78	1	18.19	3421.33
48	4	no single orientation		3	2	at	0	0	1.74	1	22.76	3426.68
49	4	357	27S	2	2	at	0	0	8.68	1	25.80	3423.61
50	4	312	45N	3	3	at	0	0	5.30	1	26.09	3426.31
51	4	0	45E	3	3	at	0	0	5.25	1	27.53	3426.00
52	4	332	29S	3	2.5	at	0	0	8.01	1	30.11	3422.01
53	4	275	35S	2	3	at	0	0	4.73	1	30.96	3421.97
54	4	7	75S	2	2.5	at	0	1	13.61	1	35.00	3424.00
55	4	4	8S	2	1.5	at	0	0	1.79	1	31.73	3425.70
56	4	351	78S	1.5	3	at	0	1	3.35	1	35.29	3422.40
57	4	330	78S	1.5	3	at	0	1	2.52	1	37.92	3421.78
58	4	336	78S	1.5	2	at	0	1	4.76	1	40.21	3421.47
59	4	too high to measure		2	2.5	at	0	0	3.60	1	41.22	3426.82
60	4	300	21N	3	3	at	0	0	2.90	1	53.35	3420.91

61	4	27	15	2	2.5	at	0	0	3.27	1	57.44	3423.58
62	4	23	3	4	2	at	0	0	7.12	1	60.43	3423.47
63	4	1	20S	2.5	2.5	at	0	0	2.27	1	62.77	3424.89
64	4	1	20S	2.5	2.5	at	0	0	2.06	1	62.84	3424.57
65	4	too varib.	toward N	5	2.5	at	0	0	12.76	1	70.02	3423.42
66	4	72	24N	4.5	3.5	at	0	0	7.69	1	72.31	3427.03
67	2	29	14S	2.5	3	at	0	0	4.20	1	1.78	3418.57
68	2	no single orientation		5	2	at	0	0	14.75	1	7.36	3416.97
69	2	35	20S	1.5	2	at	0	0	10.57	1	6.49	3419.26
70	2	27	30E	1.5	3	at	0	0	9.87	1	4.51	3413.93
71	2	340	35N	2.5	2	at	0	0	3.78	1	1.87	3414.71
72	2	40	85N	1.5	2.5	at	0	1	3.83	1	6.41	3415.70
73	2	no one orient. Low dip N		4	2-3	at	0	0	16.13	1	23.24	3417.55
74	2	52	88S	1.5	1.5	at	0	1	2.34	1	13.68	3412.79
75	2	84	81N	3	2	at	0	1	8.97	1	25.88	3414.59
76	2	no single orientation		3	2.5	at	0	0	11.72	1	34.45	3418.67
77	2	29	18S	2.5	2.5	at	0	0	5.18	1	35.38	3417.30
78	2	27	10S	2.5	2	at	0	1	3.10	1	35.66	3417.69
79	2	350	30N	3	2	at	0	0	1.00	1	36.25	3418.22
80	2	71	20N	3	2	at	0	0	7.41	1	37.20	3419.00
81	2	52	20N	2	2	at	0	0	2.64	1	36.54	3418.57
82	2	78	81N	2	1.5	at	0	1	5.22	1	38.82	3413.78
83	2	no single orientation		4	1.5	at	0	1	4.64	1	41.92	3418.75
84	2	78	25N	2	2	at	0	0	4.65	1	40.44	3419.20
85	2	332	14S	2	2-2.5	at	0	1	9.00	1	40.79	3417.01
86	2	43	21S	3	2	at	0	0	2.94	1	40.02	3417.58
87	2	43	87N	2	2	at	0	1	1.12	1	40.66	3416.46
88	2	30	31W	3	2	at	0	0	5.58	1	43.14	3416.95
89	2	no single orientation		3	3	at	0	0	6.74	1	44.50	3416.25
90	2	64	17S	2	2.5	at	0	0	10.73	1	49.58	3416.66
91	2	48	28N	2	2	at	0	0	1.37	1	45.52	3416.56

92	2	48	29W	2	2.5	at	0	0	2.71	1	46.22	3417.69
93	2	320	87N	3.5	2	at	0	1	4.30	1	54.86	3414.13
94	2	90	27N	2	2	at	0	0	4.75	1	61.10	3421.83
95	2	no single orientation		5	2	at	0	0	15.62	1	69.64	3420.41
96	2	33	29S	2	2.5	at	0	0	2.88	1	71.37	3421.18
97	2	73	74N	2	2.5	at	0	1	3.53	1	67.79	3414.01
98	2	no single orientation		3	3	at	0	0	6.93	1	77.17	3418.11
99	2	52	27S	2.5	2	at	0	0	3.45	1	86.29	3419.52
100	2	no single orientation		3	2.5	at	0	1	9.75	1	87.81	3420.95
101	2	342	34N	2.5	2.5	at	0	0	4.05	1	88.13	3417.81
102	2	195	6	2.5	2.5	at	0	0	4.34	2	21.97	3404.46
103	2	283	15N	2	3	at	0	0	12.37	2	32.30	3403.80
104	2	46	10N	3	2.5	at	0	0	8.92	2	44.28	3402.07
105	2	15	16	3	2.5	at	0	0	9.27	2	91.87	3401.43
106	2	327	90	2	1.5	at	0	1	1.08	2	93.29	3402.33
107	2	85	12N	2.5	2.5	at	0	0	7.09	2	94.74	3401.68
108	1	296	28S	3	2.5	at	0	0	2.76	2	35.39	3394.39
109	5	286	16N	3	3.5	at	0	0	4.28	3	24.16	3393.44
110	5	23	31	2	3.5	at	0	1	2.18	3	30.96	3394.80
111	5	347	28S	2	2.5	at	0	0	2.12	3	35.90	3393.95
112	5	0	26E	3	2.5	at	0	1	2.01	3	44.17	3393.55
113	5	320	29S	3.5	2	at	0	1	9.53	3	51.15	3391.44
114	5	53	29N	2	2	at	0	0	5.34	3	48.52	3391.11
115	5	35	29N	2.5	2.5	at	0	0	3.36	3	54.29	3392.06
116	5	44	41S	3.5	2	at	0	0	1.12	3	60.67	3389.62
117	5	87	33N	3	3	at	0	0	1.40	3	64.02	3391.59
118	2	382	30S	2	3.5	at	0	0	3.70	3	77.75	3381.11
119	2	85	29S	1.5	2.5	at	0	0	2.16	3	77.79	3381.47
120	2	300	32N	2	3	at	0	1	1.12	3	79.73	3382.01
121	4	17	27E	4	2	at	0	0	1.73	4	19.08	3383.71
122	4	351	17E	2.5	3.5	at	0	0	3.53	4	31.46	3383.23

123	4	317	32N	2	3	at	0	0	2.27	4	31.35	3383.60
124	4	352	46N	2.5	3	at	0	1	3.24	4	81.29	3380.72
125	4	70	37N	1	3.5	at	0	0	1.45	4	89.40	3379.41
126	4	est strike of mound, N (no plunge)		3	3	at/in	0	0	7.27	1	17.62	3429.80
127	2	60	3N	2	1.5	at/in	0	0	4.50	1	5.21	3417.55
128	2	no single orientation		4	2	at/in	0	0	8.75	1	23.72	3418.64
129	4	no single orientation		5	3	at/obs	0	0	15.45	1	30.49	3430.52
130	4	2	~NW, 20-30°	1.5	2	at/obs	0	0	2.92	1	32.85	3435.15
131	4	354	34E	1.5	1.5	in	0	0	7.13	1	4.81	3434.54
132	4	328	40N	3	2	in	0	0	2.52	1	8.42	3430.80
133	4	315	45N	1.5	2	in	0	1	2.94	1	11.13	3431.78
134	4	104	28S	3	1.5	in	0	0	2.65	1	13.69	3432.47
135	4	265	44N	4	3	in	0	0	1.07	1	28.94	3432.31
136	4	15	38N	2	3	in	0	0	3.25	1	33.24	3431.81
137	4	16	17N	2	2	in	0	0	1.44	1	41.08	3432.42
138	4	321	43N	3	2	in	0	0	3.51	1	43.23	3431.35
139	4	0	73N	1.5	2.5	in	0	1	1.44	1	41.79	3430.78
140	4	no single orientation		3	2	in	0	0	1.97	1	45.80	3434.81
141	4	294	21N	2	2.5	in	0	0	3.85	1	49.64	3430.44
142	4	40	30N	2	3	in	0	0	9.23	1	64.32	3432.62
143	4	63	31N	2.5	3.5	in	0	0	6.97	1	68.88	3433.42
144	4	63	81N	1.5	2	in	0	1	1.73	1	68.37	3433.28
145	4	50	24W	4	3.5	in	0	0	6.79	1	79.85	3433.40
146	4	no single orientation		1.5	2	in	0	0	8.99	1	82.79	3434.00
147	4	348	67N		2	in	0	1	1.94	1	88.68	3430.87
148	4	33	90	1	1.5	in	0	1	2.59	1	90.74	3434.33
149	4	66	90	1	4	in	0	1	1.23	1	96.49	3430.81
150	4	276	17S	2	1.5	in	0	0	0.84	1	97.93	3431.15
151	4	13	70W and 70E	2.5	2	in	0	0	2.97	1	8.66	3425.78
152	4	308	9N	3	3.5	in	0	0	5.95	1	9.35	3422.03
153	4	296	90	2	4	in	0	1	1.33	1	16.64	3425.63

154	4	plunges to 11°		3	2.5	in	0	0	4.62	1	16.99	3426.81
155	4	352	26S	3	2.5	in	0	0	9.07	1	23.08	3421.66
156	4	354	17S	1.5	2.5	in	0	0	2.35	1	24.97	3421.59
157	4	60	43W	2.5	3.5	in	0	0	11.25	1	33.01	3422.10
158	4	76	20E	1.5	2	in	0	0	1.83	1	28.55	3424.42
159	4	55	78S	1.5	2.5	in	0	1	5.41	1	38.40	3424.49
160	4	79	90	1.5	3	in	0	1	1.71	1	42.67	3424.45
161	4	4	90	1.5	3	in	0	1	2.39	1	46.07	3422.99
162	4	53	83N	2	2	in	0	1	1.98	1	46.65	3422.85
163	4	21	90	2	2	in	0	1	2.65	1	47.85	3422.21
164	4	20	78to106N	3	3	in	0	1	3.10	1	55.11	3425.69
165	4	305	90	2.5	3.5	in	0 to 0.5mm EI	1	0.83	1	61.54	3423.58
166	4	283	52N	2.5	2	in	0	0	13.39	1	77.69	3425.06
167	4	64	90	2	3.5	in	0	1	1.80	1	86.55	3426.77
168	2	65	74S	1.5	2.5	in	0	1	3.23	1	0.94	3413.22
169	2	280	80S	2	2.5	in	0	1	1.94	1	3.05	3415.74
170	2	275	86S	1.5	2	in	0	1	2.08	1	4.53	3414.99
171	2	45	35S	3	2.5	in	0	0	3.73	1	8.53	3412.54
172	2	20	76S	2	1.5	in	0	1	3.15	1	12.26	3419.34
173	2	40	8S	2.5	3	in	0	1	3.62	1	11.66	3414.71
174	2	345	84N	2.5	1.5	in	0	0	2.38	1	12.54	3412.76
175	2	no single orient. mostly N		4	2.5	in	0	0	13.02	1	21.56	3419.16
176	2	292	26N	2	2.5	in	0	0	2.70	1	23.91	3418.25
177	2	14	87W	1.5	1.5-2	in	0	1	4.83	1	17.70	3413.99
178	2	55	89N	2.5	1.5	in	0	0	3.37	1	20.33	3414.34
179	2	20	89N	2.5	2.5	in	0	1	3.03	1	31.10	3413.28
180	2	351	89S	1.5	1.5	in	0	1	2.76	1	34.66	3412.71
181	2	63	83N	1.5	2	in	0	1	1.80	1	42.03	3421.27
182	2	294	67N	2.5	2.5	in	0	0	2.56	1	48.39	3417.31
183	2	1	15E	3	2.5	in	0	0	4.24	1	52.39	3416.05
184	2	318	89S	2	2	in	0	1	1.46	1	55.82	3414.67

185	2	30	17N	1.5	2	in	0	0	7.58	1	57.56	3412.84
186	2	334	24S	2	2	in	0	0	4.67	1	57.54	3415.95
187	2	60	13S	2.5	2	in	0	0	3.45	1	64.00	3416.90
188	2	156	7S	3	2-2.5	in	0	0	3.57	1	67.51	3416.56
189	2	356	25S	2	2.5	in	0	0	2.72	1	67.98	3416.76
190	2	353	14N	3	2.5	in	0	0	10.95	1	67.82	3417.70
191	2	0	14E	3	3	in	0	0	9.20	1	62.97	3419.63
192	2	no single orientation		3	2.5	in	0	0	6.15	1	69.62	3422.53
193	2	no single orientation		5	3	in	0	0	5.41	1	77.32	3422.14
194	2	284	36N	2	3	in	0	0	2.56	1	73.72	3421.15
195	2	no single orientation		5	2.5	in	0	0	10.73	1	82.08	3421.29
196	2	317	16S	2	2.5	in	0	0	14.60	1	75.86	3417.49
197	2	350	78N	3	2.5	in	0	0	5.88	1	76.83	3418.04
198	2	7	90	1.5	2	in	0	1	2.54	1	76.78	3414.94
199	2	311	29N	2	2	in	0	0	0.20	1	78.27	3419.09
200	2	342	71N	2.5	1.5	in	0	0	4.36	1	85.42	3417.44
201	2	294	19S	3	2.5	in	0	0	2.03	1	86.98	3415.29
202	2	356	14S	1.5	2	in	0	0	8.26	1	89.48	3414.90
203	2	344	12N	2.5	2	in	0	0	3.49	1	95.70	3419.84
204	2	40	18N	1.5	2.5	in	0	0	6.49	1	95.90	3422.38
205	2	335	24N	1.5	2.5	in	0	0	1.87	1	99.47	3419.84
206	2	54	11N	1.5	1.5	in	0	0	5.28	2	3.41	3404.15
207	2	90	85N	3	2.5	in	0	0	2.24	2	3.08	3405.78
208	2	84	14S	2	2.5	in	0	0	3.21	2	6.55	3404.59
209	2	too variable	13N	2.5	2.5	in	0	0	15.01	2	13.46	3402.33
210	2	45	3S	2	2	in	0	0	9.34	2	24.89	3401.72
211	2	337	7S	2.5	2	in	0	0	3.38	2	26.35	3404.41
212	2	8	6N	2.5	3	in	0	0	4.43	2	28.84	3402.93
213	2	25	4N	2.5	3	in	0	0	2.65	2	29.90	3404.03
214	2	321	7N	2	3	in	0	0	3.41	2	32.14	3404.33
215	2	80	6S	3	2	in	0	0	4.55	2	34.62	3401.55

216	2	76	24N	3	3	in	0	0	9.55	2	40.36	3402.61
217	2	10	15	2.5	4	in	0	0	13.86	2	55.15	3402.34
218	2	343	10S	3	4.5	in	0	0	2.60	2	51.76	3401.91
219	2	272	7N	2	2.5	in	0	0	2.64	2	52.66	3401.46
220	2	313	5N	2	2.5	in	0	0	2.58	2	56.82	3401.33
221	2	45	72	3	3	in	0	1	3.99	2	61.81	3401.78
222	2	25	9S	3.5	3.5	in	0	0	5.29	2	69.81	3402.88
223	2	45	15N	2.5	3.5	in	0	0	4.50	2	69.38	3401.99
224	2	52	10N	3.5	3	in	0	0	3.28	2	73.86	3401.65
225	2	272	13N	2	2.5	in	0	0	3.80	2	74.27	3402.17
226	2	348	90	3	3	in	0	1	3.19	2	75.63	3401.98
227	2	7	8N	2.5	2.5	in	0	0	2.48	2	78.01	3403.25
228	2	flat	0	2.5	3	in	0	0	15.59	2	84.54	3401.78
229	1	290	26S	2.5	3	in	0	0	2.69	2	12.13	3395.80
230	1	256	6S	3	2.5	in	0	1	7.09	2	16.94	3395.54
231	1	288	23N	2	3	in	0	0	5.63	2	23.28	3395.96
232	5	316	19N	2.5	3.5	in	0	0	4.06	3	22.97	3392.34
233	5	81	23N	2.5	3	in	0	0	3.26	3	26.54	3393.71
234	5	84	22N	2.5	3	in	0	0	2.69	3	28.62	3394.30
235	5	294	37N	1.5	2.5	in	0	0	5.44	3	29.04	3390.88
236	5	350	24S	1.5	2.5	in	0	0	1.91	3	33.95	3392.29
237	5	4	25N	2	3	in	0	1	5.87	3	40.28	3393.01
238	5	342	19S	4	3	in	0	0	2.71	3	41.18	3392.22
239	5	33	21N	1.5	3	in	0	0	2.30	3	46.59	3390.38
240	5	334	20N	1.5	1.5	in	0	0	0.34	3	46.42	3389.26
241	5	290	24N	2.5	4	in	0	1	3.75	3	51.80	3390.91
242	5	301	26S	2.5	2	in	0	1	2.96	3	51.71	3389.05
243	5	63	19S	2	2	in	0	1	3.49	3	55.29	3389.75
244	5	46	31N	2.5	2	in	0	0	2.95	3	57.45	3390.50
245	5	68	39N	2.5	2.5	in	0	0	2.80	3	59.11	3391.22
246	5	350	25S	3.5	2.5	in	0	1	1.69	3	59.88	3389.94

247	5	80	23S	3	3.5	in	0	0	5.92	3	59.76	3387.29
248	5	350	30S	2.5	2.5	in	0	0	11.69	3	64.38	3388.77
249	5	35	29S	2	2.5	in	0	0	4.83	3	63.27	3386.66
250	5	285	30S	3	3.5	in	0	0	3.19	3	63.21	3389.80
251	5	90	40N	4	3.5	in	0	0	3.95	3	64.55	3391.73
252	5	55	34N	4	3-4	in	0	1	2.56	3	66.13	3391.85
253	5	22	34N	2	2	in	0	0	3.92	3	92.69	3386.22
254	2	65	33S	1.5	3.5	in	0	0	3.07	3	2.85	3388.17
255	2	80	8S	1.5	3.5	in	0	0	4.13	3	9.23	3387.60
256	2	80	14N	2	3.5	in	0	0	1.94	3	11.72	3385.47
257	2	no single orientation		4	3	in	0	0	4.77	3	18.22	3383.59
258	2	58	37N	4	3.5	in	0	0	8.31	3	24.15	3383.40
259	2	0	11E	1.5	3.5	in	0	0	3.81	3	23.19	3385.40
260	2	288	30S	2	3	in	0	0	3.22	3	26.33	3384.40
261	2	342	17W	1.5	4	in	0	0	2.31	3	28.02	3385.26
262	2	347	26W	2	3	in	0	0	3.24	3	32.46	3384.54
263	2	72	13N	2	3.5	in	0	0	3.20	3	31.30	3385.16
264	2	355	33E	1.5	3.5	in	0	0	2.35	3	35.00	3385.21
265	2	20	17W	1.5	3.5	in	0	0	2.54	3	41.49	3384.20
266	2	84	78S	2	3.5	in	NA	1	1.94	3	61.54	3382.07
267	2	307	30N	3	4	in	0	0	4.10	3	94.01	3380.38
268	2	74	90	2.5	3.5	in	0	1	1.71	3	98.12	3381.97
269	4	287	42S	1.5	2	in	0	1	2.49	4	16.75	3383.90
270	4	68	57S	2	2	in	0	1	1.21	4	17.79	3383.38
271	4	305	54S	2	2.5	in	0	1	4.91	4	21.97	3382.69
272	4	286	22N	2	2	in	0	0	2.54	4	88.64	3380.49
273	4	30	53E	1.5	3	in	0	1	1.55	4	89.25	3380.06
274	4	348	38NE	3	2	obs	0	0	8.82	1	3.70	3434.09
275	4	90	77S	1.5	3	obs	3mm EI	1	3.13	1	1.47	3434.53
276	4	10	22W	2	2	obs	0	0	2.71	1	4.11	3435.55
277	4	18	42W	3	2	obs	2mm EI	0	1.04	1	4.11	3435.70

278	4	28	74W	1.5	2.5	obs	1mm EI	1	2.98	1	6.76	3432.70
279	4	mound trend dips 14° to 190°		4	2	obs	0	0	18.57	1	13.71	3430.10
280	4	322	80W	1.5	2	obs	0.5mm EI	1	5.75	1	9.08	3433.77
281	4	46	15W	3	3	obs	0	0	2.98	1	10.47	3435.06
282	4	76	33N	2.5	2.5	obs	0	0	1.99	1	12.06	3435.41
283	4	332	74S	1.5	2	obs	2mm EI	1	1.38	1	13.69	3435.32
284	4	39	47W	2.5	1.5	obs	0	0	1.89	1	15.20	3435.69
285	4	248	51S	2	2	obs	0	1	5.18	1	17.48	3434.97
286	4	36	38N	2	2	obs	0	0	1.53	1	17.60	3435.84
287	4	no single orientation		5	2.5	obs	0	0	13.92	1	24.15	3434.29
288	4	45	43W	1.5	2	obs	0	1	1.42	1	19.04	3434.83
289	4	no single or., dip is 37°N		5	2	obs	0	0	12.36	1	35.74	3435.77
290	4	322	46N	3	1.5	obs	NA	0	4.30	1	31.76	3435.68
291	4	352	30S	2	2	obs	1 mm EI	0	2.16	1	31.69	3434.20
292	4	no single orientation		2	2.5	obs	0	0	3.09	1	43.85	3434.39
293	4	0	38E	1.5	2	obs	0	0	3.15	1	48.06	3435.72
294	4	50	50W	2	2	obs	0	1	1.14	1	48.02	3433.63
295	4	84	26N	2	2.5	obs	0	0	4.28	1	52.07	3436.26
296	4	70	29N	2.5	2	obs	NA	0	3.78	1	51.79	3436.66
297	4	58	24N	1.5	1.5	obs	0	0	2.18	1	62.31	3434.94
298	4	54	45N	2	2	obs	0	1	9.04	1	65.10	3432.97
299	4	83	27N	2.5	2	obs	NA	0	3.51	1	66.55	3435.54
300	4	no single orientation		5	2.5	obs	0	0	30.05	1	84.86	3436.46
301	4	334	36E	1.5	1.5	obs	0	0	6.40	1	75.34	3435.80
302	4	59	14W	1.5	2	obs	0	0	4.60	1	84.81	3435.72
303	4	304	88N	2.5	3	obs	0	1	0.88	1	85.41	3436.10
304	4	no single orientation		2.5	2.5	obs	0	0	9.63	1	95.24	3436.10
305	4	277	13S	2	1.5	obs	0	0	2.94	1	98.55	3435.64
306	4	90	90	3	3	obs	0	1	1.03	1	96.03	3436.29
307	4	328	31N	2.5	3.5	obs	5 mm EI	0	8.80	1	3.96	3426.81
308	4	322	21N	2.5	2.5	obs	0	0	13.47	1	6.52	3425.64

309	4	no single or:dip 15 to 35 E		3.5	3	obs	0	0	4.13	1	7.53	3427.54
310	4	43	36N	2.5	3.5	obs	0	0	14.62	1	20.14	3425.88
311	4	338	13N	2	3.5	obs	0	0	4.20	1	20.44	3427.67
312	4	332	36N	2.5	3	obs	0	0	6.27	1	22.70	3427.01
313	4	333	42S	2	2	obs	0	1	3.05	1	23.67	3426.86
314	4	46	34S	1.5	2.5	obs	0	0	19.00	1	38.61	3424.16
315	4	337	90	1.5	3	obs	0	1	1.63	1	43.91	3424.51
316	4	25	27N	2	3	obs	0	0	11.83	1	48.37	3424.53
317	4	30	13N	2	2.5	obs	0	0	15.24	1	52.29	3424.50
318	4	31	46W	2.5	2.5	obs	0	0	10.04	1	51.21	3424.01
319	4	305	90	3	3.5	obs	0	1	1.50	1	51.95	3423.73
320	4	40	25N	3	4	obs	0	0	7.46	1	61.29	3426.33
321	4	328	17N	2.5	3	obs	0	0	8.96	1	66.65	3425.71
322	4	9	90	2	3	obs	1 mm EI	1	3.98	1	75.83	3426.01
323	4	272	42N	2.5	3.5	obs	1 mm EI	0	3.79	1	78.09	3427.64
324	4	0	29W	1.5	2.5	obs	0	0	4.41	1	82.90	3427.34
325	4	0	57W	1.5	3.5	obs	0	1	4.23	1	84.72	3427.03
326	4	20	22N	2.5	2.5	obs	0	0	3.22	1	89.06	3427.91
327	4	291	12S	1.5	2	obs	0	0	3.28	1	90.71	3427.55
328	4	343	24S	2.5	3.5	obs	0	0	3.34	1	92.83	3428.86
329	4	40	34N	2	2.5	obs	0	0	4.51	1	94.37	3429.03
330	4	73	32N	2	2	obs	0	0	3.72	1	95.94	3428.70
331	4	73	34N	2	2	obs	0	0	1.69	1	96.37	3429.39
332	4	flat		1.5	3	obs	0	0	1.73	1	99.23	3430.23
333	2	78	10S	1.5	1.5	obs	0	0	9.59	1	5.09	3419.87
334	2	no single orient. mostly N		5	1.5-3	obs	0	0	13.27	1	13.09	3418.98
335	2	15	84S	3	1.5-2	obs	0	0	3.04	1	15.71	3419.55
336	2	87	40N	3	2.5	obs	0	0	18.55	1	25.30	3419.31
337	2	35	87N	2	1.5	obs	0	1	2.13	1	26.00	3420.93
338	2	323	85S	1.5	2.5	obs	0	1	1.17	1	30.47	3419.39
339	2	no single orientation		3	2.5-3.5	obs	0	0	15.48	1	41.68	3420.09

340	2	343	33N	3	2-2.5	obs	0	0	20.92	1	45.40	3420.50
341	2	83	87S	3	2.5	obs	0	1	1.35	1	61.08	3412.98
342	2	85	74S	2.5	2	obs	0	1	2.97	1	62.59	3413.90
343	2	54	23S	2.5	2.5	obs	0	0	6.62	1	55.53	3421.25
344	2	185	26	4	3	obs	0	0	7.44	1	60.02	3422.40
345	2	45	18S	2	2	obs	0	0	7.67	1	64.15	3422.18
346	2	14	37S	3	2.5	obs	0	0	8.99	1	75.57	3422.05
347	2	3	40S	3	3.5	obs	0	0	11.98	1	85.91	3421.08
348	2	288	86N	2.5	2	obs	0	1	0.97	1	89.85	3417.59
349	2	77	46S	3	3	obs	0	0	2.86	1	83.97	3422.29
350	2	313	89S	2	2	obs	0	1	1.03	1	93.35	3414.34
351	2	284	63S	3	2.5	obs	0	1	1.85	1	97.02	3420.84
352	2	8	3W	2.5	2.5	obs	0	0	19.86	2	14.86	3404.81
353	2	333	86S	1.5	1.5	obs	0	1	2.47	2	12.41	3404.02
354	2	331	90	1.5	2	obs	0	1	1.31	2	14.49	3404.69
355	2	34	18	4	2.5	obs	0	0	3.59	2	15.53	3405.10
356	2	no single orientation		2.5	2.5	obs	0	0	4.17	2	20.52	3404.79
357	2	318	8S	2	3	obs	0	0	4.06	2	27.26	3404.51
358	2	336	6N	3.5	3	obs	0	0	15.02	2	48.75	3403.63
359	2	247	90	3	2.5	obs	0	1	1.27	2	54.31	3403.11
360	2	318	90	3	3	obs	0	1	1.27	2	55.70	3403.13
361	2	385	5N	3	3	obs	0	0	3.14	2	63.41	3403.84
362	2	326	90	3	3	obs	0	1	1.23	2	78.39	3403.69
363	2	320	90	3	2	obs	0	1	1.47	2	81.26	3402.79
364	2	280	90	2.5	2	obs	0	1	1.51	2	83.44	3403.08
365	2	330	7S	2.5	2-3	obs	0	0	10.64	2	94.83	3402.69
366	2	308	90	3	2.5	obs	0	1	1.67	2	96.29	3403.28
367	2	295	90	2	2	obs	0	1	1.53	2	98.23	3403.00
368	1	285/337	30N/37N	1.5	4	obs	0	1	3.91	2	31.85	3395.46
369	1	54	34N	2.5	4	obs	0	0	9.12	2	40.51	3393.54
370	5	31	30S	2	3	obs	0	0	2.97	3	37.64	3394.13

371	5	278	27N	2.5	2.5	obs	0	1	2.53	3	46.30	3394.02
372	5	306	27N	2	3.5	obs	0	1	6.45	3	50.93	3392.66
373	5	324	38N	3	3	obs	0	0	7.39	3	56.46	3391.73
374	5	28	21N	3	3.5	obs	0	0	1.33	3	54.91	3393.12
375	5	43	31N	3	3	obs	0	0	6.10	3	61.39	3391.77
376	5	50	39N	4	3.5	obs	0	0	5.93	3	71.42	3390.63
377	5	278	16S	2	2-3	obs	0	0	12.09	3	87.38	3388.99
378	5	343	19N	3	3	obs	0	0	4.81	3	87.16	3391.16
379	2	325	26S	1.5	3	obs	2 mm EI	0	2.59	3	1.19	3388.47
380	2	293	90	2	3.5	obs	NA	1	2.46	3	14.75	3386.59
381	2	8	37E	2	3	obs	0	1	5.32	3	67.39	3381.43
382	2	71	36N	2	3	obs	0	1	3.77	3	75.53	3381.23
383	2	314	27N	3.5	3.5	obs	0	1	0.90	3	80.82	3382.19
384	2	322	44N	3.5	3.5	obs	0	1	2.18	3	79.55	3381.08
385	2	62	11S	2	3	obs	0	0	5.75	3	85.84	3381.95
386	2	348	34E	4	3	obs	NA	1	0.83	3	52.24	3383.38
387	4	no single or., dip is 40°N		3	2.5	obs/at	0	0	9.75	1	24.97	3435.33

Table A-3 Discontinuity Data for East Face of FWF

Fracture No.	Geology	Strike (°)	Dip (°)	Curvature	Roughness	Termination	Aperture	Hydr. Sig?	Length	Genetic Unit	Xmid	Xmid
1	2	330	7S	2	2	in	0	0	6.18	3	13.79	3405.08
2	3	26	8E	1.5	3.5	in	0	0	5.94	1	43.18	3446.10
3	4	44	8S	2.5	2	in	0	0	6.69	3	93.20	3416.53
4	3	322	8N	2	2	at	0	0	2.94	1	65.29	3441.33
5	4	54	9S	2.5	3	at	0	0	2.81	3	63.91	3415.56
6	4	70	9N	2.5	3	in	0	0	4.80	5	62.20	3376.08
7	4	336	9N	3.5	2	in	0	0	14.86	3	48.85	3411.45
8	3	350	9S	2.5	2.5	at	0	1	8.48	2	95.77	3426.26
9	4	350	10N	2	1.5	obs	0	0	6.34	3	96.87	3416.00
10	2	46	11N	3	3	in	0	0	6.10	3	53.07	3407.14

11	3	355	11E	3.5	3.5	at	0	0	4.83	1	45.46	3444.48
12	3	5	12E	1.5	3	at	0	1	8.76	1	54.72	3443.28
13	3	5	12W	2	3.5	in	0	0	5.37	1	46.13	3445.47
14	1	27	12S	1.5	2.5	in	0	0	4.01	4	39.54	3384.61
15	2	60	12N	2.5	2	at	0	0	4.51	5	95.09	3375.33
16	4	299	12N	2	2.5	in	0	0	2.56	3	31.26	3411.51
17	4	34	13N	2	3.5	in	0	0	3.48	4	65.62	3394.36
18	4	35	13S	2.5	1.5	at	0	0	10.02	3	54.95	3410.91
19	4	45	13N	2	2	in	0	0	13.61	3	60.03	3412.68
20	3	298	13N	1.5	3.5	at	0	1	2.19	1	47.71	3444.68
21	2	312	13S	2.5	2.5	in	0	0	4.26	3	97.89	3406.95
22	2	11	14S	3	2.5	obs	0	0	4.08	3	48.56	3406.50
23	3	294	14N	1.5	3	obs	0	0	4.52	1	50.62	3445.94
24	2	360	15E	2.5	2.5	in	0	0	9.79	3	4.97	3405.87
25	4	17	15S	3	2.5	at	0	0	4.65	4	34.45	3393.04
26	4	21	15S	2	2	at	0	0	6.21	3	91.68	3415.69
27	4	21	15S	3	2.5	at	0	0	9.61	3	35.32	3411.46
28	2	296	15S	3	2.5	at	0	0	6.16	3	35.30	3409.72
29	3	300	15N	2	2.5	obs	0	0	5.68	2	2.63	3428.05
30	2	312	15S	3	2	in	0	0	3.53	3	98.14	3407.19
31	2	351	15S	2.5	3.5	obs	0	1	3.52	3	72.81	3406.62
32	4	275	16N	2	1.5	in	0	0	3.20	3	86.77	3415.38
33	4	280	16S	3	2.5	in	0	0	3.41	4	20.65	3395.25
34	4	318	16S	1.5	2.5	in	0	0	8.57	3	91.09	3412.29
35	4	345	16S	2.5	2.5	in	0	0	5.14	3	97.33	3411.08
36	3	285	17N	2.5	2	at	0	0	7.60	2	42.36	3427.08
37	4	324	17S	2	3	at	0	0	3.32	3	54.03	3411.07
38	1	329	17N	1.5	3	obs	0	0	6.05	4	96.67	3384.27
39	2	339	17S	3	3	in	0	0	4.27	3	21.60	3403.96
40	3	4	18S	2.5	2.5	obs	0	0	6.96	2	71.57	3422.07
41	4	37	18N	3.5	3	in	0	0	7.55	4	51.44	3395.51

42	4	68	18S	2.5	3	at	0	0	2.52	3	70.06	3414.03
43	3	98	18S	2	2.5	obs	0	0	9.99	2	50.24	3425.45
44	4	309	18N	1.5	2	in	0	0	2.38	4	88.33	3395.07
45	2	320	18N	2	3	in	0	0	8.03	3	4.63	3405.17
46	2	5	19S	1.5	2.5	in	0	0	2.39	3	42.83	3404.10
47	4	34	19S	3	2.5	at	0	0	7.93	3	65.44	3410.19
48	5	55	19S	2	3	in	0	0	3.32	5	78.30	3383.46
49	4	62	19S	1.5	2.5	at	0	0	3.95	3	39.08	3412.60
50	4	71	19S	2	3.5	in	0	0	6.56	4	10.42	3398.39
51	4	344	19N	1.5	2	at	0	0	3.98	5	18.33	3383.54
52	4	357	19N	2	3	in	0	0	7.07	3	96.46	3414.39
53	4	35	20N	4	3	at	0	0	0.59	4	24.35	3394.75
54	4	76	20S	2	2.5	at	0	0	3.87	3	98.10	3412.12
55	3	316	20N	2	2.5	in	0	1	3.38	1	1.75	3446.18
56	4	317	20N	2	2.5	at	0	0	7.80	4	51.09	3390.39
57	3	325	20N	3	3	at	0	0	9.90	1	8.14	3444.19
58	3	325	20N	3	3	in	0	1	6.34	1	3.10	3444.51
59	4	329	20N	2.5	2.5	at	0	0	2.78	3	77.56	3411.30
60	3	332	20N	2.5	2.5	at	0	0	5.03	1	21.47	3442.49
61	4	332	20N	3	2.5	at	0	0	5.54	3	81.23	3410.14
62	5	344	20N	2	3.5	at	0	0	4.13	5	90.87	3382.28
63	4	348	20S	2.5	2.5	obs	0	0	16.17	3	79.43	3413.63
64	4	350	20S	1.5	2.5	in	0	0	5.67	3	97.26	3413.07
65	3	353	20W	2	2	in	0	0	1.79	2	47.16	3424.57
66	2	15	21S	3	2.5	at	0	0	3.33	3	30.13	3409.82
67	4	52	21N	3	3.5	obs	0	0	2.41	4	27.02	3394.68
68	4	61	21N	3.5	2	in	0	0	7.38	4	15.66	3398.06
69	4	83	21N	2	2.5	at	0	0	13.18	3	62.60	3411.32
70	3	296	21N	3.5	3	in	0	0	5.44	1	58.65	3443.59
71	3	315	21N	3	3	obs	0	1	17.24	2	83.42	3425.17
72	2	323	21S	2.5	3	in	0	0	8.67	3	51.57	3405.76

73	4	51	22N	2.5	2	at	0	0	5.01	3	70.58	3411.64
74	4	279	22S	2	2	in	0	0	14.63	3	88.14	3412.47
75	4	283	22N	3	2.5	at	0	0	3.75	5	66.80	3378.09
76	2	318	22S	3	2.5	in	0	0	8.77	3	67.33	3404.47
77	4	343	22N	3	3	in	0	0	5.91	3	59.94	3414.33
78	3	350	22N	2	2.5	at	0	0	4.17	2	77.37	3422.29
79	4	358	22N	2.5	3	in	0	0	8.56	3	23.04	3411.95
80	4	4	23N	2	2	in	0	0	7.83	3	49.29	3412.80
81	4	56	23N	2.5	2.5	obs	0	0	1.53	4	99.26	3398.35
82	2	58	23N	1.5	2.5	at	0	0	3.16	3	53.94	3403.92
83	4	70	23S	2.5	3.5	in	0	0	2.06	4	76.80	3396.31
84	4	90	23N	1.5	2	at	0	0	5.41	4	64.27	3394.95
85	4	285	23N	2.5	2	at	0	0	1.85	4	33.62	3391.44
86	3	288	23N	2	4	obs	0	0	5.96	1	54.83	3444.41
87	4	311	23N	2	2	in	0	0	4.90	5	92.03	3376.33
88	4	15	24N	2.5	2	in	0	0	2.36	4	82.18	3395.87
89	3	36	24N	2.5	3	obs	0	0	10.06	2	74.78	3428.54
90	5	47	24N	2	2.5	in	0	0	3.17	4	53.16	3381.95
91	2	52	24N	2.5	2	in	0	0	7.60	5	88.80	3374.90
92	2	72	24S	2.5	2	in	0	0	11.25	3	14.38	3403.58
93	4	76	24S	2.5	2.5	in	0	0	8.03	4	14.50	3396.09
94	5	82	24S	2	2.5	at	0	0	3.92	5	98.10	3383.40
95	3	281	24N	1.5	4	obs	4 mm EI	0	2.60	1	59.88	3444.82
96	4	300	24S	2	2	at	0	0	4.12	5	21.88	3382.71
97	4	300	24S	2.5	2	at	0	0	4.08	5	95.07	3376.02
98	3	4	25S	3	2	in	0	0	2.95	2	97.26	3422.57
99	4	13	25N	3	2	obs	0	0	3.31	4	30.29	3394.83
100	5	26	25S	2	2.5	in	0	0	8.49	5	84.70	3383.57
101	3	45	25N	3	3.5	at	0	0	5.19	1	52.83	3443.91
102	4	90	25S	1.5	2.5	in	0	0	3.45	4	98.39	3397.07
103	3	314	25S	3	1.5	at	0	0	7.14	2	75.51	3427.86

104	4	317	25N	2.5	2	obs	0	0	7.09	4	24.08	3394.96
105	4	339	25S	2.5	2.5	at	0	0	2.73	4	78.64	3395.34
106	3	355	25N	3	2.5	obs	0	0	17.31	2	30.92	3422.83
107	4	9	26S	3	2.5	at	0	0	4.71	5	54.42	3377.70
108	4	13	26S	2	3	in	0	0	7.81	4	77.55	3390.13
109	3	19	26E	3.5	3	in	0	0	12.43	2	46.79	3423.51
110	4	36	26N	3	3	in	0	0	6.12	3	15.62	3412.45
111	2	68	26N	3	2	in	0	0	8.85	3	92.44	3406.24
112	3	71	26S	2.5	2.5	obs	0	1	6.44	2	83.98	3427.06
113	4	72	26S	3	2.5	in	0	0	2.83	3	28.57	3411.35
114	4	75	26N	2.5	3	at	0	0	3.75	3	71.31	3410.19
115	4	273	26S	2	1.5	at	0	0	5.35	3	75.36	3411.09
116	4	288	26N	2.5	2.5	obs	0	0	17.12	3	38.25	3413.58
117	5	324	26N	1.5	3	at	0	0	4.60	5	77.94	3382.36
118	4	333	26S	2.5	2.5	at	0	0	3.88	4	42.84	3391.68
119	4	50	27N	2.5	3	obs	0	0	2.27	4	35.76	3393.54
120	4	61	27N	2.5	2.5	obs	0	0	2.75	4	17.49	3396.38
121	4	83	27S	2	2.5	in	0	0	4.18	4	71.51	3395.38
122	4	275	27N	2.5	3	at	0	0	3.99	3	54.85	3413.52
123	4	283	27N	2.5	2.5	at	0	0	5.40	5	54.69	3376.80
124	4	293	27S	3.5	2.5	at	0	0	4.17	5	95.51	3376.27
125	4	296	27N	2	2.5	obs	0	0	10.15	4	93.30	3396.72
126	4	310	27S	2.5	3	in	0	0	3.70	4	60.44	3394.16
127	4	27	28N	3	2.5	at	0	0	8.40	3	24.66	3409.65
128	2	36	28S	4	2.5	at	0	0	7.61	3	48.91	3409.36
129	4	38	28N	3	2.5	at	0	0	8.95	3	59.36	3415.22
130	3	82	28N	2.5	2	in	0	1	3.14	1	1.50	3445.30
131	3	118	28S	2.5	2.5	at	0	0	10.91	2	50.83	3424.93
132	3	283	28N	2.5	2.25	at	0	0	6.03	2	2.77	3427.10
133	4	283	28S	2	2.5	in	0	0	5.37	4	97.54	3396.34
134	4	300	28N	1.5	4	in	0	0	3.14	4	62.70	3396.88

135	5	310	28S	1.5	3	at	0	0	9.10	5	75.87	3382.80
136	3	348	28N	3.5	2.5	at	0	0	15.24	2	92.49	3423.73
137	4	24	29S	2	2	in	0	0	17.75	5	15.75	3383.55
138	3	38	29S	1.5	3	at	0	0	1.73	1	46.28	3443.73
139	4	51	29S	2	3	obs	0	0	8.26	4	57.11	3397.01
140	4	56	29S	2	2	in	0	0	3.37	4	85.56	3395.00
141	4	60	29S	3	2.5	at	0	0	5.89	3	73.23	3410.99
142	4	70	29S	2.5	2	in	0	0	6.12	3	4.06	3413.63
143	4	87	29N	2	3	in	0	0	3.57	3	33.90	3413.02
144	4	296	29S	3	1.5	obs	0	0	8.94	3	72.36	3414.50
145	3	320	29N	2.5	2.5	at	0	0	3.82	2	65.60	3423.90
146	3	48	30N	3	1.5	at	0	0	3.87	1	31.79	3444.51
147	3	53	30N	3	3	obs	0	1	10.85	1	11.87	3445.35
148	4	67	30N	3	2.5	at	0	0	9.44	5	89.02	3376.83
149	4	334	30N	3.5	3	obs	0	0	1.76	4	70.92	3396.87
150	5	45	31S	2	2.5	at	0	0	3.40	5	95.83	3383.27
151	4	53	31S	2.5	2.5	at	0	0	11.76	4	28.86	3393.10
152	3	75	31S	3	2.5	in	0	0	11.32	2	10.03	3425.81
153	4	75	31S	2.5	2.5	in	0	0	4.24	4	69.29	3395.82
154	3	90	31S	1.5	1.5	at	0	0	4.41	1	33.37	3441.61
155	4	296	31N	1.5	2	at	0	0	3.94	4	64.71	3394.71
156	3	298	31N	1.5	2	in	0	0	7.48	2	3.52	3425.05
157	4	325	31N	2	2.5	in	0	0	2.66	3	25.55	3410.80
158	3	337	31N	2.5	2.5	obs	0	0	10.23	2	40.87	3427.38
159	3	356	31W	3.5	3	in	0	0	19.52	1	55.32	3443.30
160	4	358	31N	2.5	3.5	at	0	0	6.90	4	66.51	3396.86
161	4	61	32S	2.5	2.5	in	0	0	8.25	5	64.95	3376.74
162	4	68	32S	1.5	2.25	at	0	0	3.89	5	18.25	3382.20
163	4	80	32S	2	1.5	at	0	0	1.89	3	77.64	3410.45
164	4	86	32S	2	3.5	in	0	0	3.75	4	22.85	3397.35
165	4	290	32N	2	3	in	0	0	4.44	4	80.07	3396.53

166	2	291	32N	3	2	at	0	0	4.61	3	27.64	3409.52
167	4	292	32N	2.5	3.5	obs	0	0	6.28	4	53.93	3390.95
168	4	302	32N	3.5	3	in	0	0	3.73	4	82.54	3388.77
169	4	315	32S	2.5	2.5	obs	0	0	5.49	4	59.14	3390.88
170	4	320	32S	2	2.5	obs	0	0	3.62	3	65.23	3415.63
171	3	333	32W	2.5	2	at	0	0	6.44	2	59.49	3425.44
172	4	355	32S	4	2.5	obs	0	0	1.16	4	39.29	3393.43
173	4	357	32N	2	3	obs	0	0	3.97	4	61.79	3391.25
174	4	21	33S	3	2.5	in	0	0	7.29	5	58.29	3376.60
175	3	39	33N	2	4	obs	0	0	4.24	1	62.97	3443.33
176	4	49	33S	4	2	in	0	0	12.82	3	10.75	3412.83
177	4	275	33S	2	2	at	0	0	1.58	3	79.29	3411.27
178	3	276	33S	2	2	obs	0	0	12.40	2	20.55	3426.63
179	4	295	33S	2	2	obs	0	1	11.78	5	37.10	3380.04
180	4	336	33N	2.5	2.5	in	0	0	8.47	5	39.83	3377.23
181	3	356	33S	3	3	obs	0	0	6.24	2	64.45	3429.25
182	4	360	34E	2.5	2	in	0	0	3.11	4	21.45	3396.77
183	4	49	34S	2	2	at	0	0	3.90	4	94.98	3396.49
184	4	51	34S	2	2.5	at	0	0	2.31	5	54.77	3376.16
185	4	57	34S	1.5	2.5	in	0	0	4.37	5	74.12	3377.05
186	4	61	34S	2.5	2.5	at	0	0	3.34	5	35.25	3378.34
187	4	276	34N	1.5	3	obs	0	0	2.78	4	15.25	3397.46
188	4	290	34S	2	1.5	at	0	0	2.70	3	76.22	3410.10
189	4	300	34N	3	3	at	0	0	2.76	4	63.25	3396.15
190	3	310	34S	3	2.5	in	0	0	2.67	1	18.79	3441.45
191	4	316	34S	1.5	2.5	at	0	0	2.30	4	41.15	3386.21
192	4	327	34S	3	2	in	0	0	9.44	3	86.71	3412.10
193	4	336	34N	2	2	at	0	0	6.17	5	44.05	3379.13
194	3	350	34N	2.5	2.5	in	0	0	9.80	1	70.55	3442.73
195	4	351	34N	3	2	at	0	0	3.53	4	21.82	3394.47
196	3	18	35N	3	2	in	0	0	13.83	1	27.70	3442.02

197	4	39	35S	2.5	2	at	0	0	3.48	5	58.73	3378.75
198	3	66	35N	3	2.5	obs	0	0	9.06	2	66.31	3426.27
199	4	67	35S	2.5	2	in	0	0	6.90	4	84.81	3389.37
200	4	296	35S	3	3	obs	0	0	5.83	5	56.09	3378.99
201	4	333	35S	3.5	3	obs	0	0	5.19	5	69.42	3379.19
202	4	340	35S	3.5	2.5	obs	0	1	1.14	4	39.15	3387.64
203	4	343	35N	3.5	2.25	in	0	0	10.87	5	80.56	3377.78
204	3	345	35S	2.5	1.5	at	0	0	4.65	1	21.81	3441.18
205	4	353	35S	2	3	obs	0	0	10.62	4	74.83	3389.49
206	4	355	35N	2.5	2.5	in	0	1	4.29	5	79.14	3377.12
207	4	18	36N	2.5	3.5	obs	0	0	0.62	4	52.62	3392.49
208	4	48	36N	2	2	at	0	0	3.42	3	9.66	3410.96
209	4	59	36S	2.5	2.5	at	0	0	6.79	5	50.22	3377.75
210	1	62	36N	2	2.5	obs	0	0	0.67	4	6.99	3386.03
211	4	70	36S	2	2	in	0	0	9.87	5	71.30	3377.44
212	4	90	36N	2.5	3	obs	0	0	3.12	5	73.43	3378.65
213	2	285	36S	4	2.5	in	0	0	6.92	3	61.64	3402.90
214	4	297	36N	2.5	2.5	in	0	0	3.91	4	69.15	3388.71
215	4	311	36N	1.5	1.5	obs	0	0	3.01	4	10.28	3397.83
216	4	312	36	3.5	3.5	obs	NA	0	0.63	4	12.71	3398.84
217	4	332	36N	1.5	3	in	0	0	5.03	4	29.86	3397.18
218	3	351	36S	5	2.5	obs	0	0	14.42	2	62.53	3428.86
219	5	353	36N	3	2	in	0	0	5.97	5	91.40	3382.47
220	4	82	37S	2	2.5	at	0	0	2.64	3	69.93	3413.02
221	4	273	37S	2	2.5	obs	0	0	4.35	4	97.88	3391.66
222	3	276	37N	1.5	2	at	0	0	0.39	2	0.20	3425.74
223	1	296	37N	2	3.5	in	0	0	9.04	4	51.00	3384.46
224	3	329	37N	1.5	1.5	obs	0	0	8.84	2	95.87	3422.43
225	1	346	37N	1.5	3	obs	0	0	5.38	4	72.56	3385.34
226	4	360	38E	2	2.5	in	0	0	4.53	4	26.98	3397.57
227	4	11	38S	4.5	2.5	obs	0	1	5.63	5	87.59	3379.46

228	5	52	38S	2.5	2.5	at	0	0	3.67	5	89.04	3382.90
229	4	273	38S	2.5	2	obs	0	0	3.55	5	92.23	3379.24
230	3	345	38W	2	3	obs	0	0	9.17	2	58.05	3425.75
231	4	49	39N	3.5	2.5	at	0	0	3.22	3	41.16	3414.01
232	4	325	39N	2.5	2.5	at	0	0	4.03	5	11.57	3382.37
233	3	344	39S	4	3	obs	0	1	4.32	2	82.85	3427.93
234	4	20	40S	2.5	2	at	0	0	3.25	5	14.44	3382.95
235	4	23	40S	3	2.5	obs	0	0	15.23	4	92.46	3390.95
236	3	35	40S	3	2.5	in	0	0	4.01	1	40.22	3442.93
237	4	35	40S	3	2.5	in	0	0	11.40	5	89.16	3379.03
238	4	302	40S	2.5	3	at	0	0	4.08	5	76.70	3378.71
239	3	326	40S	2	2.5	obs	0	1	11.44	2	34.87	3425.94
240	3	330	40S	2.5	2	in	0	1	29.60	1	40.32	3445.71
241	4	346	40N	2	2.5	at	0	1	2.10	4	59.52	3389.42
242	3	76	41S	3.5	2	at	0	0	10.06	2	88.76	3422.11
243	3	302	41N	3	2.5	at	0	0	5.58	1	11.01	3443.67
244	3	320	41N	2.5	2	obs	0	0	18.76	2	88.70	3424.72
245	4	344	41N	2.5	2.5	at	0	0	2.62	5	29.82	3377.59
246	4	50	42S	2	2	in	0	1	3.21	4	75.52	3394.61
247	4	72	42N	2	3.5	obs	0	1	5.73	4	32.33	3386.61
248	4	304	42S	2.5	1.5	in	0	0	3.93	5	29.49	3379.07
249	4	316	42N	2	2	at	0	1	3.19	5	85.95	3376.93
250	4	317	42N	1.5	2.5	obs	0	1	3.31	4	72.05	3397.06
251	4	346	42N	2	2.5	in	0	1	3.74	4	37.67	3386.33
252	4	13	43S	3	3	obs	0	1	7.60	5	45.59	3380.15
253	4	60	44S	2	2.5	in	0	0	4.87	4	95.37	3391.53
254	1	82	44S	2.5	2.5	in	0	1	4.16	4	3.80	3384.48
255	4	326	44N	2	1.5	at	0	0	5.27	5	19.98	3381.38
256	4	360	45W	2.5	2	in	0	0	9.99	3	86.05	3411.25
257	3	282	45N	1.5	2	at	0	1	8.22	2	68.65	3425.95
258	3	9	46E	3	2.5	at	0	1	8.72	1	5.79	3444.23

259	4	20	46S	2.5	2	in	0	0	7.29	5	31.02	3377.04
260	4	81	46N	3	2.5	at	0	0	2.95	5	90.17	3375.68
261	4	98	46	4	3.5	in	0	0	5.29	5	38.59	3382.40
262	3	305	46S	2	2	obs	0	0	5.39	2	31.52	3427.40
263	3	33	47S	1.5	2	at	0	1	3.30	1	61.72	3442.27
264	3	292	47S	1.5	2	at	0	0	3.33	1	73.80	3441.96
265	4	340	47N	2.5	2	obs	0	1	2.84	5	52.39	3380.41
266	4	7	48S	2.5	2.5	at	0	0	11.12	5	49.37	3378.83
267	5	324	49S	1.5	3.5	in	0	1	3.34	4	63.61	3382.81
268	4	298	50N	1.5	2	at	0	1	5.71	5	33.85	3379.11
269	3	323	51S	2	2.5	at	0	1	0.88	1	39.15	3441.16
270	3	19	52S	2	2	at	0	0	2.32	1	78.30	3441.63
271	3	27	52N	2.5	2.5	at	0	0	2.00	1	33.73	3443.04
272	1	28	52S	3	2.5	in	0	0	2.20	5	52.31	3385.66
273	3	292	52S	2.5	2	in	0	0	2.46	1	38.25	3445.29
274	3	10	53S	2	2	in	0	0	3.44	2	35.93	3426.20
275	3	308	53N	3	3	in	0	1	7.55	1	11.82	3444.13
276	3	35	54S	2	2	in	0	1	3.92	1	65.23	3441.86
277	3	350	54N	2	2.5	obs	0	1	3.29	1	26.57	3444.18
278	3	293	55N	4	3	in	0	1	3.03	1	11.14	3444.06
279	3	77	57S	2	2.5	in	0	1	1.56	1	85.90	3441.84
280	3	50	59S	3	2	at	0	0	2.11	1	49.07	3444.29
281	4	44	60S	2	2	in	0	1	8.60	3	79.03	3415.82
282	3	274	60S	1.5	2	in	0	1	4.65	1	34.67	3443.74
283	3	70	63S	2	2	at	0	1	4.26	1	85.80	3442.55
284	3	354	68W	2	2.5	in	0	1	0.93	1	40.85	3441.19
285	2	330	69S	2	1.5	in	0	1	1.79	3	63.06	3407.08
286	4	10	74N	2	1.5	obs	0	1	1.68	3	21.38	3410.31
287	4	77	75S	1.5	2	obs	0	1	4.36	3	2.09	3412.21
288	4	345	75N	2	2.5	obs	0	1	1.26	3	47.25	3415.55
289	2	353	75N	2	1.5	obs	0	1	3.26	3	69.56	3406.10

290	3	161	78W	3	3	obs	0	1	3.89	2	44.45	3425.74
291	4	3	79S	1.5	1.5	obs	0	1	2.05	3	33.33	3414.14
292	3	345	80S	2	1.5	in	0	1	4.14	2	18.52	3424.50
293	4	325	81S	1.5	1.5	obs	unknown	1	1.68	3	43.98	3413.75
294	4	10	82S	2.5	2	obs	unknown	1	1.84	3	31.35	3414.07
295	3	17	82N	2	2.5	obs	unknown	1	1.74	1	37.61	3442.60
296	3	82	83S	1.5	2	at	0	1	2.72	1	93.53	3441.38
297	4	303	83S	2.5	2	in	0	1	1.94	3	22.23	3410.82
298	2	319	84S	2	2	obs	0	1	2.27	3	46.03	3405.74
299	3	339	84N	2.5	3	at	0	1	1.54	1	24.31	3444.27
300	4	29	85N	2.5	2.5	obs	0	1	3.06	3	22.69	3413.42
301	3	44	86N	2	2.5	in	0	0	1.37	1	49.45	3441.69
302	3	72	86S	1.5	3	at	0	1	2.07	1	47.96	3444.46
303	2	85	86N	2.5	2	in	0	1	2.29	3	78.21	3406.11
304	3	330	86N	1.5	3.5	at	0	1	3.12	1	43.40	3444.44
305	3	22	87E	3	2	obs	0	1	3.79	2	54.46	3424.81
306	3	85	87N	3	3	obs	unknown	1	1.62	1	93.37	3444.41
307	4	64	88N	2	2	obs	0	1	1.86	3	37.00	3414.38
308	4	77	88N	1.5	2.5	obs	0	1	1.87	4	75.61	3391.03
309	3	290	88N	2	3	at	0	1	2.61	1	41.47	3444.58
310	3	294	89S	2.5	3.5	at	0	1	2.53	1	53.18	3443.19
311	4	4	90	2	1.5	obs	0	1	1.82	3	39.61	3414.83
312	3	25	90	2.5	2.5	obs	0	0	1.39	2	68.52	3423.12
313	3	42	90	2	2.5	in	0	1	1.23	1	42.13	3441.40
314	3	48	90	2.5	2.5	obs	0	0	1.96	2	76.10	3426.14
315	3	54	90	1.5	4	at	0	1	1.71	1	55.66	3442.11
316	3	57	90	1.5	2	in	0	1	2.96	2	6.91	3424.68
317	3	75	90	1.5	4	at	0	1	2.43	1	50.32	3442.25
318	3	90	90	2	3	obs	0	1	2.07	1	76.74	3444.25
319	3	273	90	1.5	1.5	in	0	1	2.14	2	20.56	3424.33
320	2	273	90	2	2	obs	0	1	2.53	3	33.42	3405.84

321	3	305	90	1.5	1.5	obs	0	1	4.41	2	27.53	3426.10
322	3	323	90	1.5	3.5	at	0	1	1.94	1	54.95	3441.96
323	3	337	90	1.5	1.5	in	0	1	2.64	2	14.82	3424.39
324	2	357	90	2.5	2.5	in	0	1	1.81	3	72.11	3402.56
325	2	311	5S	3	2	in	0	0	4.13	3	56.07	3405.58

Table A-4 Discontinuity Data for South Face of FWF

Fracture No.	Geology	Strike (°)	Dip (°)	Curvature	Roughness	Termination	Aperture	Hydr. Sig?	Length	Genetic Unit	Xmid	Ymid
1	2	62	1E	2	2	in	0	0	7.54	3	96.24	3408.13
2	4	84	2S	1.5	1.5	in	0	0	10.69	5	42.19	3377.21
3	2	320	2N	2	2	in	0	0	4.48	5	62.38	3373.40
4	3	30	3S	2.5	2.5	at	0	0	8.21	2	79.11	3420.64
5	4	73	3S	3.5	3	in	0	0	5.00	5	64.38	3376.81
6	4	142	3S	2.5	2.5	in	0	0	17.87	3	74.10	3411.53
7	2	318	4S	2.5	2.5	obs	0	0	5.10	3	47.58	3407.26
8	4	88	5N	1.5	2.5	in	0	0	3.69	3	13.40	3411.73
9	2	18	6W	3	2.5	in	0	0	8.99	3	84.65	3409.00
10	4	35	6N	3	2	in	0	0	3.70	2	90.56	3437.96
11	4	80	6N/30S	4	2.5	at/in	0	0	13.50	2	27.26	3440.59
12	4	112	7S	2.5	2	at	0	0	3.67	3	89.70	3410.38
13	3	273	8N	2.5	2.5	at	0	1	3.99	2	56.08	3421.36
14	2	352	8E	4	2.5	at	0	0	11.23	5	94.42	3374.20
15	4	24	9N	2	3.5	in	0	0	6.63	3	7.01	3416.02
16	5	31	9N	2.5	3	in	0	0	7.66	5	94.69	3382.99
17	4	103	9S	4	2.5-3.5	obs	0	0	17.36	3	55.72	3412.35
18	4	335	9N	2	2.5	in	0	0	2.72	3	1.39	3414.95
19	4	58	10S	3	2	at	0	0	7.29	3	25.06	3410.79
20	4	283	10N	2.5	2.5	in	0	0	4.35	2	61.74	3441.42
21	4	316	10N	2	2.5	obs	0	0	5.36	4	70.32	3398.35
22	2	331	10S	3	2.5	obs	0	0	4.60	3	64.42	3407.07

23	2	13	12E	2	2	in	0	0	4.38	5	32.93	3373.32
24	4	78	12S	3	3	obs	0	0	10.29	3	94.89	3412.39
25	3	80	12N	2	2.5	in	0	0	3.85	2	98.06	3421.58
26	4	273	12N	4	2-3	in	0	0	5.62	5	69.94	3376.81
27	2	304	12N	3	2.5	obs	0	0	7.30	3	41.09	3407.18
28	4	320	12S	2	3	in	0	0	3.95	2	30.89	3440.61
29	3	326	12N	2	2	at	0	0	5.09	1	15.88	3442.59
30	3	281	13N	3.5	3	in	0	0	4.07	1	10.85	3442.58
31	4	298	13S	2.5	2.5	in	0	0	2.85	5	75.45	3376.31
32	4	300	13S	3	3.5	in	0	0	7.53	5	70.96	3376.74
33	4	14	14N	3	3	in	0	0	3.65	2	78.82	3438.21
34	4	29	14N	2	3	in	0	0	10.29	4	71.46	3396.10
35	4	74	14S	3	2.5	at	0	0	2.72	3	14.64	3414.20
36	4	78	14S	2.5	3	obs	0	0	12.79	3	86.26	3412.02
37	4	289	14N	2.5	2.5	at	0	1	4.40	3	44.66	3410.87
38	2	325	14S	2.5	3.5	in	0	0	9.32	3	89.56	3405.82
39	4	332	14S	1.5	3	in	0	0	2.72	4	1.41	3395.81
40	3	334	14N	2	2	in	0	0	4.55	1	7.73	3443.00
41	3	8	15N	2.5	3	in	0	0	4.40	1	2.22	3442.67
42	4	13	15W	3	2.5	in	0	0	5.60	3	50.58	3412.84
43	2	36	15S	2.5	3	obs	0	0	4.31	3	96.41	3406.14
44	4	298	15N	2.5	3	obs	NA	0	4.57	4	5.43	3390.93
45	4	8	16W	2	2.5	at	0	0	19.61	5	62.87	3376.50
46	3	20	16N	3.5	3	in	0	0	3.81	2	35.62	3426.56
47	2	100	16N	2	2.5	at	0	0	3.31	3	65.34	3409.10
48	3	277	16N	3	3	in	0	0	12.29	2	9.60	3421.80
49	5	295	16S	2	3	in	0	0	2.50	5	11.23	3381.82
50	3	9	17N	2	2.5	at	0	0	2.68	2	53.18	3422.32
51	4	38	17W	2.5	2.5	obs	NA	0	5.00	4	70.65	3391.15
52	2	85	17N	2.5	2.5	at	0	0	15.65	5	81.03	3375.89
53	4	87	17S	3	2	at	0	0	4.59	3	67.15	3410.75

54	2	337	17N	3	2	in	0	0	2.25	5	74.30	3373.07
55	3	4	18S	2.5	2	at	0	0	3.07	2	1.55	3427.19
56	3	68	18N	2.5	3	in	0	1	7.53	2	13.04	3426.05
57	4	86	18N	4	2.5	in	0	0	17.48	3	90.63	3411.69
58	3	273	18S	3.5	3.5	at	0	0	19.04	2	58.65	3421.30
59	2	280	18S	2	2.5	in	0	1	1.71	3	99.12	3406.26
60	2	282	18N	2	2.5	in	0	0	4.32	5	75.38	3374.77
61	4	285	18N	3	2.5	at	0	0	1.70	4	76.99	3395.73
62	4	303	18N	2	2.5	in	0	0	11.05	3	34.40	3410.78
63	2	320	18N	3.5	2	in	0	0	4.99	5	57.39	3373.79
64	4	5	19N	3	2.5	in	0	0	3.46	2	62.07	3440.91
65	2	22	19N	3.5	2	at	0	0	6.05	5	45.90	3375.64
66	3	29	19S	2	3	obs	0	1	19.59	2	29.68	3424.12
67	4	30	19W	2	2	at	0	0	18.67	3	71.38	3410.40
68	4	39	19S	1.5	2.5	in	0	0	3.46	4	79.79	3395.69
69	4	285	19N	3	2	at	0	0	7.87	2	81.08	3441.23
70	3	303	19N	3	2.5	in	0	0	3.21	2	92.30	3423.58
71	2	305	19N	3	3	obs	0	0	3.24	3	47.63	3407.11
72	2	3	20E	2	2	at	0	0	6.65	5	51.01	3374.55
73	4	7	20N	2	2	in	0	0	7.81	4	95.31	3396.21
74	3	20	20S	4	3	obs	0	0	10.60	2	87.13	3425.36
75	2	37	20S	2.5	2.5	obs	0	0	9.80	3	64.28	3405.35
76	2	60	20S	2.5	2.5	in	0	0	5.06	3	19.87	3405.75
77	2	81	20N	2.5	2	in	0	0	4.28	3	22.39	3407.24
78	4	83	20S	2.5	2.5	in	0	0	8.24	2	71.87	3440.01
79	2	274	20S	2.5	2.5	obs	0	0	6.70	3	73.51	3406.91
80	4	283	20N	3	1.5	in	0	0	5.71	4	48.31	3394.52
81	4	295	20S	3	2.5	at	0	0	6.90	5	50.21	3376.60
82	4	316	20N	2	2	in	0	0	18.57	3	24.99	3412.00
83	4	317	20N	2	2	obs	0	0	0.50	2	83.96	3440.91
84	3	340	20S	2	2.5	at	0	0	2.75	2	54.16	3422.05

85	3	360	20S	3	2.5	obs	0	0	12.81	2	87.90	3423.83
86	4	90	20N/27S	3.5	2.5	in	0	0	7.62	4	87.17	3396.33
87	2	15	21S	1.5	2	in	0	0	4.49	5	29.07	3374.88
88	2	19	21N	2	2.5	in	0	0	3.17	3	46.91	3408.95
89	4	35	21S	2	2.5	at	0	0	1.40	2	83.05	3440.27
90	4	35	21S	2	3	at	0	0	15.52	3	31.01	3411.31
91	4	47	21S	2.5	3	obs	0	0	9.48	3	11.42	3415.31
92	4	57	21N	3	3	at	0	0	4.16	3	91.44	3410.87
93	3	62	21N	3	2.5	in	0	1	3.11	2	16.61	3426.37
94	4	73	21S	3.5	2.5	at	0	0	3.89	2	91.57	3438.77
95	4	80	21S	2.5	2.5	in	0	0	8.18	3	12.26	3414.22
96	4	327	21N	2.5	2.5	in	0	0	9.40	5	10.43	3375.89
97	4	345	21S	2	2	at	0	0	6.78	3	7.71	3411.32
98	4	350	21S	1.5	2.5	in	0	0	3.35	4	6.86	3397.08
99	4	360	22E	2.5	2	in	0	0	7.57	4	68.31	3388.72
100	4	360	22W	2.5	2.5	obs	0	0	3.94	5	51.93	3376.73
101	4	9	22N	1.5	3	in	0	0	5.72	4	60.09	3394.72
102	4	19	22N	2.5	1.5	in	0	0	3.26	2	89.99	3441.33
103	4	20	22N	2.5	3	in	0	0	3.91	2	36.42	3439.15
104	4	20	22S	2	3	obs	NA	0	2.60	4	34.28	3397.59
105	3	24	22S	2.5	2.5	in	0	0	3.73	2	79.28	3424.18
106	4	67	22S	2.5	3	in	0	0	6.00	2	51.57	3441.01
107	3	85	22N	2.5	3	obs	0	0	8.10	2	67.84	3423.84
108	4	302	22S	4	2	at	0	0	8.61	2	89.34	3439.96
109	3	328	22S	3.5	2.5	at	0	0	8.98	2	59.70	3421.25
110	2	360	23E	3	2	in	0	0	6.78	5	16.98	3374.66
111	2	14	23W	2.5	1.5-2.5	obs	0	0	16.51	5	91.42	3376.83
112	4	37	23N	3	2.5	in	0	1	2.16	2	74.35	3441.61
113	4	61	23N	1.5	2	obs	0	0	11.37	2	63.47	3439.55
114	4	72	23N	1.5	2	in	0	0	4.72	5	26.73	3376.96
115	4	142	23N	2.5	2-3	obs	0	0	9.91	3	89.56	3412.17

116	2	288	23N	4	2.5	in	0	0	2.77	3	98.17	3405.05
117	2	297	23N	2.5	2.5	at	0	0	3.46	5	88.51	3372.71
118	4	306	23S	3	2.5	in	0	0	4.94	5	39.37	3379.14
119	4	330	23S	2.5	2	at	0	0	6.40	2	33.45	3439.09
120	3	343	23N	4	2.5	at	0	0	3.79	2	37.06	3423.37
121	2	356	23S	1.5	2	at	0	0	2.49	3	64.11	3404.37
122	4	275	23N/36N	4	2.5	obs	NA	0	0.73	4	41.13	3397.75
123	5	2	24N	2.5	3	in	0	0	3.99	5	68.92	3382.30
124	4	4	24S	2	2.5	at	0	0	2.60	2	65.67	3437.71
125	4	15	24N	1.5	3	obs	8 mm EI	0	2.92	3	69.80	3398.82
126	2	70	24S	2.5	2.5	obs	0	0	4.48	5	36.00	3375.16
127	2	72	24S	2.5	2.5	in	0	0	3.25	5	72.41	3372.23
128	4	282	24N	2.5	2.5	in	0	0	4.20	4	60.24	3391.83
129	2	287	24N	2	1.5-2.5	in	0	0	12.23	5	6.05	3374.75
130	3	306	24S	3.5	2.5	obs	0	0	6.44	2	46.45	3420.75
131	4	308	24N	2.5	2	obs	0	0	1.64	5	10.81	3378.27
132	2	312	24S	3	3.5	in	0	1	5.17	3	40.18	3409.51
133	4	330	24S	2	2	obs	0	0	2.52	4	68.40	3397.92
134	4	334	24N	3	2.5	obs	0	0	11.28	2	80.72	3441.82
135	5	337	24N	2.5	3	in	0	0	4.76	5	13.95	3382.39
136	4	17	25N	3	2	in	0	0	10.90	2	78.30	3439.54
137	3	20	25S	3.5	2-3.5	at	0	0	19.55	2	53.60	3423.33
138	4	29	25N	3	1.5-2.5	in	0	0	6.49	5	21.85	3376.53
139	4	81	25N	3	3	at	0	0	6.59	5	93.30	3377.03
140	4	90	25N	2	2	in	0	0	3.84	4	49.13	3395.65
141	2	295	25S	3.5	2	obs	0	0	8.16	3	60.96	3406.69
142	1	331	25N	2.5	3.5	obs	0	0	3.68	4	46.58	3385.95
143	4	355	25S	3	2.5	in	0	0	7.14	5	29.70	3377.53
144	4	8	26N	2	2.5	obs	0	0	8.11	4	81.10	3388.88
145	4	18	26S	2.5	3	in	0	0	4.06	4	6.43	3395.44
146	4	29	26E	2	3	obs	0	0	5.92	3	54.94	3413.19

147	3	65	26S	3	2.5-3.5	at	0	0	14.01	2	38.97	3421.84
148	3	80	26S	4	3	at	0	0	8.48	2	31.03	3421.41
149	4	277	26N	3.5	3.5	obs	0	0	3.92	4	12.16	3398.19
150	2	292	26N	2.5	2	at	0	0	5.69	5	60.70	3375.59
151	4	328	26S	2	2	in	0	0	4.59	4	66.17	3394.37
152	4	332	26N	2	3	at	0	1	3.70	4	14.88	3397.06
153	4	34	26N/33N	4	2.5	in	0	0	7.17	4	48.73	3390.14
154	2	360	27E	2.5	2	at	0	0	4.67	5	86.96	3372.54
155	5	4	27N	1.5	2.5	in	0	0	2.66	5	38.74	3384.11
156	4	5	27S	2	2	obs	0	0	5.29	4	36.53	3396.84
157	4	25	27N	3	3	obs	0	0	3.12	4	1.46	3391.63
158	4	31	27N	2.5	2.5	at	0	0	9.36	3	9.96	3412.45
159	4	63	27N	2	3.5	obs	0	0	8.69	4	95.97	3397.78
160	5	88	27N	3	3.5	in	0	0	4.57	5	61.53	3382.98
161	2	273	27S	2	2	in	0	0	8.33	5	83.89	3373.13
162	2	275	27N	2	3	in	0	0	2.51	3	81.82	3406.42
163	4	316	27S	2	2	in	0	0	12.88	4	31.18	3395.13
164	4	342	27E	3.5	3.5	in	0	0	4.52	4	73.41	3390.17
165	3	300	27S/40N	3.5	2.5	obs	0	0	6.69	2	92.35	3424.83
166	3	4	28N	2	2	in	0	0	6.09	2	73.02	3419.66
167	2	37	28W	3.5	2.5	at	0	0	5.47	5	81.50	3376.72
168	5	42	28N	1.5	2	obs	0	0	9.77	5	80.09	3383.28
169	3	292	28N	2	2.5	at	0	0	3.64	2	75.06	3423.35
170	4	307	28N	2.5	3	obs	0	0	4.36	4	17.91	3397.47
171	4	310	28W	2.5	3	in	0	1	2.74	3	42.11	3414.20
172	3	317	28N	2.5	2.5	in	0	1	6.09	2	19.42	3426.22
173	4	326	28N	2.5	2.5	at	0	0	6.36	4	25.13	3394.89
174	4	334	28S	1.5	2.5	obs	0	1	5.36	4	15.28	3398.22
175	4	340	28N	4	3	in	0	0	2.52	2	57.53	3440.49
176	1	62	28N/15S	3	4	in	0	0	5.00	4	2.52	3384.89
177	4	13	29E	3	3	at	0	0	6.12	5	5.81	3377.04

178	4	25	29N	2.5	2	in	0	0	6.49	2	48.17	3438.06
179	4	67	29N	1.5	3	obs	0	0	4.48	4	97.98	3398.72
180	4	75	29N	3	3	in	0	0	3.98	2	7.40	3440.31
181	4	305	29N	2.5	3.5	at	0	0	3.72	4	8.46	3397.35
182	4	343	29N	3	2.5	in	0	0	6.00	5	16.29	3376.90
183	2	354	29W	2.5	2	at	0	0	6.17	5	90.06	3373.16
184	3	2	30S	2	2	at	0	0	2.65	2	86.49	3424.22
185	4	77	30S	4	2	at	0	0	7.97	5	80.22	3377.99
186	4	78	30N	2	2	obs	NA	0	3.42	4	29.15	3391.14
187	4	84	30N	2.5	2	at	0	0	11.14	2	81.20	3439.29
188	4	287	30N	2	2.5	at	0	0	1.72	4	0.88	3391.16
189	2	303	30N	2	2.5	at	0	0	2.63	3	84.69	3406.42
190	2	314	30S	3	2	in	0	0	8.78	3	48.02	3409.82
191	4	322	30S	2	2	obs	0	0	7.87	3	3.56	3412.05
192	3	346	30S	2	2	at	0	0	10.89	2	68.54	3423.86
193	4	61	31N	2	2	in	0	0	10.26	2	69.21	3438.89
194	4	76	31N	3	2.5	in	0	0	19.57	3	12.70	3413.27
195	4	337	31S	3	2	at	0	0	4.72	2	40.79	3438.67
196	5	343	31N	4	3.5	in	0	0	5.64	5	17.25	3384.14
197	4	360	32E	1.5	2	obs	0	0	4.40	5	2.13	3377.68
198	4	41	32E	2	2.5	at	0	0	4.78	3	74.08	3410.06
199	5	48	32S	4	2.5	in	0	0	6.44	5	28.95	3384.26
200	5	50	32S	4	3.5	in	0	0	5.18	5	18.08	3381.98
201	3	66	32N	3	2.5	at	0	0	6.26	2	72.91	3423.77
202	4	164	32S	2	2.5	at	0	1	8.07	3	62.55	3410.21
203	2	296	32N	2	2	in	0	0	9.70	5	81.28	3374.36
204	1	306	32S	2	2.5	in	0	0	2.68	4	98.64	3384.83
205	4	311	32N	3	2.5	obs	0	0	0.53	2	89.70	3439.43
206	4	332	32N	3.5	2.5	in	0	0	6.63	2	51.75	3439.93
207	4	76	32N/30N	2	3.5	obs	NA	0	1.47	4	62.67	3397.73
208	2	5	33N	2.5	3	obs	0	0	3.27	3	48.16	3405.74

209	4	16	33E	1.5	2	at	0	0	4.55	3	88.26	3410.94
210	5	36	33N	2	2.5	in	0	0	3.79	5	27.60	3381.46
211	4	45	33S	2	2	in	0	1	3.03	4	12.88	3395.48
212	4	50	33N	3	2	at	0	0	6.09	3	46.40	3411.79
213	4	51	33E	2.5	2.5	obs	0	0	3.49	3	48.89	3413.90
214	4	278	33N	3.5	1.5	obs	0	0	0.50	2	93.45	3440.19
215	2	303	33N	3.5	2.5	in	0	0	3.49	5	63.05	3372.81
216	4	360	34W	3.5	2.5	obs	0	0	5.62	3	41.24	3413.60
217	4	10	34N	4.5	2	at	0	0	7.24	2	49.17	3438.20
218	3	33	34S	5	2	at	0	0	8.43	2	72.55	3422.29
219	3	39	34S	1.5	3	obs	0	0	5.55	2	2.53	3426.99
220	4	280	34S	2	2	in	0	0	6.01	4	77.86	3396.66
221	4	325	34N	4.5	2	in	0	0	3.71	5	98.00	3376.52
222	3	344	34S	2	2	obs	0	0	2.52	1	21.87	3442.63
223	4	357	34S	1.5	2.5	obs	0	0	3.15	4	77.00	3398.45
224	4	27	35N	2	2.5	in	0	0	3.03	2	5.74	3439.51
225	4	80	35S	2	3	in	0	0	3.02	3	40.98	3410.82
226	4	288	35N	3	3	at	0	0	3.91	4	82.63	3387.05
227	4	322	35S	2.5	3	in/at	0	0	3.39	5	61.35	3376.95
228	2	342	35S	2	2.5	at	0	0	6.04	3	29.92	3409.24
229	1	352	35N/41N	3	3.5	obs	NA	0	4.15	4	64.35	3385.63
230	3	85	35S/48S	3	2.5	obs	0	0	28.15	2	14.03	3425.21
231	5	11	36N	2.5	2.5	in	0	0	6.06	5	78.55	3382.67
232	4	14	36N	1.5	3	at	0	0	3.92	4	55.28	3395.71
233	3	69	36N	1.5	2.5	obs	0	0	4.52	2	70.05	3423.88
234	4	77	36N	2.5	2	at	0	0	1.66	2	79.25	3440.17
235	3	79	36N	2.5	2.5	in	0	0	4.97	2	74.24	3424.44
236	3	87	36N	3	2-3	at	0	0	11.88	2	80.95	3422.18
237	4	93	36N	4	3.5	in	0	0	8.26	4	58.14	3388.48
238	4	277	37S	2.5	2	in	0	0	5.94	4	69.16	3388.62
239	4	295	37N	3	2.5	in	0	0	8.51	4	6.51	3397.44

240	3	303	37S	3	3	at	0	0	3.19	2	32.72	3426.72
241	2	342	37S	2	1.5-2	at	0	0	5.39	5	89.07	3375.32
242	2	345	37N	2	2	obs	0	0	15.43	5	75.88	3375.53
243	2	4	38E	2.5	2.5	in	0	0	9.01	5	82.59	3373.49
244	4	288	38N	3	2.5	in	0	0	0.75	2	91.57	3438.39
245	5	303	38S	1.5	3	in	0	0	5.46	5	2.56	3382.19
246	5	55	39S	2	1.5	in	0	1	8.73	5	40.89	3382.58
247	4	295	39S	3	2.5	at	0	0	7.47	2	26.27	3439.71
248	4	48	40S	2.5	2.5	in	0	0	5.69	4	42.61	3395.76
249	4	59	40N	3	2.5	obs	0	0	3.98	3	38.22	3413.64
250	4	298	40N	2	2	in	0	1	1.21	2	14.33	3438.76
251	4	321	40N	3	2.5	in	0	0	3.54	4	77.73	3388.70
252	3	339	40N	1.5	2.5	in	0	1	3.54	1	20.32	3442.10
253	4	19	41S	2.5	3.5	obs	0	0	6.32	3	45.50	3413.19
254	3	62	41S	2.5	2.5	obs	0	1	10.64	2	47.16	3423.59
255	5	63	42N	3	1.5	at	0	0	4.62	5	44.45	3381.99
256	3	352	42N	2.5	2.5	at	0	0	3.83	2	66.72	3421.17
257	3	355	42N	4.5	2.5	at	0	0	2.93	1	24.12	3441.48
258	5	358	42N/28N	3	2.5	in	0	1	4.49	5	86.74	3382.30
259	3	40	42S	4.5	2.5	at	0	0	16.28	2	17.95	3425.57
260	5	16	43S	2	2	in	0	1	4.51	5	23.00	3381.69
261	5	18	43N	1.5	3.5	in	0	0	5.41	5	63.40	3383.02
262	4	90	43S	1.5	1.5	in	0	1	2.66	2	1.37	3440.99
263	2	308	43N	4.5	2	in	0	0	7.21	5	94.67	3373.48
264	4	341	43S	2.5	2	at	0	0	5.87	2	54.68	3438.64
265	4	315	44N	2.5	3	at	0	0	3.16	2	96.87	3438.02
266	4	343	44S	2	2	at	0	1	4.26	4	75.01	3388.01
267	4	35	44	5	3.5	in	0	0	4.13	4	78.54	3387.00
268	5	50	45S	1.5	2.5	in	0	0	3.70	5	50.79	3383.76
269	4	58	45N	3.5	4	obs	0	0	10.07	5	54.81	3377.01
270	4	300	45S	2.5	2.5	obs	0	0	4.23	3	31.94	3414.83

271	4	321	45N	3	3	in	0	0	2.29	4	95.76	3388.58
272	4	325	45N	2	2.5	obs	0	1	7.09	2	20.63	3441.21
273	4	207	45	5	3	in	0	0	3.01	4	49.43	3387.25
274	4	26	46N	5	2	in	0	0	4.17	4	88.55	3388.96
275	3	323	46N	4	3.5	obs	0	0	5.78	2	97.11	3424.95
276	5	339	46N	2	3	in	0	1	5.39	5	38.53	3382.16
277	5	353	46S	1.5	3	in	0	1	6.90	5	96.88	3384.26
278	4	32	47S	2.5	3	in	0	0	4.02	4	43.49	3388.63
279	5	323	48N	2.5	1.5	obs	NA	0	2.27	5	71.60	3384.80
280	3	53	50N	3	3	at	0	0	2.44	1	18.12	3441.70
281	3	333	50N	3	2.5	at	0	0	3.58	2	94.99	3423.70
282	5	84	51N	2.5	2	in	0	0	3.31	5	95.82	3381.74
283	4	65	52N	3	3	obs	0	0	3.75	5	95.73	3379.43
284	4	72	52S	2	2.5	in	0	1	3.88	2	57.84	3439.27
285	3	80	54N	2.5	3	at	0	0	3.65	2	71.28	3423.65
286	4	62	56S	1.5	2	at	0	0	2.70	2	62.10	3438.49
287	3	297	58N	3.5	3	obs	0	0	1.36	1	38.44	3441.64
288	4	321	58S	3	2	in	0	0	2.77	2	46.01	3437.86
289	4	283	59S	3	2.5	inat	0	1	4.57	5	22.27	3376.03
290	4	81	63S	2	3.5	at	0	1	3.00	2	79.83	3437.63
291	3	296	64N	2	3	obs	0	1	1.61	2	85.83	3421.76
292	3	350	66S	2	2	in	0	1	2.34	1	5.90	3441.75
293	4	300	68N	3.5	2.5	in	0	1	3.20	2	13.19	3439.54
294	4	274	69N	3	3	obs	0	0	0.87	2	30.51	3440.34
295	4	351	70S	3	3	in	0	0	2.52	2	8.89	3439.77
296	4	73	72S	3	2.5	obs	0	0	4.00	2	53.89	3439.98
297	4	26	74S	2.5	2	in	0	0	3.13	2	38.83	3440.98
298	2	285	76N	2.5	2	obs	0	1	1.42	3	26.12	3404.25
299	3	84	77S	2	3.5	obs	0	1	1.54	1	35.45	3441.53
300	3	282	77N	1.5	1.5	obs	0	1	1.75	2	84.08	3423.41
301	2	281	79N	2	2	obs	0	1	1.48	3	23.71	3405.97

302	3	345	80S	2.5	3	in	0	1	2.79	1	9.72	3440.91
303	3	296	81N	4	3.5	obs	unknown	1	0.94	1	75.85	3442.28
304	3	304	81N	3	4	obs	0	1	1.23	1	47.51	3441.33
305	2	84	83N	2.5	2	obs	0	1	1.87	3	33.92	3405.79
306	2	285	83N	2.5	1.5	obs	0	1	1.42	3	55.40	3406.83
307	2	86	84N	3	1.5	obs	0	1	1.57	3	51.59	3406.38
308	2	302	84N	2.5	2.5	obs	0	1	0.54	3	49.81	3407.43
309	4	292	85N	3	1.5	obs	0	1	1.11	3	16.21	3415.99
310	3	134	86S	3	2.5	obs	0	1	1.36	2	98.71	3422.29
311	2	72	87S	3	1.5	in	0	1	2.62	3	8.55	3406.05
312	2	294	87N	1.5	1.5	obs	0	1	0.90	3	7.64	3406.90
313	2	327	87N	3	1.5	obs	0	1	1.57	3	52.72	3406.48
314	3	299	88N	2	2	obs	0	1	1.33	2	47.13	3426.00
315	3	302	88N	2	2.5	obs	0	1	1.45	2	44.15	3422.49
316	3	45	90	3.5	3	obs	0	0	2.68	1	24.89	3441.62
317	2	54	90	1.5	2	in	0	1	1.78	3	55.68	3402.88
318	4	70	90	2	2	obs	0	1	1.59	2	41.66	3440.66
319	4	80	90	4	2.5	obs	0	1	2.64	2	15.12	3440.03
320	2	310	90	2	2	obs	0	1	2.07	3	12.56	3406.12
321	4	332	90	3	3.5	at	unknown	1	2.13	2	72.43	3440.00

Appendix B

STEREOPLOTS OF DISCONTINUITIES

FOR EACH GELOGIC UNIT AND COMBINED GENETIC UNIT OF CWF AND FWF

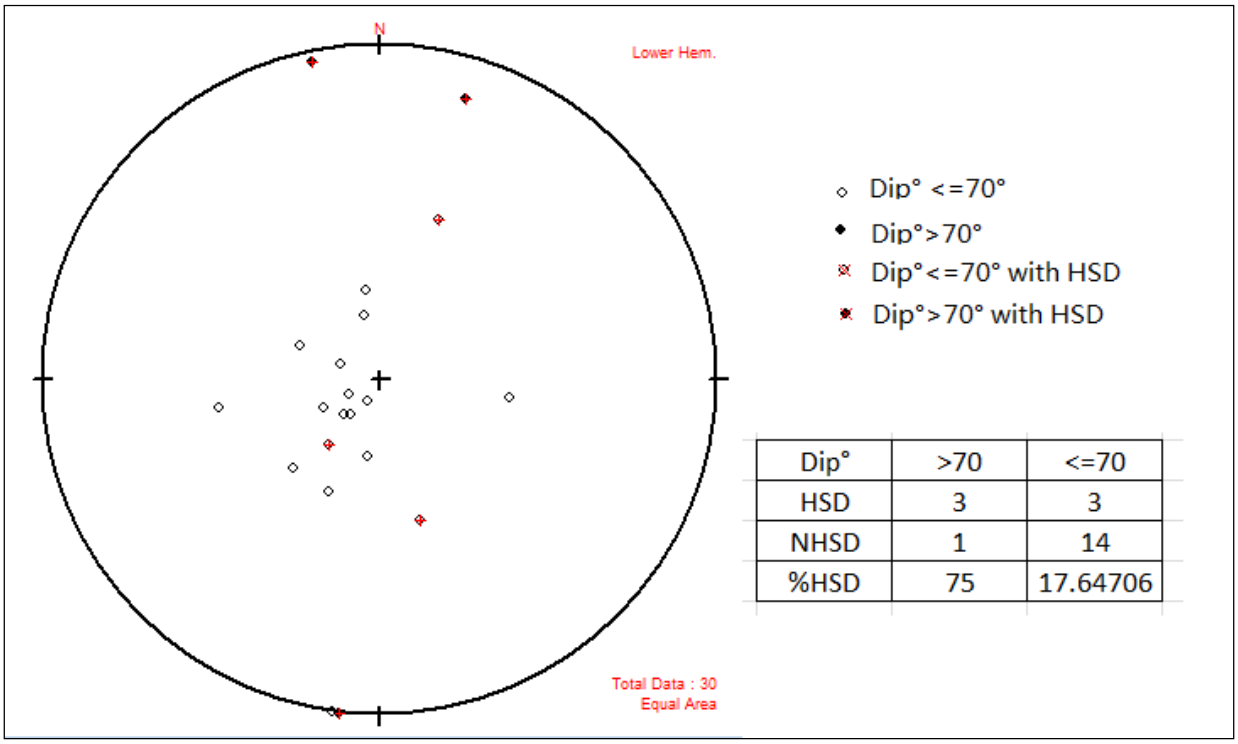

Dip°	>70	<=70
HSD	3	3
NHSD	1	14
%HSD	75	17.64706

Figure B-1. Stereoplot of Discontinuities Mapped Faces of Geologic Unit 1 of the CWF

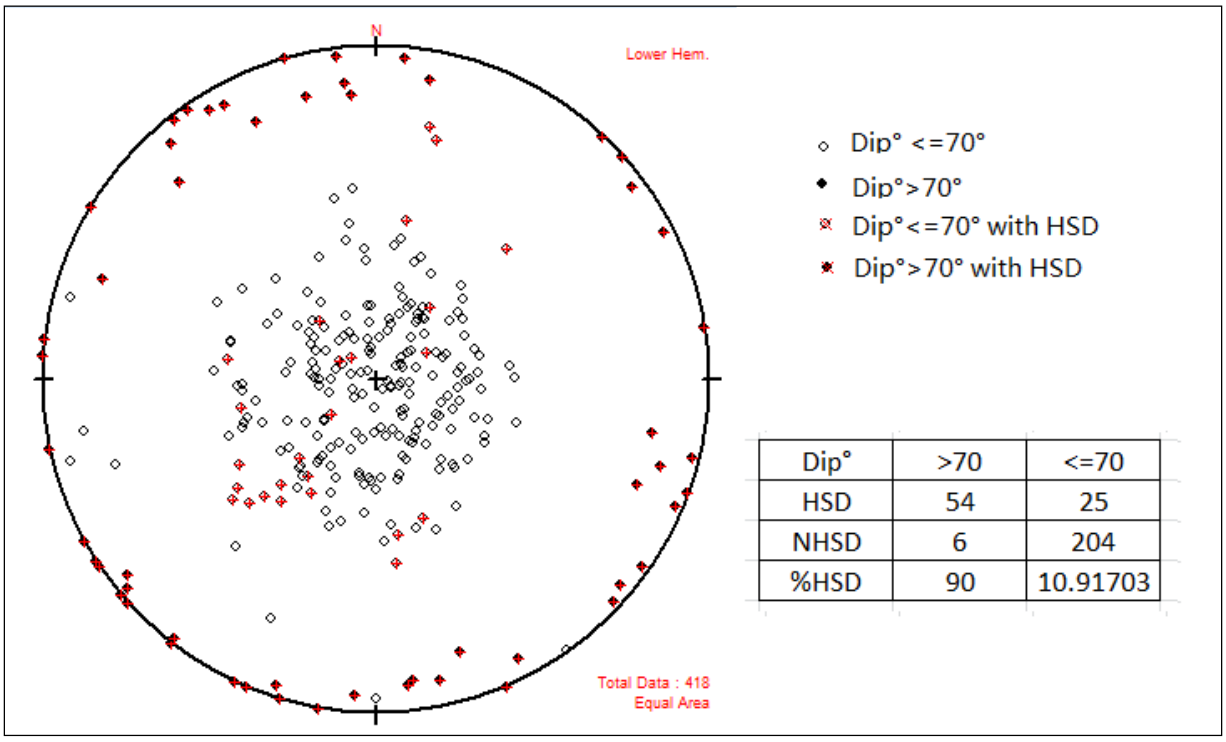

Dip°	>70	<=70
HSD	54	25
NHSD	6	204
%HSD	90	10.91703

Figure B-2. Stereoplot of Discontinuities Mapped Faces of Geologic Unit 2 of the CWF

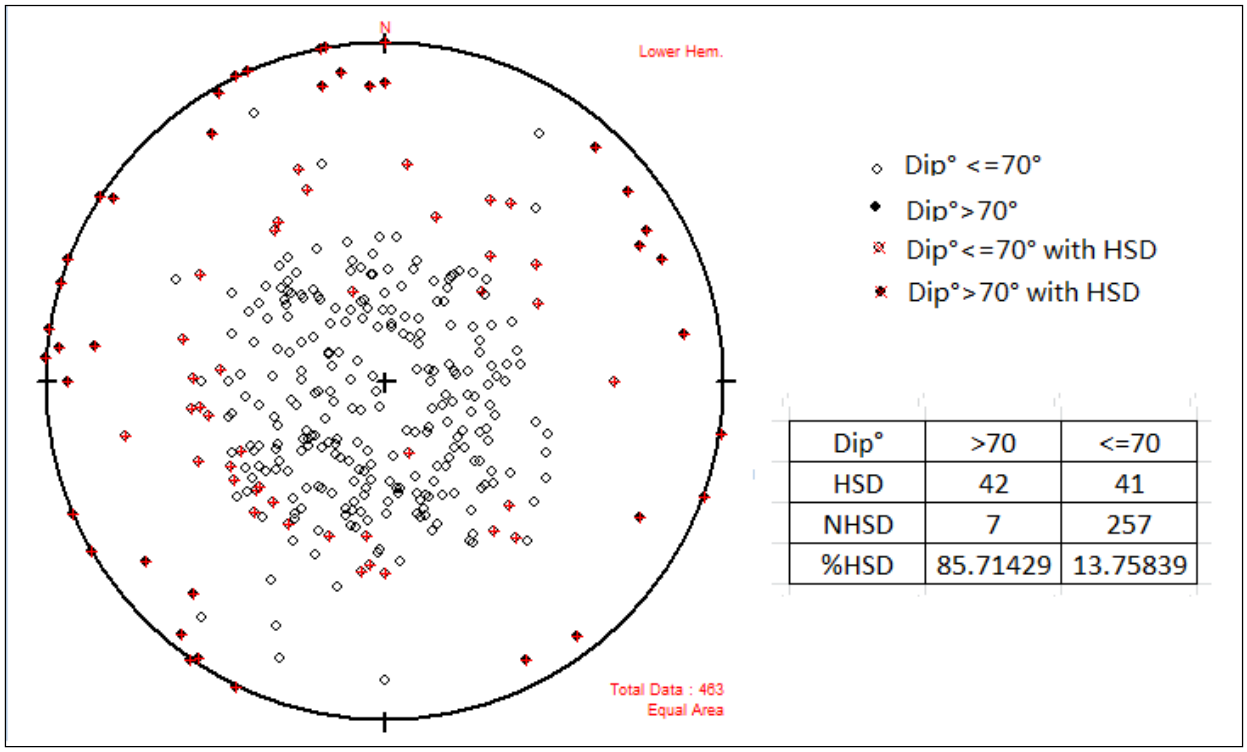

Dip°	>70	<=70
HSD	42	41
NHSD	7	257
%HSD	85.71429	13.75839

Figure B-3. Stereoplot of Discontinuities Mapped Faces of Geologic Unit 4 of the CWF

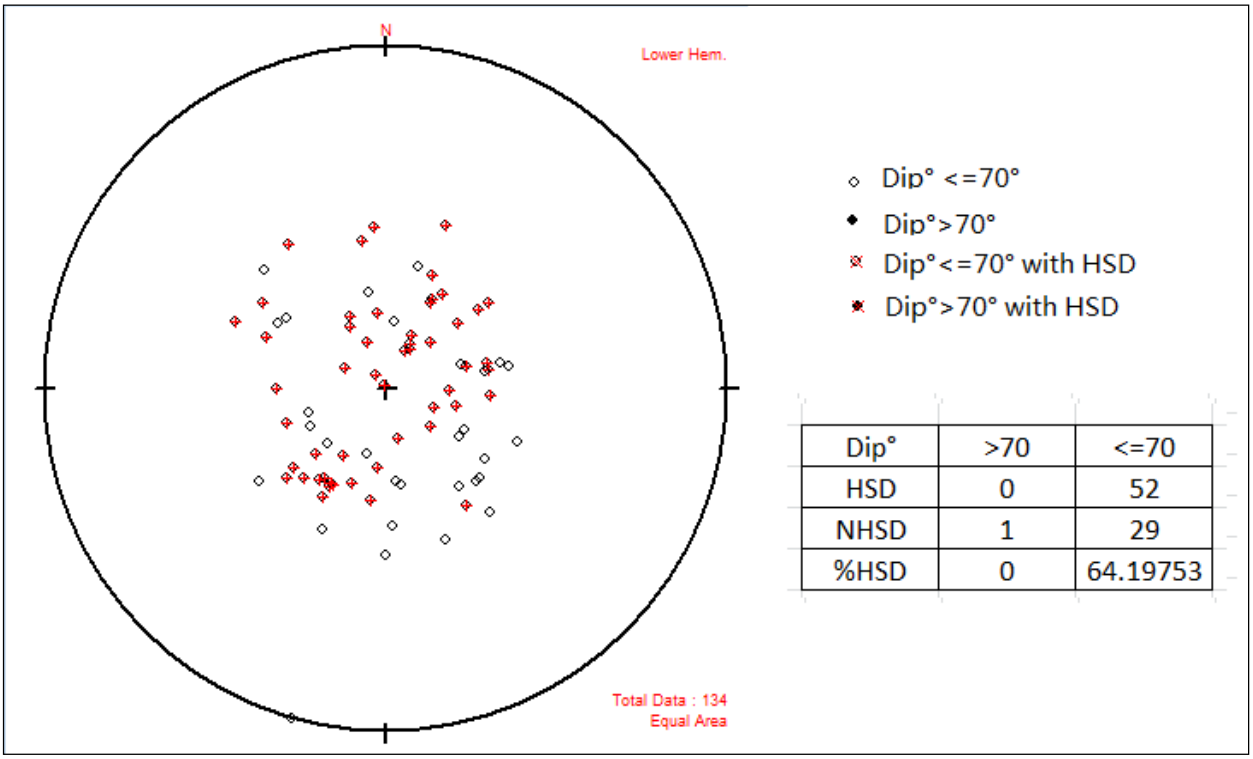

Dip°	>70	<=70
HSD	0	52
NHSD	1	29
%HSD	0	64.19753

Figure B-4. Stereoplot of Discontinuities Mapped Faces of Geologic Unit 5 of the CWF

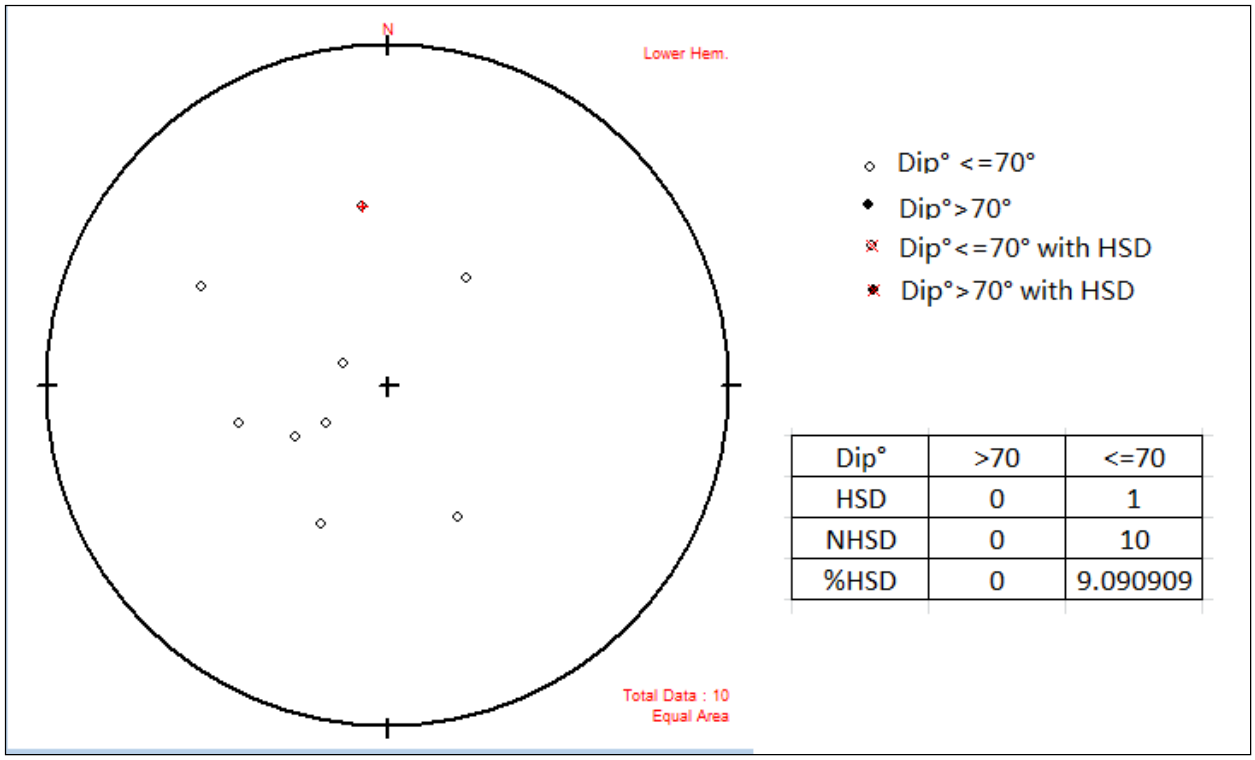

Dip°	>70	<=70
HSD	0	1
NHSD	0	10
%HSD	0	9.090909

Figure B-5. Stereoplot of Discontinuities Mapped Faces of Geologic Unit 1 of the FWF

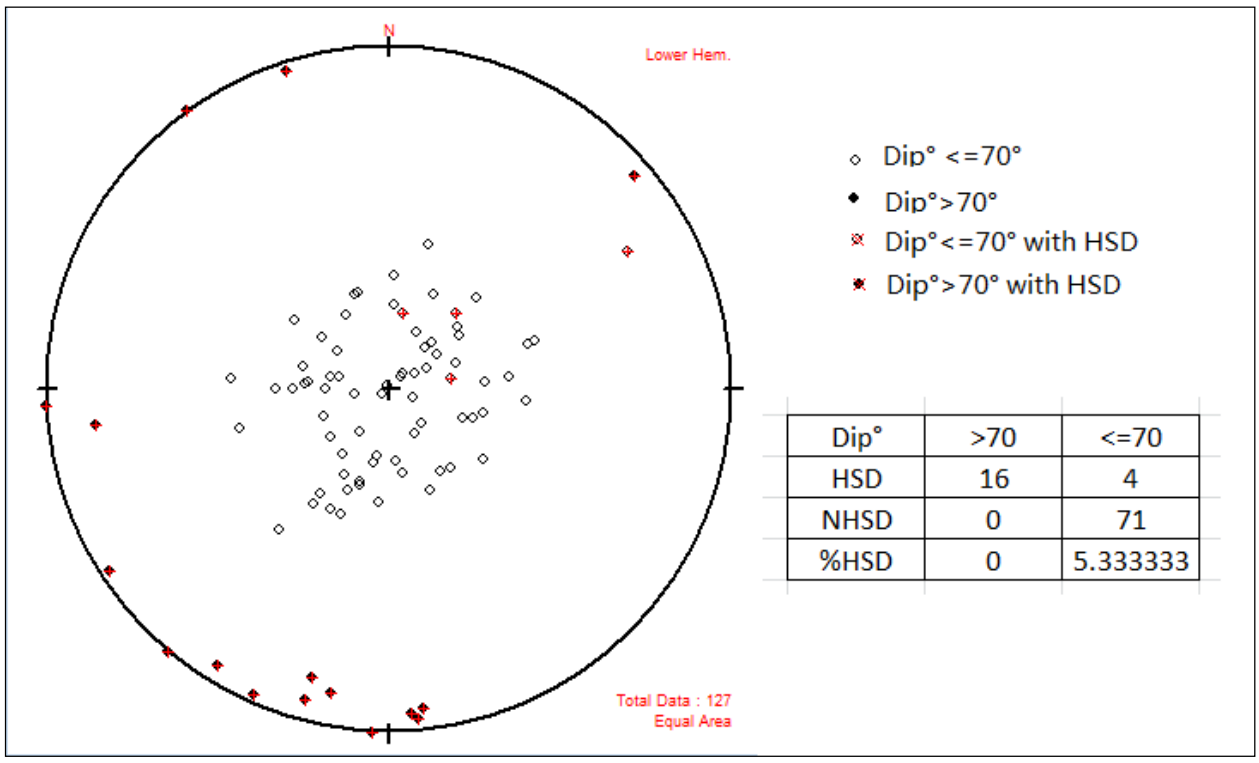

Dip°	>70	<=70
HSD	16	4
NHSD	0	71
%HSD	0	5.333333

Figure B-6. Stereoplot of Discontinuities Mapped Faces of Geologic Unit 2 of the FWF

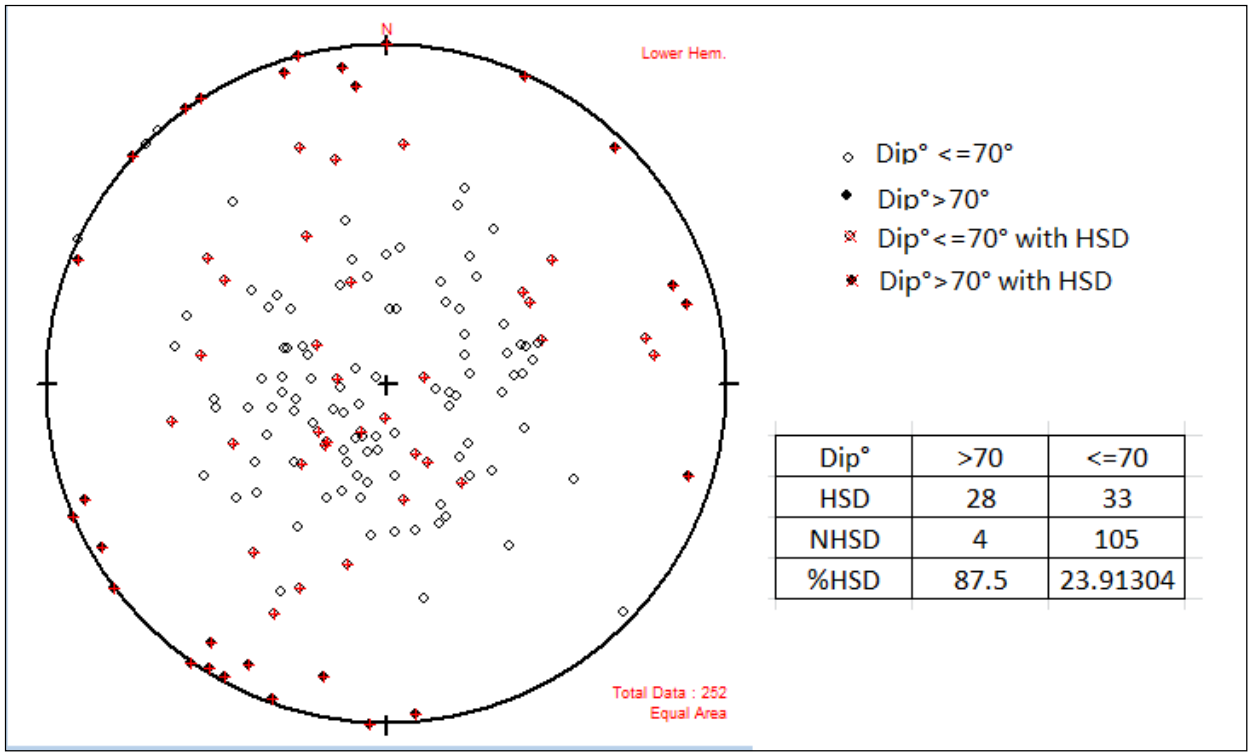

Dip°	>70	<=70
HSD	28	33
NHSD	4	105
%HSD	87.5	23.91304

Figure B-7. Stereoplot of Discontinuities Mapped Faces of Geologic Unit 3 of the FWF

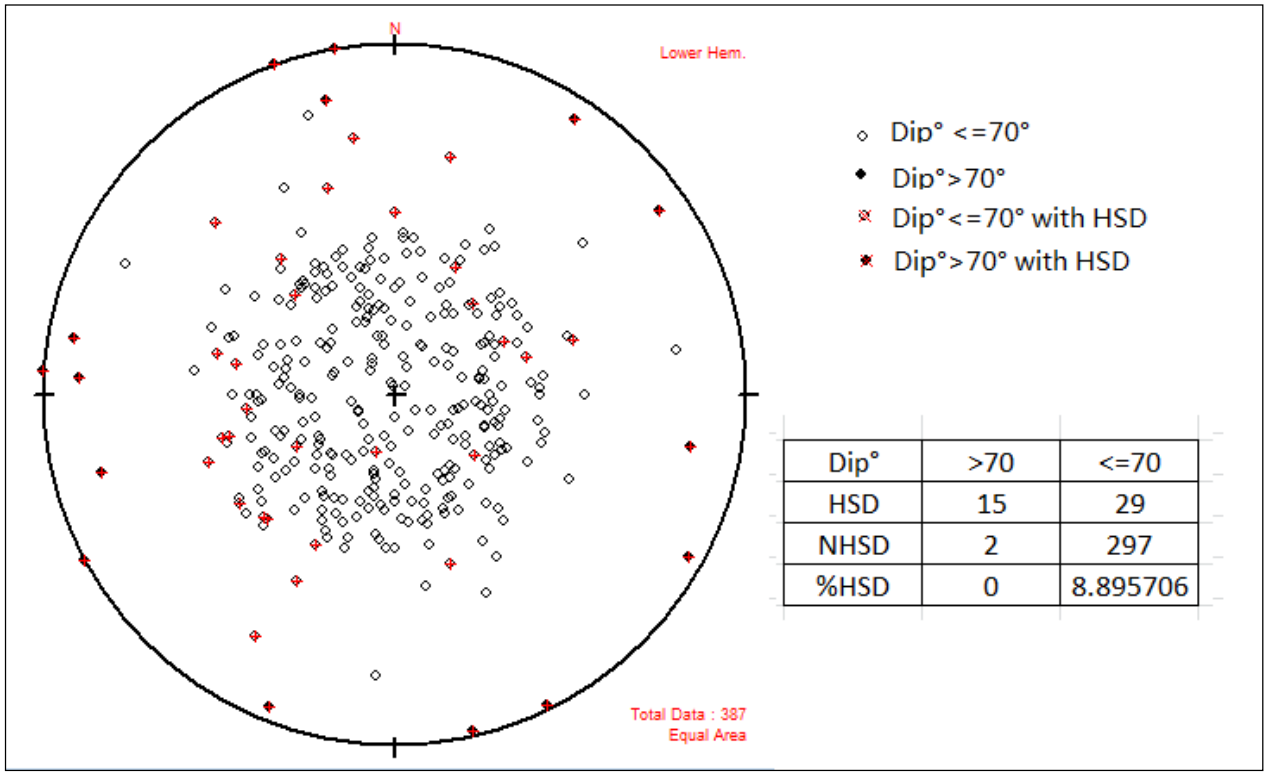

Dip°	>70	<=70
HSD	15	29
NHSD	2	297
%HSD	0	8.895706

Figure B-8. Stereoplot of Discontinuities Mapped Faces of Geologic Unit 4 of the FWF

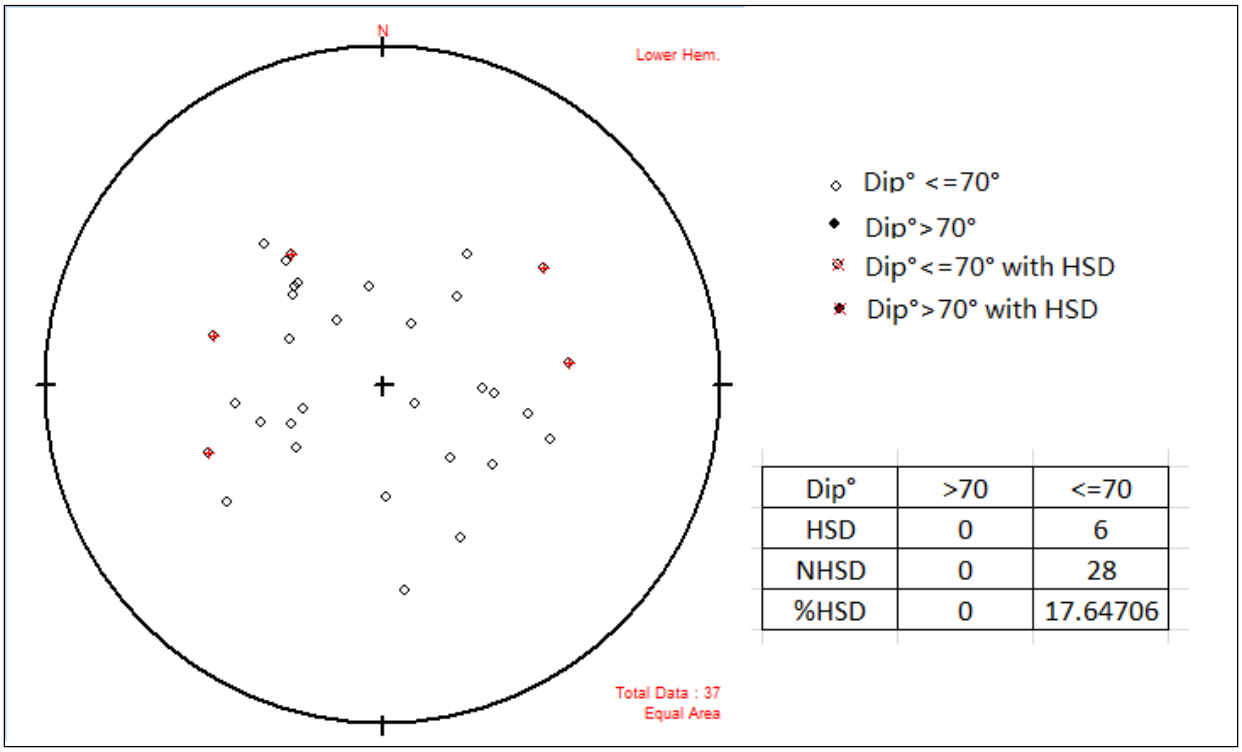

Dip°	>70	<=70
HSD	0	6
NHSD	0	28
%HSD	0	17.64706

Figure B-9. Stereoplot of Discontinuities Mapped Faces of Geologic Unit 5 of the FWF

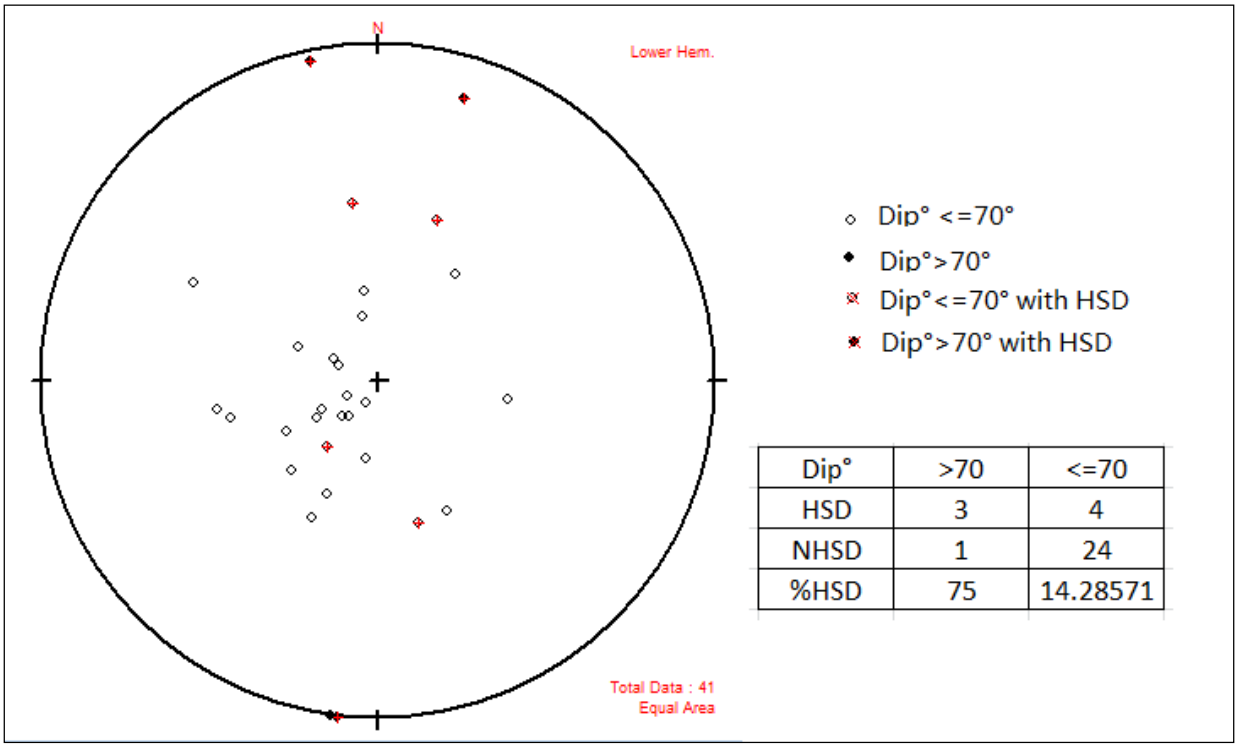

Dip°	>70	<=70
HSD	3	4
NHSD	1	24
%HSD	75	14.28571

Figure B-10. Stereoplot of Discontinuities Mapped Faces of Geologic Unit 1 of the CWF& FWF

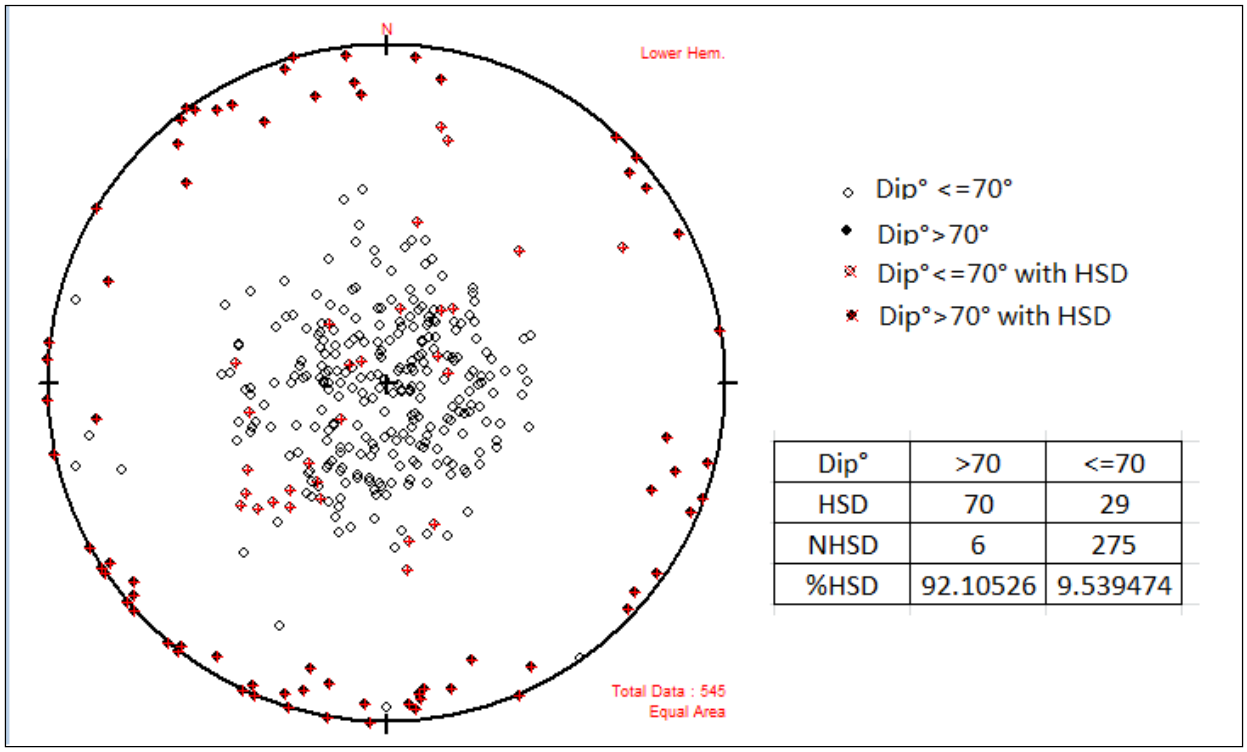

Dip°	>70	<=70
HSD	70	29
NHSD	6	275
%HSD	92.10526	9.539474

Figure B-11. Stereoplot of Discontinuities Mapped Faces of Geologic Unit 2 of the CWF&FWF

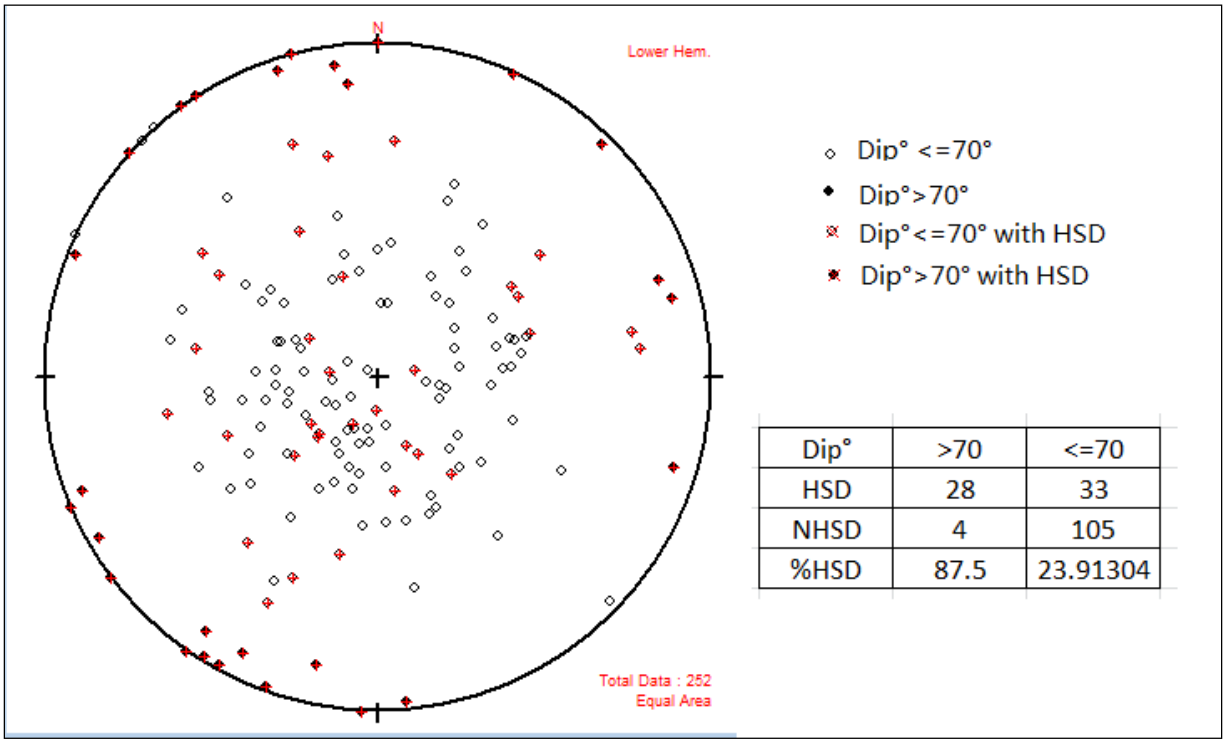

Dip°	>70	<=70
HSD	28	33
NHSD	4	105
%HSD	87.5	23.91304

Figure B-12. Stereoplot of Discontinuities Mapped Faces of Geologic Unit 3 of the CWF&FWF

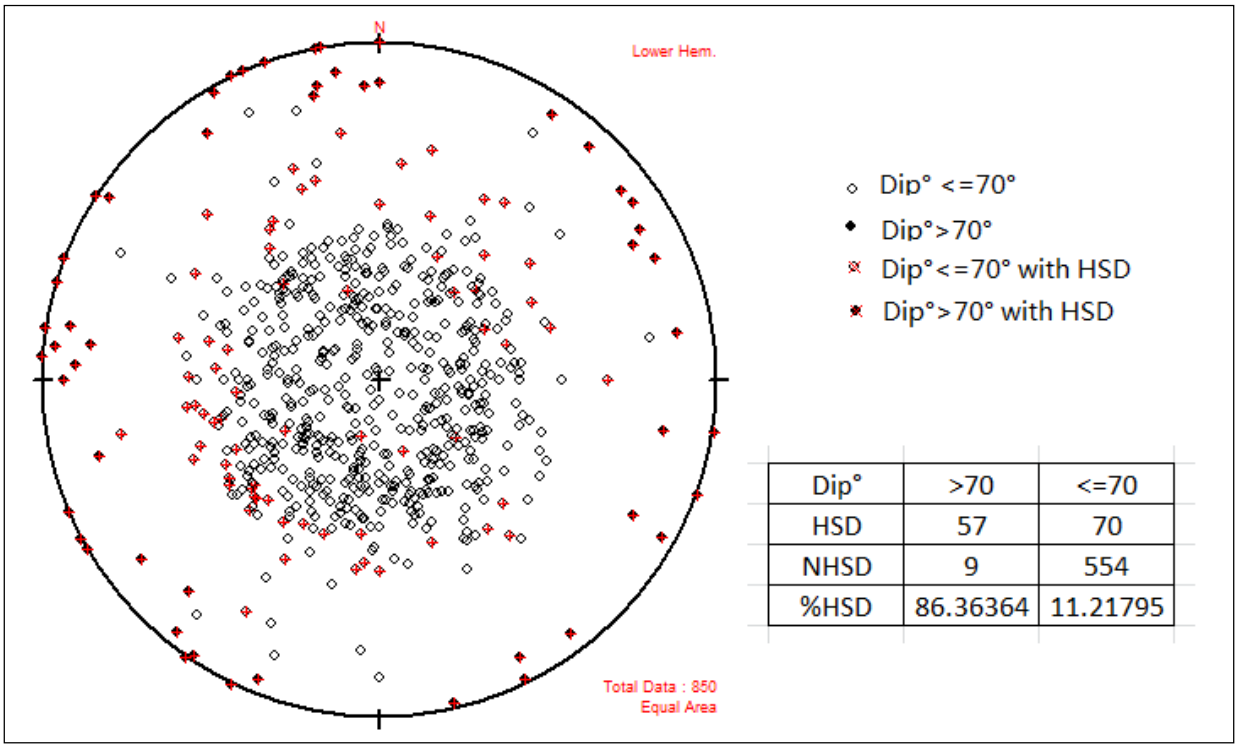

Dip°	>70	<=70
HSD	57	70
NHSD	9	554
%HSD	86.36364	11.21795

Figure B-13. Stereoplot of Discontinuities Mapped Faces of Geologic Unit 4 of the CWF&FWF

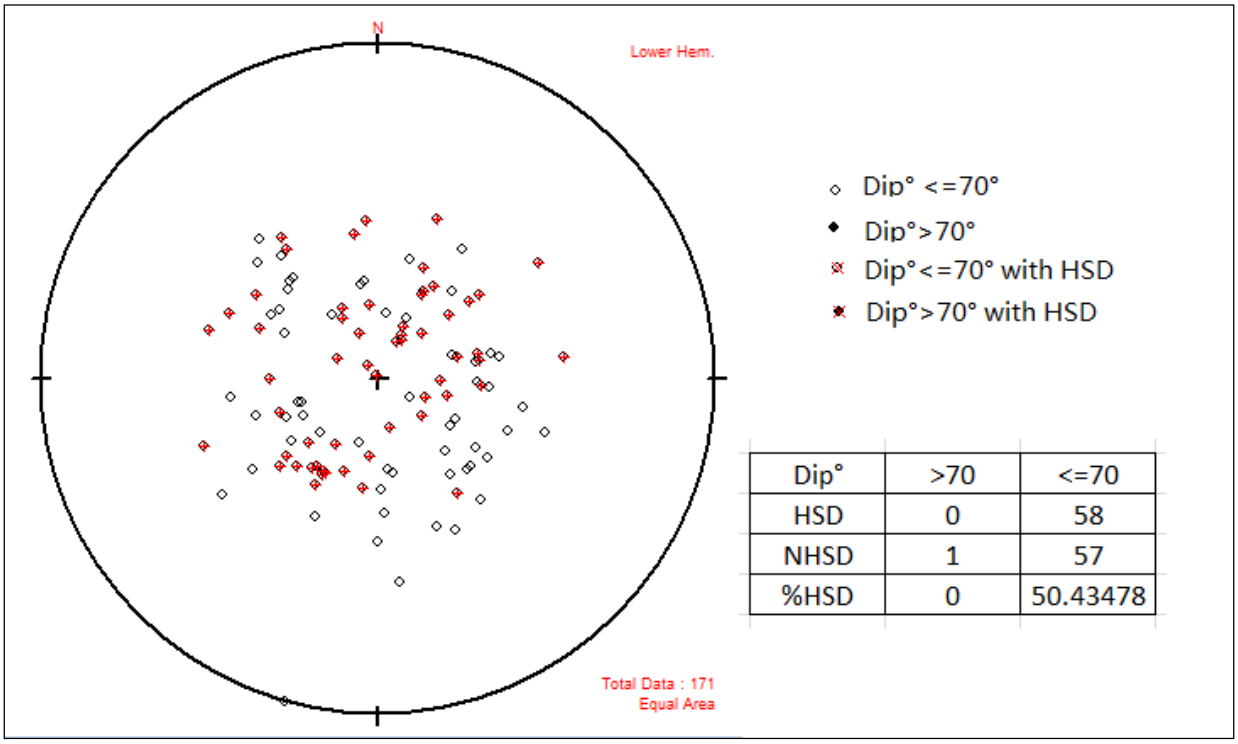

Dip°	>70	<=70
HSD	0	58
NHSD	1	57
%HSD	0	50.43478

Figure B-14. Stereoplot of Discontinuities Mapped Faces of Geologic Unit 5 of the CWF&FWF

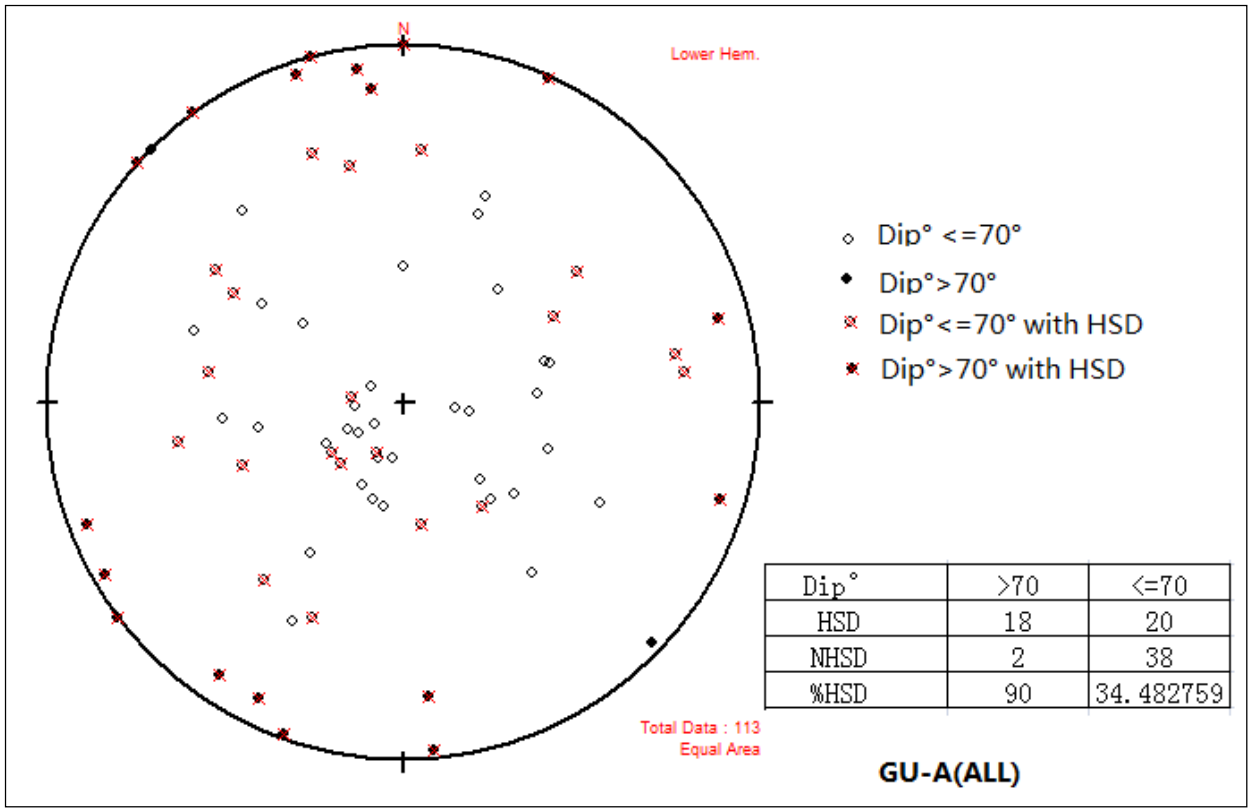

Dip°	>70	<=70
HSD	18	20
NHSD	2	38
%HSD	90	34.482759

Figure B-15. Stereoplot of Discontinuities Mapped Faces of Genetic Unit A

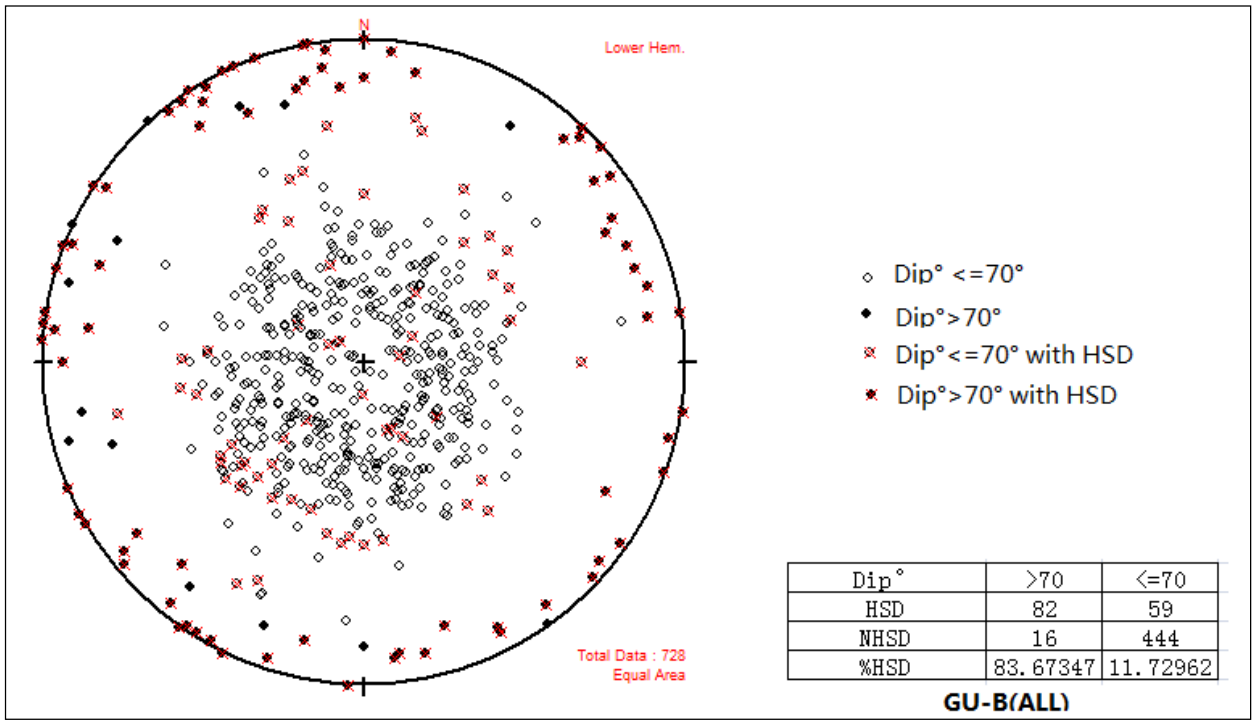

Dip°	>70	<=70
HSD	82	59
NHSD	16	444
%HSD	83.67347	11.72962

Figure B-16. Stereoplot of Discontinuities Mapped Faces of Genetic Unit B

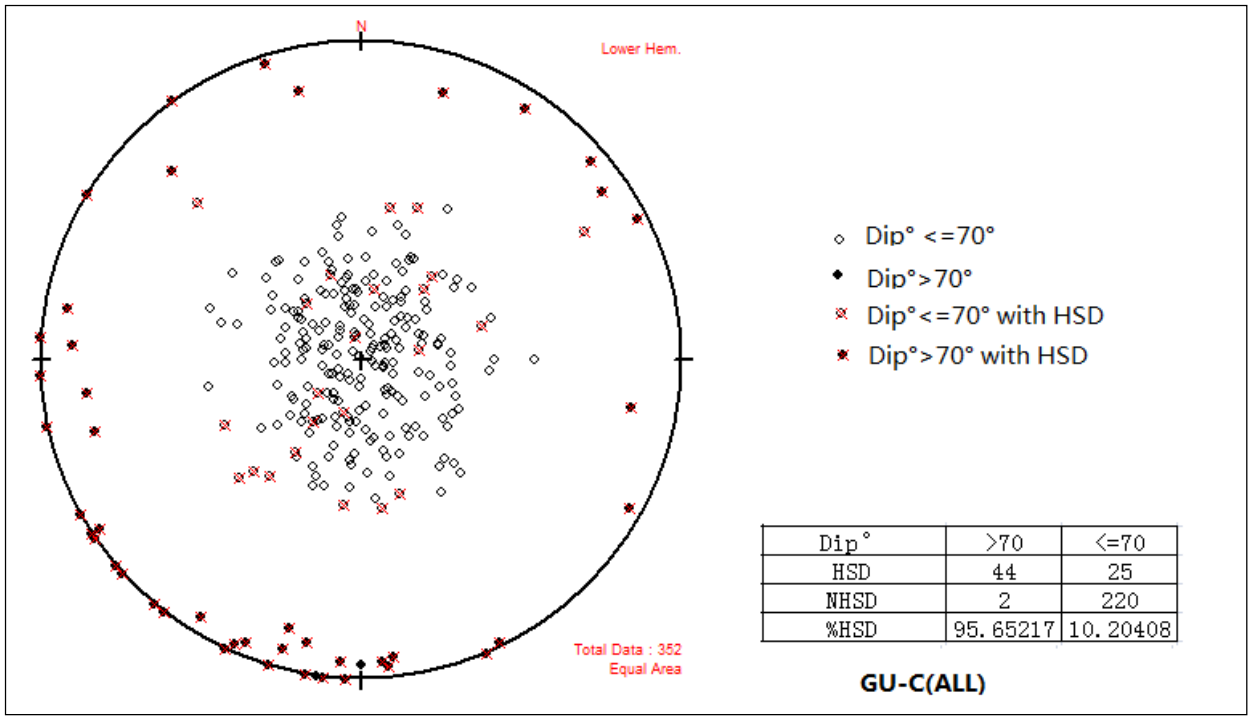

Dip°	>70	<=70
HSD	44	25
NHSD	2	220
%HSD	95.65217	10.20408

Figure B-17. Stereoplot of Discontinuities Mapped Faces of Genetic Unit C

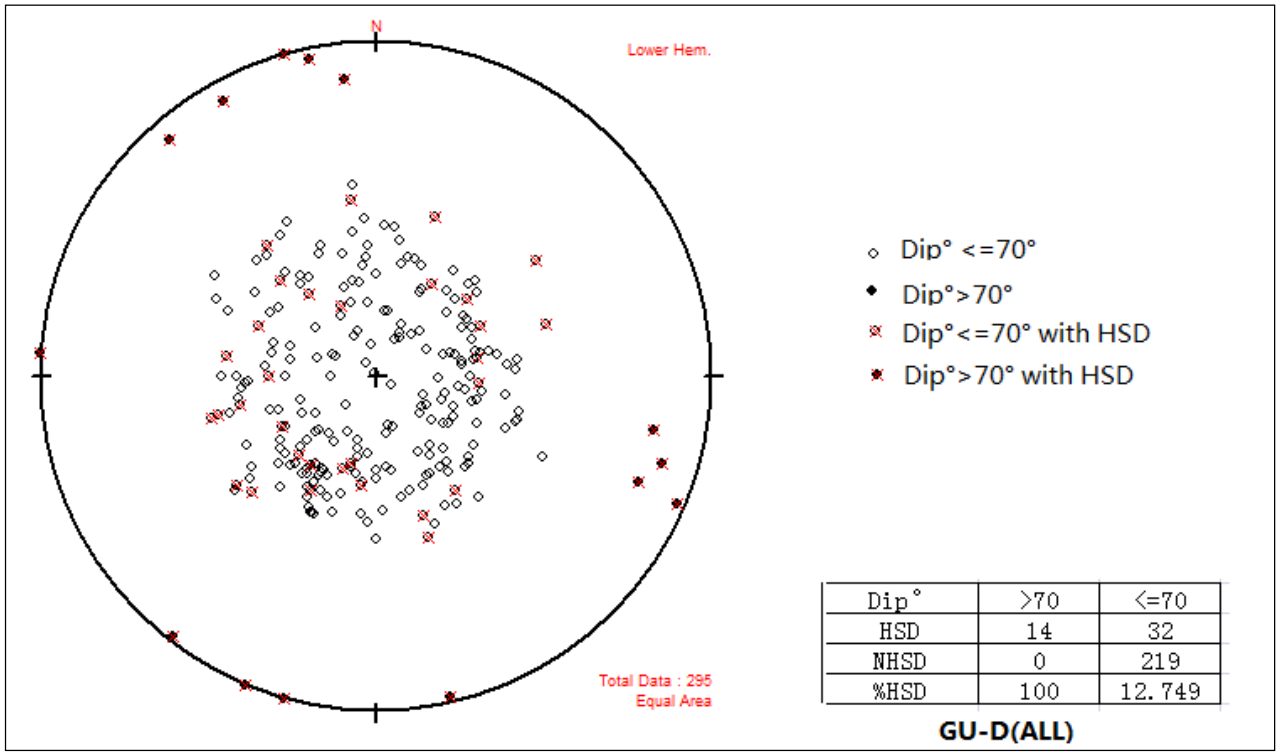

Dip°	>70	<=70
HSD	14	32
NHSD	0	219
%HSD	100	12.749

Figure B-18. Stereoplot of Discontinuities Mapped Faces of Genetic Unit D

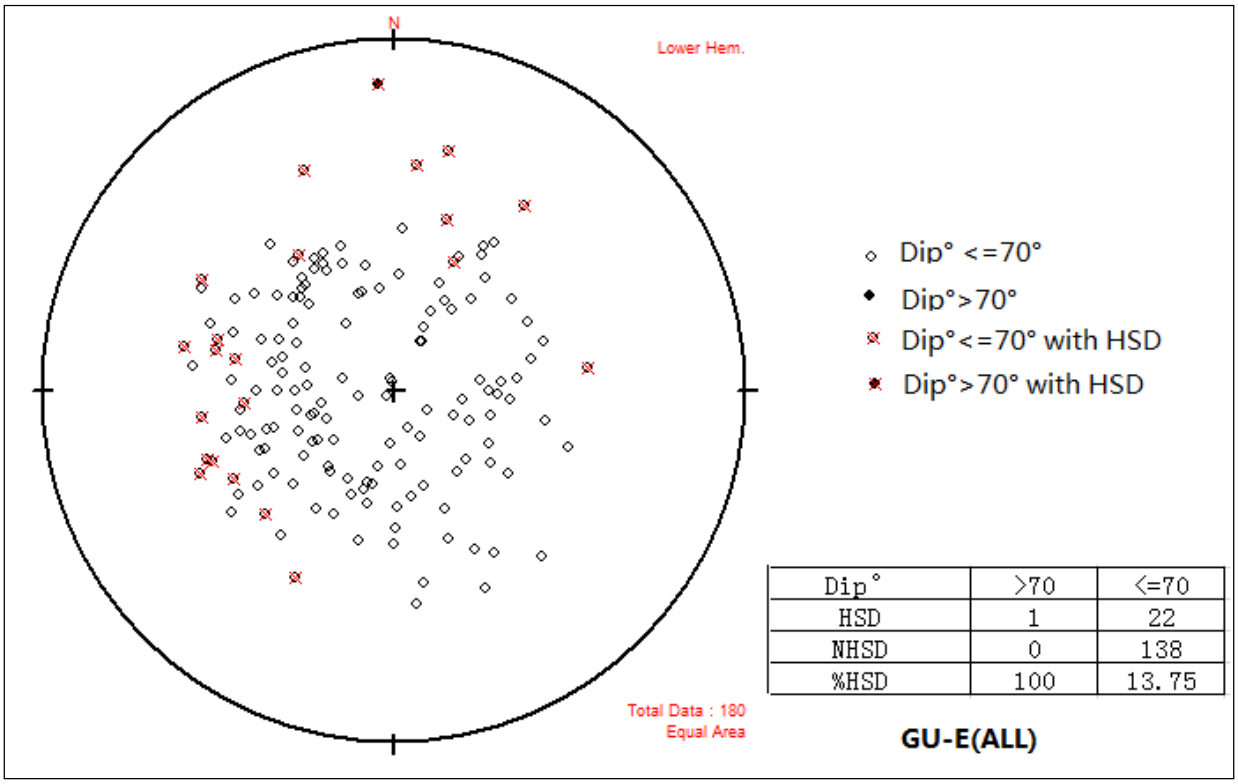

Dip°	>70	<=70
HSD	1	22
NHSD	0	138
%HSD	100	13.75

Figure B-19. Stereoplot of Discontinuities Mapped Faces of Genetic Unit E

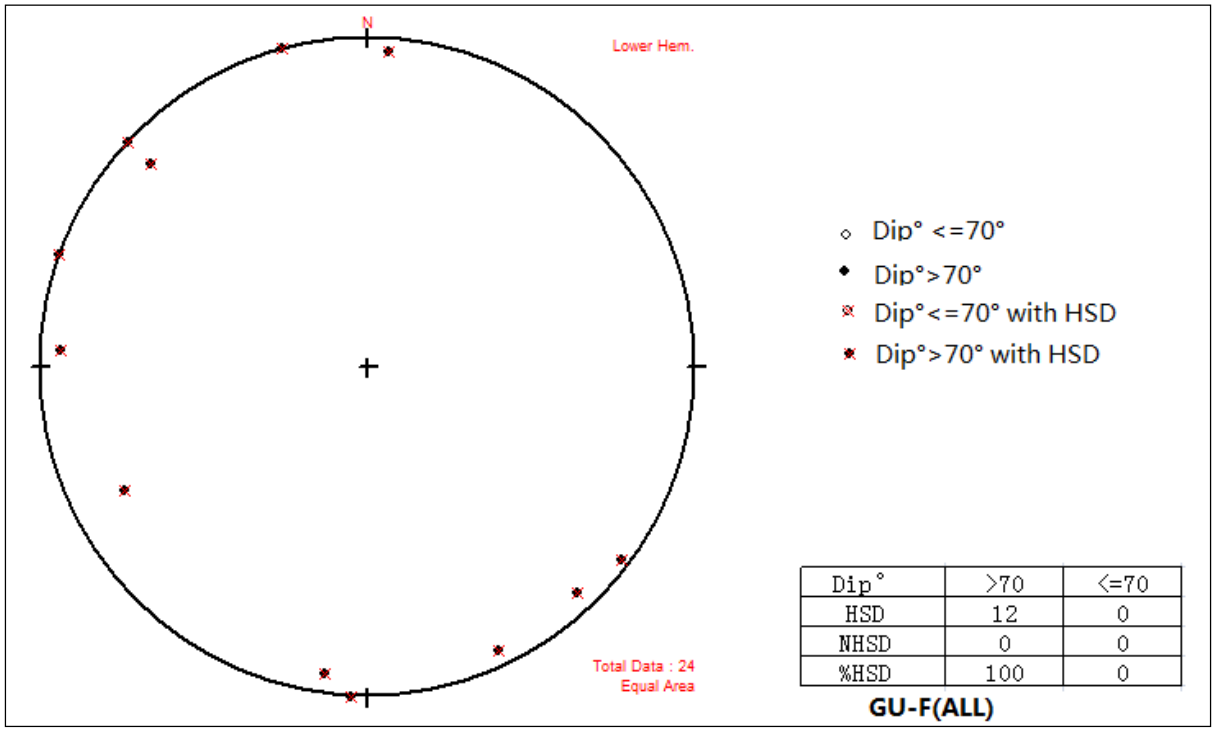

Dip°	>70	<=70
HSD	12	0
NHSD	0	0
%HSD	100	0

Figure B-20. Stereoplot of Discontinuities Mapped Faces of Genetic Unit F

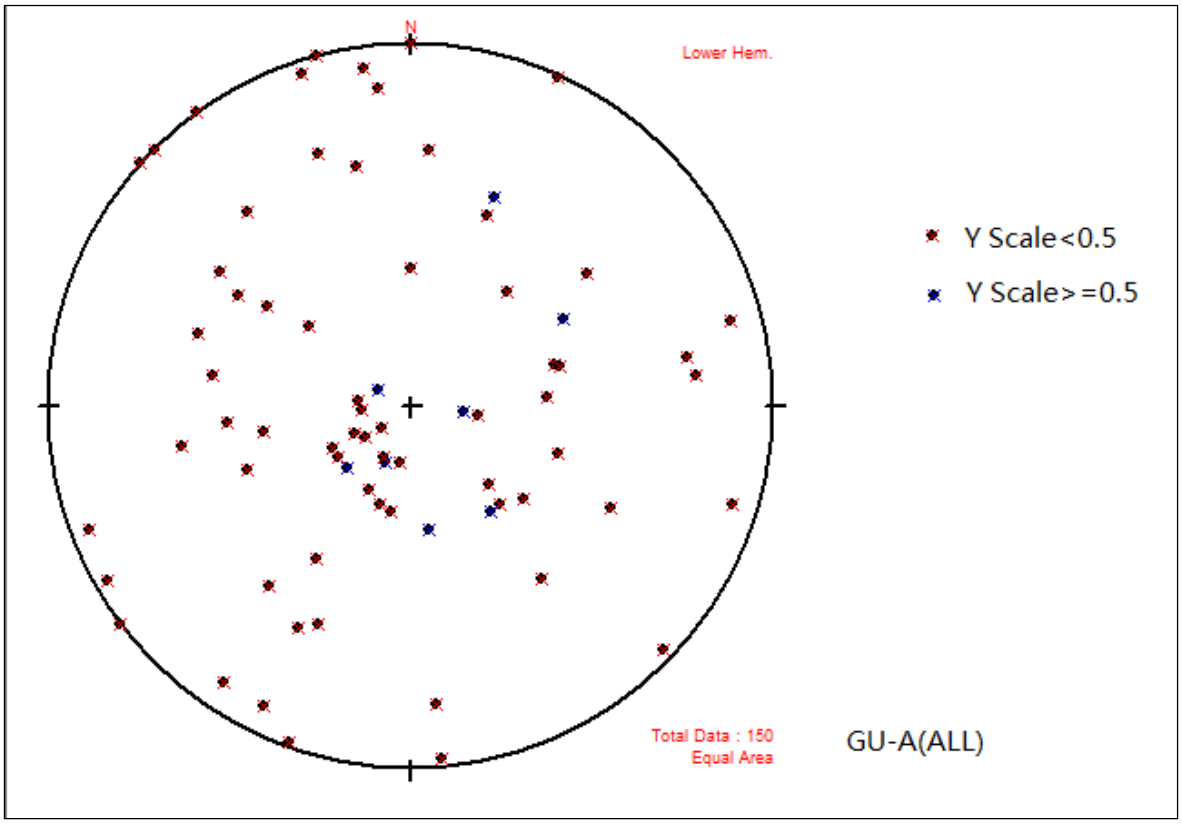

Figure B-21. Stereoplot of All Discontinuities with Y_{scale} Mapped in Genetic Unit A

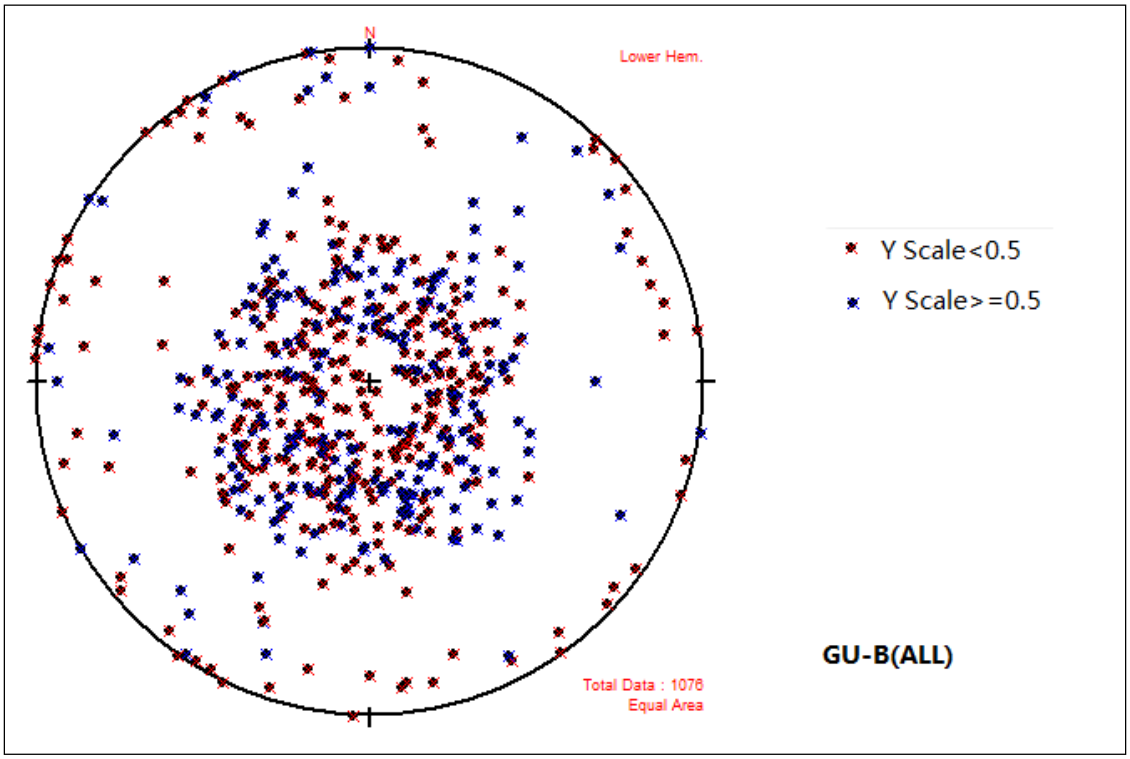

Figure B-22. Stereoplot of All Discontinuities with Y_{scale} Mapped in Genetic Unit B

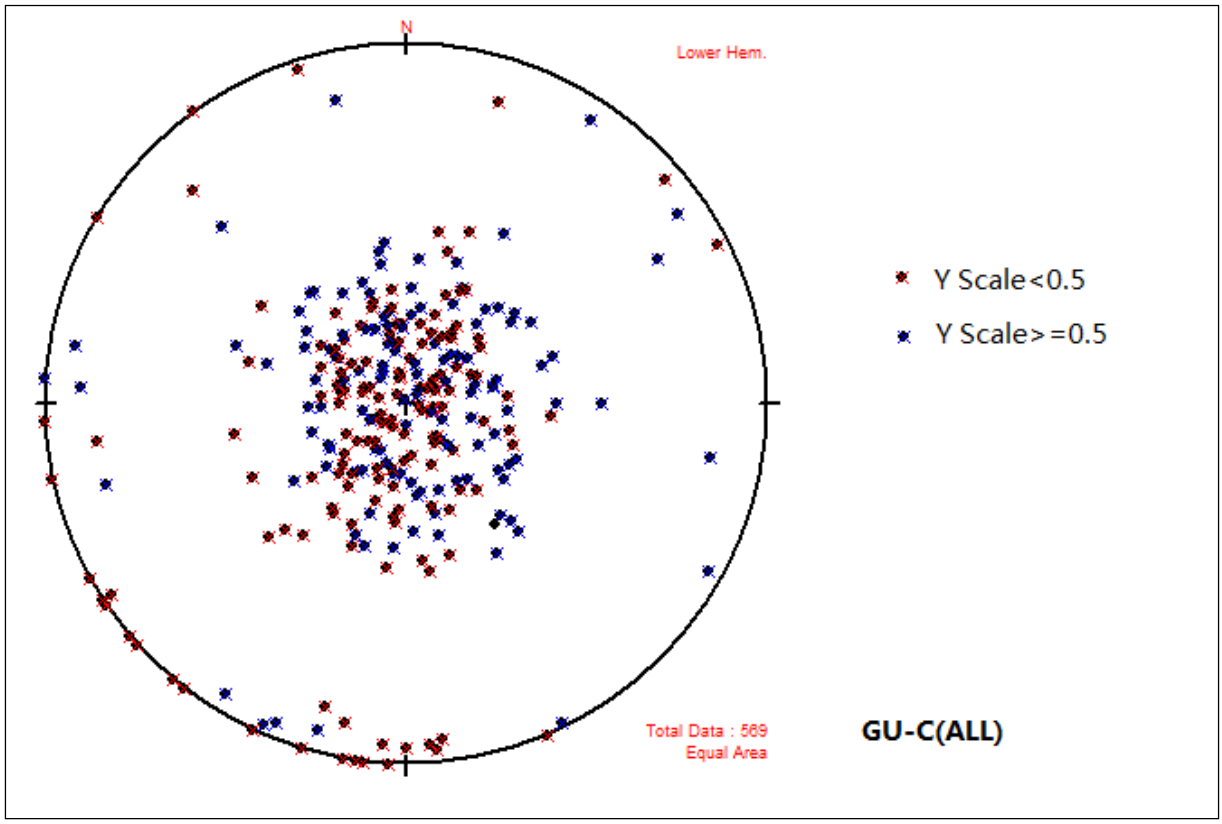

Figure B-23. Stereoplot of All Discontinuities with Y_{scale} Mapped in Genetic Unit C

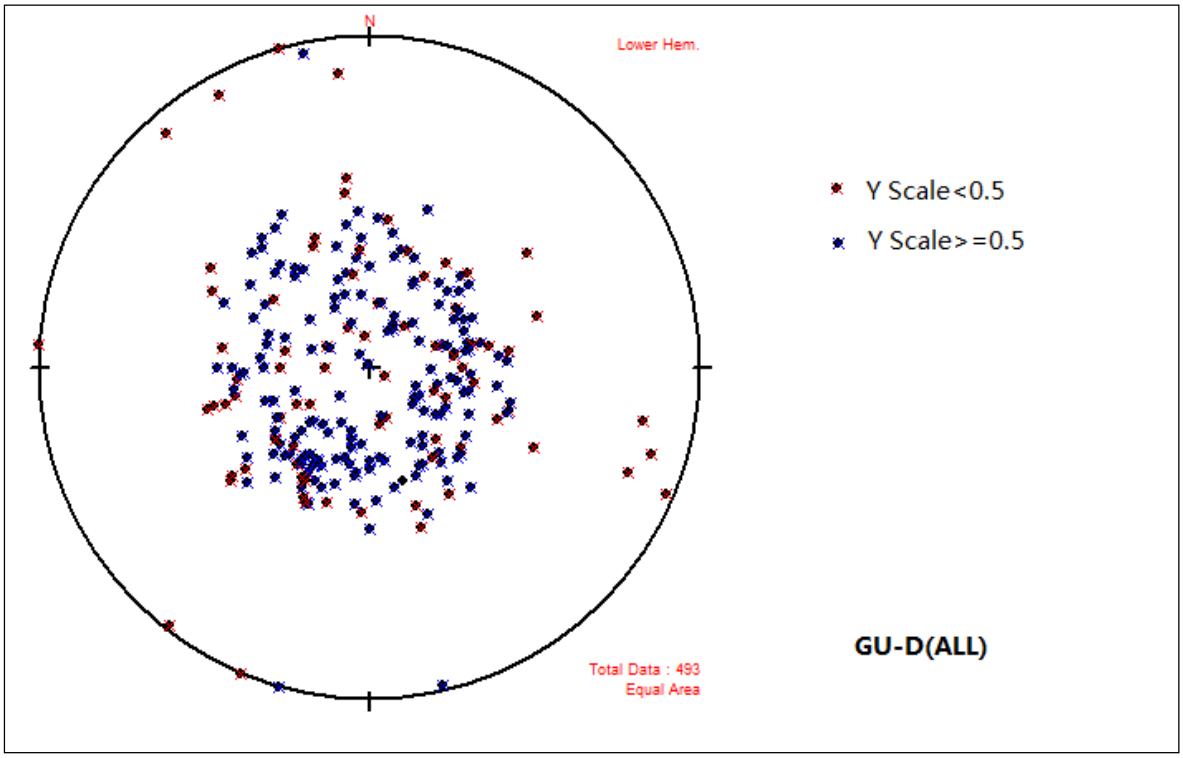

Figure B-24. Stereoplot of All Discontinuities with Y_{scale} Mapped in Genetic Unit D

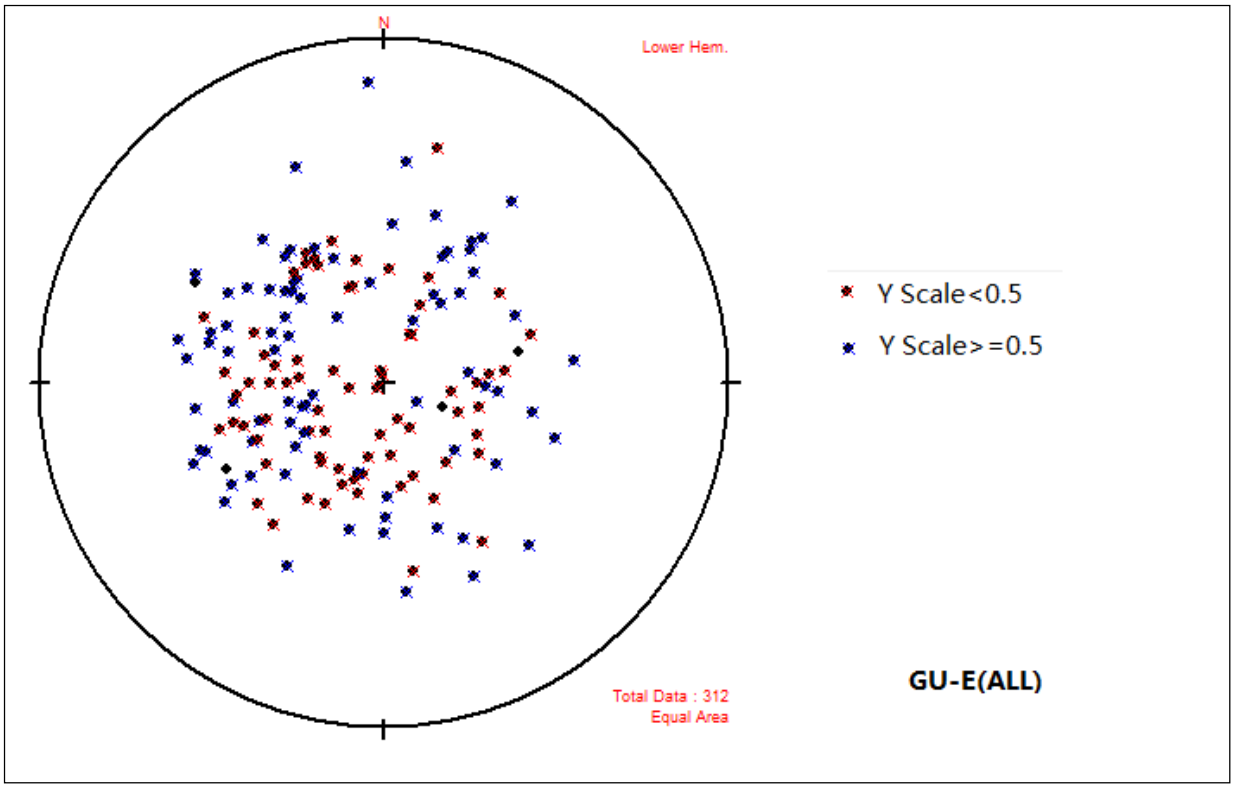

Figure B-25. Stereoplot of All Discontinuities with Y_{scale} Mapped in Genetic Unit E

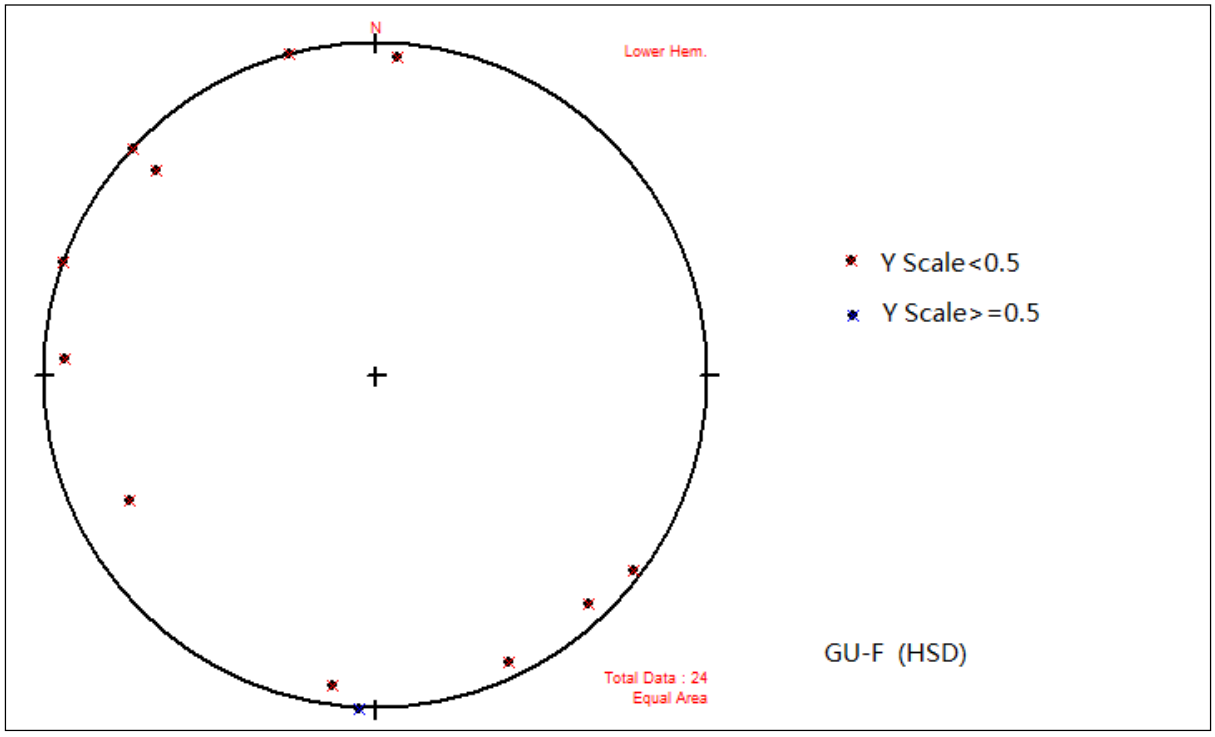

Figure B-26. Stereoplot of All Discontinuities with Y_{scale} Mapped in Genetic Unit F

Appendix C

HISTOGRAM AND KRIGING PREDICTION MAP OF DISCONTINUITIES PROPERTIES FOR CWF AND FWF

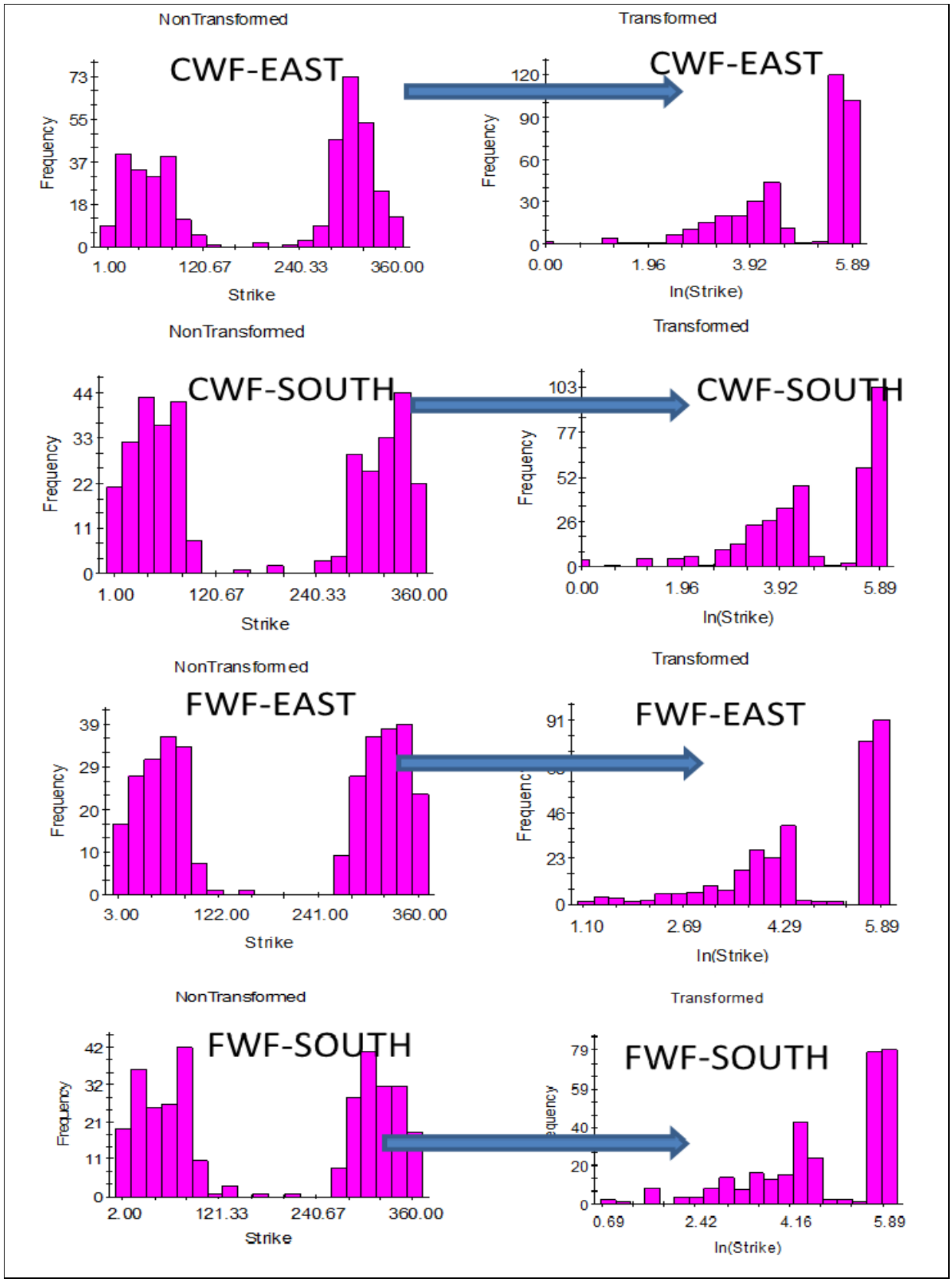

Figure C-1. Histogram of Discontinuity Strike for CWF and FWF

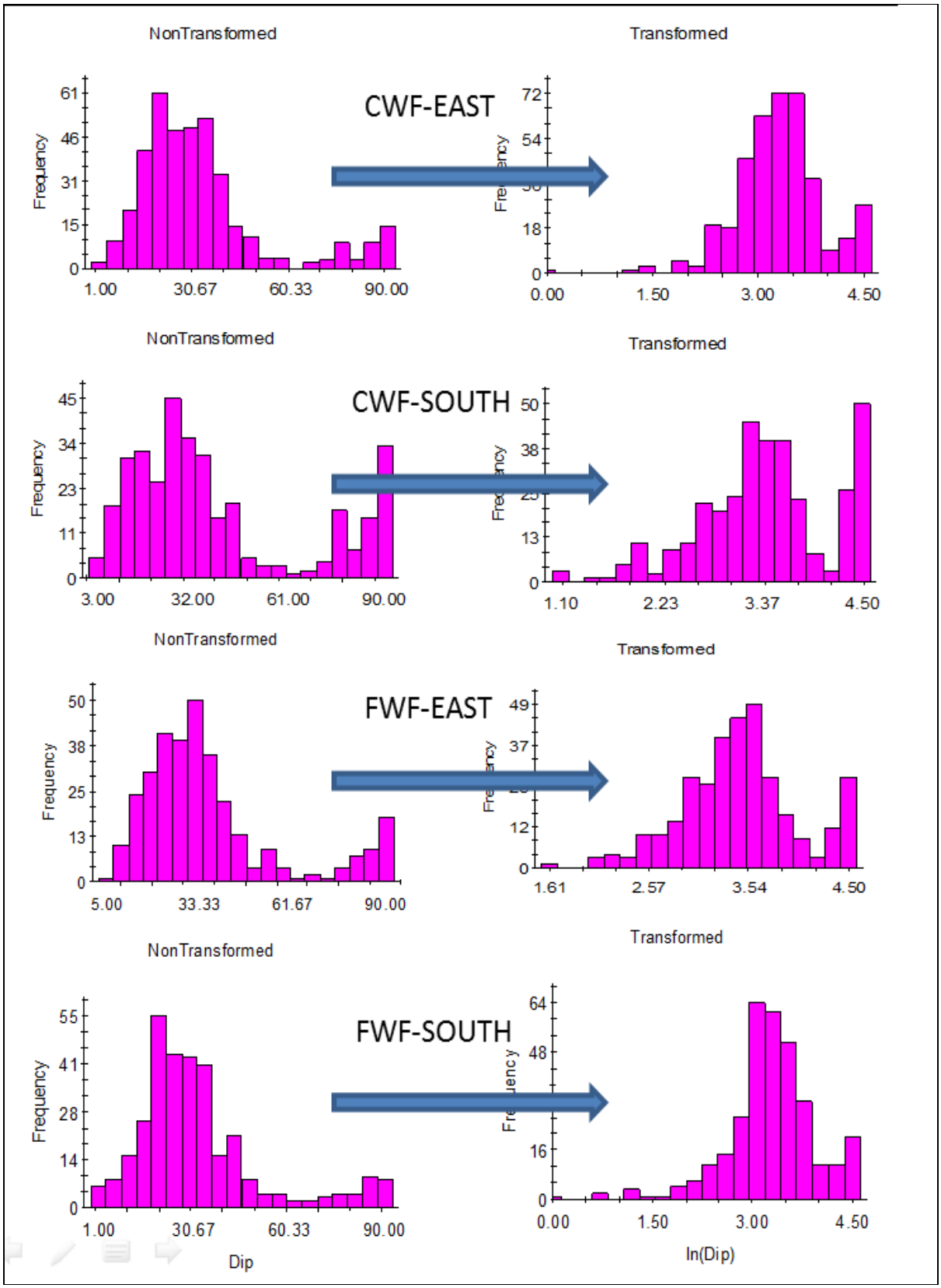

Figure C-2. Histogram of Discontinuity Dip Angle for CWF and FWF

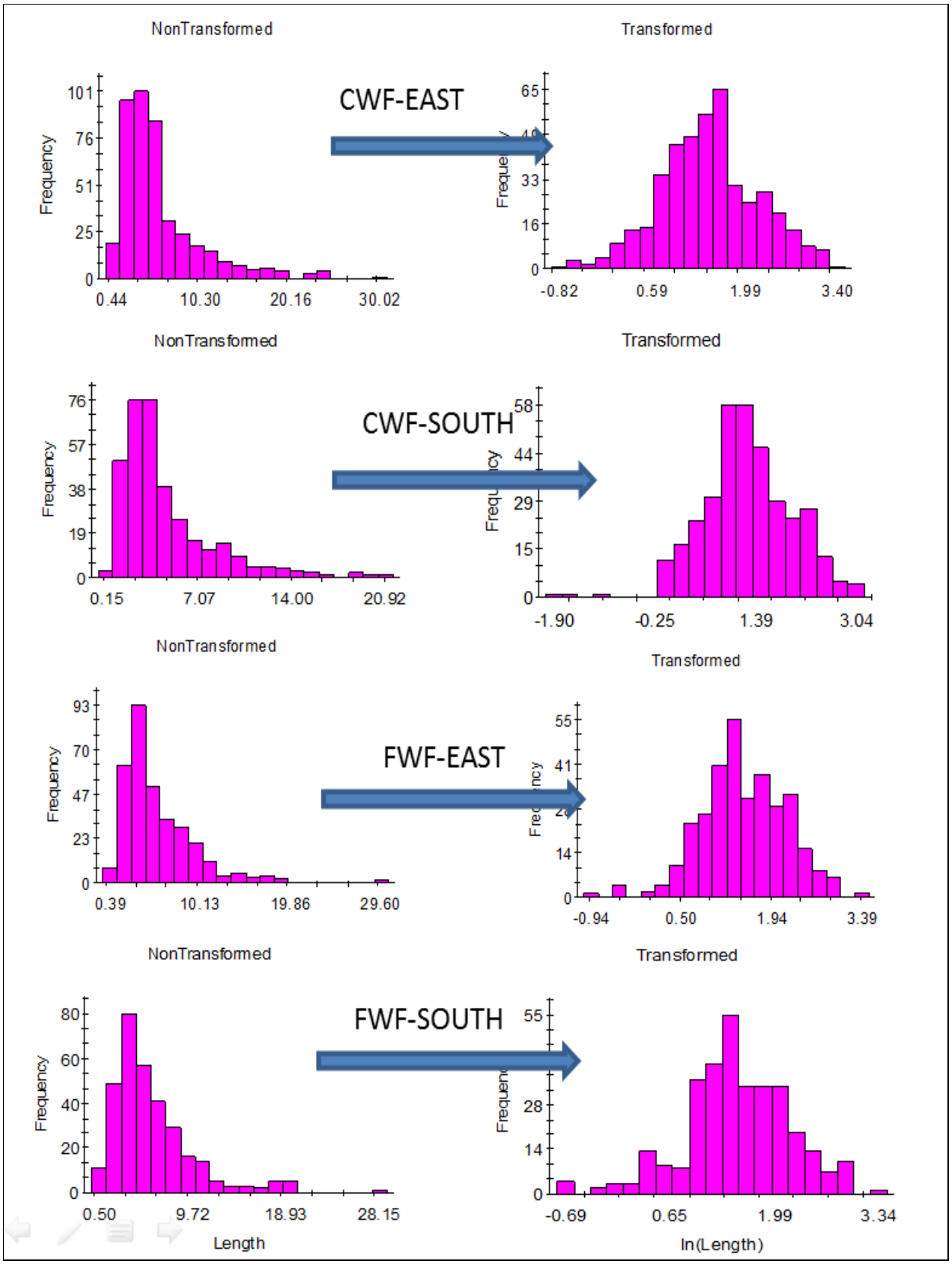

Figure C-3. Histogram of Discontinuity Length for CWF and FWF

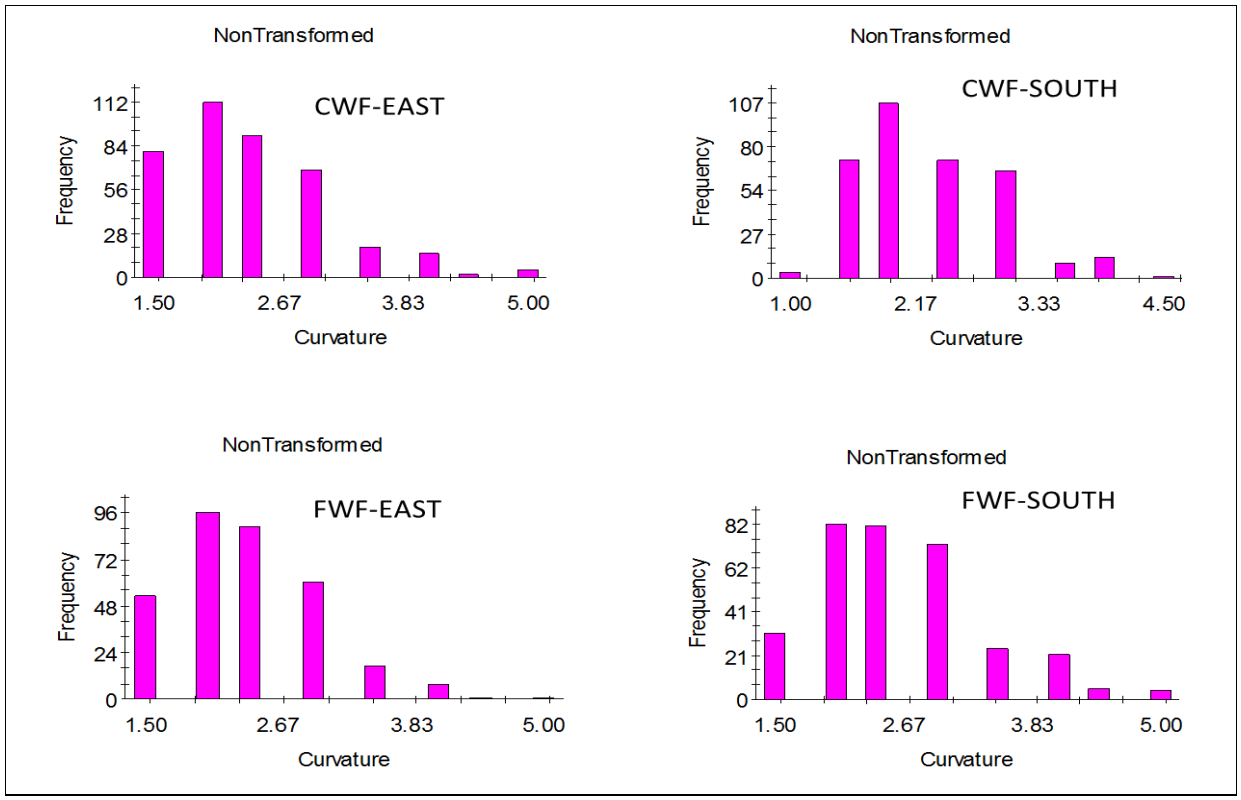

Figure C-4. Histogram of Discontinuity Curvature for CWF and FWF

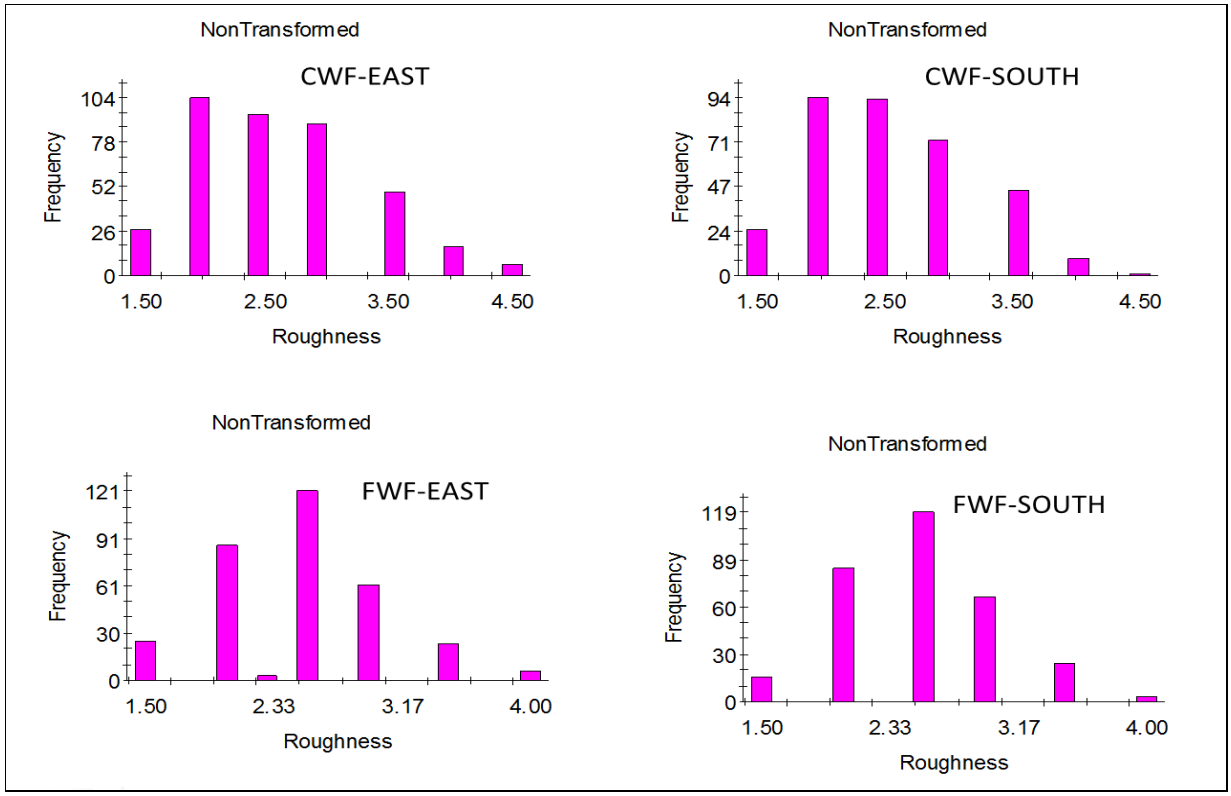

Figure C-5. Histogram of Discontinuity Roughness for CWF and FW

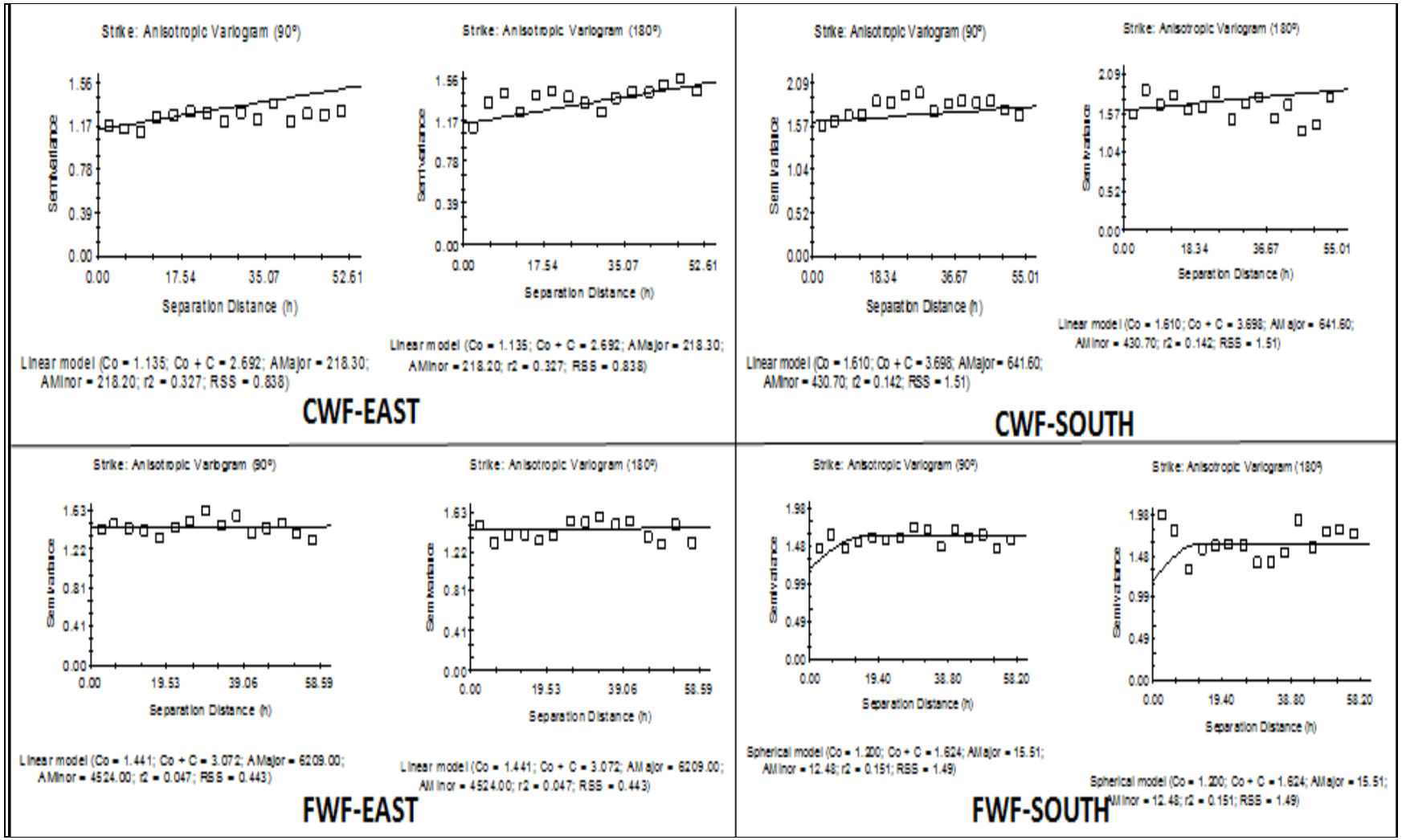

Figure C-6. Fitted Variogram Models of Strike for CWF and FWF

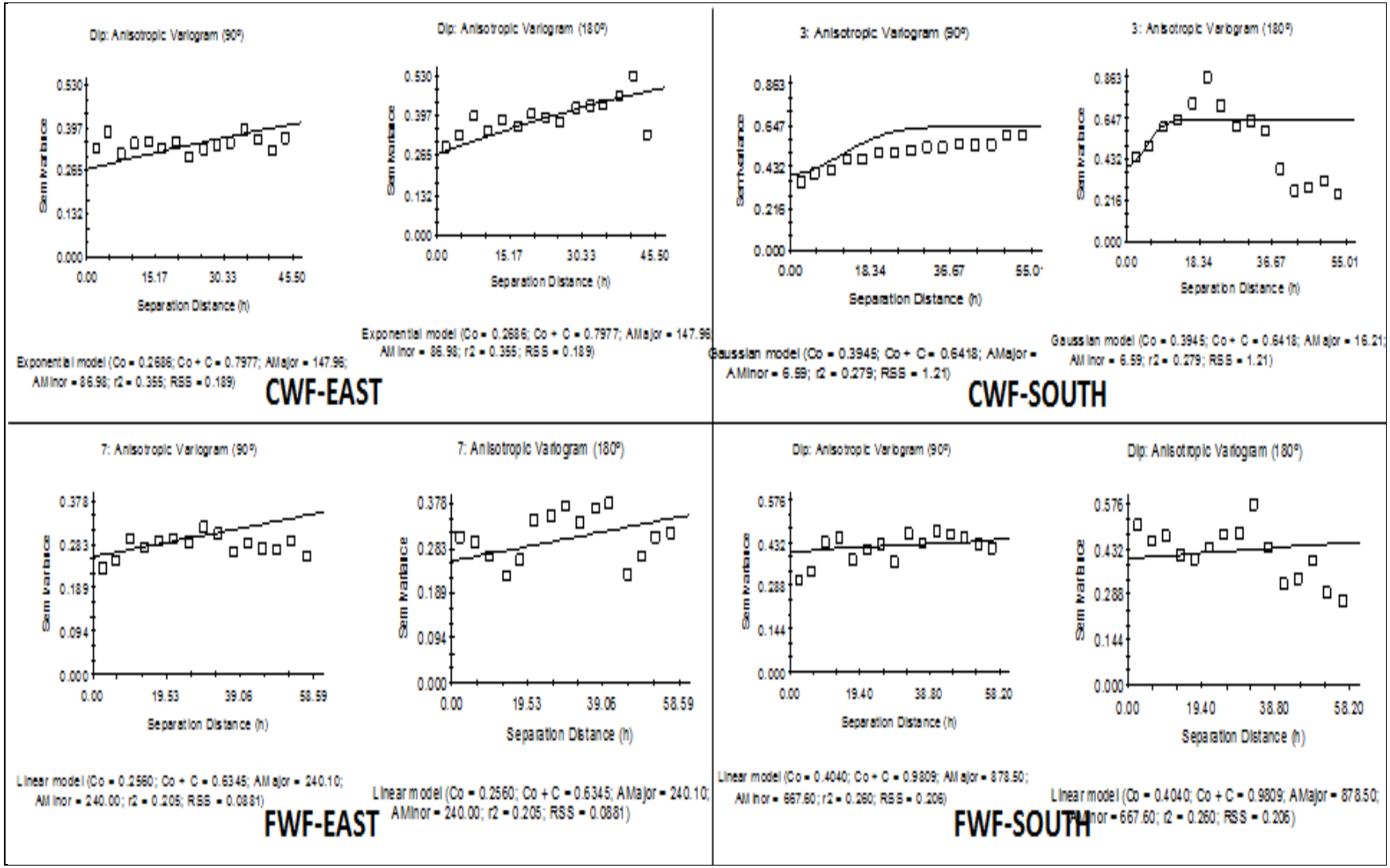

Figure C-7. Fitted Variogram Models of Dip Angle for CWF and FWF

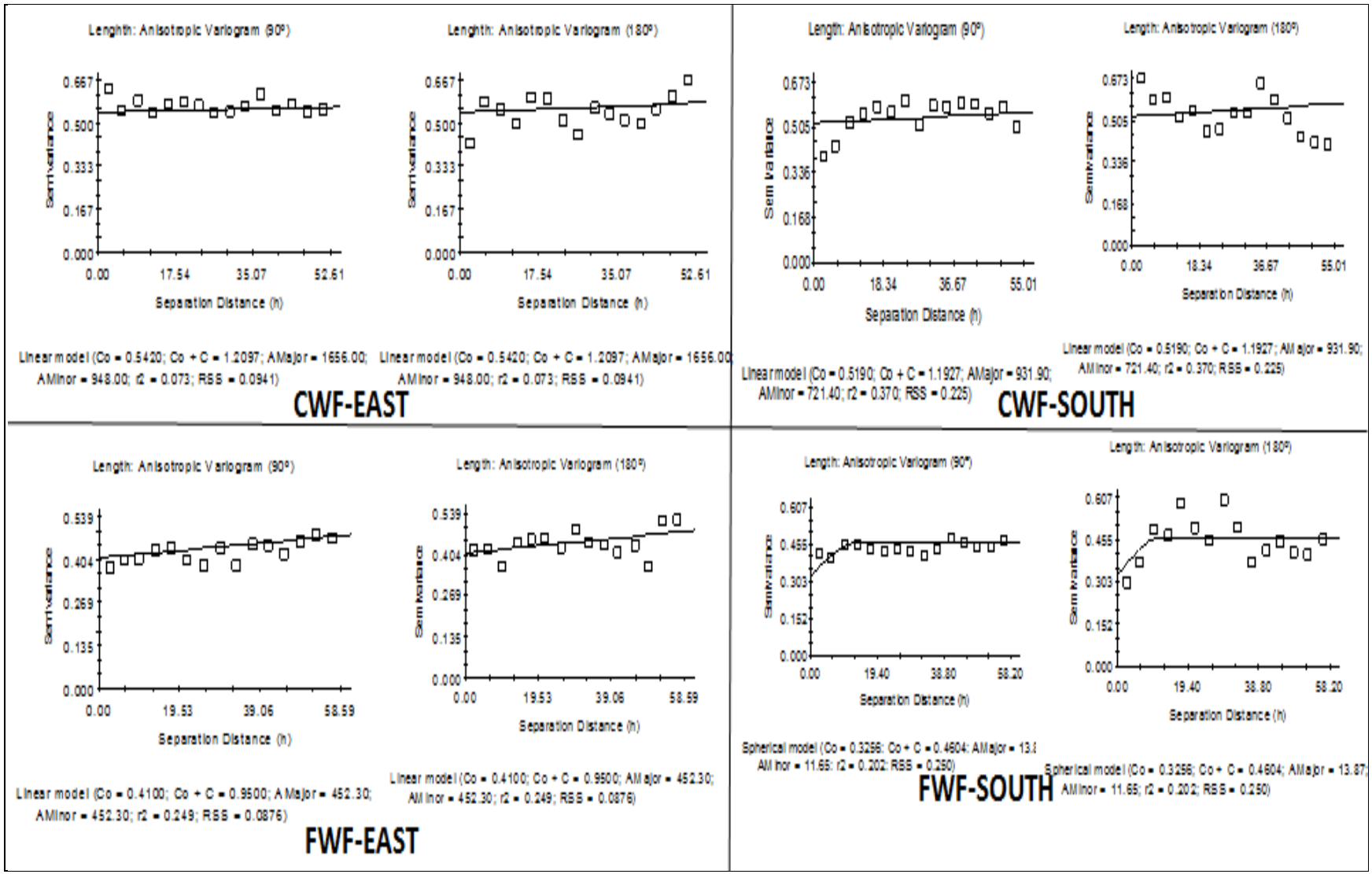

Figure C-8. Fitted Variogram Models of Length for CWF and FWF

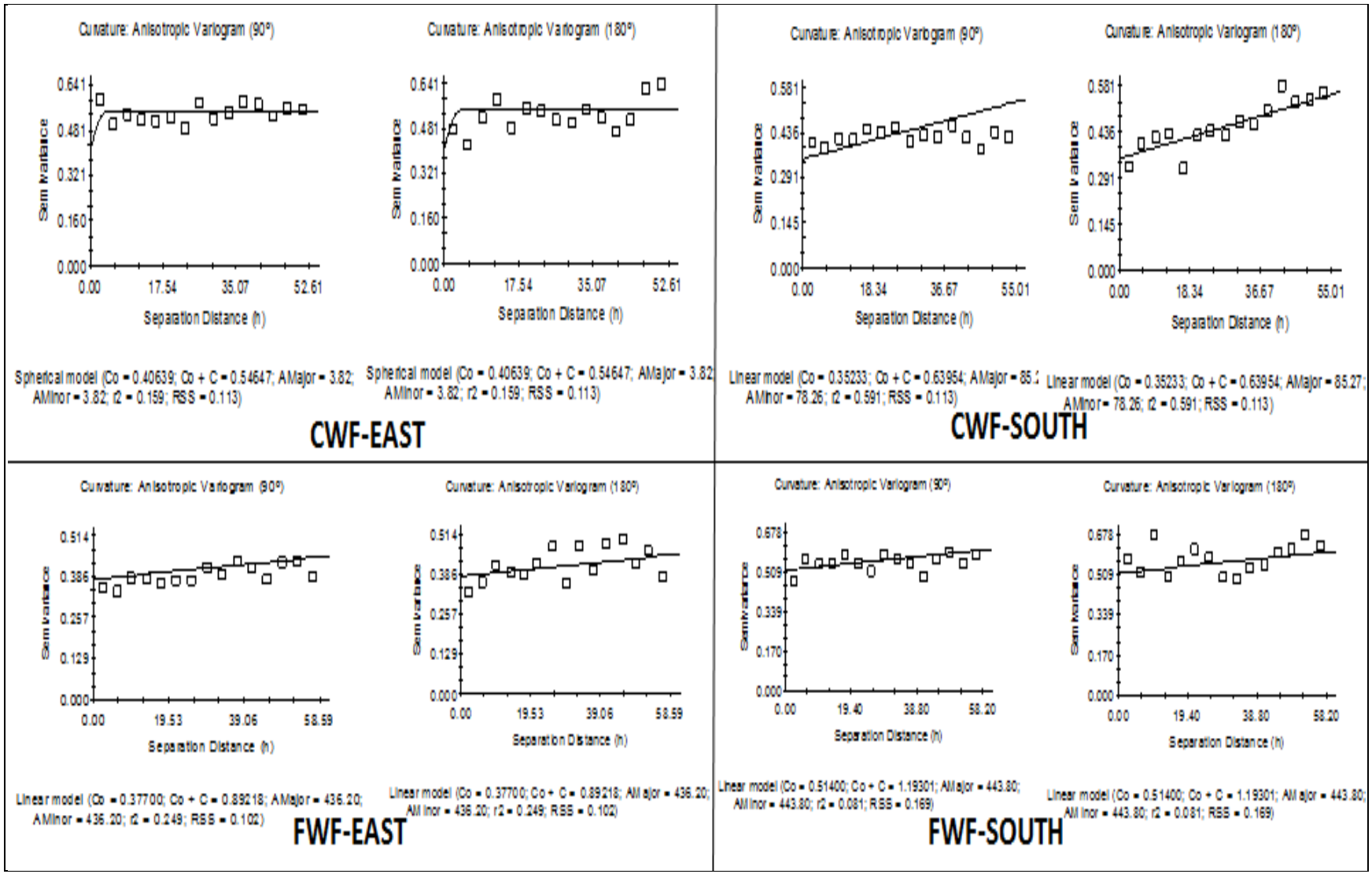

Figure C-9. Fitted Variogram Models of Curvature for CWF and FWF

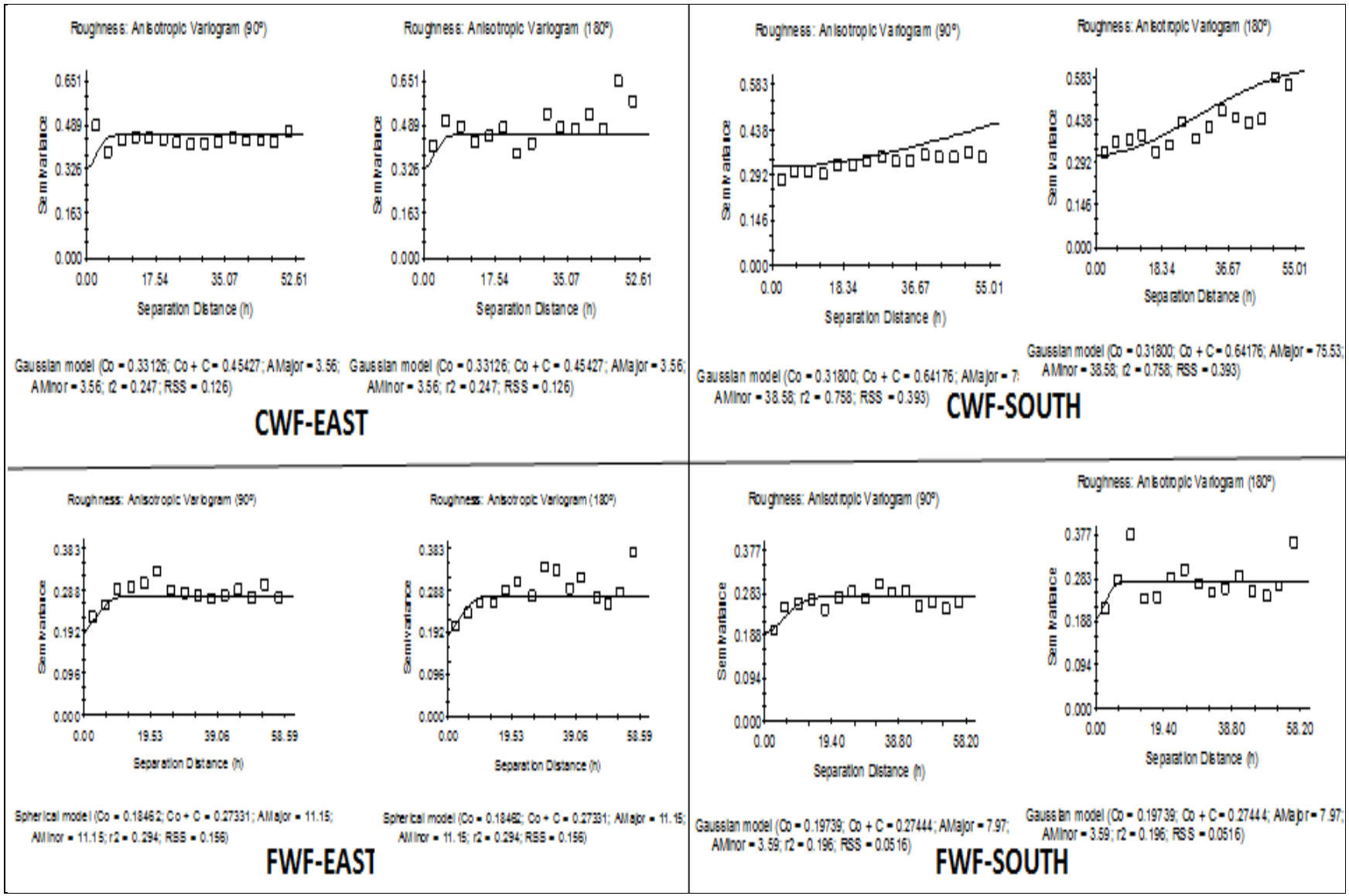

Figure C-10. Fitted Variogram Models of Roughness for CWF and FWF

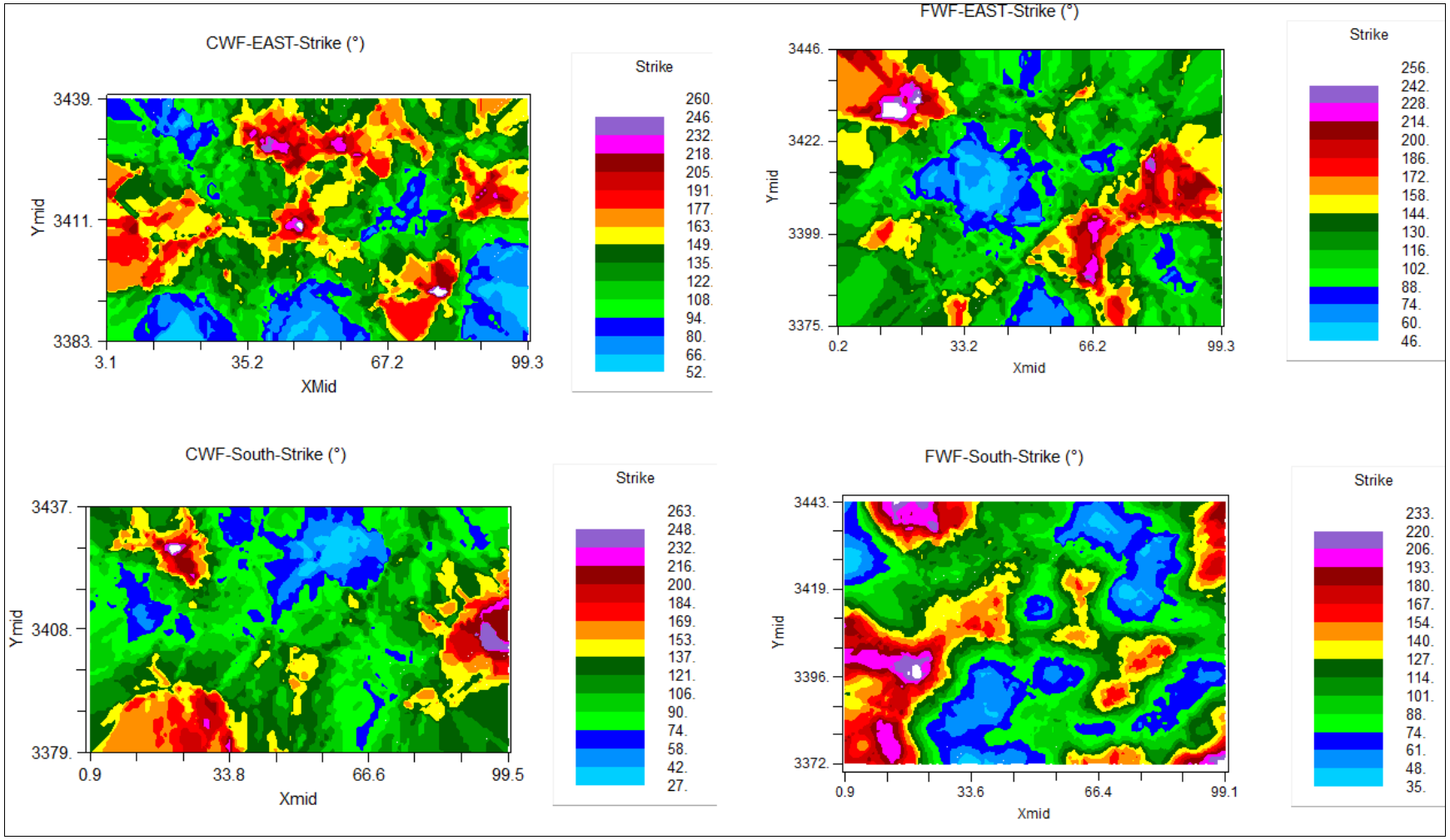

Figure C-11. Kriging Prediction Maps of Strike for CWF and FWF

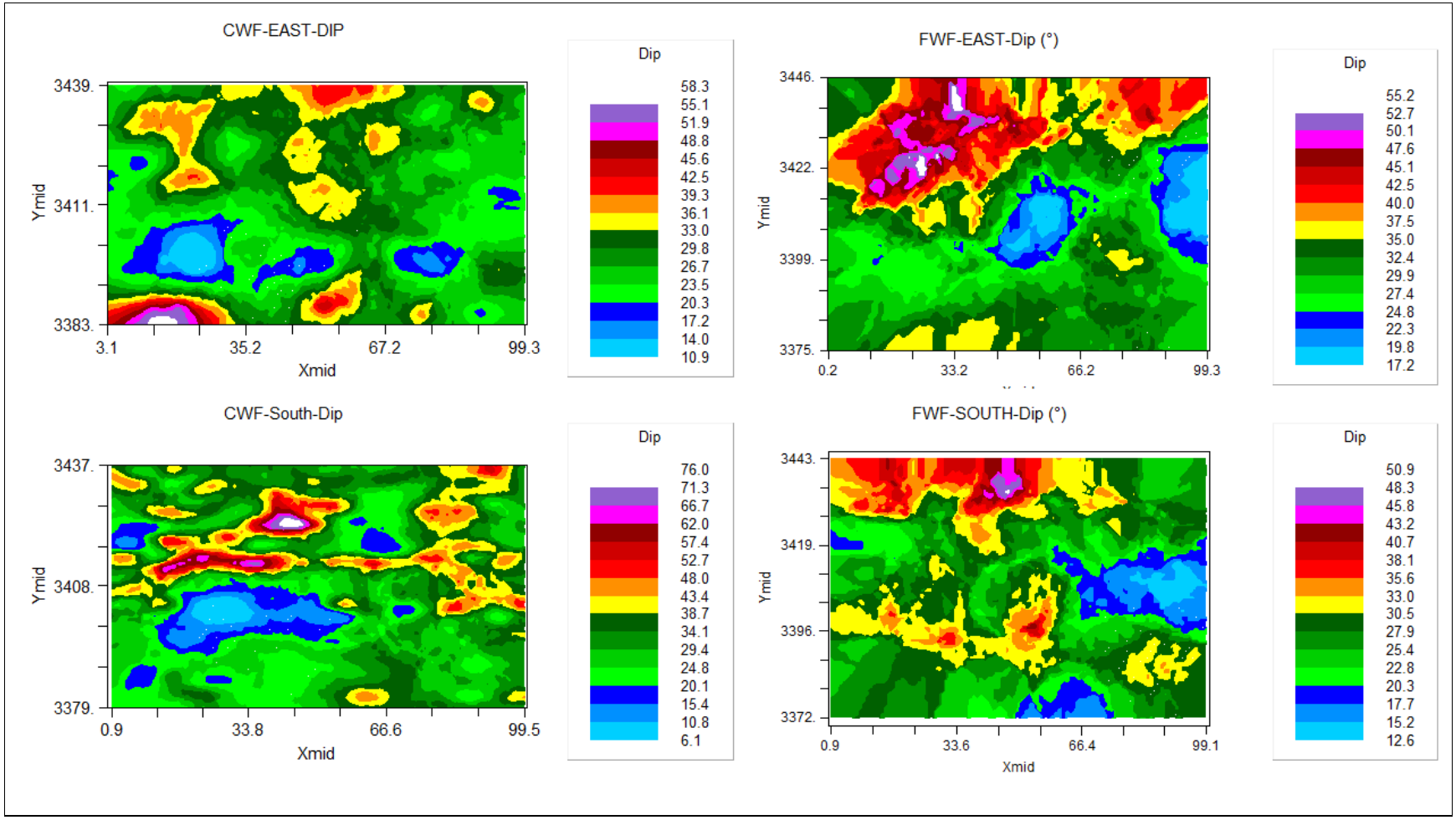

Figure C-12. Kriging Prediction Maps of Dip Angle for CWF and FWF

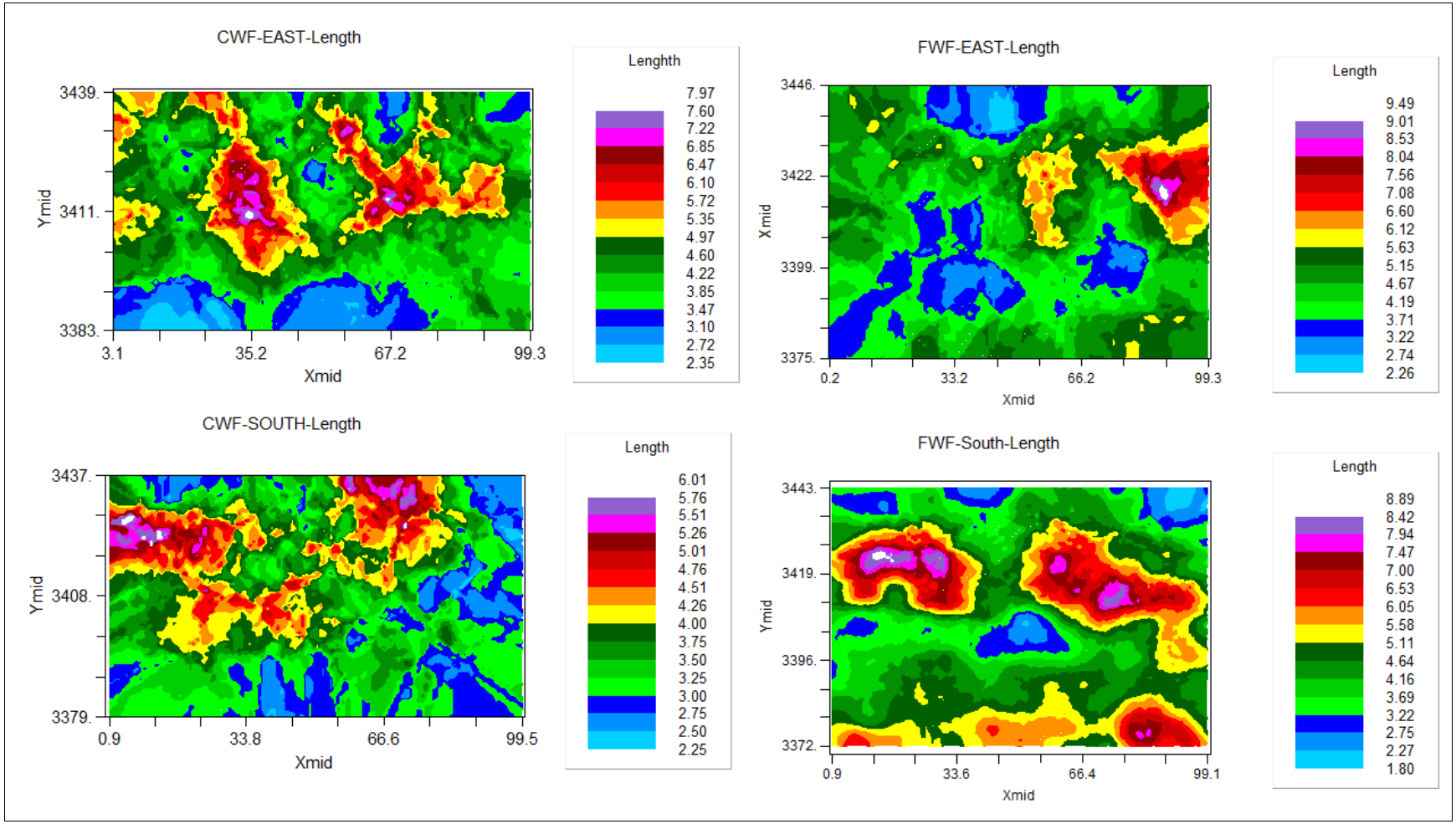

Figure C-13. Kriging Prediction Maps of Length for CWF and FWF

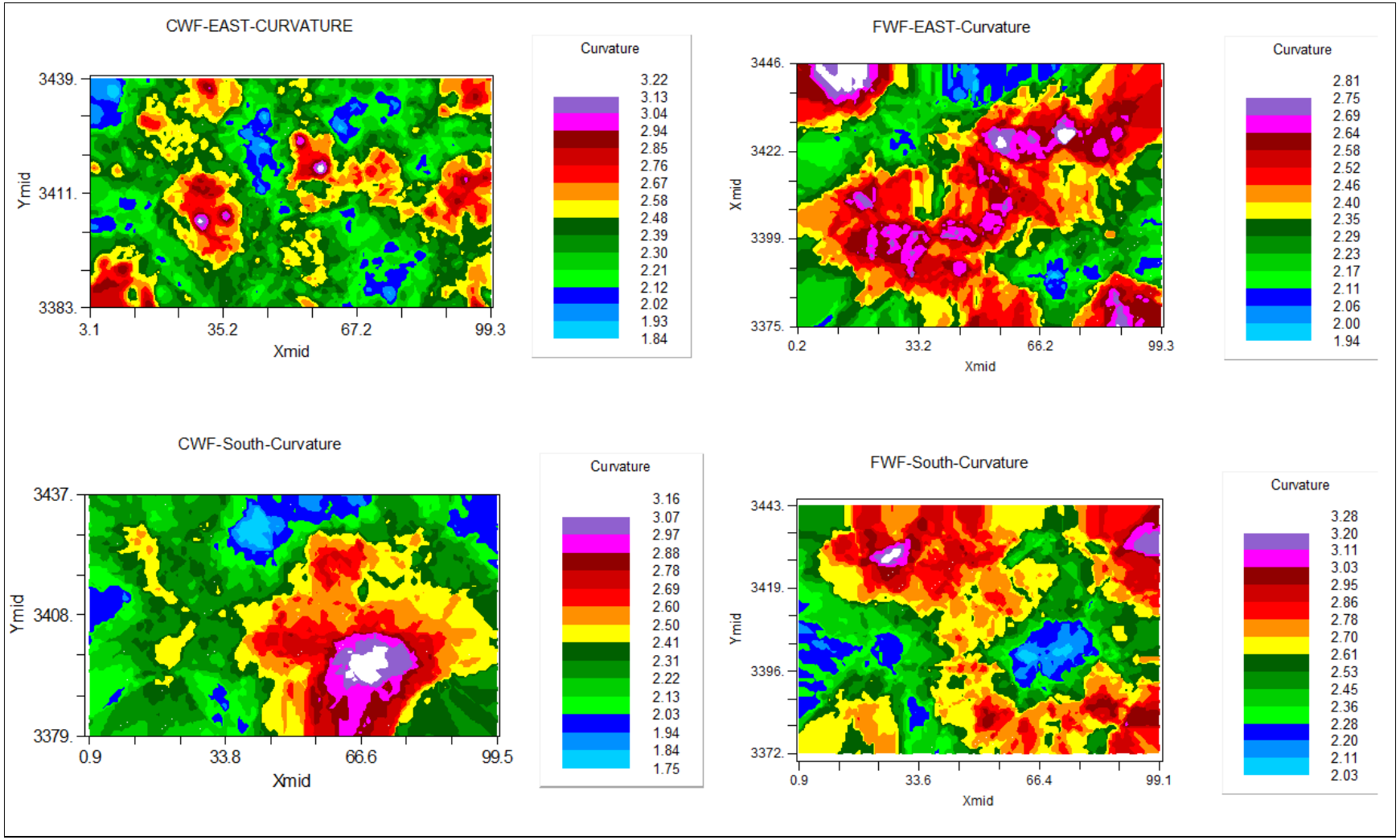

Figure C-14. Kriging Prediction Maps of Curvature for CWF and FWF

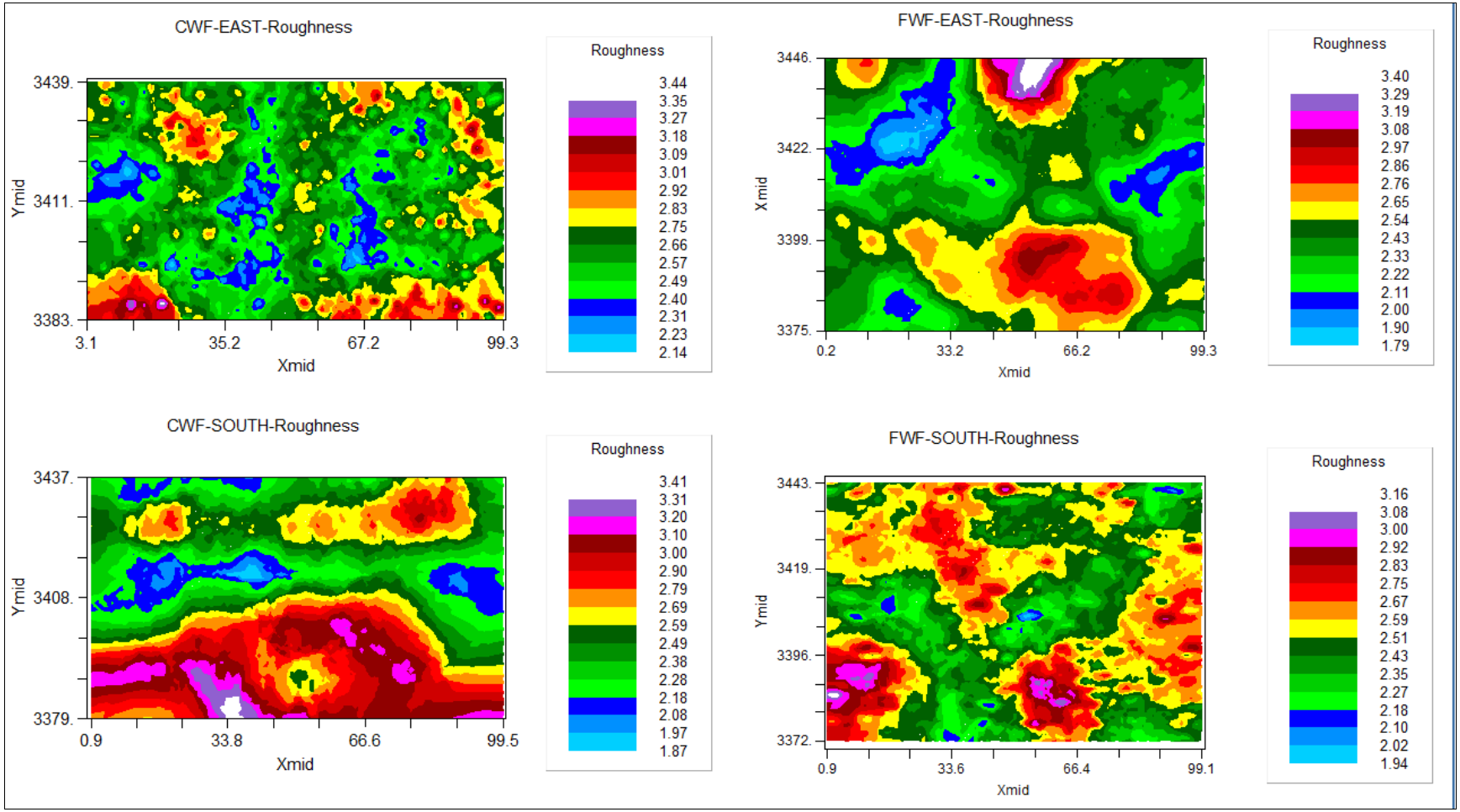

Figure C-15. Kriging Prediction Maps of Roughness for CWF and FWF

Appendix D

STATISTICAL ANALYSIS OF EACH FRACTURE SET IN EACH REGION OF CWF AND FWF HSD FOR THREE- DIMENSIONAL MODEL

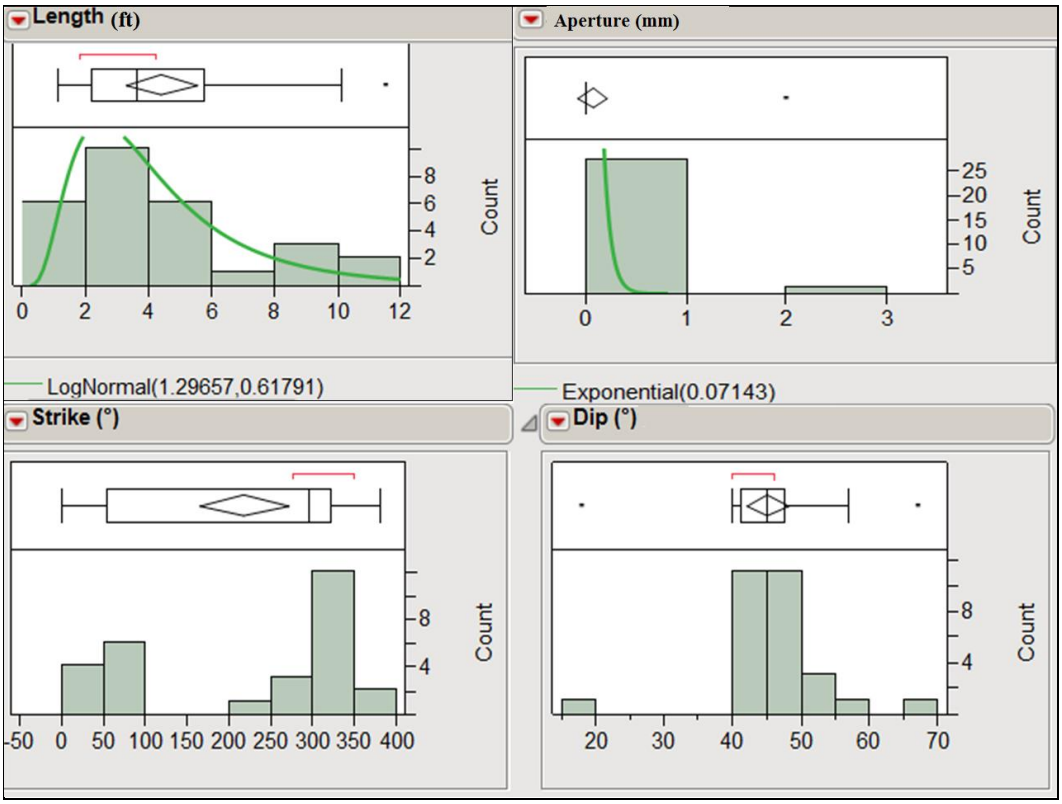

Figure D-1 Histograms of Fracture Set 1 in CWF Region-A

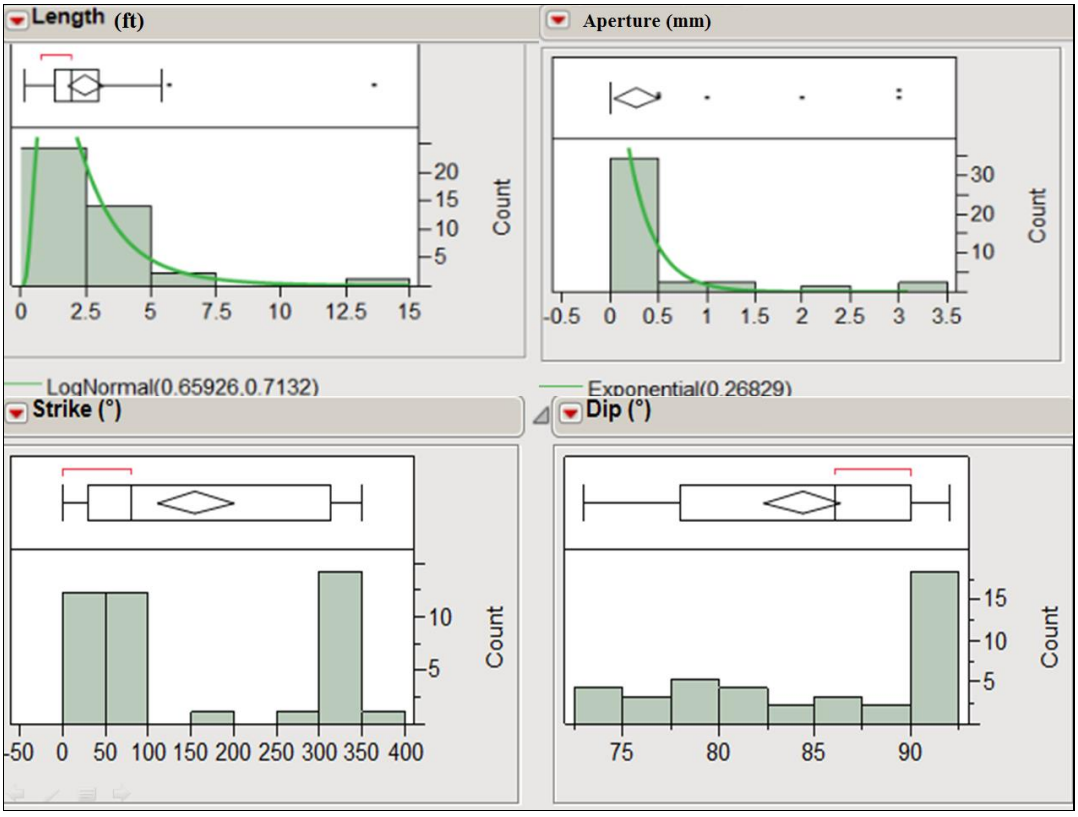

Figure D-2 Histograms of Fracture Set 2 in CWF Region-A

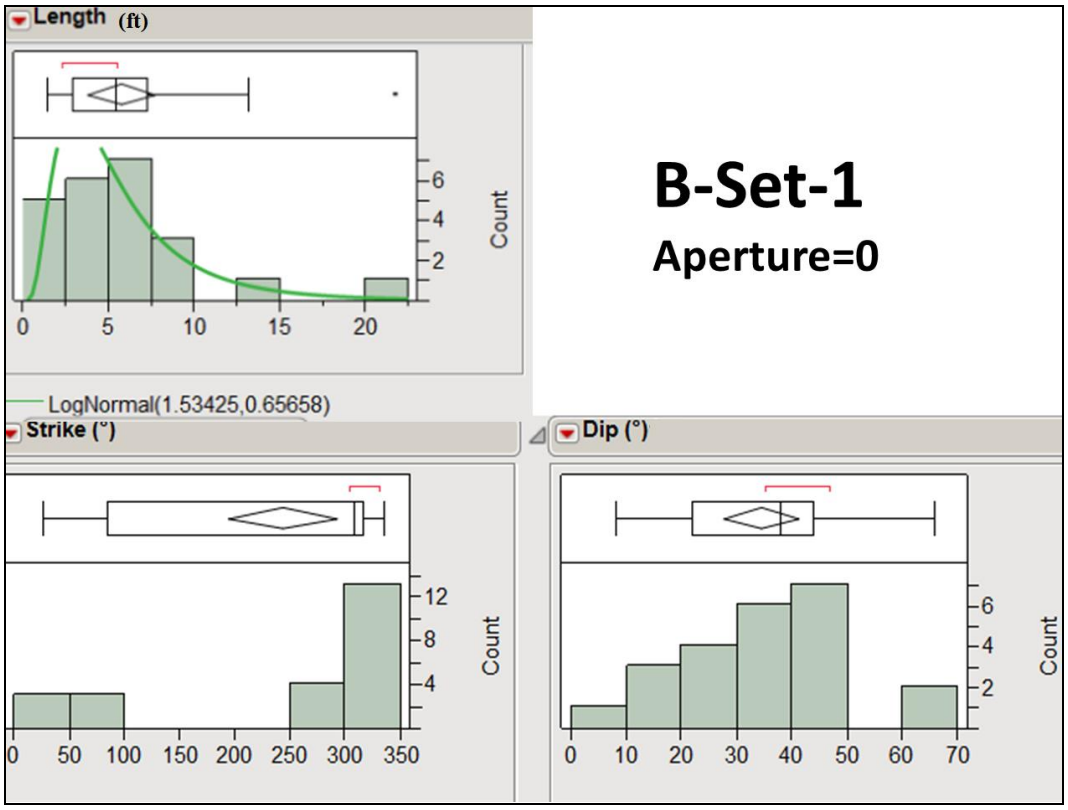

Figure D-3 Histograms of Fracture Set 1in CWF Region-B

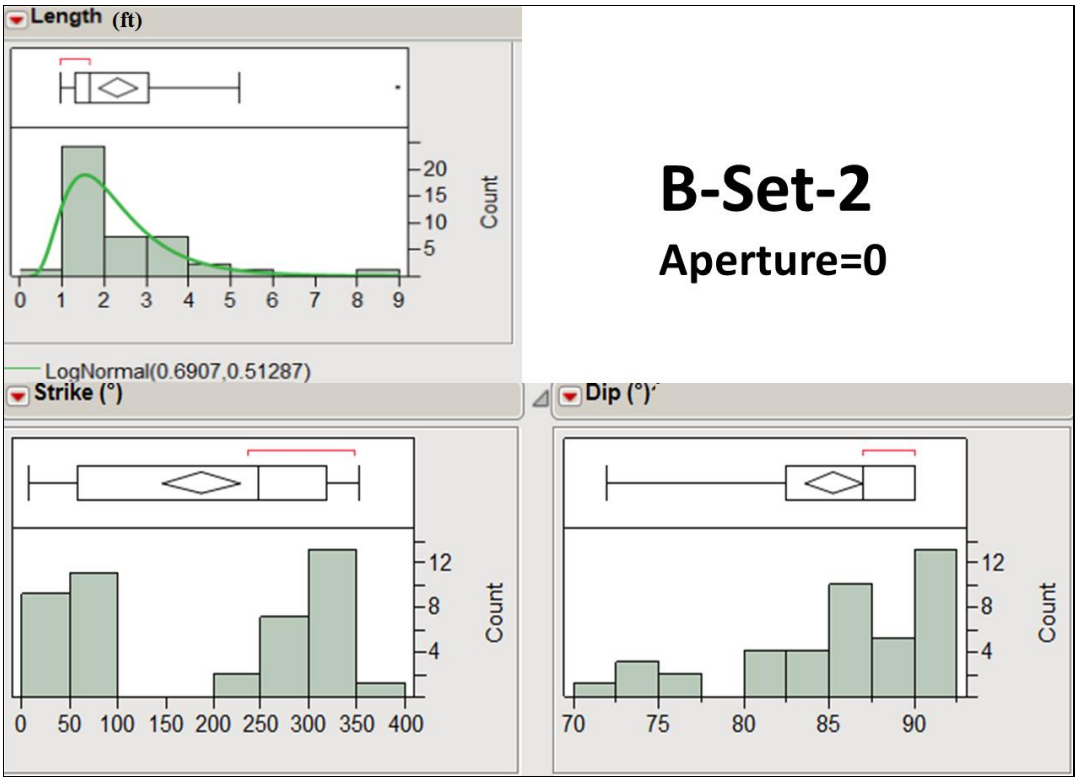

Figure D-4 Histograms of Fracture Set 2in CWF Region-B

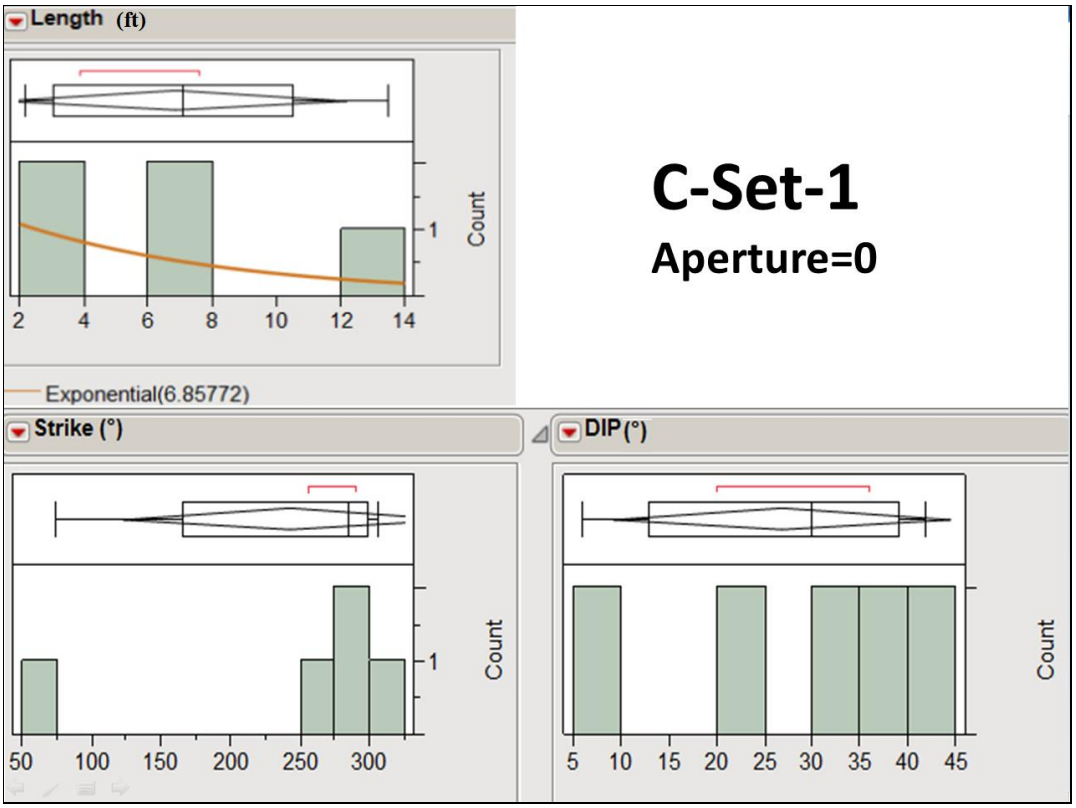

Figure D-5 Histograms of Fracture Set 1in CWF Region-C

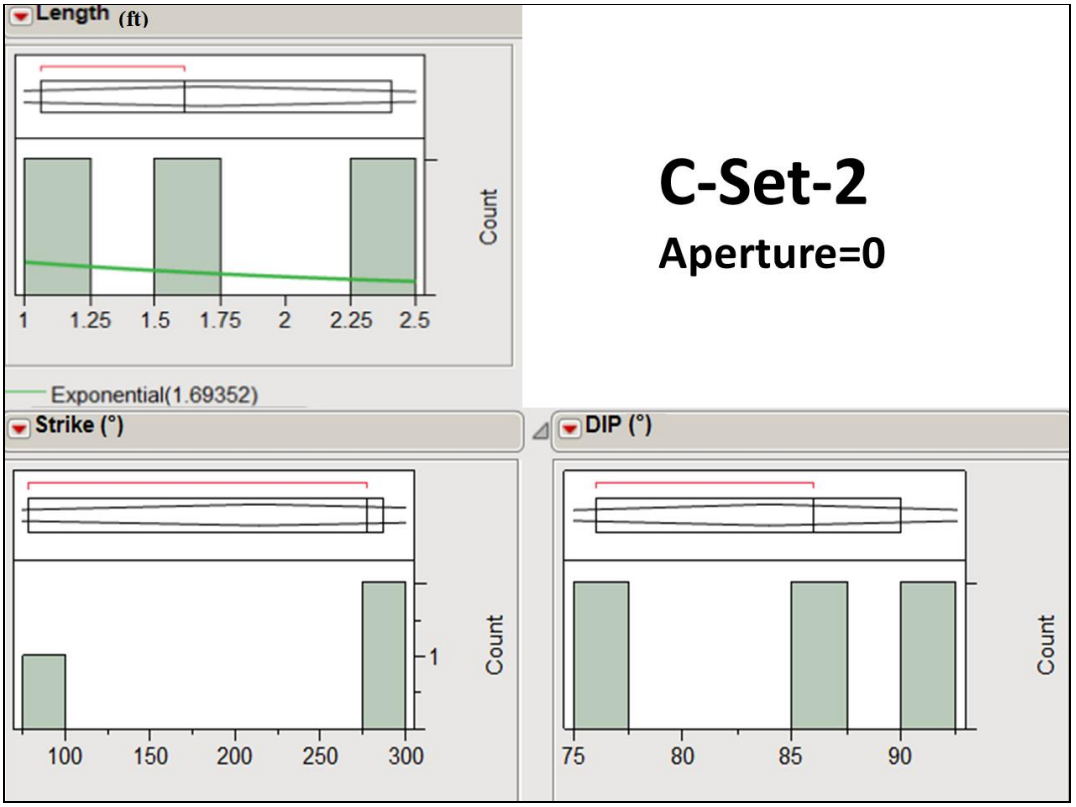

Figure D-6 Histograms of Fracture Set 2in CWF Region-

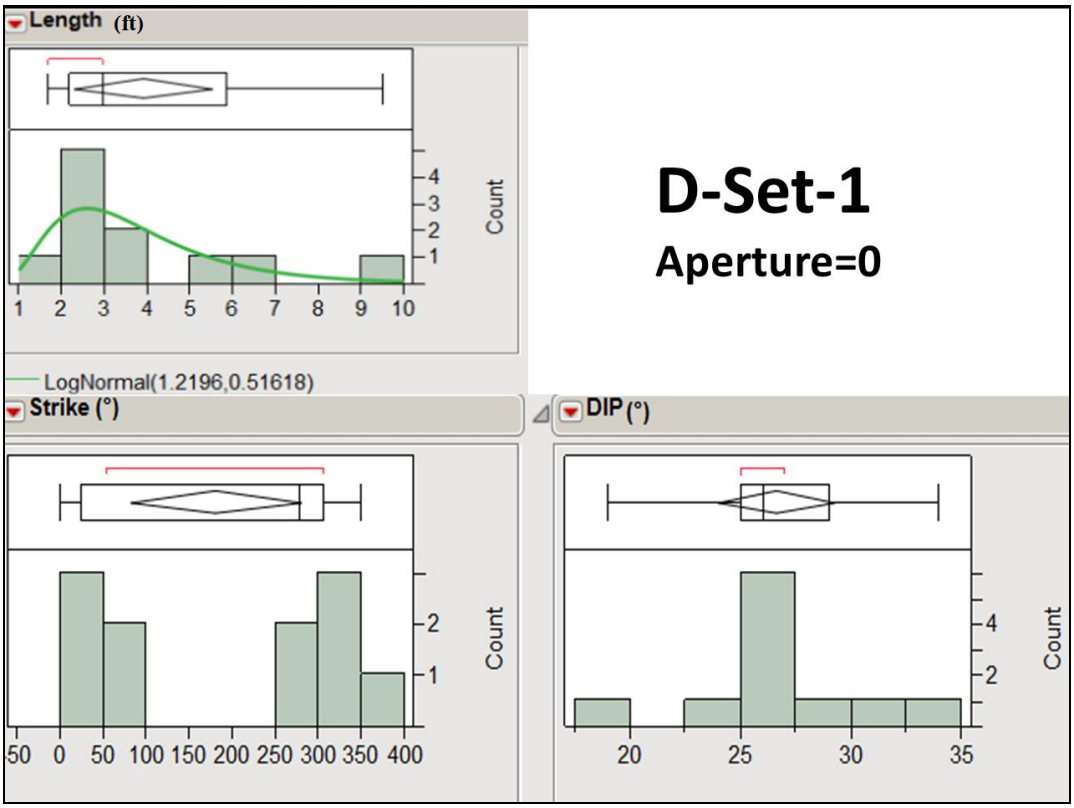

Figure D-7 Histograms of Fracture Set 1in CWF Region-D

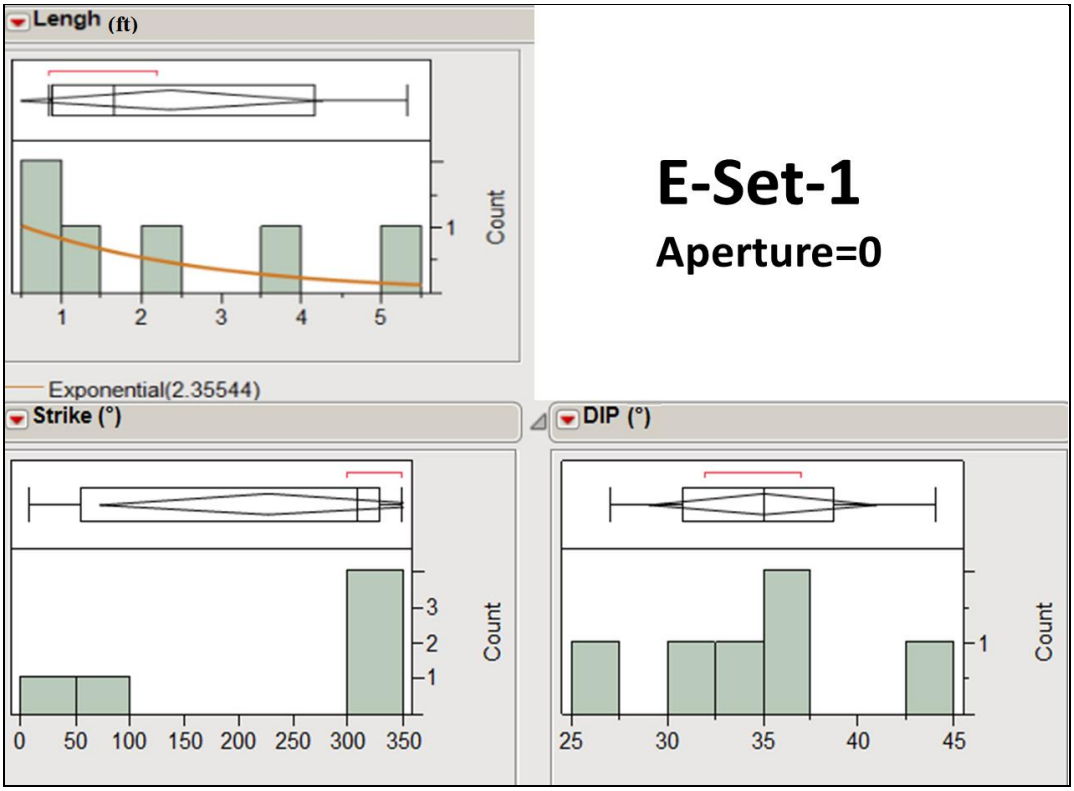

Figure D-8 Histograms of Fracture Set 1in CWF Region-E

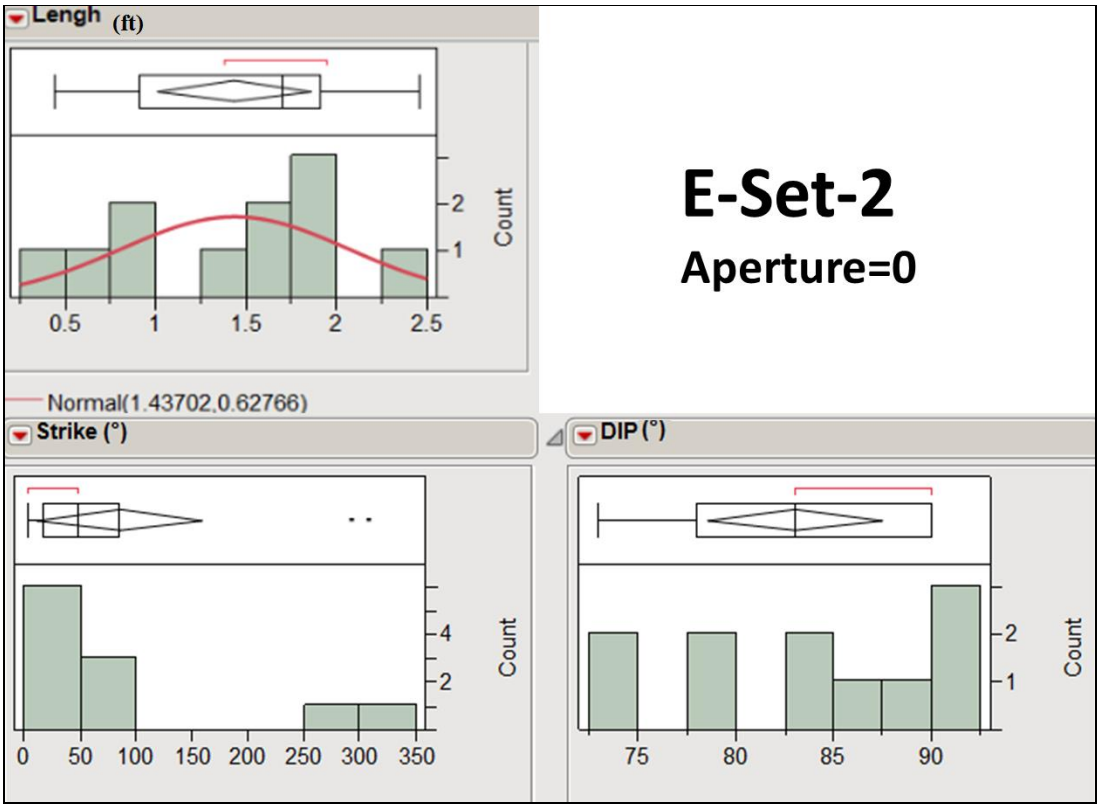

Figure D-9 Histograms of Fracture Set 2in CWF Region-E

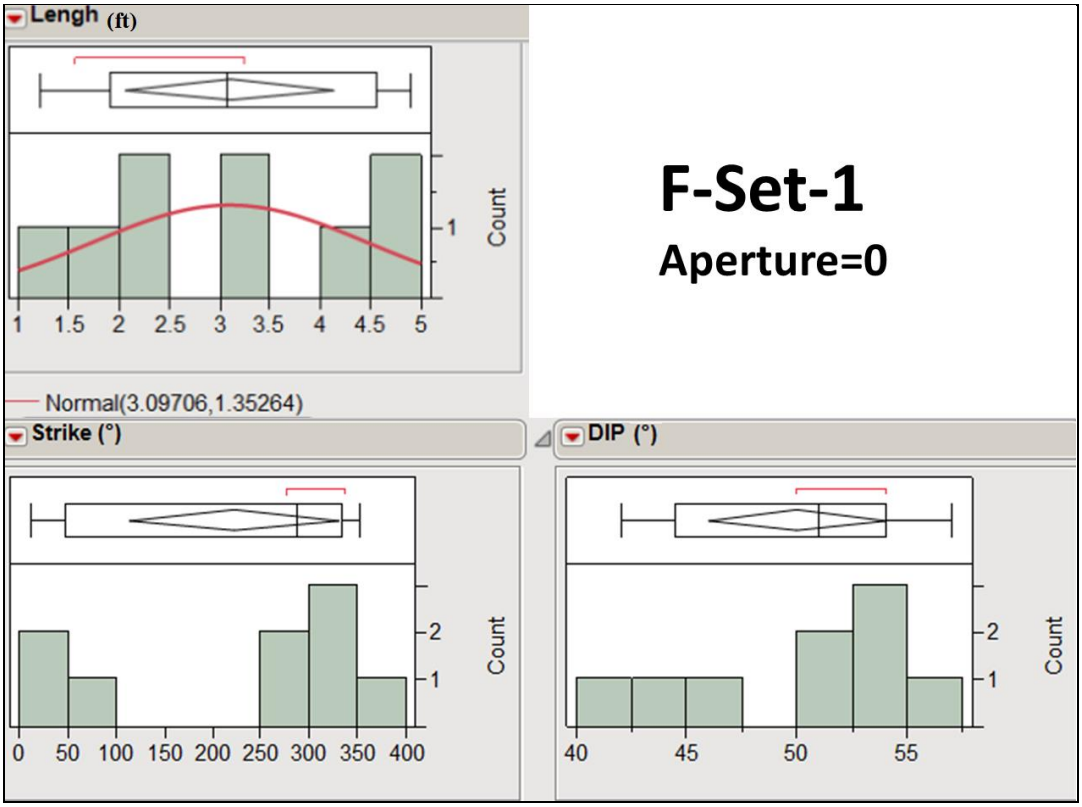

Figure D-10 Histograms of Fracture Set 1 in CWF Region-F

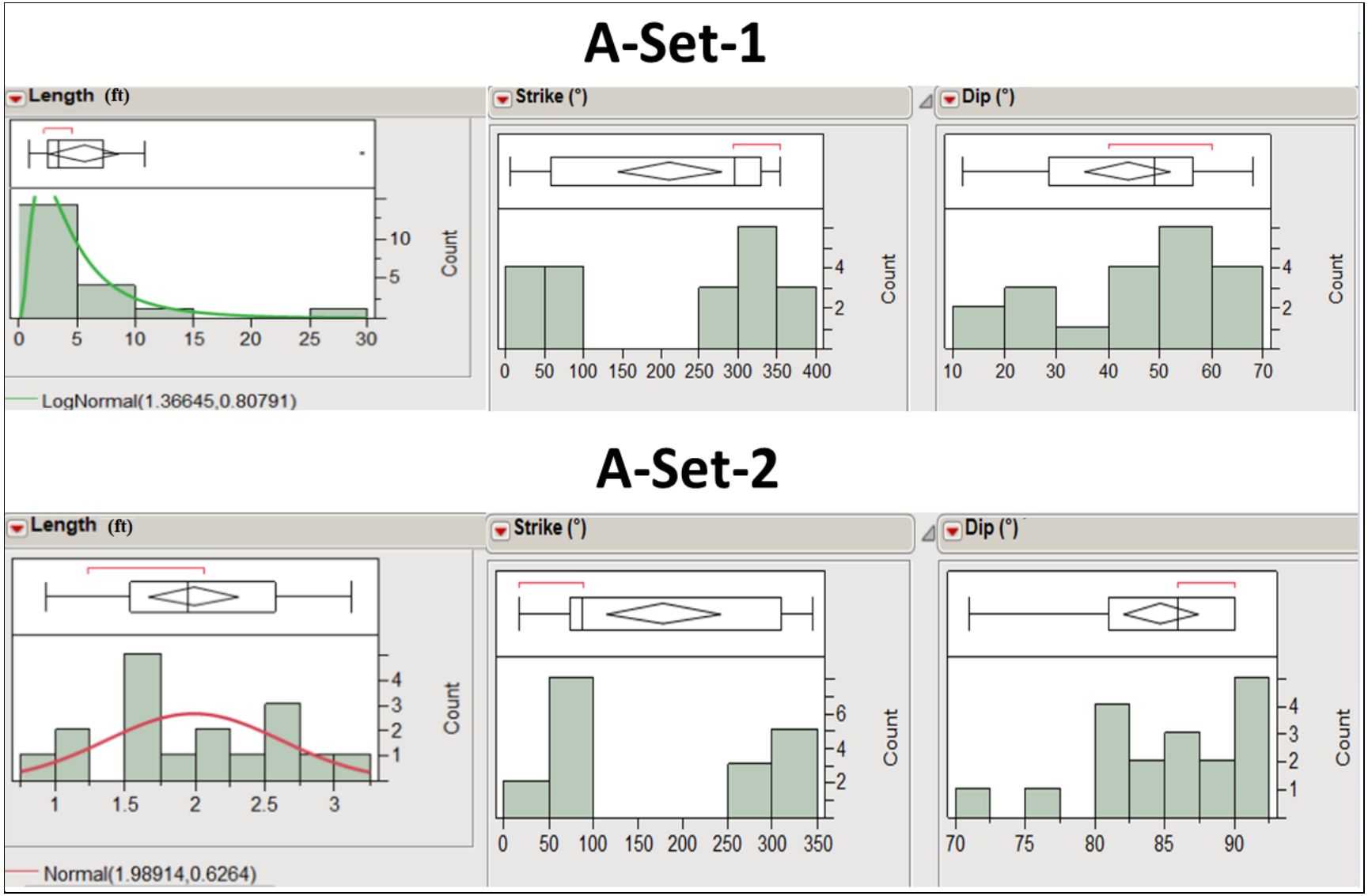

Figure D-11 Histograms of Fracture Set 1& Set 2 in FWF Region-A

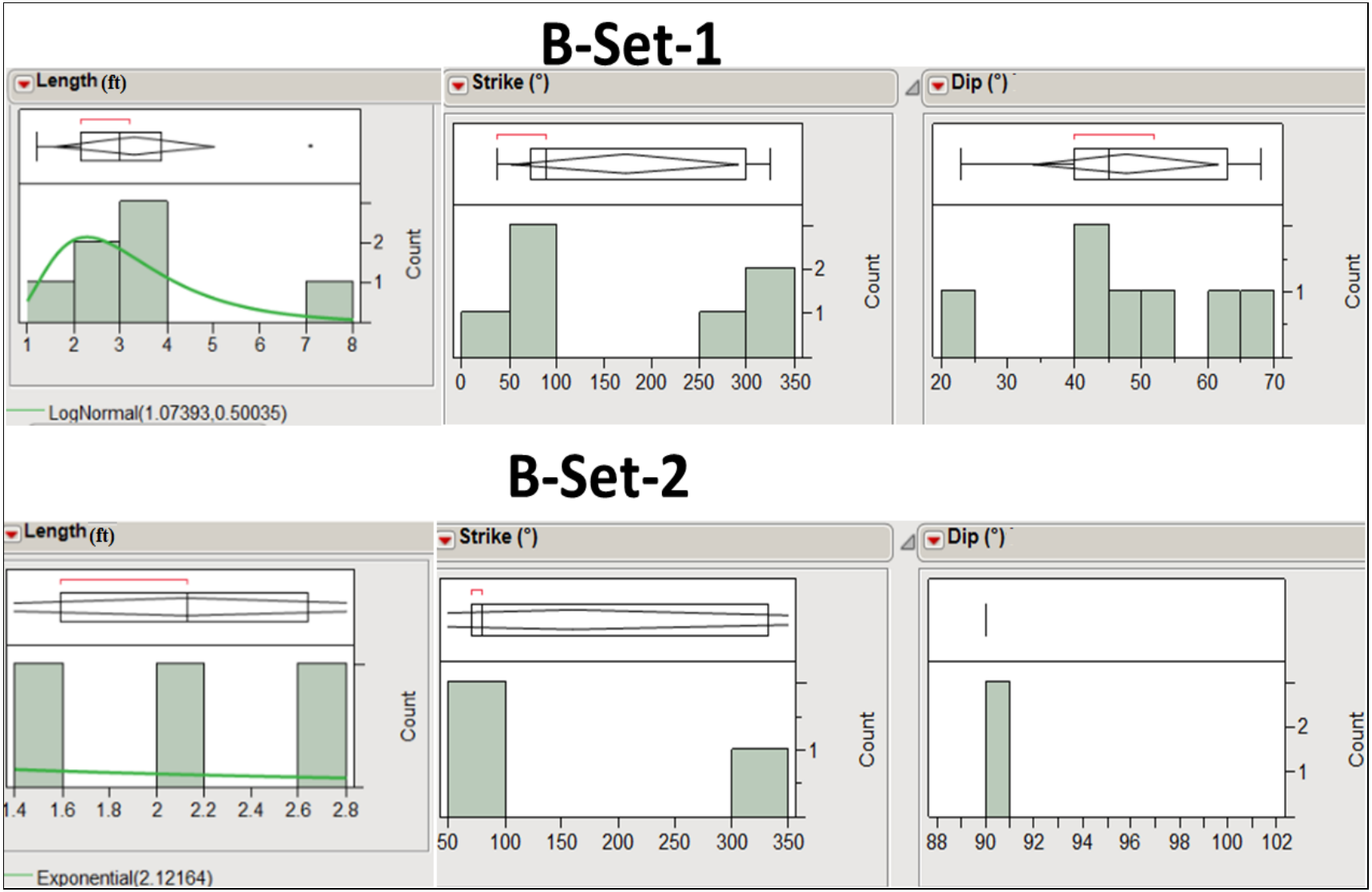

Figure D-12 Histograms of Fracture Set 1& Set 2 in FWF Region-B

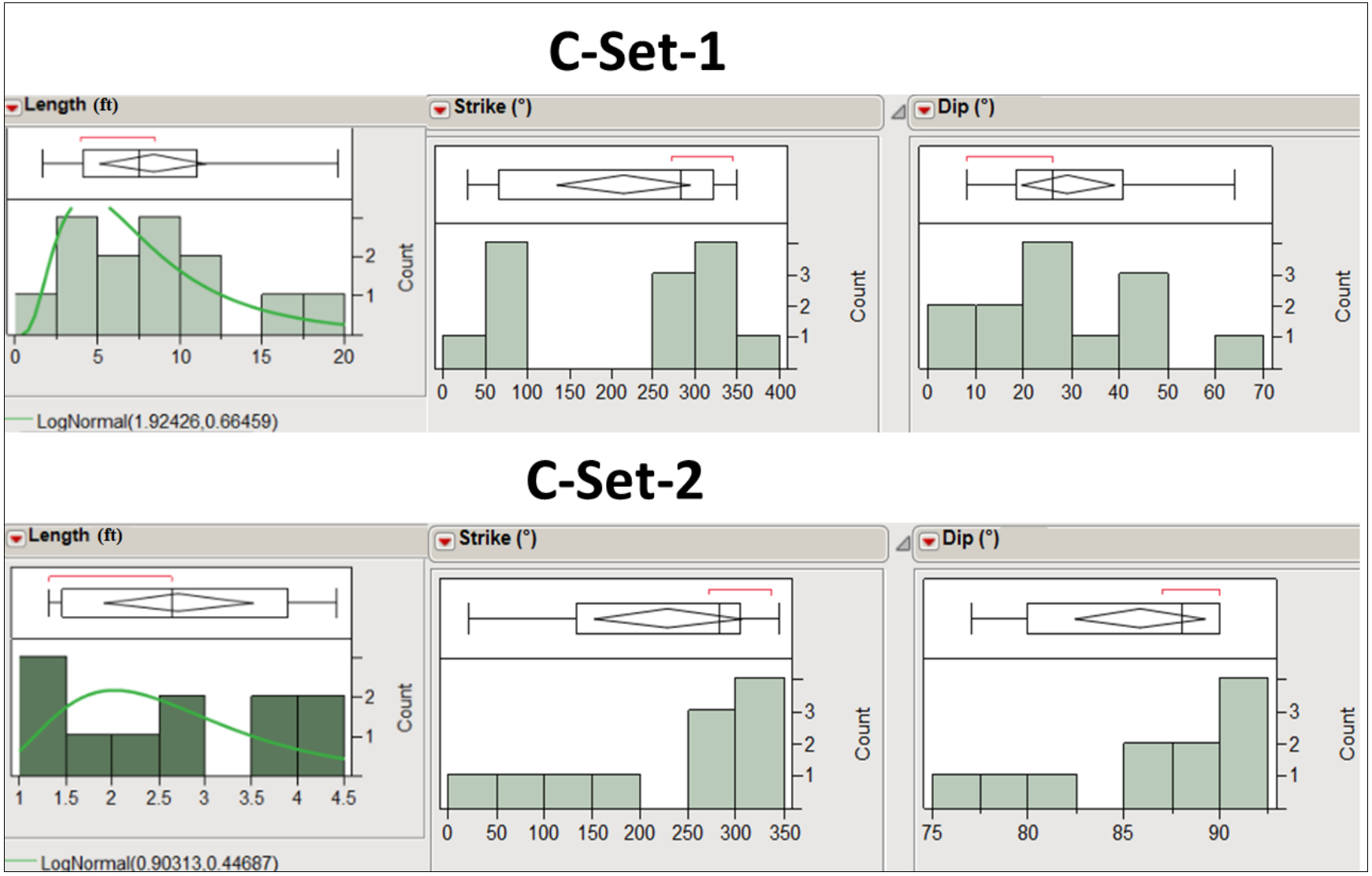

Figure D-13 Histograms of Fracture Set 1& Set 2 in FWF Region-C

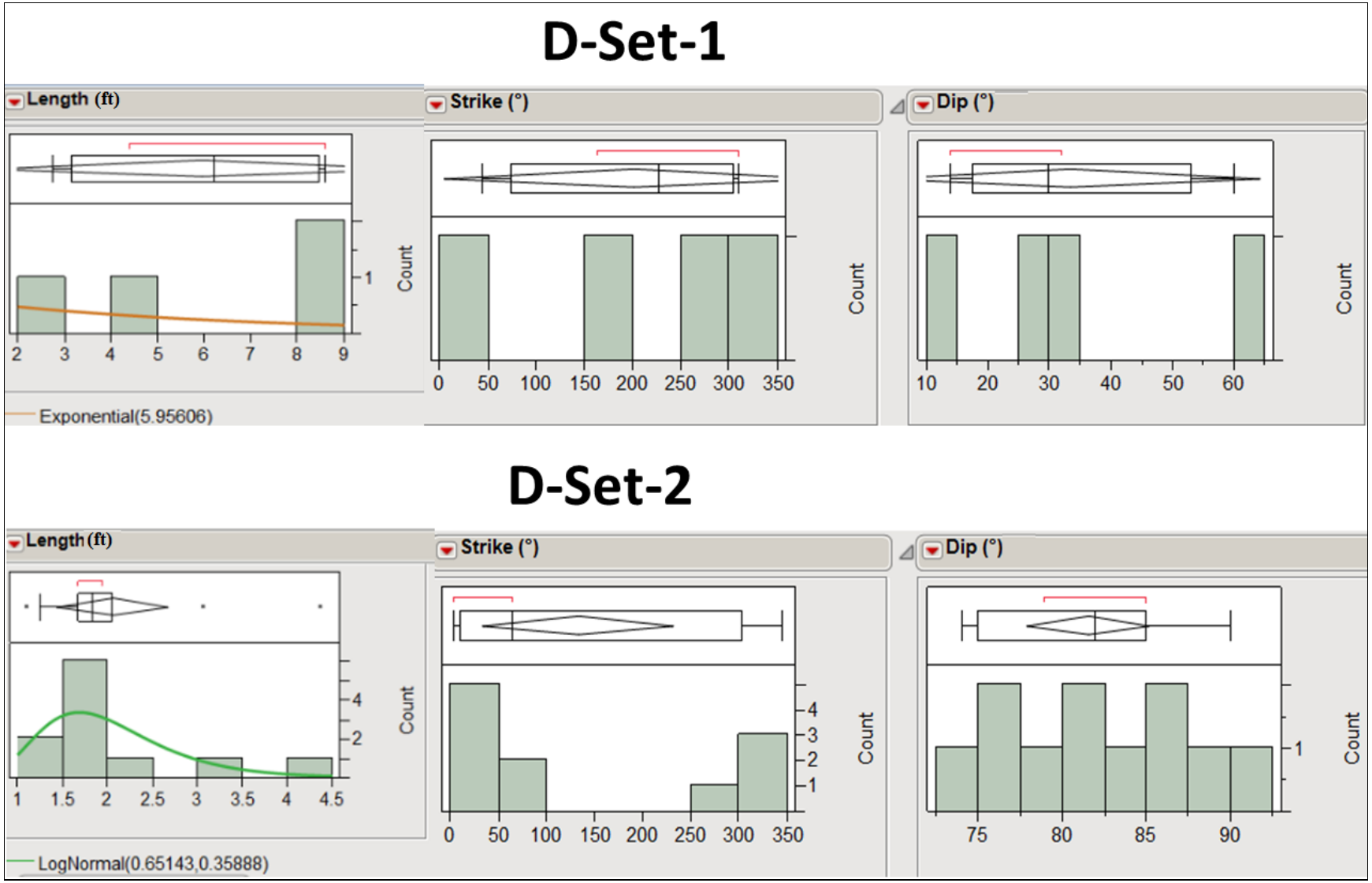

Figure D-14 Histograms of Fracture Set 1& Set 2 in FWF Region-D

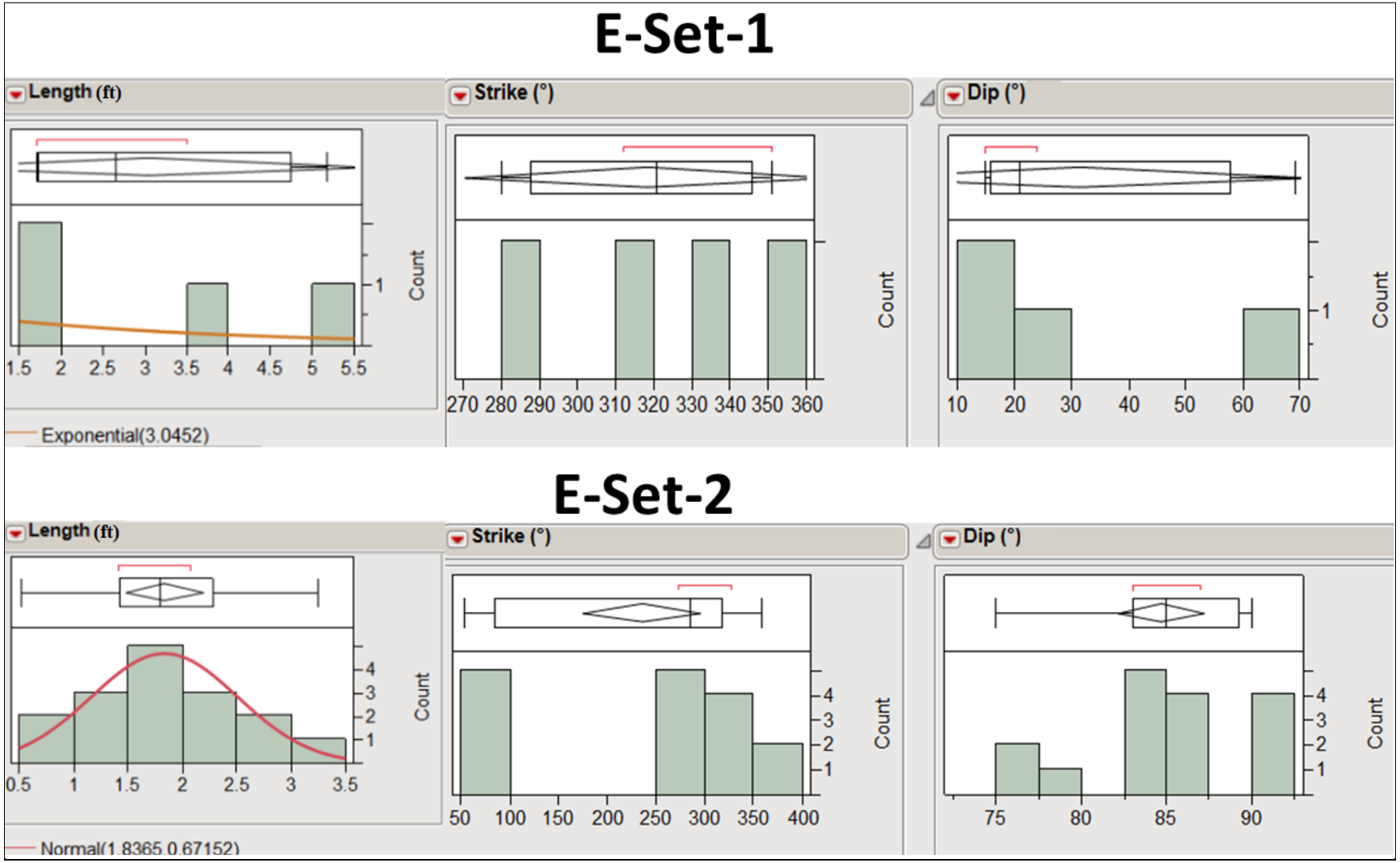

Figure D-15 Histograms of Fracture Set 1& Set 2 in FWF Region-E

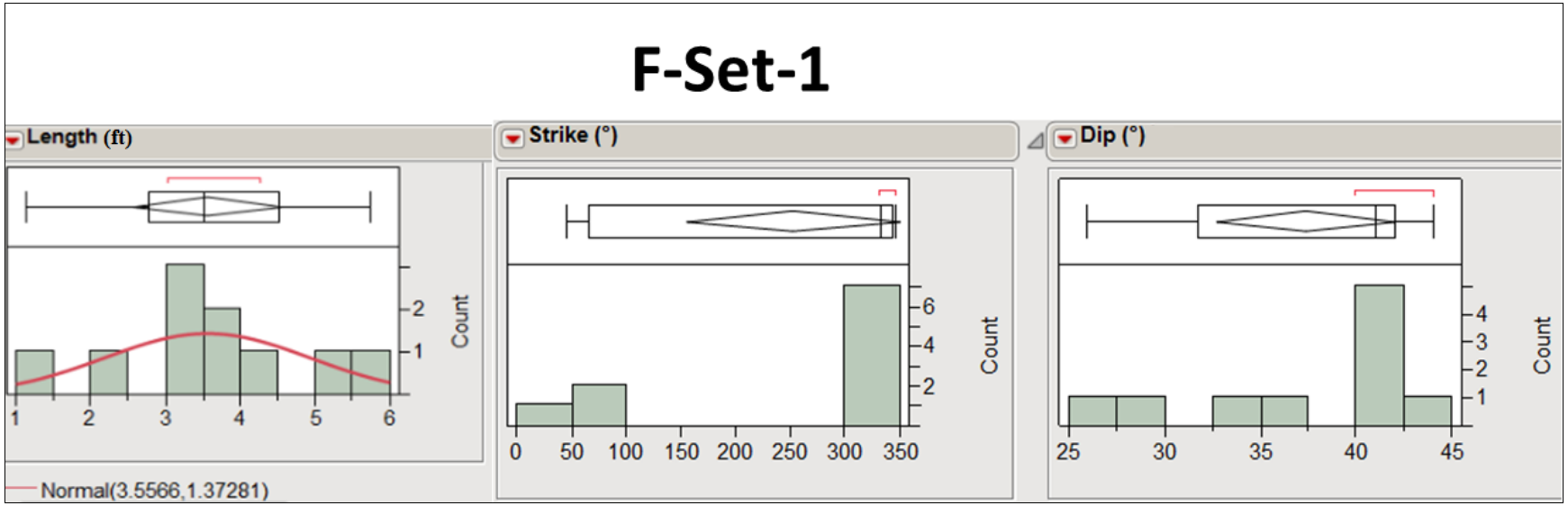

Figure D-16 Histograms of Fracture Set 1& Set 2 in FWF Region-F

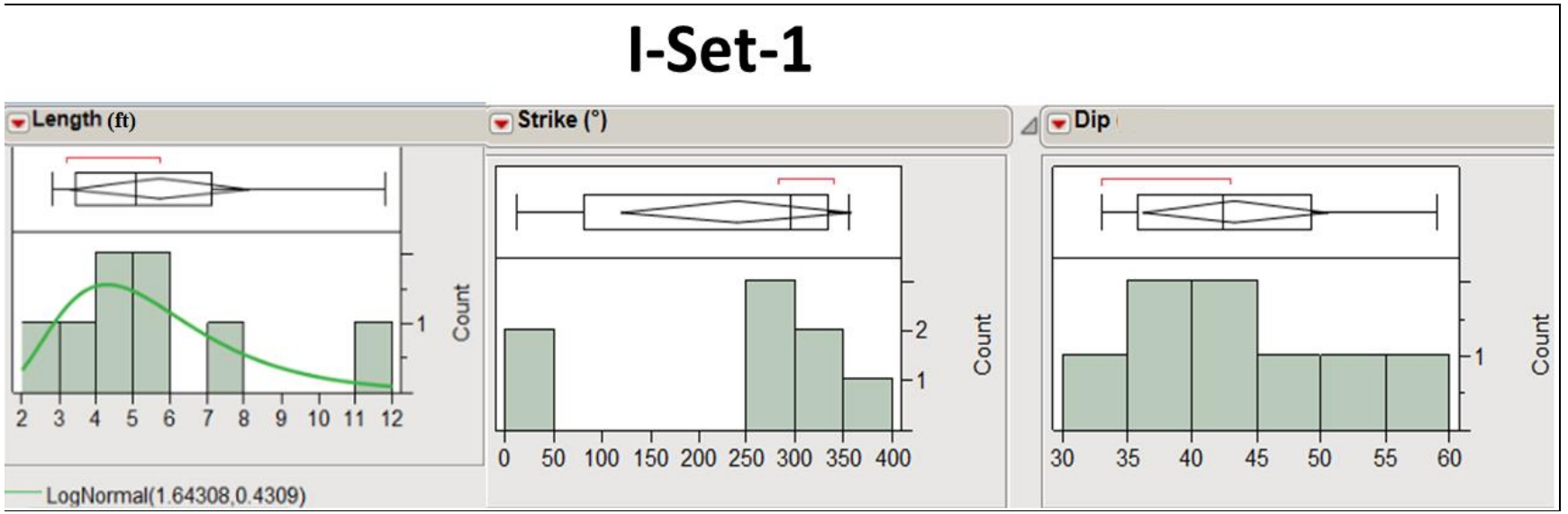

Figure D-17 Histograms of Fracture Set 1& Set 2 in FWF Region-I

Appendix E

THREE-DIMENSIONAL MODELS AND COMPARTMENTALIZATION ANALYSIS OF CWF AND FWF

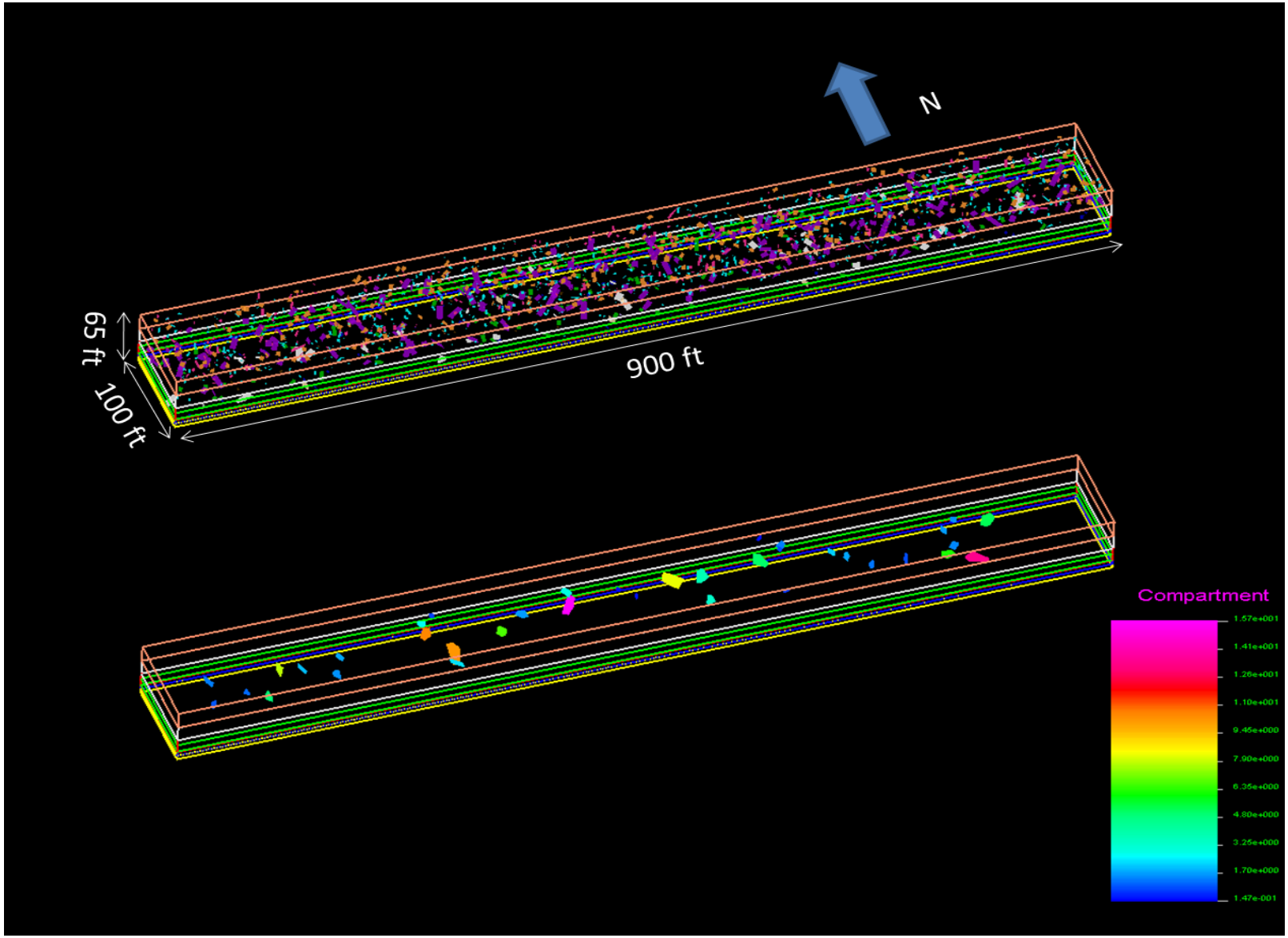

Figure E-1 Example of Three-Dimensional fracture realization and compartments analysis for CWF Assumption-A Model

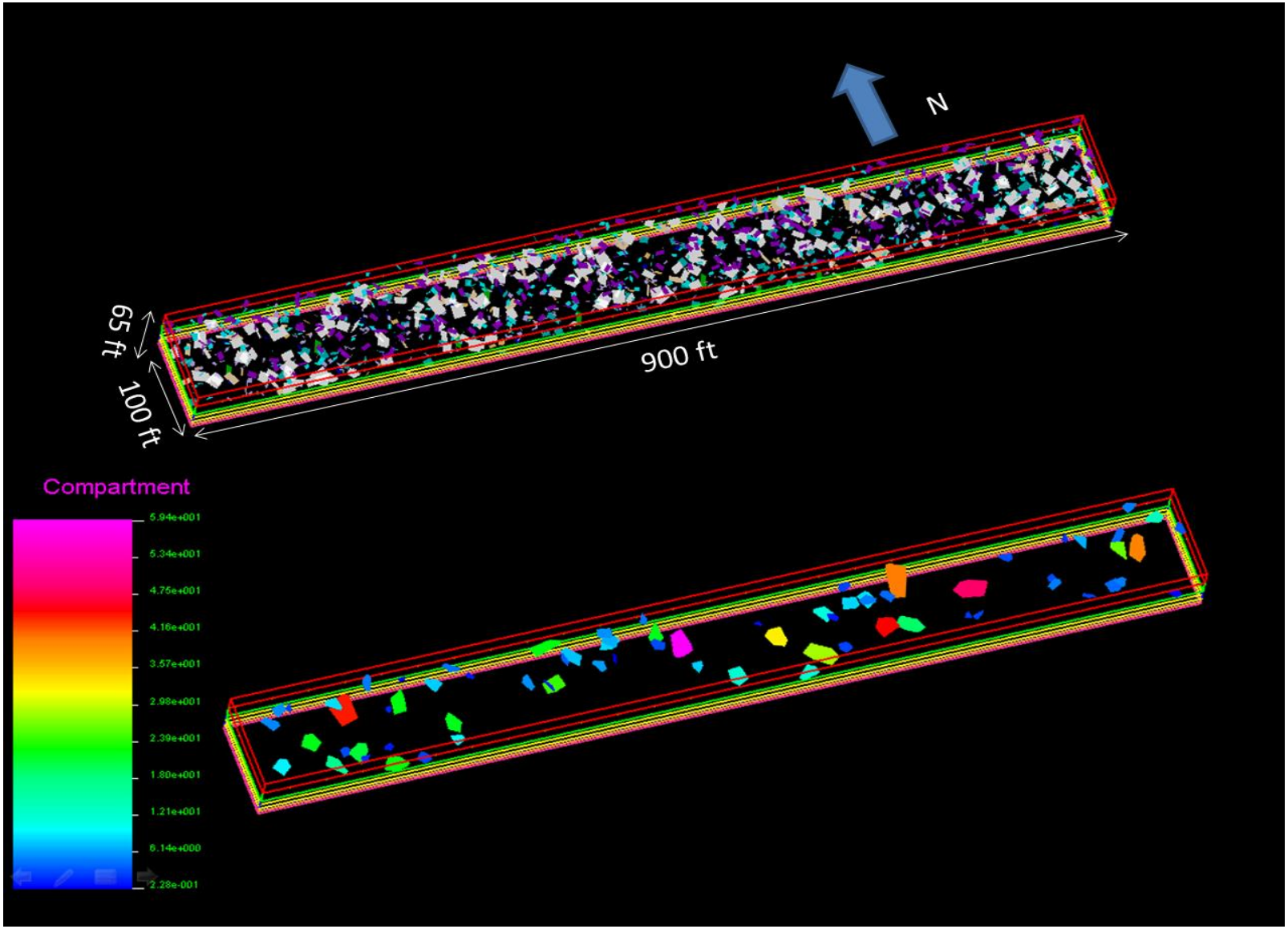

Figure E-2 Example of Three-Dimensional fracture realization and compartments analysis for CWF Assumption-B Model

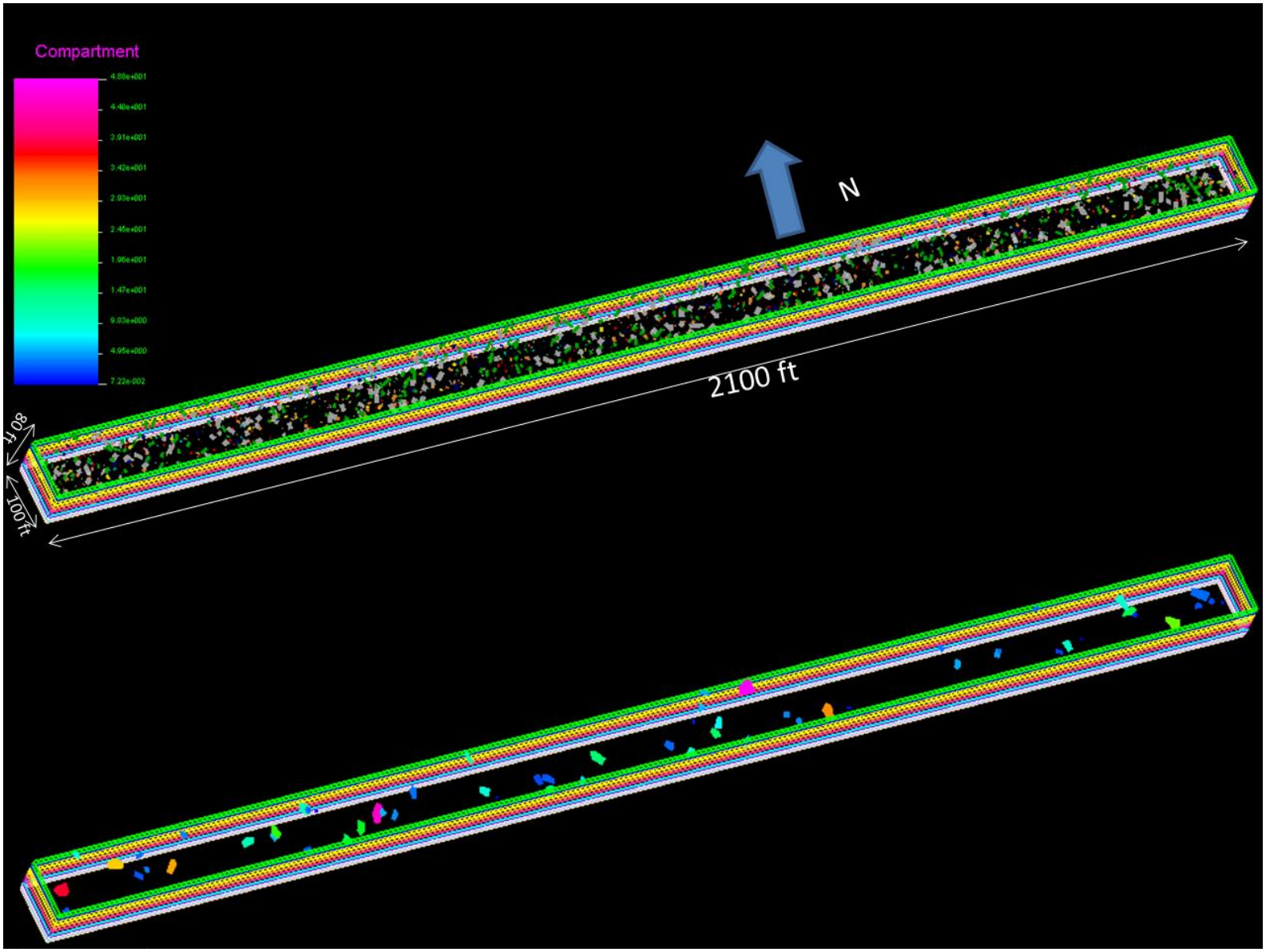

Figure E-3 Example of Three-Dimensional fracture realization and compartments analysis for FWF Assumption-A Model

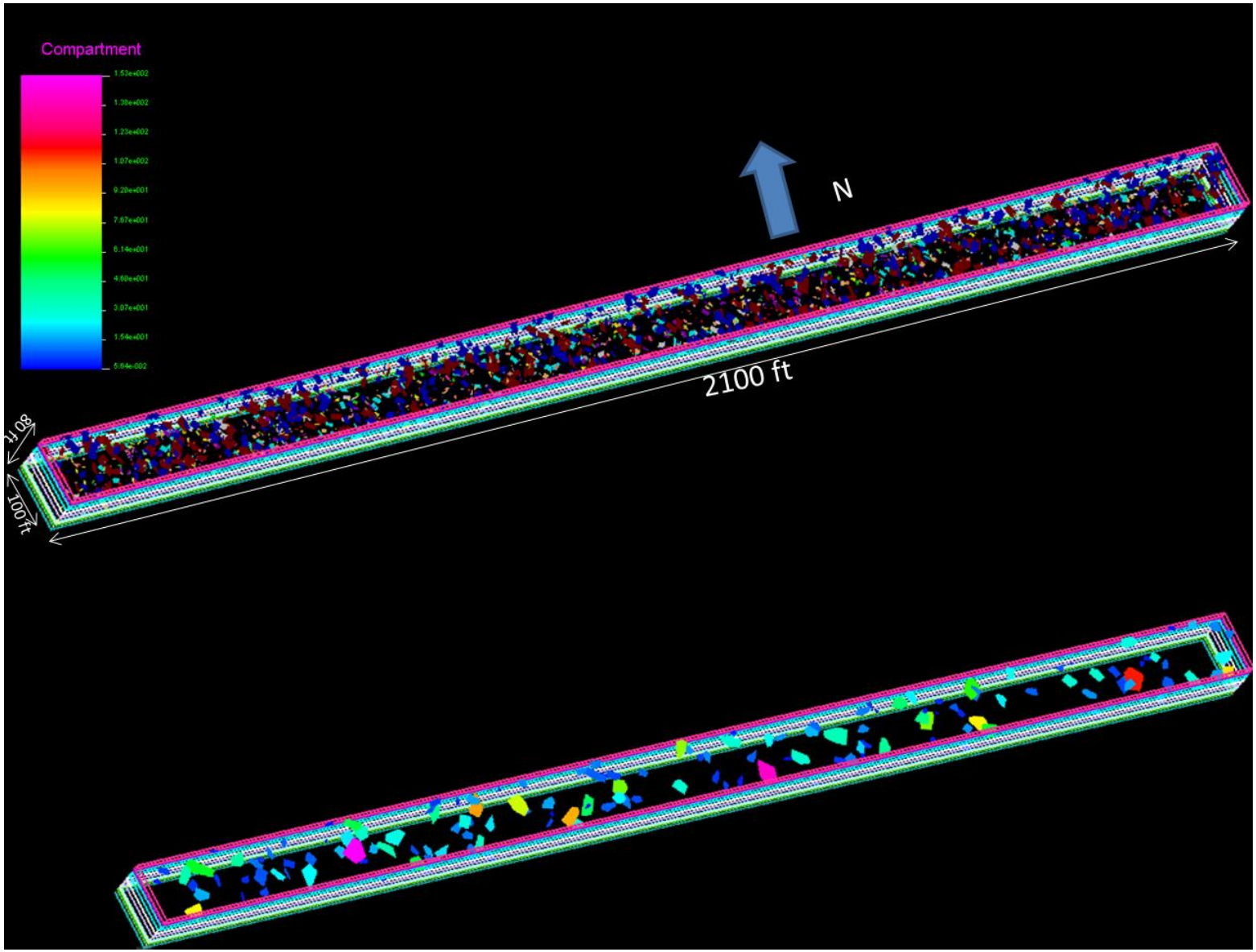

Figure E-4 Example of Three-Dimensional fracture realization and compartments analysis for FWF Assumption-B Model

Table E-1 Compartments Volume Statistics of 33 Realizations for CWF and FWF

Realization		1	2	3	4	5	6	7	8	9	10	11	12	13	14	15	16	17	18	19	20	21	22	23	24	25	26	27	28	29	30	31	32	33	Mean
CWF-A	Max. Vol (m^3)	25.2	10.3	18	18.2	51	15.7	25.2	10.3	18	13.3	28	37.8	19.1	17.6	38.8	23.4	30.4	64.8	47.2	15.9	17.3	32.6	13.3	101	25.5	48.7	14.2	15.7	38.1	21.9	34.7	22.5	19.6	28.28
	Total No. Com	45	34	38	29	35	37	45	34	38	45	36	34	43	33	39	41	41	27	44	49	39	38	32	33	36	33	40	39	27	37	41	45	40	37.79
	0-8(M^3)	42	33	35	27	30	32	40	33	35	44	28	27	38	28	32	35	30	23	37	41	34	30	29	26	30	26	34	35	17	35	35	38	36	32.58
	8.1-18(M^3)	2	1	2	1	2	5	1	1	2	1	6	3	4	5	5	4	8	3	6	8	5	5	3	4	5	6	6	4	7	1	4	4	2	3.82
	18.1-28(m^3)	1	0	1	1	1	0	4	0	1	0	1	3	1	0	0	2	2	0	0	0	0	2	0	2	1	0	0	0	2	1	1	3	2	0.97
	28.1-38(m^3)	0	0	0	0	1	0	0	0	0	0	1	1	0	0	1	0	1	1	0	0	0	1	0	0	0	0	0	0	0	0	1	0	0	0.24
	38.1-48(m^3)	0	0	0	0	0	0	0	0	0	0	0	0	0	0	1	0	0	0	1	0	0	0	0	0	0	0	0	0	1	0	0	0	0	0.09
	48.1-58(m^3)	0	0	0	0	1	0	0	0	0	0	0	0	0	0	0	0	0	0	0	0	0	0	0	0	0	1	0	0	0	0	0	0	0	0.06
	58.1-68(m^3)	0	0	0	0	0	0	0	0	0	0	0	0	0	0	0	0	0	0	0	0	0	0	0	0	0	0	0	0	0	0	0	0	0	0.00
	68.1-78(m^3)	0	0	0	0	0	0	0	0	0	0	0	0	0	0	0	0	0	0	0	0	0	0	0	0	0	0	0	0	0	0	0	0	0	0.00
	78.1-88(m^3)	0	0	0	0	0	0	0	0	0	0	0	0	0	0	0	0	0	0	0	0	0	0	0	0	0	0	0	0	0	0	0	0	0	0.00
	88.1-98(m^3)	0	0	0	0	0	0	0	0	0	0	0	0	0	0	0	0	0	0	0	0	0	0	0	0	0	0	0	0	0	0	0	0	0	0.00
	98.1-108(m^3)	0	0	0	0	0	0	0	0	0	0	0	0	0	0	0	0	0	0	0	0	0	0	0	1	0	0	0	0	0	0	0	0	0	0.03
	108.1-118(m^3)	0	0	0	0	0	0	0	0	0	0	0	0	0	0	0	0	0	0	0	0	0	0	0	0	0	0	0	0	0	0	0	0	0	0.00
CWF-B	Max Vol (m^3)	59.9	170	103	51.1	84.8	50.5	141	118	149	75	179	103	51.1	84.8	50.5	141	96	110	32.4	103	118	145	59.6	102	99.8	160	82	86	68.6	85.1	119	37.9	42.7	95.72
	Total No. Com	69	72	74	70	75	71	64	80	64	78	72	74	70	75	71	64	54	68	65	75	84	87	76	66	76	70	73	66	70	62	74	75	66	71.21
	0-8(M^3)	44	51	41	45	52	49	48	56	47	51	49	44	46	62	48	40	28	41	30	53	57	68	50	43	52	58	49	48	50	37	40	35	41	47.06
	8.1-18(M^3)	2	8	25	14	11	9	3	5	9	10	14	13	13	4	13	14	16	18	24	9	13	10	11	10	11	6	11	7	12	13	18	30	15	12.15
	18.1-28(m^3)	11	5	1	7	8	5	5	12	1	12	2	10	7	5	2	2	3	2	8	4	6	1	7	6	5	0	7	4	2	6	4	4	3	5.06
	28.1-38(m^3)	7	1	2	1	1	3	5	3	4	1	2	2	1	0	4	5	3	5	3	5	4	4	2	3	4	0	2	1	3	0	7	6	6	3.03
	38.1-48(m^3)	3	2	0	1	2	2	2	2	0	2	1	2	1	2	1	2	2	0	0	0	0	2	5	1	0	1	2	2	0	4	4	0	1	1.48
	48.1-58(m^3)	1	2	2	2	0	3	0	0	1	0	1	0	2	1	3	0	0	1	0	0	2	0	0	0	1	2	0	2	2	0	0	0	0	0.85
	58.1-68(m^3)	1	0	1	0	0	0	0	0	0	1	0	1	0	0	0	0	0	0	0	1	1	1	1	2	1	0	1	0	0	0	0	0	0	0.36
	68.1-78(m^3)	0	0	1	0	0	0	0	0	1	1	0	1	0	0	0	0	1	0	0	2	0	0	0	0	0	0	0	0	1	1	0	0	0	0.27
	78.1-88(m^3)	0	1	0	0	1	0	0	0	0	0	1	0	0	1	0	0	0	0	0	0	0	0	0	0	1	0	1	2	0	1	0	0	0	0.27
	88.1-98(m^3)	0	0	0	0	0	0	0	1	0	0	0	0	0	0	0	0	1	0	0	0	0	0	0	0	0	1	0	0	0	0	0	0	0	0.09
	98.1-108(m^3)	0	1	1	0	0	0	0	0	0	0	1	1	0	0	0	0	0	0	0	1	0	0	0	1	1	1	0	0	0	0	0	0	0	0.24
	108.1-118(m^3)	0	0	0	0	0	0	0	0	0	0	0	0	0	0	0	0	0	1	0	0	0	0	0	0	0	0	0	0	0	0	0	0	0	0.03
	118.1-128(m^3)	0	0	0	0	0	0	0	1	0	0	0	0	0	0	0	0	0	0	0	0	1	0	0	0	0	0	0	0	0	0	1	0	0	0.09
	128.1-138(m^3)	0	0	0	0	0	0	0	0	0	0	0	0	0	0	0	0	0	0	0	0	0	0	0	0	0	0	0	0	0	0	0	0	0	0.00
	138.1-148(m^3)	0	0	0	0	0	0	1	0	0	0	0	0	0	0	0	1	0	0	0	0	0	1	0	0	0	0	0	0	0	0	0	0	0	0.09
	148.1-158(m^3)	0	0	0	0	0	0	0	0	1	0	0	0	0	0	0	0	0	0	0	0	0	0	0	0	0	0	0	0	0	0	0	0	0	0.03
	158.1-168(m^3)	0	0	0	0	0	0	0	0	0	0	0	0	0	0	0	0	0	0	0	0	0	0	0	0	0	1	0	0	0	0	0	0	0	0.03
	168.1-178(m^3)	0	1	0	0	0	0	0	0	0	0	0	0	0	0	0	0	0	0	0	0	0	0	0	0	0	0	0	0	0	0	0	0	0	0.03
	178.1-188(m^3)	0	0	0	0	0	0	0	0	0	0	1	0	0	0	0	0	0	0	0	0	0	0	0	0	0	0	0	0	0	0	0	0	0	0.03
	188.1-198(m^3)	0	0	0	0	0	0	0	0	0	0	0	0	0	0	0	0	0	0	0	0	0	0	0	0	0	0	0	0	0	0	0	0	0	0.00

Realization		1	2	3	4	5	6	7	8	9	10	11	12	13	14	15	16	17	18	19	20	21	22	23	24	25	26	27	28	29	30	31	32	33	Mean
FWF-A	Max. Vol (m^3)	36	42.4	41.7	45.1	73.7	69.4	36	42.4	41.7	45.1	73.7	33.3	37.4	53.2	38.4	36.5	56.3	39.6	49.2	56.1	48.5	78.7	41.2	70.7	45.9	35.5	95.8	32.7	31.1	66.5	34.3	32.3	36.2	48.38
	Total No. Com	43	36	52	55	58	55	43	36	52	57	58	49	37	69	49	56	54	64	56	46	47	55	42	42	56	52	51	50	58	53	66	44	51	51.27
	0-8(M^3)	20	12	27	33	40	38	31	15	27	33	37	22	17	39	31	36	32	39	30	22	31	40	22	31	30	24	31	30	34	36	40	32	34	30.18
	8.1-18(M^3)	20	14	12	16	6	12	9	16	16	18	13	14	18	23	14	14	16	18	13	18	9	8	11	7	19	20	10	15	20	11	19	8	14	14.27
	18.1-28(m^3)	2	6	10	5	5	1	1	1	6	5	2	12	1	5	3	4	4	2	6	3	3	3	7	2	5	7	6	2	3	3	5	3	2	4.09
	28.1-38(m^3)	1	3	2	0	5	3	2	3	2	0	4	1	1	1	0	2	1	2	5	1	2	1	1	1	0	1	1	3	1	0	2	1	1	1.64
	38.1-48(m^3)	0	1	1	1	1	0	0	1	1	1	1	0	0	0	1	0	0	3	1	1	1	2	1	0	2	0	1	0	0	1	0	0	0	0.67
	48.1-58(m^3)	0	0	0	0	0	0	0	0	0	0	0	0	0	1	0	0	1	0	1	1	1	0	0	0	0	0	0	0	0	1	0	0	0	0.18
	58.1-68(m^3)	0	0	0	0	0	0	0	0	0	0	0	0	0	0	0	0	0	0	0	0	0	0	0	0	0	0	0	0	0	1	0	0	0	0.03
	68.1-78(m^3)	0	0	0	0	1	1	0	0	0	0	1	0	0	0	0	0	0	0	0	0	0	0	0	1	0	0	1	0	0	0	0	0	0	0.15
	78.1-88(m^3)	0	0	0	0	0	0	0	0	0	0	0	0	0	0	0	0	0	0	0	0	0	1	0	0	0	0	0	0	0	0	0	0	0	0.03
	88.1-98(m^3)	0	0	0	0	0	0	0	0	0	0	0	0	0	0	0	0	0	0	0	0	0	0	0	0	0	0	1	0	0	0	0	0	0	0.03
	98.1-108(m^3)	0	0	0	0	0	0	0	0	0	0	0	0	0	0	0	0	0	0	0	0	0	0	0	0	0	0	0	0	0	0	0	0	0	0.00
FWF-B	Max Vol (m^3)	115	107	213	148	106	360	125	220	274	182	151	219	153	141	304	180	246	159	148	135	233	102	319	255	123	98.6	377	195	159	301	92.8	157	125	188.6
	Total No. Com	119	125	144	127	132	143	130	138	144	132	129	137	139	128	143	120	130	112	121	125	119	118	127	145	130	124	133	122	124	141	117	134	127	129.7
	0-8(M^3)	40	56	80	48	34	86	56	69	88	76	42	83	72	56	78	63	76	37	40	40	71	37	83	84	47	31	82	51	122	82	41	61	58	62.73
	8.1-18(M^3)	27	19	10	33	39	0	23	22	7	15	36	0	23	19	0	18	0	26	41	29	0	15	0	0	21	26	0	4	-41	0	23	29	23	14.76
	18.1-28(m^3)	3	9	8	4	20	24	17	3	10	2	9	13	2	2	33	4	17	9	1	10	8	10	11	50	21	15	30	29	1	33	15	2	15	13.33
	28.1-38(m^3)	27	18	10	9	19	13	15	5	13	7	6	5	3	8	14	8	5	7	7	15	2	21	17	4	2	19	9	5	4	6	25	7	4	10.27
	38.1-48(m^3)	6	6	6	17	12	6	4	20	5	1	9	2	8	26	-1	5	4	8	10	18	12	14	0	0	7	14	2	14	8	3	5	5	6	7.94
	48.1-58(m^3)	8	3	6	6	1	0	4	1	2	9	11	1	18	0	6	9	0	10	13	2	1	6	1	1	20	2	0	3	13	2	5	5	11	5.45
	58.1-68(m^3)	2	4	12	3	1	0	2	8	1	13	1	21	2	4	0	2	6	1	3	2	8	6	8	1	0	5	0	7	12	0	1	17	2	4.70
	68.1-78(m^3)	1	4	5	1	4	0	3	5	0	2	5	6	2	5	0	1	12	5	1	2	6	1	1	0	1	7	0	1	0	0	1	0	1	2.52
	78.1-88(m^3)	2	2	0	0	1	0	3	2	11	2	3	0	2	1	0	3	6	2	2	1	4	5	0	2	4	3	0	5	0	4	0	1	3	2.24
	88.1-98(m^3)	1	1	2	1	0	0	2	1	3	1	2	1	0	1	4	2	0	1	1	1	1	1	1	1	6	1	0	1	0	4	1	2	1	1.36
	98.1-108(m^3)	1	3	0	1	1	4	0	0	0	0	0	1	0	3	0	2	0	1	0	2	2	2	0	1	0	1	0	1	0	0	0	0	1	0.82
	108.1-118(m^3)	1	0	0	2	0	2	0	0	0	1	2	1	0	1	0	0	0	2	0	2	1	0	1	0	0	0	5	0	0	2	0	3	0	0.79
	118.1-128(m^3)	0	0	2	0	0	0	1	0	1	1	2	0	1	0	1	0	1	1	0	0	0	0	2	0	1	0	1	0	4	2	0	1	2	0.73
	128.1-138(m^3)	0	0	0	0	0	2	0	0	1	1	0	1	2	0	6	0	1	0	0	1	0	0	0	0	0	0	1	0	0	0	0	0	0	0.48
	138.1-148(m^3)	0	0	1	0	0	4	0	0	0	0	0	0	2	2	0	1	0	1	0	0	2	0	0	0	0	0	0	0	0	0	0	0	0	0.39
	148.1-158(m^3)	0	0	0	2	0	0	0	1	1	0	1	1	2	0	0	0	0	0	2	0	0	0	1	0	0	0	2	0	0	1	0	1	0	0.45
	158.1-168(m^3)	0	0	0	0	0	0	0	0	0	0	0	0	0	0	0	0	1	1	0	0	0	0	0	0	0	0	0	0	1	0	0	0	0	0.09
	168.1-178(m^3)	0	0	0	0	0	0	0	0	0	0	0	0	0	0	0	0	0	0	0	0	0	0	0	0	0	0	0	0	0	0	0	0	0	0.00
	178.1-188(m^3)	0	0	0	0	0	0	0	0	0	1	0	0	0	0	0	2	0	0	0	0	0	0	0	0	0	0	0	0	0	0	0	0	0	0.09
	188.1-198(m^3)	0	0	0	0	0	0	0	0	0	0	0	0	0	0	1	0	0	0	0	0	0	0	0	0	0	0	0	1	0	0	0	0	0	0.06
	198.1-208(m^3)	0	0	0	0	0	0	0	0	0	0	0	0	0	0	0	0	0	0	0	0	0	0	0	0	0	0	0	0	0	0	0	0	0	0.00
	208.1-218(m^3)	0	0	2	0	0	0	0	0	0	0	0	0	0	0	0	0	0	0	0	0	0	0	0	0	0	0	0	0	0	0	0	0	0	0.06
	218.1-228(m^3)	0	0	0	0	0	1	0	1	0	0	0	1	0	0	0	0	0	0	0	0	0	0	0	0	0	0	0	0	0	0	0	0	0	0.09
	228.1-238(m^3)	0	0	0	0	0	0	0	0	0	0	0	0	0	0	0	0	0	0	0	0	1	0	0	0	0	0	0	0	0	0	0	0	0	0.03
	138.1-248(m^3)	0	0	0	0	0	0	0	0	0	0	0	0	0	0	0	0	1	0	0	0	0	0	0	0	0	0	0	0	0	1	0	0	0	0.06
	248.1-258(m^3)	0	0	0	0	0	0	0	0	0	0	0	0	0	0	0	0	0	0	0	0	0	0	0	1	0	0	0	0	0	0	0	0	0	0.03
	258.1-268(m^3)	0	0	0	0	0	0	0	0	0	0	0	0	0	0	0	0	0	0	0	0	0	0	0	0	0	0	0	0	0	0	0	0	0	0.00
	268.1-278(m^3)	0	0	0	0	0	0	0	0	1	0	0	0	0	0	0	0	0	0	0	0	0	0	0	0	0	0	0	0	0	0	0	0	0	0.03
	278.1-288(m^3)	0	0	0	0	0	0	0	0	0	0	0	0	0	0	0	0	0	0	0	0	0	0	0	0	0	0	0	0	0	0	0	0	0	0.00
	288.1-298(m^3)	0	0	0	0	0	0	0	0	0	0	0	0	0	0	0	0	0	0	0	0	0	0	0	0	0	0	0	0	0	0	0	0	0	0.00
	298.1-308(m^3)	0	0	0	0	0	0	0	0	0	0	0	0	0	0	1	0	0	0	0	0	0	0	0	0	0	0	0	0	0	1	0	0	0	0.06

	308.1-318(m^3)	0	0	0	0	0	0	0	0	0	0	0	0	0	0	0	0	0	0	0	0	0	0	0	0	0	0	0	0	0	0	0	0	0	0.00
	318.1-328(m^3)	0	0	0	0	0	0	0	0	0	0	0	0	0	0	0	0	0	0	0	0	0	0	1	0	0	0	0	0	0	0	0	0	0	0.03
	328.1-338(m^3)	0	0	0	0	0	0	0	0	0	0	0	0	0	0	0	0	0	0	0	0	0	0	0	0	0	0	0	0	0	0	0	0	0	0.00
	338.1-348(m^3)	0	0	0	0	0	0	0	0	0	0	0	0	0	0	0	0	0	0	0	0	0	0	0	0	0	0	0	0	0	0	0	0	0	0.00
	348.1-358(m^3)	0	0	0	0	0	0	0	0	0	0	0	0	0	0	0	0	0	0	0	0	0	0	0	0	0	0	0	0	0	0	0	0	0	0.00
	358.1-368(m^3)	0	0	0	0	0	1	0	0	0	0	0	0	0	0	0	0	0	0	0	0	0	0	0	0	0	0	0	0	0	0	0	0	0	0.03
	368.1-378(m^3)	0	0	0	0	0	0	0	0	0	0	0	0	0	0	0	0	0	0	0	0	0	0	0	0	0	0	1	0	0	0	0	0	0	0.03
	378.1-388(m^3)	0	0	0	0	0	0	0	0	0	0	0	0	0	0	0	0	0	0	0	0	0	0	0	0	0	0	0	0	0	0	0	0	0	0.00

VITA

Shuang (Cindy) Cao was born in Lenghu, Qinghai, China on July 10, 1988. In September 2006, she enrolled in China University of Petroleum, in Beijing, China; In August 2009, she enrolled in University of Alaska Fairbanks, in Fairbanks, Alaska. In May 2011, she received her Bachelor of Science degree in Geological Engineering from both China University of Petroleum and University of Alaska Fairbanks. In the fall of 2011, she enrolled in the University of Mississippi and will receive her Master of Science in Geological Engineering in December of 2013.